Advanced Solar combisystems

Yazdanshenas, Eshagh

Publication date:
2010

Document Version
Publisher's PDF, also known as Version of record

Eshagh Yazdanshenas

Advanced Solar combisystems

Ph.D. Thesis

DTU Byg
2010
Byg R-219
ISBN 9788778772985

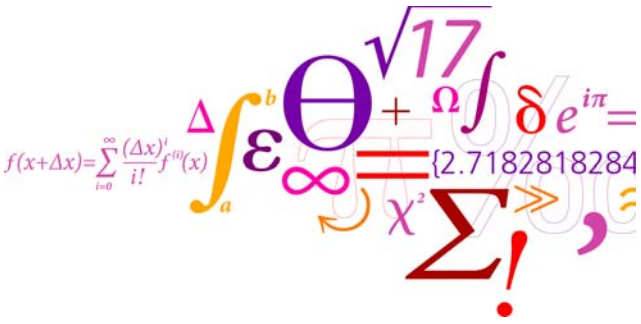

DTU Civil Engineering
Department of Civil Engineering

Eshagh Yazdanshenas

Advanced Solar combisystems

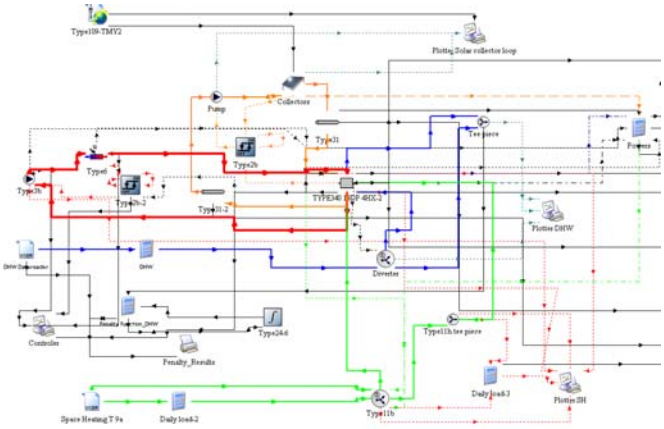

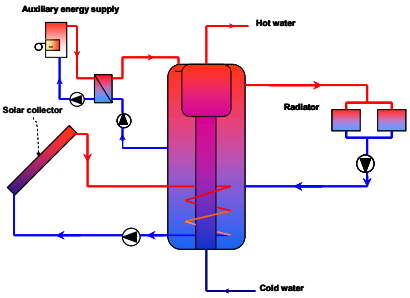

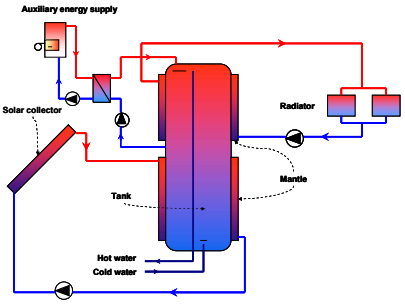

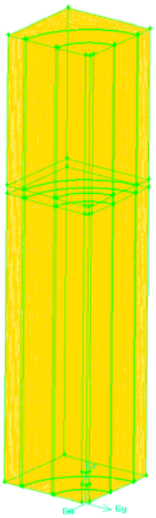

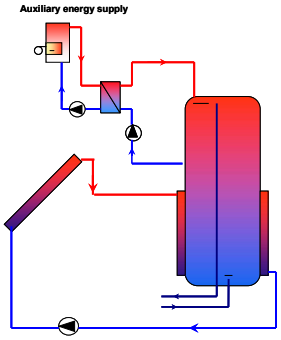

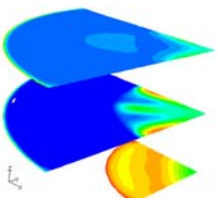

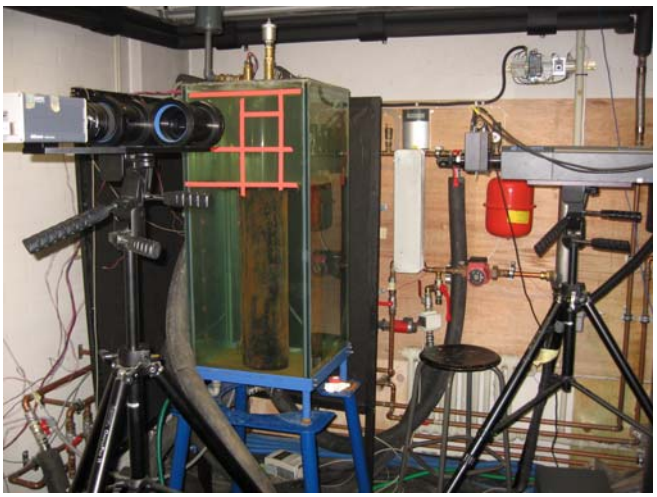

2010
Byg R-219
ISBN 9788778772985

Acknowledgements

This thesis concludes my Ph.D. work entitled 'Advanced Solar Combisystems'. The work was carried out in the period between October 2006 and March 2010 at Department of Civil Engineering at the Technical University of Denmark. This research work has been financed by the European Unions 6th research framework program, Marie-Curie early stage research training network Advanced solar heating and cooling for buildings: SOLNET under the contract MEST-CT-2005-020498.
I would like to offer my deepest gratitude to my supervisor Associate Professor Simon Furbo who was available for discussions and support at any time. I really enjoyed working with and learning from Simon.

Further, I would like to thank my colleagues from Technical University of Denmark especially Jianhua Fan, Janne Dragsted, Elsa Andersen and Bengt Peres for many helpful discussions and support regarding the investigations described in the thesis. I acknowledge and appreciate the help and support with experiments that I was offered by Martin Dandanell and other colleagues from the laboratory.

I would like to thank my former colleague, Alexander Thür for his support at the beginning of my arrival to Denmark which made my life easier at that period. I like to thank my friends having fun and living together in Lyngby during the years of my PhD study.

It was a great honour for me to work within the SOLNET project and I would like to thank all coordinators and supervisors for the good and valuable cooperation during the PhD courses and meetings within this project. Thanks go to Dr. Chris Bales for his support on my three months study stay abroad at Solar Energy Research Center, Dalarna University, Sweden. I would like to thank all PhD students; Juliane, Alexandra, Antoine, Michel, Janne, Bahy, Corry, Ricardo, Oleg within SOLNET network for making it successful, constructive and enjoyable.

Especial thanks to Michel Haller for the very good cooperation on having joint publication within SOLNET project.

I would like to thank my first solar energy teacher, Hessam Taherian for his support during my MSc study.

Finally, I wish to express my gratitude to my parents, brothers, sister and my wife Mona for their admirable patience and support, and many thanks for supporting me in the last intensive month of my Ph.D. study.

Eshagh Yazdanshenas,

Lyngby, March 2010

MARIE CURIE ACTIONS

Marie Curie Early Stage Research Training Network

Advanced solar heating and cooling in buildings, 2006-2010

Abstract

Investigations have shown that the energy consumption during summer periods for space heating and domestic hot water supply is unexpectedly high in many Danish residential buildings. Therefore solar combisystems for combined space heating and domestic hot water supply can be attractive solutions in the future.
Other investigations have shown that a good heat storage design for a solar combisystem is a domestic hot water tank placed in a tank.
In Denmark the auxiliary energy supply system for most solar heating systems is natural gas boilers or oil burners. Both the thermal efficiency and cost-efficiency of a solar combisystem are strongly influenced by the efficiency of the auxiliary energy supply system and by the interplay between the solar collectors and the auxiliary energy supply system. In this connection it is very important that the heat storage is designed in such a way that thermal stratification in the heat storage is built up in the best possible way.
This study is focused on research of the thermal behavior of differently designed solar combisystems for one family houses. The heat storage can either be a hot water tank-in-tank heat storage or a bikini tank with one mantle welded around the lower part of the tank and with one mantle welded around the upper part of the tank. The upper mantle is connected to the space heating system and the lower mantle is connected to the solar collector loop. The study is carried out using a combination of experimental and numerical methods. Thermal experiments of bikini tank and tank-in-tank heat stores are carried out to elucidate the effect of space heating and DHW discharge on thermal stratification for both stores.
The heat transfer and flow structure in the inner and outer side of the tank-in-tank heat store are rather complex and the thermal experiments were followed by investigations by means of advanced experimental and numerical techniques such as Particle Image Velocimetry (PIV) and Computational Fluid Dynamics (CFD). Using a transparent glass tank-in-tank store, experimental flow visualisation was carried out with a PIV system. The flow structures inside the DHW tank and space heating tank were visualised and then compared with the flow structures predicted by CFD-models. The investigations showed that the CFD-models were able to model the flow in the inner and outer side of the tank-in-tank system correctly. With the validated CFD-models, analyses were carried out for differently designed tank-in-tank heat store for different typical conditions to reveal how the design influence the flow structure and heat transfer in the tank-in-tank store.
The yearly thermal performance of solar combisystems based on bikini tanks and on tank-in-tank stores are determined by means of TRNSYS calculations. In this way it is elucidated which system is suitable for three different houses: A low energy house, a house with medium space heating demand and an old house. The study showed that bikini solar combisystems are suitable for low energy houses, while the tank-in-tank stores are suitable for the houses with medium and high space heating demands.

Resumé

Ph.D. projektet med titlen ”Advanced solar combisystems” omhandler solvarmeanlæg til kombineret rum- og brugsvandsopvarmning til enfamiliehuse. Arbejdet er koncentreret om solvarmeanlæg med to forskellige typer varmelagre.
Det ene varmelager er et tank-i-tank varmelager, hvor en varmtvandsbeholder er placeret i en trykløs vandfyldt tank. Solvarme tilføres varmelageret via den trykløse tank. Varme til husets varmeafgivelsessystem tappes fra den trykløse tank, og varmt brugsvand tappes direkte fra varmtvandsbeholderen. Det andet varmelager er en såkaldt bikinibeholder, som er en cylinderformet opretstående varmtvandsbeholder med to påsvejste kapper. En kappe omgiver den nederste del af beholderens lodrette sider, og en kappe omgiver den øverste del af beholderens lodrette sider. Den nederste kappe kobles til solfangerkredsen og den øverste kappe kobles til husets varmeafgivelsessystem. Solvarme tilføres varmelageret ved at solfangervæske langsomt føres gennem den nederste kappe fra top til bund, samtidig med at varme overføres fra solfangervæsken gennem varmtvandsbeholderens sider til brugsvandet. Varme til husets varmeafgivelsessystem tappes fra varmelageret ved at vand føres gennem den øverste kappe fra bund til top, hvorved varme overføres fra brugsvandet til vandet, der strømmer gennem kappen.
Arbejdet, som har omfattet teoretiske såvel som eksperimentelle undersøgelser, er beskrevet kort i det følgende:
Der er gennemført eksperimentelle undersøgelser i en lagerprøvestand af hvorledes der opbygges temperaturlagdeling i en bikinibeholder i perioder, hvor varme til varmeafgivelsessystemet tappes fra varmelageret. Temperaturlagdelingen opbygges på en god måde når volumenstrømmen gennem den øverste kappe er lav. Til gengæld nedbrydes temperaturlagdelingen i varmelageret ved høje volumenstrømme. Der er gennemført eksperimentelle undersøgelser i en lagerprøvestand af hvorledes der opbygges temperaturlagdeling i et tank-i-tank varmelager i perioder, hvor varmt brugsvand tappes fra varmelageret. Temperaturlagdelingen opbygges på en god måde, specielt når der benyttes lave volumenstrømme ved varmtvandstapningen.
Der er opbygget en CFD (Computational Fluid Dynamics) model til beregning af varmestrømme og massestrømme i et tank-i-tank varmelager under typiske driftsforhold. Modellen er valideret ved hjælp af termiske målinger med et forsøgsvarmelager og ved hjælp af målinger af massestrømme i varmelageret med PIV (Particle Image Velocimetry) udstyr.
Med den validerede CFD model er der gennemført beregninger af varmestrømme og massestrømme i forskelligt udformede tank-i-tank varmelagre. Blandt andet er det undersøgt hvorledes temperaturlagdeling opbygges i varmelageret under og efter varmtvandstapninger for varmelagre med forskellige diametre for varmtvandsbeholderen..
Der er desuden gennemført TRNSYS beregninger af ydelsen af solvarmeanlæg baseret på de to varmelagre. Beregningerne viste at solvarmeanlæg med bikinitanke er velegnede til lavenergihuse, mens solvarmeanlæg med tank-i-tank varmelagre er velegnede til huse med mellemstore og store varmebehov.
Resultaterne udgør et forbedret grundlag til videreudvikling af solvarmeanlæg til kombineret rum- og brugsvandsopvarmning.

Nomenclature

A	Heat transfer area, [m²]
c_p	Specific heat capacity of water, [J/kgK]
A_h	Total horizontal cross section area of the tank, [m²]
$A_{h,j}$	Horizontal cross section area of face number 'j' of the tank, [m²]
A_w	Total area of the wall, [m²]
$A_{w,i}$	Area of face number 'i' on the surface, [m²]
Fsav,therm	Fractional energy savings
G	Total radiation on the collector surface, [W/m²]
G_i	Gravity, $g_i = (g_x,g_y,g_z)$, [m/s²]
H	Total enthalpy, $H = h + ½u_i^2$, [J/kg]
h	Thermodynamic enthalpy, h = h(T,p), [J/kg]
k	Turbulence kinetic energy, [m²/s²]
K_θ	The incidence angle modifier, [-]
$LMTD$	Logarithmic mean temperature difference, [K]
m	Total number of faces on the horizontal cross section area of the tank, [-]
n	Total number of faces of the wall, [-]
P	Pressure, [kg/(m·s²)]
q	Area-weighted average of the heat flux, [W/m²]
q_i	Heat flux at face number 'i', [W/m²]
$Q_{vol(i)}$	The power transferred from layer i to the fluid through the upper mantle, [W]
Q_1	The actual energy amount discharged from the tank, [J]
Q_2	Maximum possible discharged energy amount, [J]
u_i	Fluid velocity, $u_i = (u,v,w)$, [m/s]
U	Heat transfer coefficient, [W/m².K]
V	Volume flow through mantle, [m³]
$\dot{V}$	Volume flow rate, [m³/s]
V_i	Volume of layer i, [m³]
t	Time, [s]
T	Area-weighted average of the temperature, [K]
T_a	Ambient temperature, [ºC]
T_j	Temperature of sensor j, [°C]
T_j	Temperature of face number 'j', [K]
T_m	Mean temperature of inlet and outlet of the solar collector, [ºC]
$T_{min,inlet}$	The minimum temperature of the inlet during the whole test period, [°C]
T_{max}	The maximum temperature of all tank temperatures during the whole test period, [°C]
$T_{initial}$	Initial tank temperature, [°C]
$T_{iaverage,inlet}$	Average inlet temperature during the experiment, [°C]
T_{inlet}	Inlet temperature, [°C]
T_{outlet}	Outlet temperature, [°C]
$T_{vol(i)}$	The average temperature of volume i, [°C]

Greek symbols

β	Thermal expansion coefficient [K^{-1}]
$\Delta T_{vol(i)}$	The change in temperature of volume i, [K]
Δt	Period of four minutes, [s]
$\Delta \rho$	Difference in density (difference from reference condition), [kg/m³]
ε	Turbulence dissipation rate, [m²/s³]
η	Collector efficiency, [-]
λ	Thermal conductivity, [W/(m·K)]
$\lambda_{eff,tank}$	Effective thermal conductivity, [W/(m·K)]
μ	Dynamic viscosity, [kg/(m·s)]
ν	Kinematic viscosity, [m²/s]
θ	Angle of incidence, [°]
θ_j	Dimensionless temperature of sensor j, [-]
ρ	Water density, [kg/ m³]
σ	Turbulent Prandtl number, [-]

Subscripts and abbreviations

a	ambient
DHW	domestic hot water
i	Number of layer, [-]
insidewater	Inner tank water
insidetank	Inside tank wall
j	Number of temperature sensor, [-]
outertank	Outer tank water
SCS	Solar combisystem
SDHW	Solar domestic hot water system
SH	Space heating
steel	Steel
start	Start of the test, [-]
stop	Stop of the test, [-]
TRNSYS	Transient Energy System Simulation Tool

Table of Contents

1 Introduction

This thesis describes the Ph.D. study of Eshagh Yazdanshenas carried out at Department of Civil Engineering, Technical University of Denmark. The study is financed by the EU project SOLNET from 2006 to 2010. In this introduction first the outline of the report will briefly be explained, followed by a summary of previous research and background information on the project. Based on this, aims and scope of the study will be described and a short description of the method used will be explained at the end of this chapter.

1.1 Structure of the thesis

This thesis in total has seven chapters with the following contents:

1) Introduction

The outline is explained, followed by a summary of previous research and background information, aims and scope of the project and the method used to achieve the goals.

2) Thermal experiments for a bikini tank and tank-in-tank heat store

In this chapter, thermal measurements of two different solar combisystems; bikini tank solar combisystems and tank-in-tank solar combisystem are investigated. Thermal stratification in both heat storages has been investigated and analyzed.

3) CFD calculations and PIV measurements on tank-in-tank heat store

In this chapter, the tank-in-tank model has been built for the thermal experiments and PIV measurements. Further, the CFD model is made for validation between CFD and measurements.

4) CFD calculations on tank-in-tank stores

CFD calculations on a reference tank-in-tank store and a tank with a small DHW tank diameter is investigated in this chapter to elucidate, how the diameter of the DHW tank influence the thermal stratification in the store.

5) TRNSYS calculations for two solar combisystems and one SDHW system

Bikini tank solar combisystems are investigated numerically and compared to SDHW systems based on mantle tanks. Three different houses with four different radiator systems are considered for the simulations. Solar combisystems based on bikini tanks and tank-in-tank stores have also been compared for three different houses: A low energy house, a house with a medium space heating demand and an old house with a high space heating demand.

6) Conclusions and suggestions for further investigations

A brief review is done to summarize the results of two concepts of solar combisystems. Some suggestions for further work are brought forward in this chapter.

References

The list of references as they are referred to within the thesis.

1.2 Solar heat world wide

Solar energy might become a major component of future sustainable energy supply in the form of solar thermal heating, photovoltaics (PV) and concentrating solar power (CSP). Solar thermal heating has potential to cover up to 50% of the heating and cooling demand in Europe by 2050, according to the workshops on sustainable energies, DTU, Denmark (Bindslev, (2009)).
Solar thermal systems consist of solar domestic hot water (SDHW) systems, solar combisystems for heating of buildings and domestic hot water supply, solar heating plants for heating a whole town or a part of a town by means of a district heating system, solar cooling systems, solar heating systems for desalination and purification of water and air collectors for dehumidification of buildings.
Nowadays the financial payback times of Danish solar heating systems are 5-15 years, and it could be improved by 50% simply by making technological improvements. At present, worldwide, the solar heating market grows by more than 30% a year, and the growth is expected to continue.
A report on the worldwide installed solar collector capacity prepared within the Solar Heating and Cooling Programme (SHC) of the International Energy Agency (IEA), (Weiss et.al. (2009)) presents a study of the solar heating market. The study includes 49 countries with 4 billion people, which is about 60% of the world's population. The installed capacity in these countries is estimated to represent 85–90% of the solar thermal market worldwide. The solar thermal collector capacity in operation worldwide equalled 146.8 GWth corresponding to 209.7 million square meters at the end of the year 2007. Of this, 120.5 GWth were accounted for by flat-plate and evacuated tube collectors and 25.1 GWth by unglazed plastic collectors. The air collector capacity installed was 1.2 GWth.
The main markets for flat-plate and evacuated tube collectors world wide are in China and Europe as well as in Australia and New Zealand. The average annual growth rate between 1999 and 2007 was 24% in China, 20% in Europe, 26% in Canada and the USA and 16% in Australia and New Zealand.
The annual collector yield of all solar thermal systems in operation by the end of 2007 in the 49 countries is 88,845 GWh (319.841 TJ). This corresponds to an oil equivalent of 12.09 million tons and an annual avoidance of 39.3 million tons of CO_2.
Fig. 1-1 shows the total renewable energy sources in the world. Solar thermal heating has the second rank after wind energy on renewable energy production worldwide. Actually, public discussions about the energy policy are increasing dramatically in Europe and worldwide as well. At the Copenhagen climate change conference 2009, the dramatic change of the global climate and the need of reducing CO_2 emissions were in focus.

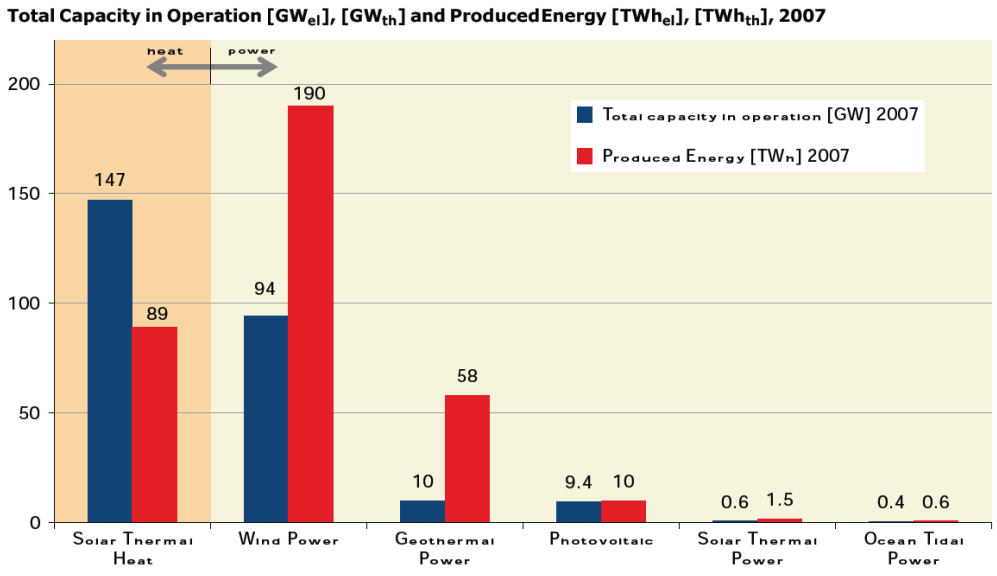

Figure 2: Total capacity in operation [GW_{el}], [GW_{th}] 2006 and annually energy generated [TWh_{el}], [TWh_{th}].
Sources: EPIA, GEWC, EWEA, EGEC, REN21 and IEA SHC 2008

Fig. 1-1. Renewable energy sources worldwide in 2007.

Fig. 1-2 shows the total capacity of glazed flat-plate and evacuated tube collectors in operation at the end of 2007. There is a considerable gap between the first countries compared to the rest of the countries on the list regarding market contribution of solar collectors. Actually the energy policy of the countries and subsidies on renewable energies influences the market share of each individual country.

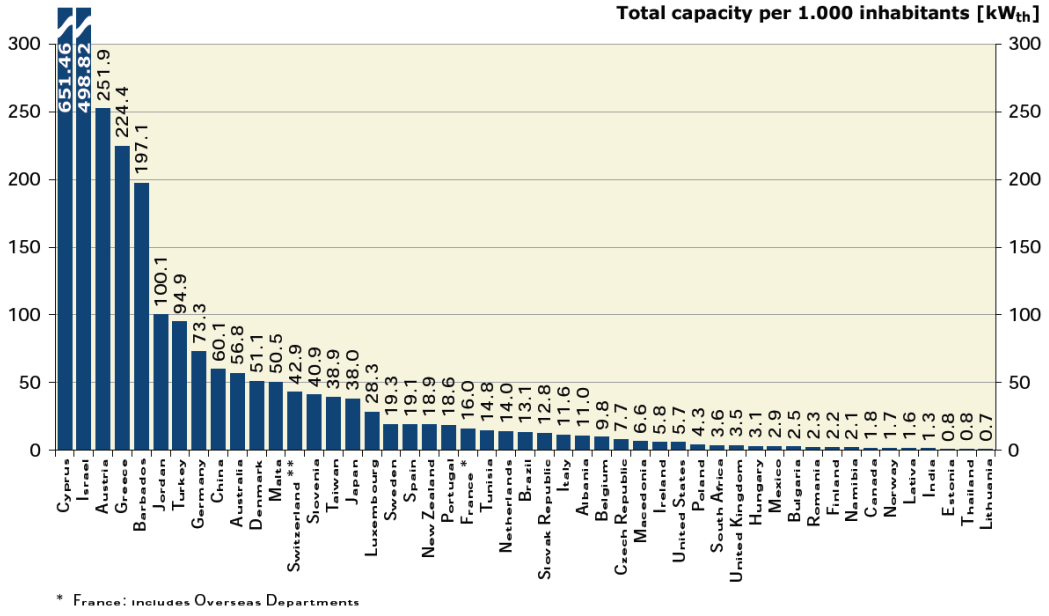

Figure 6: Total capacity of glazed flat-plate and evacuated tube collectors in operation at the end of 2007 in kW_{th} per 1,000 inhabitants

Fig. 1-2. Market contributions in 49 countries per inhabitant , 2007 (Weiss et al. 2009).

Europe has the most sophisticated market for different solar thermal applications. It includes systems for hot water preparation, solar heating systems for space heating of

single- and multi-family houses and hotels, large-scale plants for district heating as well as a growing number of systems for air conditioning, cooling and industrial applications.
In Austria, Germany, Switzerland and the Netherlands the share of applications other than hot water preparation in single-family houses is 20% and higher. Figure 30 gives the distribution of the applications for the 10 countries in Europe with the largest collector area in operation.

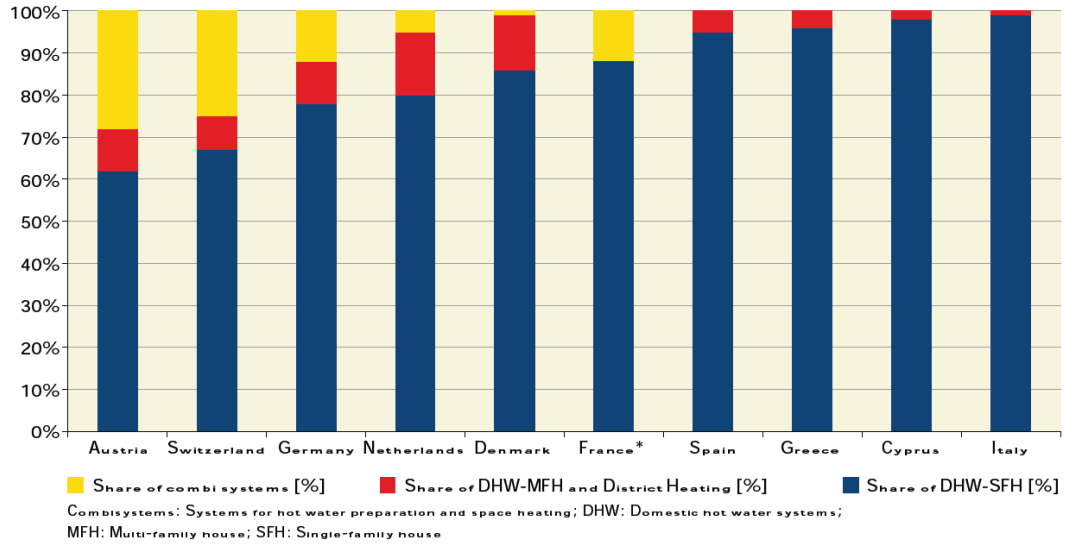

Figure 30: Distribution of different applications in the European top-10-countries related to the total capacity in operation of glazed and evacuated tube collectors in 2007

Fig. 1-3. Distribution of different applications in the European top-10-countries related to the total capacity in operation of glazed and evacuated tube collectors in 2007 (Weiss et.al. 2009).

Education plays an important role to make solar energy an integral part of our energy system. Therefore, in some countries, large efforts have been put on education on solar thermal energy. In Europe, the first coordinated international PhD education program on Solar Thermal Engineering, Advanced Solar Heating and Cooling for Buildings, SOLNET is organized and supported by European Commission within Marie Curie fellowship. 10 Ph.D. projects started in 2006 and 2007 in the field of solar thermal energy. The SOLNET consortium consists of nine university research groups from seven different European countries and involves six commercial enterprises as second hosts. In Fig. 1-4 the network of participants of this project is shown: Technical University of Denmark (DTU), Högskolan Dalarna University (SERC), Kassel University, Czech Technical University, Lund Institute of Technology (LIT), University of Applied Sciences Stuttgart, Graz University of Technology, Politecnico de Milano and Lleida University.

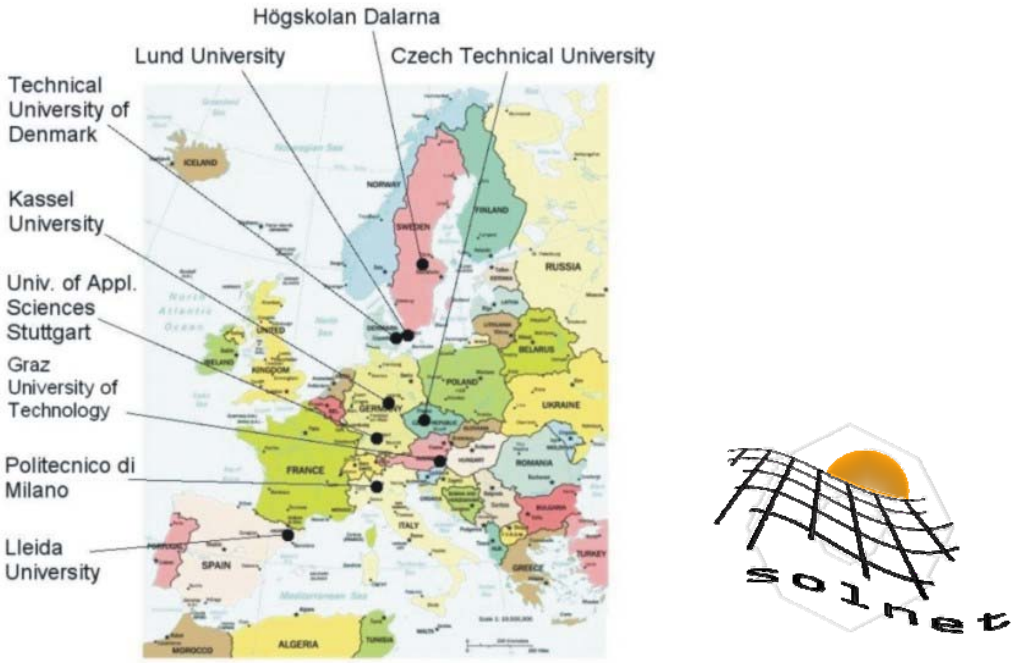

Fig. 1-4. The SOLNET project supported by European Commission among 7 EU countries.

This PhD-project was carried out as one out of 10 PhD studies in the framework of the SOLNET project.

1.3 Previous research

For many years, SDHW (solar domestic hot water) systems based on mantle tanks have been available on the market. Mantle tanks are cylindrical hot water stores with a double-walled ring-shaped mantle wrapped around the lower part of the store. The solar collector fluid heated by the solar collectors is slowly pumped through the mantle and heat is transferred from the solar collector fluid to the domestic water in the tank. Solar collector fluid flow into the top of the mantle, and the cooled fluid is pumped back to the collectors from the bottom of the mantle. In the upper 20% of the mantle, a re-circulating buoyancy-driven flow pattern is created when a hot inlet temperature is applied (Shah et al. (1999)). Mantle heat exchangers have the advantage that the fluid from the solar collector passes neither directly through the tank nor through an internal heat exchanger, both of which are a source of internal mixing. Mantle heat exchangers cause considerably less tank mixing and actually create temperature stratification inside the store – as a result the system efficiency becomes higher as investigated by Baur et al. (1993), Knudsen et al. (2005) and Furbo et al. (2006). Another important reason of using mantle heat exchangers is that it facilitates low-flow systems. Low-flow SDHW principles differ from traditional SDHW systems by having a low flow rate in the solar collector loop. In traditional SDHW systems, the collector flow rate is about 1.2 l/(min·m² collector) while the collector flow rate in low-flow systems is about 0.2 l/(min·m² collector). The main reason for using the high flow rates is to achieve a high efficiency for the solar collector (Duffie and Beckman (1991)).Van Koppen et al. (1979) introduced solar heating systems using highly stratified heat stores and the low-flow principle because the entire solar heating system performance can be strongly increased by this

approach. By the low flow approach, the thermal stratification in the heat store can be further improved resulting in increased thermal performance of the solar heating system. The reason is both that the high temperatures at the upper part of the tank will result in a reduced auxiliary energy consumption and that the low temperatures at the lower part of the tank will increase the solar collector efficiency and operation time of the solar collectors.
A survey carried out within the IEA-SHC Task 14 (1996) project further showed that the cost efficiency of low flow SDHW systems with highly stratified heat stores are much better than the cost efficiency of normal high flow SDHW systems with poorly stratified heat stores, both due to increased thermal performance and due to decreased system costs.
Furbo and Mikkelsen (1987) have shown that the thermal performance is about 20% higher for a low-flow SDHW system based on a mantle tank than for a high-flow SDHW system with an internal coil heat exchanger. Furbo (1993) carried out another experimental investigation to elucidate which of three different low-flow SDHW systems has the best thermal performance. One system with an internal coil heat exchanger from the top to the bottom of the tank, one system with an external heat exchanger and one system with a vertical mantle heat exchanger were analyzed in low-flow mode. It was found that the SDHW system based on the vertical mantle heat exchanger performed best, and also had the best performance/cost ratio. The fact that heat exchanger and heat store are combined into one element makes the system quite compact. At the same time as being a heat exchanger, the mantle can also serve as a drainback tank for drainback solar heating systems. As the mantle heat transfer area to tank volume ratio decreases with increasing store capacity, SDHW stores based on mantle tanks are most effective in small systems.
The solar heating market worldwide grows by 20-40% each year. In most European countries the percentage part of solar heating systems, which are solar combisystems is growing. Solar combisystems can cover both a part of the space heating demand and a part of the domestic hot water consumption. In principle, a solar combisystem consists of a solar collector loop, solar heat exchanger, heat store, auxiliary energy supply system, DHW preparation, space heating system and controllers to control the hydraulics of a system. There are different boundary conditions that influence the performance of a solar combisystem such as the fuel which is used for the auxiliary boiler/burner, the performance of the auxiliary boiler/burner, the control system, the type of the heat store, the solar collector and space heating system, DHW and space heating loads etc. Therefore, the optimal solar combisystem type might change from house to house, on the boundary conditions.
The first solar combisystems were built in US to cover the space heating demand in 1950s (Bliss (1955), Engebretson (1964), Löf et al. (1963) and Löf et al. (1964)). Their solar combisystems were designed for high solar fractions while the cost/performance ratio of the systems had less importance. The working fluid in their collector was water and air.
In Denmark one of the first solar combisystems was used for the so called the Zero Energy House at the Technical University of Denmark (Esbensen and Korsgaard (1977)). A solar fraction of 100% was planned for this system. However, the aim was not achieved, mainly due to high heat loss from the heat store. New Danish solar combisystems have much lower solar fractions. The studies on solar combisystems in practice in Denmark continued (Andersen (1988), Ellehauge (1993) and Ellehauge (2000)). The studies showed that there is little correlation between the solar fraction and the yearly net utilized solar energy per m² collector for the Danish systems. The

main reasons for this are that there are large variations in the space heating demand during the summer months from system to system and that there are large variations in the heat loss from the heat storage of the systems (Andersen et al. (2004)).
In IEA-SHC Task 26, Weiss (2003), the combined coverage of DHW load and Space Heating (SH) load by Solar Combisystems was investigated. Solar Combisystems require a bigger solar collector area than SDHW systems, as they also need to provide energy for Space Heating. The space heating load is considerably higher than the DHW load. The DHW load accounts for 10-40% of the total heat demand. As the SH load varies significantly from season to season, an auxiliary energy supply system powered by biomass, gas, oil or electricity is usually included in a Solar Combisystem, so that in winter no problems on covering heat demand arise. The efficiency of the auxiliary energy supply system strongly influences the thermal efficiency and cost-efficiency of a Solar Combisystem. It is important that the heat store and the auxiliary energy supply are controlled in such a way that both the auxiliary volume and the temperature to which the volume is heated are as low as possible without causing discomfort.
Twenty one different solar combisystems were investigated, numerically in detail in different IEA member countries within the IEA-SHC Task 26 project. A design hand book for solar combisystems was published, Weiss (2003). In order to gain high energy savings for solar combisystems, it is important to have:

- A small auxiliary volume in the heat storage.
- A low auxiliary set point temperature of the auxiliary volume in the heat storage.
- A low tank heat loss
- A high efficiency of the auxiliary energy supply system
- A good thermal stratification in the heat storage tank

Two different small and medium sized solar combisystems have been studied within the Task 26 project in Denmark. Ellehauge (2002) investigated the small solar combisystems "Generic system #2" with a 280 litre DHW tank volume, 10 m² collector area and a gas boiler. The study shows that $F_{sav,therm}$ increased from 19 to 22% while the auxiliary volume decreased from 126 to 70 litre.
Shah (2002) investigated a medium sized solar combisystem "Generic system #4" with a 750 litre DHW tank volume, 15 m² collector area and a gas boiler. The study showed that $F_{sav,therm}$ increased from 22 to 26% while the auxiliary volume decreased from 375 to 75 litre. Furthermore, it was found that $F_{sav,therm}$ increased from 24 to 27% while the auxiliary set point temperature decreased from 60°C to 40°C.
In IEA-SHC Task 26, a simulation study of a dream system was carried out at SERC, Sweden (Tepe et al. (2003)). The thermal performance of the solar combisystem "Generic System #11" with a 700 liter space heating tank volume and with an oil boiler and 10 m² collector area was improved by installation of an external heat exchanger hot water unit, a stratifier for the space heating return flow and a four way mixing valve for space heating.
Drück and Hahne (1998) investigated four different solar combisystems in detail. They found that the most important parameters for a well performing combistore are low heat losses due to a good thermal insulation. They also suggested using a small auxiliary volume and a low set point temperature of the auxiliary boiler. Moreover, the connections for the auxiliary and the space heating loop should be in appropriate positions.

Andersen and Furbo (2007) investigated theoretically three solar combisystem designs in three different houses with different space heating systems. The solar combisystems are initially equipped with solar heat exchanger spirals and direct inlets from the space heating system to the tank. A step-by-step investigation was performed demonstrating the influence on the thermal performance of using inlet stratification pipes at the different inlets. Based on TRNSYS simulations, they found increased thermal performance of solar heating systems by using stratifiers instead of internal heat exchangers and direct inlet to the tank. They found that the best performing solar combisystem is based on a tank-in-tank storage with stratifiers both in the solar collector loop and the space heating loop.

Andersen and Furbo (2009) investigated the thermal performances of solar collectors and solar combisystems with different solar fractions with weather data of the Danish Design Reference Year, DRY data file, and with measured weather data from a solar radiation measurement station situated at the Technical University of Denmark. Their study showed that solar combisystems with high efficient solar collectors are more influenced by weather variations from one year to another than systems with low efficient solar collectors. Their investigation also showed that the space heating consumption is strongly correlated to the ambient temperature and not to the solar radiation. It was also reported that evacuated tubular solar collectors utilize less sunny years with large parts of diffuse radiation relatively better than flat plate collectors.

Fiedler et al. (2006) investigated four different commercial combined solar and pellet heating systems. Two systems had a pellet stove, one with a store integrated pellet burner and one with a pellet boiler. The systems were simulated by TRNSYS taking the experimental parameters into account. The results of this study showed that the room structure of the building performance has a strong impact of the performance of the stove systems. The results from this study can only be applied for buildings with the same or equivalent design. For buildings with an open internal design a system with a pellet stove is the most efficient solution.

Thür (2007) investigated a new compact solar combisystem with an integrated condensing natural gas boiler in his PhD thesis. Advanced control strategy to control a hot water circulation pump and the very high overall hydraulic efficiency of the developed compact solar combisystem in the space heating period demonstrated a successful concept. The solar combisystem with a 360-liter tank achieved a hydraulic efficiency of around 94 %, whereas the conventional heating system with a 50-liter hot water tank achieved around 95 % to 96 % at comparable total heat loads.

The advantage of the developed solar combisystem is due to its compactness of the hydraulic system, which is installed within a closed 60 x 60 cm cabinet, and a new designed 360-liter tank with a comparable low heat loss coefficient of about 2 W/K, thanks to a totally closed insulation at the top and the side of the tank.

By integration of the solar collector into the building envelope, the heat loss from the collector decreases and also there is a possibility to gain passive heat from the collectors to the building in winter periods (Bergmann and Weiß (2002); Metzger et al.(2007) and Metzger et al. (2008)). The use of solar façade collectors have several advantages especially for solar combisystems due to natural removal of summer extreme solar gains from oversized tilted solar collector areas. Use of vertical solar collectors result in a more uniform profile of the radiation.

Thermal stratification in the tank has a great importance for the thermal performance of the solar heating system. It can considerably increase the system performance, especially for low flow solar heating systems (Lavan and Thompson (1977), Phillips and Dave (1982), Hollands and Lightstone (1989), Cristofari et al. (2003); Andersen

and Furbo(2007)). Some numbers have been introduced to characterize thermal stratification in heat storages during charge, stand-by and discharge (Davidson et al. (1994a), van Berkel, (1997) Shah and Furbo (2003), Panthalookaran et al. (2007) and Andersen et al. (2007)). Haller et al. (2009) and (2010) investigated thermal stratification in heat storages and presented an overview of the methods used to characterize thermal stratification. Moreover, a new method based on the second law of thermodynamics for calculation of a stratification efficiency of heat storages was proposed. According to this study - a part of the current study is a part of the paper - it does not in theory make a difference if the stratification efficiency is calculated based on entropy balances or based on exergy balances. In practice, however, exergy balances are less affected by measurement uncertainties, whereas entropy balances can not be recommended if measurement uncertainties are not corrected in a way that the energy balance of the storage process is in agreement with the first law of thermodynamics.

Thermal stratification can be established during charge and discharge. During charge periods, the solar heat can be transferred to the heat store to a level where the temperature is close to the inlet temperature of the fluid. Vertical mantle heat exchanger is a kind of the heat exchanger where the incoming fluid goes to a level where it can transfer heat to the tank. Therefore, there is less mixing in such a tank than in a spiral tank.

During discharge periods when the cold water enters the tank from the bottom during hot water draw-off in SDHW and solar combisystems, thermal stratification can be established in the tank. If the return water from the space heating system enters the tank through inlet stratifiers in solar combisystems, thermal stratification can be built up in the tank too, Weiss (2003) and Furbo et al. (2004).

Knudsen and Furbo (2004) suggested the use of three-way valves to a mantle heat exchanger into which the fluid is injected at the correct level. They used a top inlet position for high temperatures and an intermediate height position for moderate inlet temperatures.

Furbo et al. (2005) also investigated the thermal advantages by utilizing discharge from different levels in solar storage tanks, both for a small SDHW system and for a solar combisystem. The investigations showed that it is possible to increase the thermal performance of both types of systems by using two draw-off levels from the solar tanks instead of one draw-off level at a fixed position. The best position of the second draw-off level is in the middle or just above the middle of the tank. For the investigated small SDHW system with a realistic hot water draw-off, the increase of the thermal performance by the second draw-off level is about 6%.

For the investigated solar combisystem the extra thermal performance by using one extra draw-off level, either for the domestic hot water heat exchanger or for the heating system, is about 3%, while an improvement of about 5% is possible by using a second draw-off level both for the domestic hot water heat exchanger and for the heating system.

Andersen et al. (2007) investigated a number of different fabric stratification pipes compared to a rigid inlet stratifier. Detailed investigations of the flow structure close to fabric stratification pipes were investigated for one set of operating conditions by means of the optical PIV (Particle Image Velocimetry) method. The investigation showed that the performance of fabric stratification pipes can be improved significantly by using two fabric layers with a distance of about 10 mm between each fabric layer instead of using one fabric layer. The biggest drawback of fabric stratification pipes is the high horizontal heat transfer through the very thin fabric.

Thus, when hot water enters a cold tank from the bottom to the top of a stratification pipe, rigid stratifiers have an advantage because of the low horizontal heat transfer through the pipe wall compared to fabric stratifiers. For the cooling test, fabric layer stratification pipes perform better than the rigid stratifiers, while two fabric layer stratification pipes and rigid stratifiers perform identical during stratified heating tests. Davidson et al. (1994b) found that fabrics with limited ability to stretch like woven fabrics were not suitable as stratification inlet pipes when the water enters the stratification inlet pipe through the top of the tank.
CFD models, in addition to the use of less detailed one dimensional simulations and measurements, make it possible to describe the near reality of the physical phenomena and thus to understand the flows inside solar tanks better. In comparison with one-dimensional models, CFD models involve less assumptions, therefore it is more realistic and accurate. A wider range of operation conditions as well as complex tank designs can be modelled by means of CFD. Oliveski et al. (2005) carried out a numerical and experimental study of the thermal stratification inside a tank containing thermal oil. Starting from an initial condition of uniform temperature, the tank was submitted to cooling by the thermal losses to the environment. The numerical analysis was accomplished with a two-dimensional model in cylindrical coordinates with the Finite Volumes method. The bottom and the top of the tank were thermally insulated. The temperatures of the tank sidewall and centerline were measured with copper-constantan thermocouples. The numerical and experimental results showed that, as time passes, the oil volume is divided into two regions: a stratified region (at the bottom) and another at a uniform temperature (at the top). The interface between these two regions advances towards the top. It was numerically verified that the tank under natural convection regime, in terms of convective flow direction, presented two different regions. The numerical results show a good agreement with the experimental results.
Johannes et al. (2005) compared the ability of TRNSYS's Types 60 and 140 to reproduce the temperature field in a storage tank. Also fluid motions by means of CFD simulations were studied. This part has highlighted the mixing in the top of the tank due to the inlet configuration, but also the limits of the stratified fluid models with the multinode approach used in TRNSYS.
CFD simulations take a considerable computing time (around 5 days for one physical hour of simulation), making annual performance prediction impossible by means of CFD calculations. The main conclusion of comparisons of calculations with a multi-layer model and with a CFD model and measurements was a need to develop a simple one dimensional model, which is a compromise between a reasonable calculation accuracy and a reasonable duration of simulation times.

1.4 Aims and Scope

Many different Solar Combisystem designs have been commercialized over the years. In the IEA-SHC Task 26, twenty one solar combisystems have been described and analyzed. Maybe the attractive mantle tank approach also for solar combisystems can be used with advantage? This might be possible if the solar heating system is based on a so called bikini tank. A bikini tank is a vertical hot water tank with two mantles welded around the surface of the hot water tank. One mantle placed around the upper part of the tank is connected to the heating system of the house and one mantle placed around the lower part of the tank is connected to the solar collectors. The charging of the bikini tank by solar collectors takes place in the same way as the previously

described SDHW mantle tank system, namely through the lower mantle - preserving and improving thermal stratification. Domestic hot water is tapped directly from the inner tank, the hot outlet pipe connection placed at the bottom of the tank and a plastic pipe running all the way to the top of the tank, preventing thermal bridges between the top and the ambient, which would otherwise have been a cause of strong internal mixing and of a high heat loss. The cold water inlet is placed at the tank at the bottom, and is shielded by a baffle plate to prevent a strong inlet jet from causing mixing in the tank. The SH load is supplied by the upper mantle. Hot water going to the SH system is supplied from the top of the mantle, while the cooled return flow enters the mantle from the bottom. An auxiliary heater is heating up the domestic hot water in the top of the tank. In this way, the high space heating load in the winter months can be covered, and the DHW consumption can be covered as well.

Investigations of bikini tanks are carried out. Moreover, two solar combisystems: Tank-in-tank solar combisystems and solar combisystems based on bikini tanks have been compared. Tank-in-tank heat stores have the advantage of having high peak power on the demand side, low heat loss due to its compact design, no lime problems and a reduced hot water volume compared to hot water tanks which makes it easy to avoid restrictions in the design due to legionella considerations. The advantage of bikini tank is that it is compact; no lime problems in the tank, low heat loss due to the compact design and the disadvantages of the bikini tank is a low heat transfer area of the upper mantle used for discharge for space heating and equalization of temperature differences during space heating discharge. Further, the design is due to legionella considerations only suitable for small systems.

The aim of the investigation is to study two different heat storage tanks: Tank-in-tank and bikini tank stores. Those components are experimentally tested individually to elucidate how thermal stratification is built up during space heating discharge for the bikini tanks and DHW discharge from the tank-in-tank store. Based on the thermal experimental studies, the tank-in-tank store was chosen to be investigated more in details by means of the CFD calculations and PIV measurements. A CFD model is validated by the thermal experiments and PIV measurements. Based on the validated CFD model, a CFD model is used to investigate how the geometry of the tank influences the thermal stratification in the tank.

Moreover, solar combisystems based on bikini tanks and solar domestic hot water systems based on mantle tanks are investigated by means of TRNSYS calculations. Furthermore, two solar combisystems based on bikini tanks and tank-in-tank stores are compared by means of TRNSYS calculations to elucidate which of these two systems is suitable for three different houses: A low energy house, a house with medium space heating demand and an old house with a high space heating demand.

2 Thermal experiments of the bikini tank and tank-in-tank heat store

2.1 Thermal experiments of the bikini tank

2.1.1. Introduction

There are different kinds and sizes of solar combisystems on the market. The size of solar combisystems differs from country to country, first of all due to different traditions.
In central Europe, most solar combisystems have large collector areas, typically more than 10 m². In Denmark, it is normal to have small solar combisystems based on a hot water tank as heat storage.
One of the marketed systems which have been used in the Netherlands since 1994 is a compact unit for both space heating and DHW, with an integrated gas burner. The 240 litre or 650 litre DHW tank is surrounded by a double-wall tank connected to the solar collector. This mantle tank simultaneously works as a heat exchanger and a drainback tank for the collector. And at the top of the tank, an internal heat exchanger is installed and connected to the space heating system. A typical system with 4.2 m² of collector and a 240 litre storage tank with an integrated gas burner is shown in Fig. 2-1.

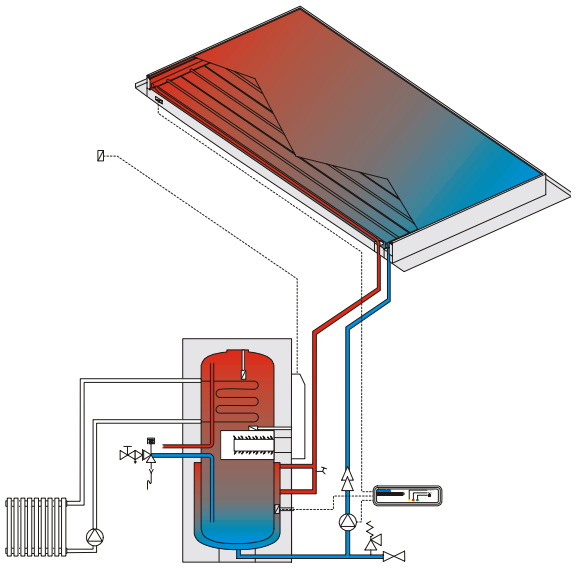

Fig. 2-1. Schematic sketch of the DHW tank as space heating storage with drainback capability.

As mentioned before, earlier investigations have shown that solar domestic hot water systems based on vertical mantle tanks are very attractive from a thermal performance point of view.
Maybe solar combisystems based on bikini tanks with two mantles working in a similar way as the Dutch system (Fig. 2-1) are attractive? In order to answer this question, preliminary investigations with a hot water tank with two mantles are

carried out. Fig. 2-2 shows a schematic illustration of the investigated solar heating system. Solar heat is transferred from the solar collector fluid to the domestic water by means of a mantle around the lower part of the hot water tank. Heat is transferred from the domestic water to the water coming from the space heating system by means of a mantle around the upper part of the tank.

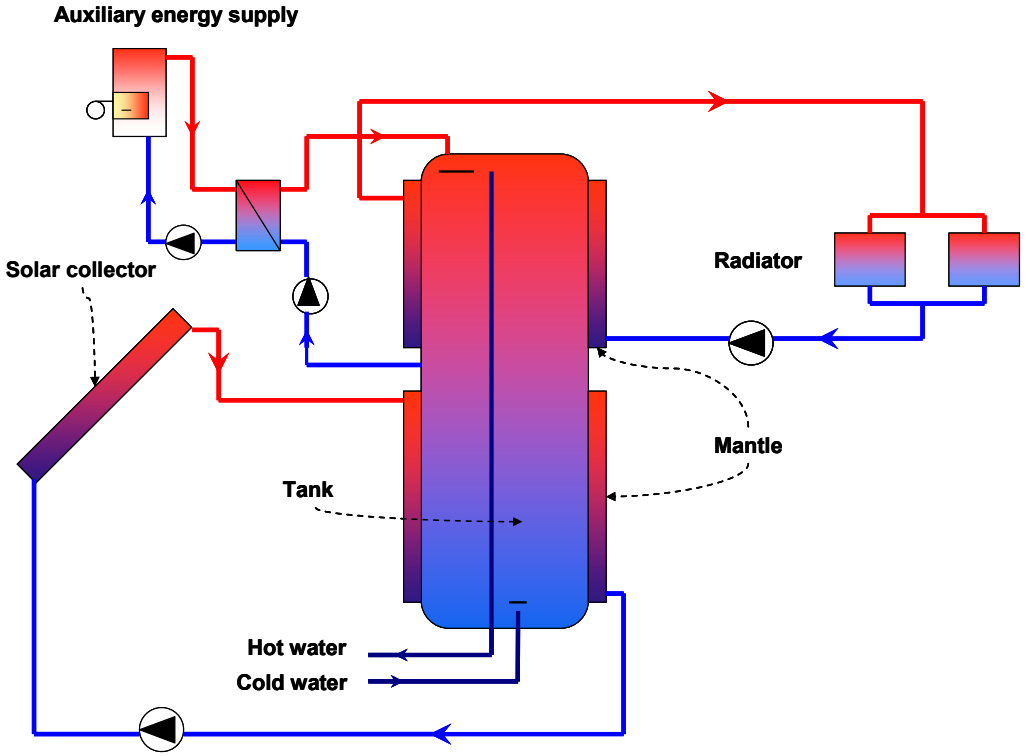

Fig. 2-2. Schematic sketch of the investigated solar combisystem.

Thermal experiments are carried out as discharge tests for a bikini tank with two mantles. The aim of the tests is to investigate how the heat exchange capacity rate between the tank and the water in the upper mantle and the thermal stratification in the tank are influenced by the volume flow rate through the upper mantle and the temperature level of the tank.

2.1.2. Experimental set up

Fig. 2-3 is the photo of the tested bikini tank including dimensions. The data of the bikini tank are also given in Table 2-1. A cold and a hot loop is used in the experiments. In the heat storage test facility, the hot loop is connected to the lower mantle acting as a solar collector loop and the flow rate and the temperature is controlled. Water is used in the loop. The cold loop is connected to the upper mantle and acts as a space heating system. The water flowing through the upper mantle is cooled down by a counter flow heat exchanger in the loop. The volume flow rate and the inlet temperature of the upper mantle are controlled and regulated in a precise way.

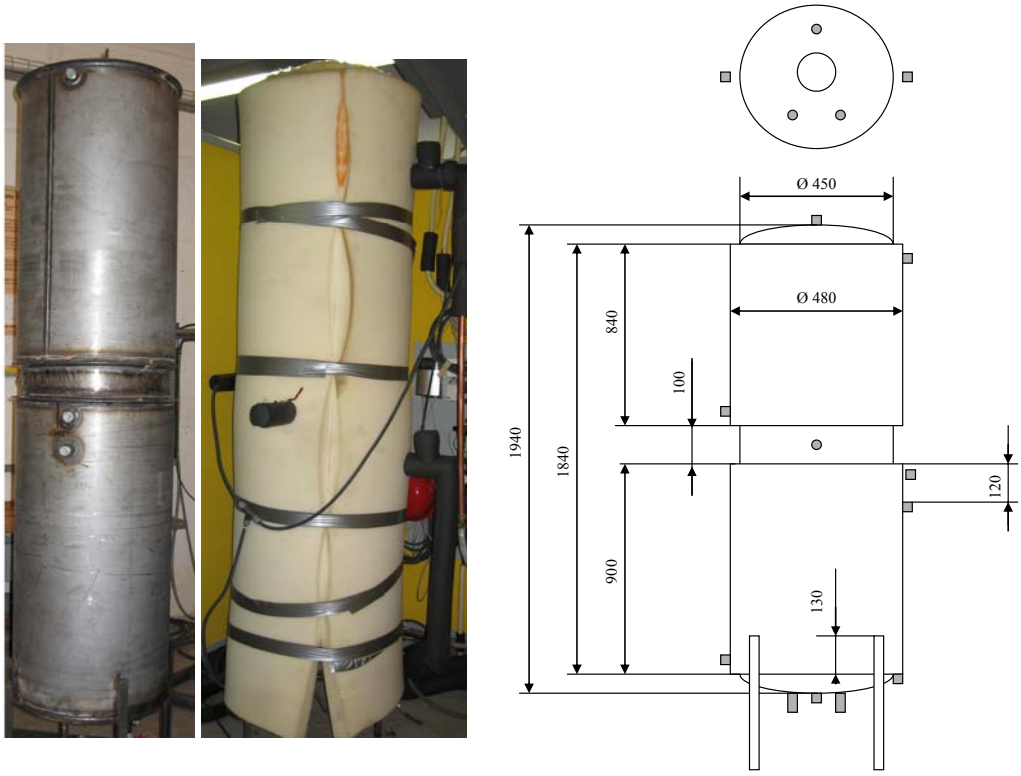

Fig. 2-3. The bikini tank used for the experiments.

Table 2-1. Data for the tested bikini tank.

Tank volume, l	292
Lower mantle volume, l	16.5
Upper mantle volume, l	16.0
Tank height, m	1.94
Inner tank diameter, m	0.444
Upper mantle height, m	0.84
Lower mantle height, m	0.90
Mantle gap, m	0.015
Tank material thickness, mm	2.5
Top and bottom of the mantle thickness, mm	3
Insulation material	Latex foam
Insulation thickness top, m	0.20
Insulation thickness side, m	0.07
Insulation thickness bottom, m	0
Empty tank mass, kg	125

The ambient temperature and the temperatures of the water in the inner tank are measured at twelve measuring points inside the bikini tank by means of copper/constantan thermocouples, Type TT placed in a glass tube that is placed in the tank through the bottom and the top. The inlet and outlet temperatures of the upper and lower mantles are also measured by means of copper/constantan thermocouples, type TT. The temperature differences between inlet and outlet are measured by copper/constantan thermopiles.

The twelve temperature sensor positions in the tank and their distance from the top of the tank is shown in Fig. 2-4. The accuracy of the measuring thermocouples is estimated to be about ± 0.5 K and for the thermopiles about ± 0.03 K (Ellehauge

(1993)). The upper mantle flow rate is measured with an electro magnetic inductive flow meter, type HGQ1 from Brunata HG A/S. The flow meter has an accuracy of about ± 1 %. The lower mantle flow rate is measured by Combimeter 5 EPD flow meter with the accuracy of ± 1 %. The data are logged by PC (using the software: IMPVIEW) and two Schlumberger IMP measuring cards (Type 35951C and Type 35952A).

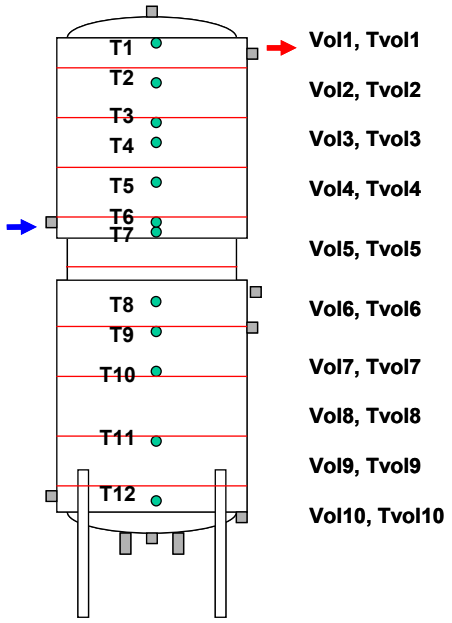

Middle tank temperature sensors	Distance from the top of tank, m
T1	0.06
T2	0.24
T3	0.44
T4	0.53
T5	0.65
T6	0.86
T7	0.86
T8	1.07
T9	1.20
T10	1.28
T11	1.54
T12	1.88

Fig. 2-4. Thermal measuring points and their position.

2.1.3. Test conditions

Tests are carried out with five different flow rates of 0.5, 1, 2, 3, 5 l/min with two different inlet temperatures of 20°C and 30°C to the lower inlet of the upper mantle. Furthermore, the tests are carried out with different initial conditions for the temperatures inside the tank. The initial conditions are that the tank is either ‘‘mixed’’ or ‘‘stratified’’. In the ‘‘mixed’’ tests, the temperature at the bottom of the tank is about 47°C and 60°C at the start of the tests. In the stratified tests, the temperature at the bottom of the tank is about 25°C at the start of the tests. The start temperature in the upper part of the tank is in the interval 50-59°C or in the interval 70-75°C. The initial conditions in four tests are shown in Fig. 2-5. Prior to the tests, the tank is heated via the lower mantle with an inlet temperature of about 80°C and a constant flow rate followed by a 3 hr period without heating. After this period, the tests are carried out. The measured data is logged every one second and averaged every four minutes.

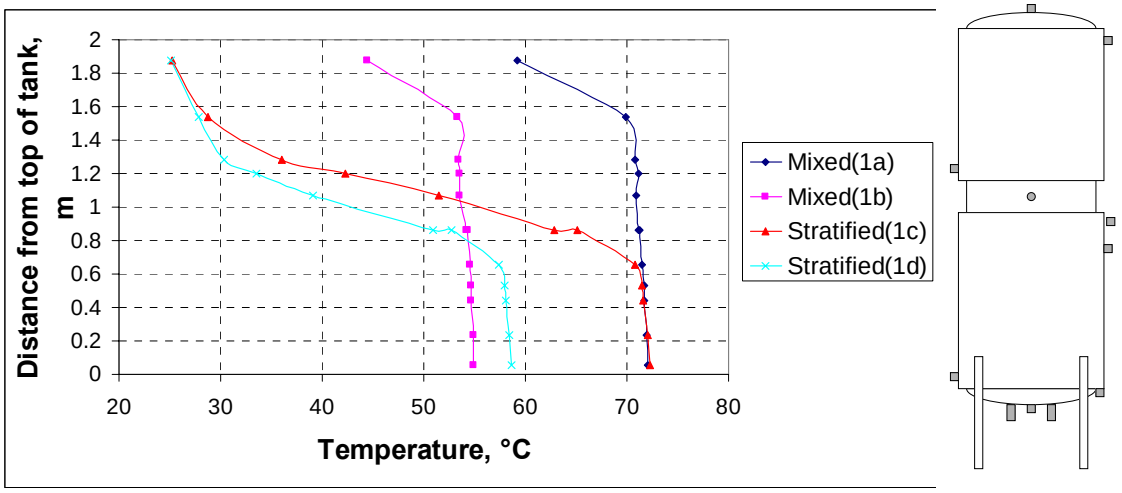

Fig. 2-5. Initial temperatures in four tests.

The duration of the test is different from test to test due to different flow rates, inlet temperatures and initial temperatures. The test conditions of the tests are shown in Table 2-2.

Table 2-2. Description of 19 tests.

Test no.	Inlet temperature [°C]	Flow rate [l/min]	Start tank temperatures at top and bottom of tank [°C]	Initial condition
1a	25	0.5	72-59	Mixed
2a	25	1	72-59	Mixed
3a	21	2	75-62	Mixed
4a	21	3	72-59	Mixed
5a	21	5	72-59	Mixed
1b	20	0.5	55-45	Mixed
2b	20	1	60-50	Mixed
3b	21	2	57-45	Mixed
4b	21	3	60-50	Mixed
5b	22	5	55-45	Mixed
1c	22	0.5	72-25	Stratified
2c	21	1	70-25	Stratified
3c	21	2	70-26	Stratified
4c	21	3	70-26	Stratified
5c	22	5	71-26	Stratified
1d	21	0.5	59-25	Stratified
2d	21	1	55-25	Stratified
1e	31	0.5	57-51	Mixed
2e	36	0.5	61-55	Mixed

2.1.4. Methods of analyzing results

The tank is divided into ten equal volumes of 29.2 l as shown in Fig. 2-4. The temperature of each volume is obtained by assuming a linear relation between measured temperatures in the tank. The rate of heat transfer from each water volume

is obtained by Eq. (2.1). A time step of four minutes is used in the calculations of the heat transfer.

$$Q_{vol(i)} = \frac{\rho_i . V_i . c_p . \Delta T_{vol(i)}}{\Delta t} \tag{2.1}$$

where ρ_i is the density of water, V_i is the volume of layer i, c_p is specific heat capacity of water, $\Delta T_{vol(i)}$ is the change in temperature of volume i, Δt is the period of four minutes.

The thermal stratification in the tank for the different tests with different flow rates and inlet temperatures and start temperatures are compared. In order to eliminate the small differences in the initial temperatures and inlet temperatures, the temperatures are shown dimensionless as Eq. (2.2):

$$\theta_j = \frac{T_j - T_{min,inlet}}{T_{max} - T_{min,inlet}} \tag{2.2}$$

where θ_j is dimensionless temperature of sensor j, T_j is temperature of sensor j, $T_{min,inlet}$ is the minimum temperature of the inlet during the whole test period, T_{max} is the maximum temperature of all tank temperatures during the whole test period.

The discharge efficiency of the tank for discharge tests with an initially mixed tank is defined as an actual energy amount discharged from the tank over the maximum possible exchanged energy amount. The actual energy amount discharged from the tank Q_1 and the maximum possible exchanged energy amount, Q_2 are obtained using Eqs. (2.3) and (2.4).

$$Q_1 = \int_{t_{start}}^{t_1} \dot{V} . \rho . c_p . (T_{outlet} - T_{inlet}) . dt \tag{2.3}$$

$$Q_2 = V . \rho . c_p . (T_{initial} - T_{iaverage,inlet}) \tag{2.4}$$

where $\dot{V}$ is the volume flow rate in the upper mantle, T_{outlet} is the outlet temperature of the upper mantle, T_{inlet} is the inlet temperature of the upper mantle, t_1 is the end of the calculation, t_{start} is the start of the test. V is total volume passing through the upper mantle. $T_{initial}$ is the average of the initial tank temperatures and $T_{iaverage,inlet}$ is the average inlet temperature during the experiment.

The heat transfer coefficient of the upper mantle is obtained by the equation:

$$U = \frac{\dot{V} . \rho . c_p . (T_{outlet} - T_{inlet})}{A . LMTD}, \quad \text{where} \quad LMTD = \frac{(T_{tank} - T_{outlet}) - (T_{tank} - T_{inlet})}{Ln \frac{(T_{tank} - T_{outlet})}{(T_{tank} - T_{inlet})}} \tag{2.5}$$

where A is heat transfer area and T_{tank} is the tank average temperature at the upper mantle level.
Dimensionless time is defined as the time at a certain time of the test divided by the time when the total amount of 324.5 l corresponding to the sum of the domestic hot water tank volume and the lower and upper mantle volumes, have passed through the upper mantle. Discharge efficiency η can be obtained by Eq. (2.6).

$$\eta = \frac{Q_1}{Q_2} \tag{2.6}$$

Dimensionless volume is defined as the discharged volume at a specific time divided by the total volume discharged during the whole test. The total volume discharged during the whole test is the sum of the domestic hot water tank volume and the volumes of the upper and the lower mantles.

2.1.5. Effect of mantle flow rate

''Experiment 1a-5a'' [Initially mixed (59-72°C), Inlet temperature (21-25°C)]

The measured temperatures inside the tank, inlet and outlet temperatures for the upper mantle for experiments 1a, 2a, 3a, 4a and 5a for different mantle volume flow rates and initially mixed temperature of around 70°C are shown in Fig. 2-6a, Fig. 2-6b, Fig. 2-7a, Fig. 2-7b, Fig. 2-8a, Fig. 2-8b, Fig. 2-9a and Fig. 2-9b. The mantle inlet temperature is around 23°C.
In experiment 1a, with a volume flow rate of 0.5 l/min, the tank temperatures decrease. Thermal stratification is built up in the upper part of the tank surrounded by the upper mantle (T1-T7), while in the lower part a little thermal stratification is built up inside the tank. At the end of the experiment almost no stratification is seen inside the tank. It can also be seen that the outlet temperature from the upper mantle is very high between T1 and T2.
In experiment 2a, the volume flow rate is 1 l/min. The thermal stratification in the tank is somewhat smaller than in experiment 1a. The outlet temperature from the upper mantle is close to T2. In experiment 3a with a volume flow rate of 2 l/min, the thermal stratification in the tank is much lower than in experiments 1a and 2a. The outlet temperature from the upper mantle is higher than T3 in the first 80 min of the test period. During the test, the outlet temperature decreases below the tank bottom temperature. In experiment 4a with a volume flow rate of 3 l/min, thermal stratification is lower than for the lower flow rates and the outlet temperature from the upper mantle is now lower than the lowest tank temperature. The same result is obtained for experiment 5a with a volume flow rate of 5 l/min. The reason for the low outlet temperature from the upper mantle for the high volume flow rates is the short time it takes the water to pass the upper mantle.

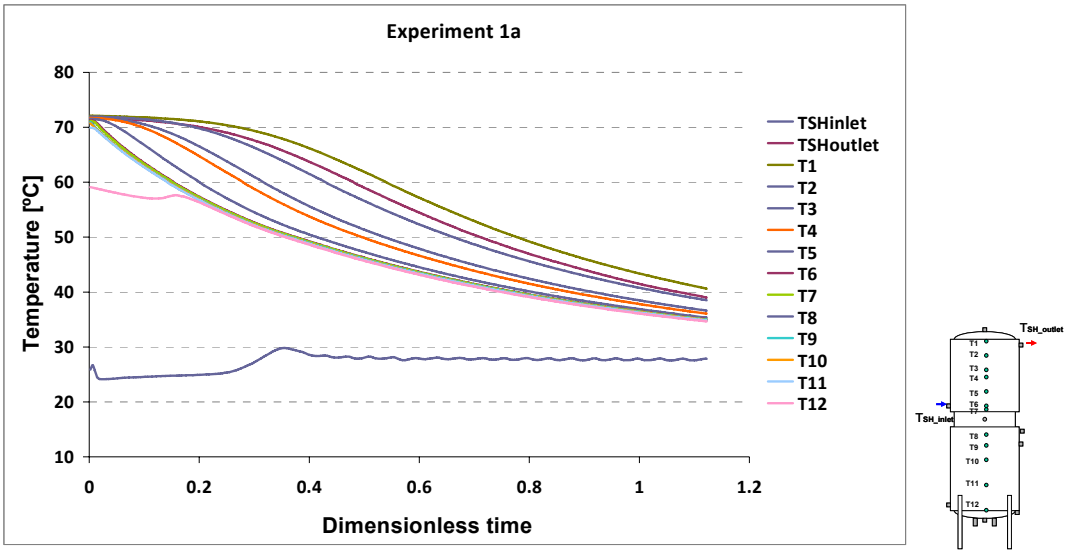

Fig. 2-6a. Measured temperatures with a volume flow rate of 0.5 l/min, experiment 1a.

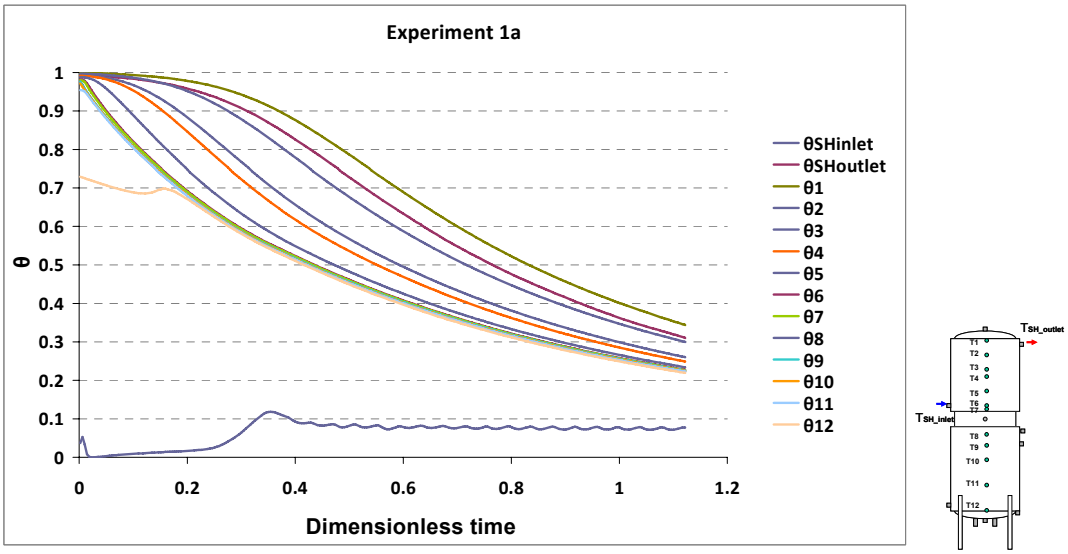

Fig. 2-6b. Dimensionless temperatures for experiment 1a with a volume flow rate of 0.5 l/min.

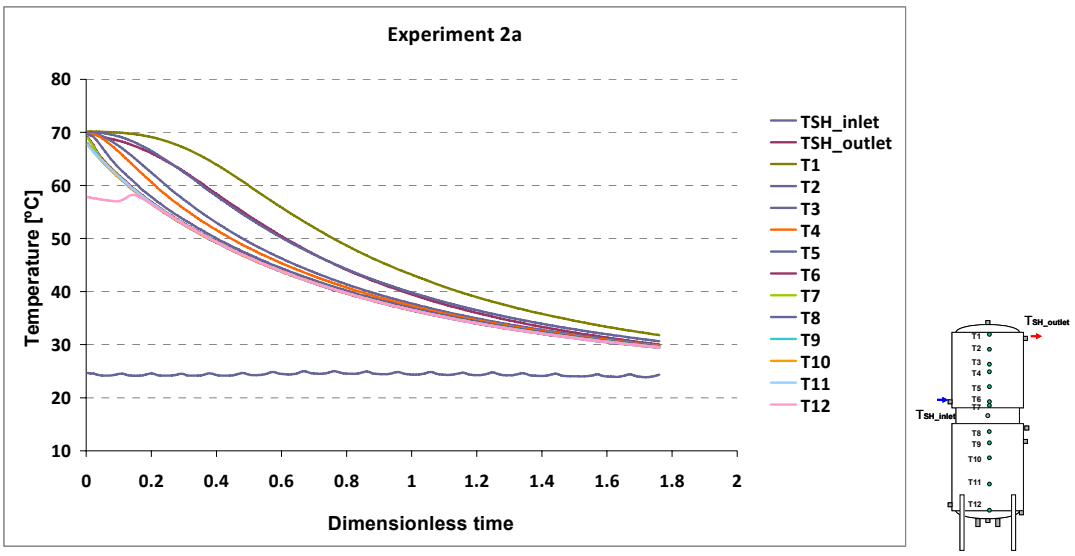

Fig. 2-7a. Measured temperatures with a volume flow rate of 1 l/min, experiment 2a.

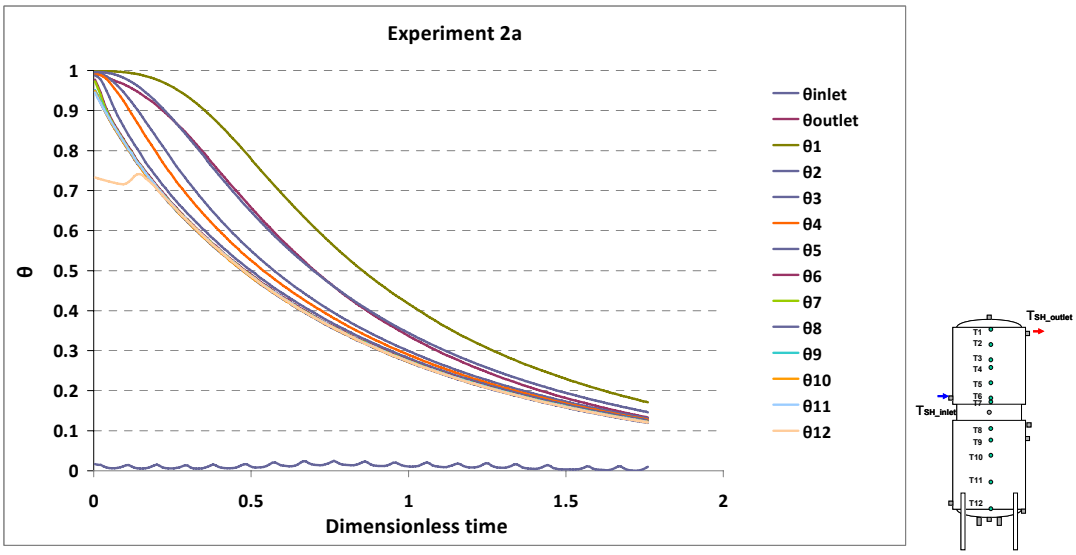

Fig. 2-7b. Dimensionless temperatures for experiment 2a with a volume flow rate of 1 l/min.

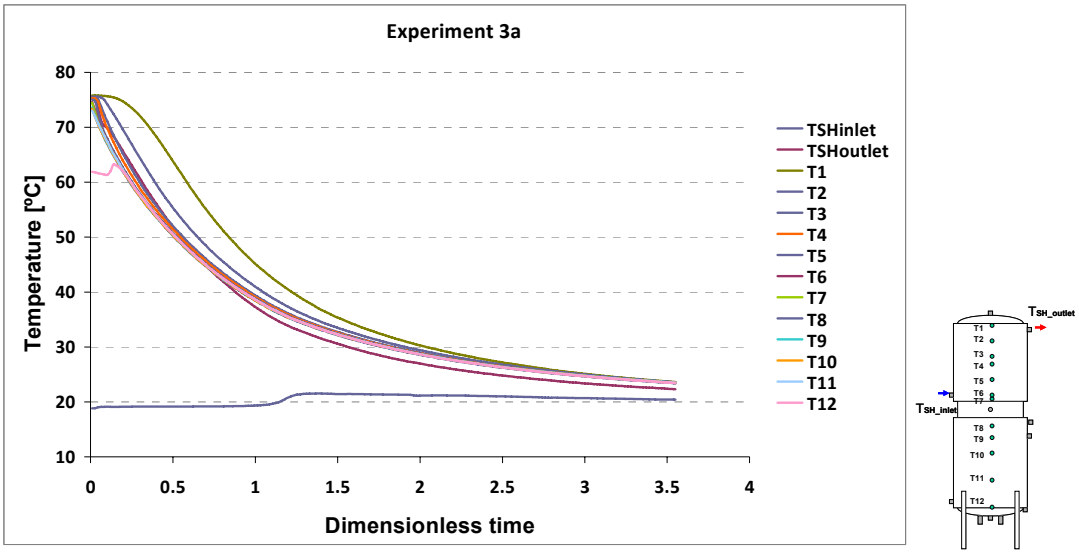

Fig. 2-8a. Measured temperatures with a volume flow rate of 2 l/min, experiment 3a.

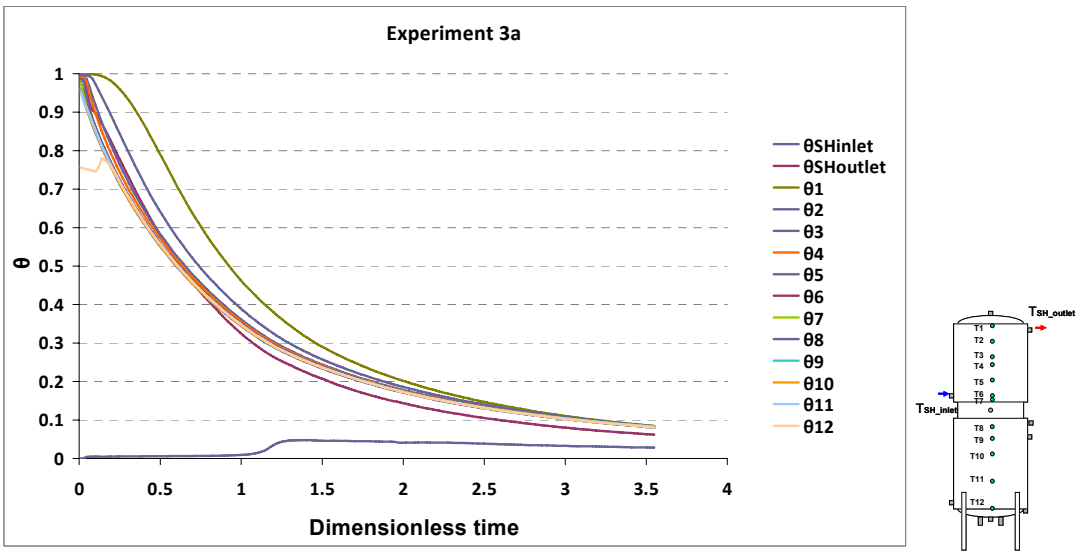

Fig. 2-8b. Dimensionless temperatures for experiment 3a with a volume flow rate of 2 l/min.

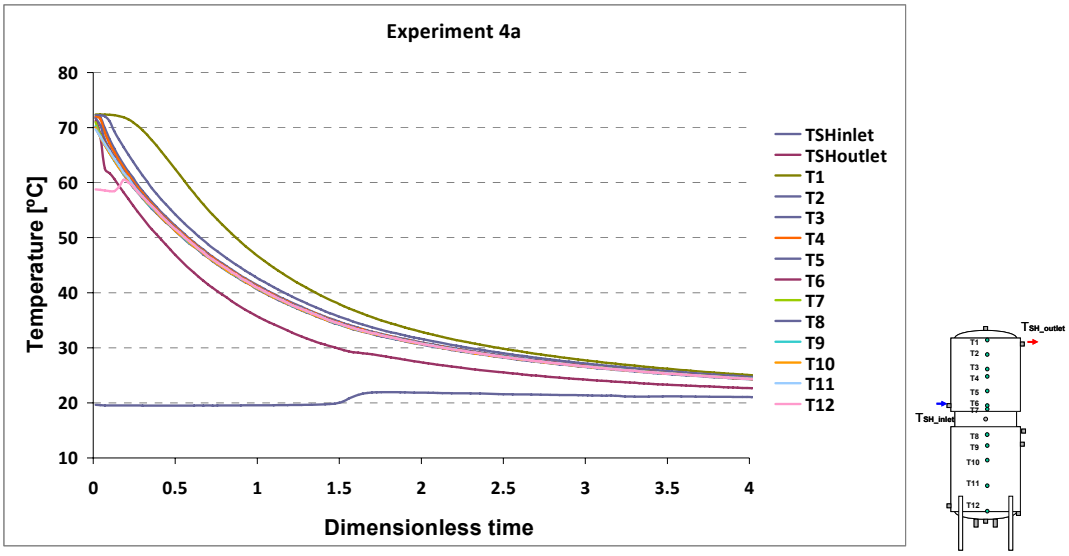

Fig. 2-9a. Measured temperatures with a volume flow rate of 3 l/min, experiment 4a.

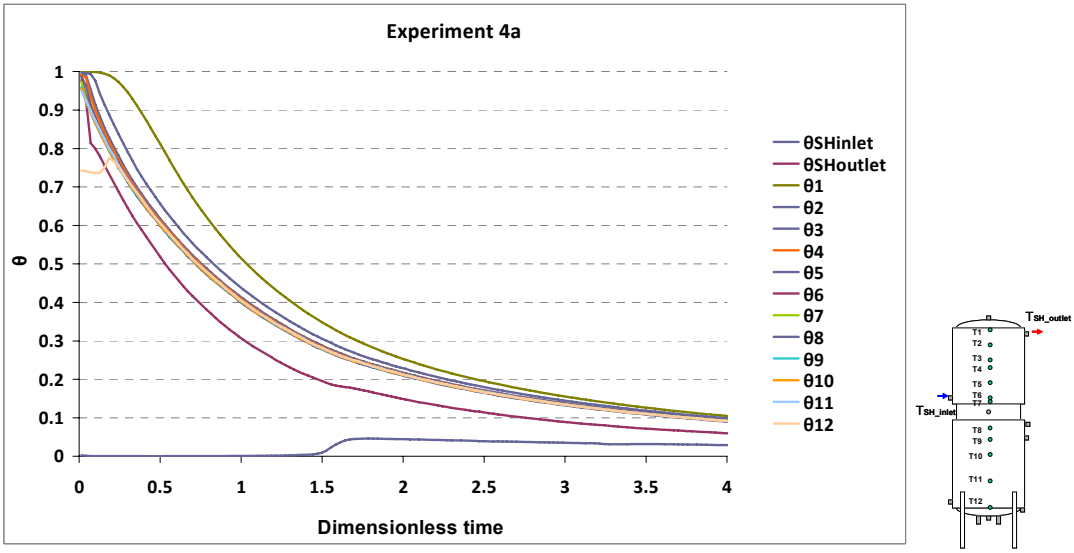

Fig. 2-9b. Dimensionless temperatures for experiment 4a with a volume flow rate of 3 l/min.

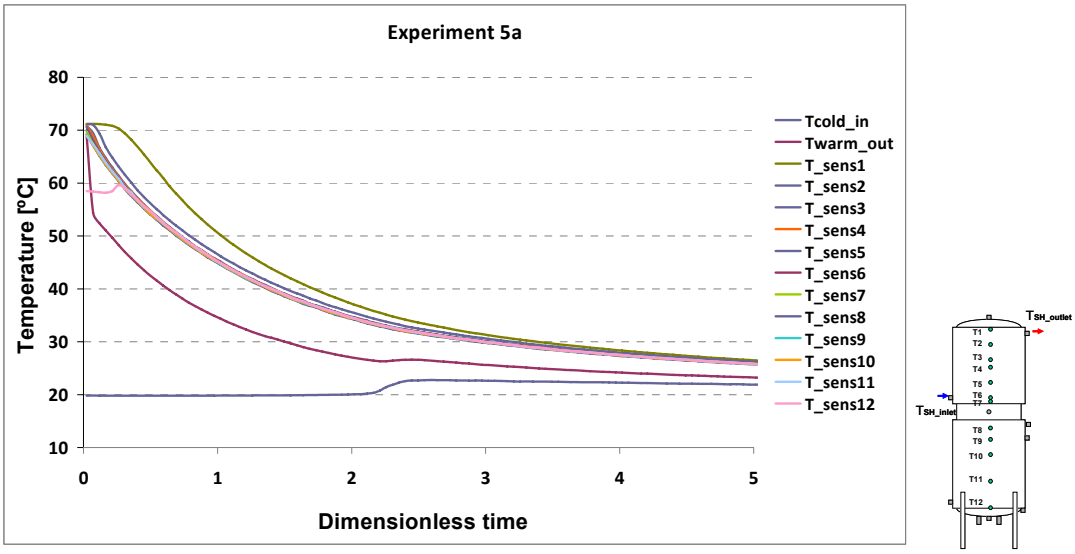

Fig. 2-10a. Measured temperatures with a volume flow rate of 5 l/min, experiment 5a.

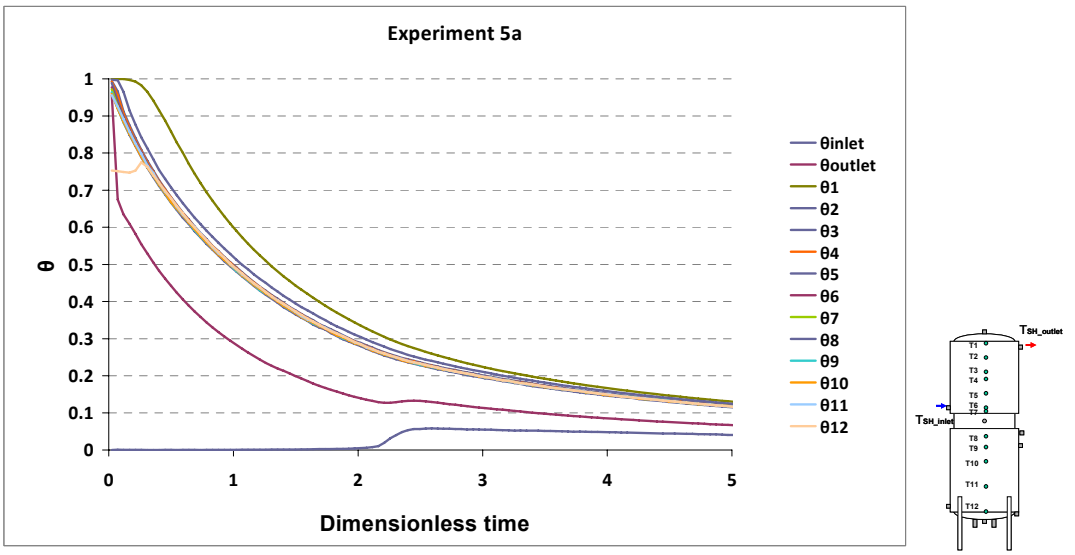

Fig. 2-10b. Dimensionless temperatures for experiment 5a with a volume flow rate of 5 l/min.

The heat transfers from each tank volume during the five experiments are shown in Fig. 2-11a till Fig. 2-15a. It is always desirable to discharge the tank from the bottom so that the cold water is positioned at the bottom and the hot water at the top. That is, it is an advantage if thermal stratification is built up in the tank and as a result, the thermal performance of the system will increase. The heat transfer coefficient of the upper mantle and the discharge power is shown in Fig. 2-11b till Fig. 2-15b. The test period can be divided to three main parts for analyzing the results, the first part is the time period when by discharge, heat is mainly taken from the lower part of the tank and from the upper mantle. The second part is a period where the heat discharge level changes from the lower part to the upper part of the tank and from the upper mantle volume. And the third part is where more heat is taken from the upper part than from the lower part of the tank.

In experiment 1a with a volume flow rate of 0.5 l/min, heat is in the first period of the test mostly discharged from Volume 7, then from Volume 6, followed by Volumes 8, 5, 9, 10, 4, 3, 2 and 1. In this way, thermal stratification is established in the tank. The

peak power is about 360 W from one tank volume. In the second part of the test, the discharge powers from volumes 9 and 10 decreases to the minimum value so that after 100 min, dimensionless time of 0.15, heat is supplied to volume 10. Therefore, mixing occurs somewhat at the bottom part of the tank and it disturbs somewhat the thermal stratification. Further, the power discharge from volumes 8, 7, 6 and 5 decreases all the time, and the power discharge from volumes 4, 3, 2 and 1 increases and then decreases. In the third period of the test, most heat is taken from volume 1, second most from volume 2, third most from volume 3 followed by volumes 4, 5, 6, 7, 8, 9 and 10. In Fig. 2-11b, the power discharge from the tank and the heat transfer coefficient of the upper mantle is shown. The power discharge is about 350-1500 W and the heat transfer coefficient is about 80-140 W/m²K.

In experiment 2a with a volume flow rate of 1 l/min, heat is in the first period of the test mostly discharged from volume 6, second most from volume 8, third most from volume 7 followed by volumes 5, 9, 4, 10, 3, 2 and 1. Therefore, like experiment 1a, heat in the start is mostly taken from the lower part of the tank which is desirable for creating thermal stratification. However, this situation exists only for short period of about 50 min, dimensionless time of 0.15. For the second period of the test, power discharge from volumes 9 and 10 decreases and energy is supplied to volume 10 as in experiment 1a. The power discharge from volumes 5, 6, 7 and 8 decreases and the power discharge from volumes 1, 2, 3 and 4 increases and decreases in the second period. In the third period of the test, most heat is taken from volume 1, second most from volume 2, third most from volume 3 followed by volumes 4, 5, 6, 7, 8, 9 and 10. The peak power is 650 W from one tank volume which is higher than in experiment 1a due to the fact that the volume flow rate is higher. The power discharge and heat transfer coefficient is also increased to 450-3000 W and 100-250 W/m²K.

In experiment 3a with a volume flow rate of 2 l/min, heat is in the first period of the test mostly discharged from volume 5, second most from 6, third most from volume 7 followed by volumes 4, 8, 9, 10, 3, 2 and 1. It can be seen that heat is taken from the tank at a somewhat higher level than in experiment 1a and 2a. For the second period of the test, power discharge from volumes 9 and 10 decreases and energy is supplied to volume 10 as in experiments 1a and 2a. The power discharge from volumes 5, 6, 7 and 8 decreases and the power discharge from volumes 1, 2 and 3 increases and decreases. In the third period of the test, most heat is taken from volume 1, second most from volume 2, third most from volume 3 followed by volumes 4, 5, 6, 7, 8, 9 and 10. The peak power is about 1350 W from one tank volume which is higher than in experiments 1a and 2a due to the higher volume rate. The power discharge is 500-8500 W and the heat transfer coefficient is 100-330 W/m²K.

In experiment 4a, the flow rate is 3 l/min. Heat is in the first period of the test mostly discharged volume 4, second most from volume 3, third most from volume 5 followed by volumes 6, 7, 8, 9, 2, 1 and 10. The period of desirable building up the stratification is short, about 30 minutes, dimensionless time of 0.15, for this experiment, shorter than for experiments 1a, 2a and 3a. For the second period of the test, power discharge from volumes 9 and 10 decreases and energy is supplied to volume 10 as for experiments 1a, 2a and 3a. The power discharge from volumes 5, 6, 7 and 8 decreases and the power discharge from volumes 1, 2 and 3 increases and decreases. In the third period of the test, most heat is taken from volume 1, second most from volume 2, third most from volume 3 followed by volumes 4, 5, 6, 7, 8, 9 and 10. The peak power is 1550 W from one tank volume. The discharge power is about 500-13000 W and the heat transfer coefficient is between 100-400 W/m²K.

In experiment 5a with volume flow rate of 5 l/min, heat is in the first period of the test mostly discharged from volume 3, second most from volume 4 followed by volumes 6, 7, 5, 2, 8, 9, 1 and 10. This first period of the experiment has the duration of about 25 min, dimensionless time of 0.13. For the second period of the test, power discharge from volumes 9 and 10 decreases and energy is supplied to volume 10 as in experiments 1a, 2a, 3a and 4a. The power discharge from volumes 5, 6, 7 and 8 decreases and the power discharge from volumes 1, 2 and 3 increases and decreases. In the third period of the test, most heat is taken from volume 1, second most from volume 2, third most from volume 3 followed by volumes 4, 5, 6, 7, 8, 9 and 10. The peak power is 2200 W from one tank volume. The discharge power is about 500-10000 W and the heat transfer coefficient is between 100-330 W/m²K.

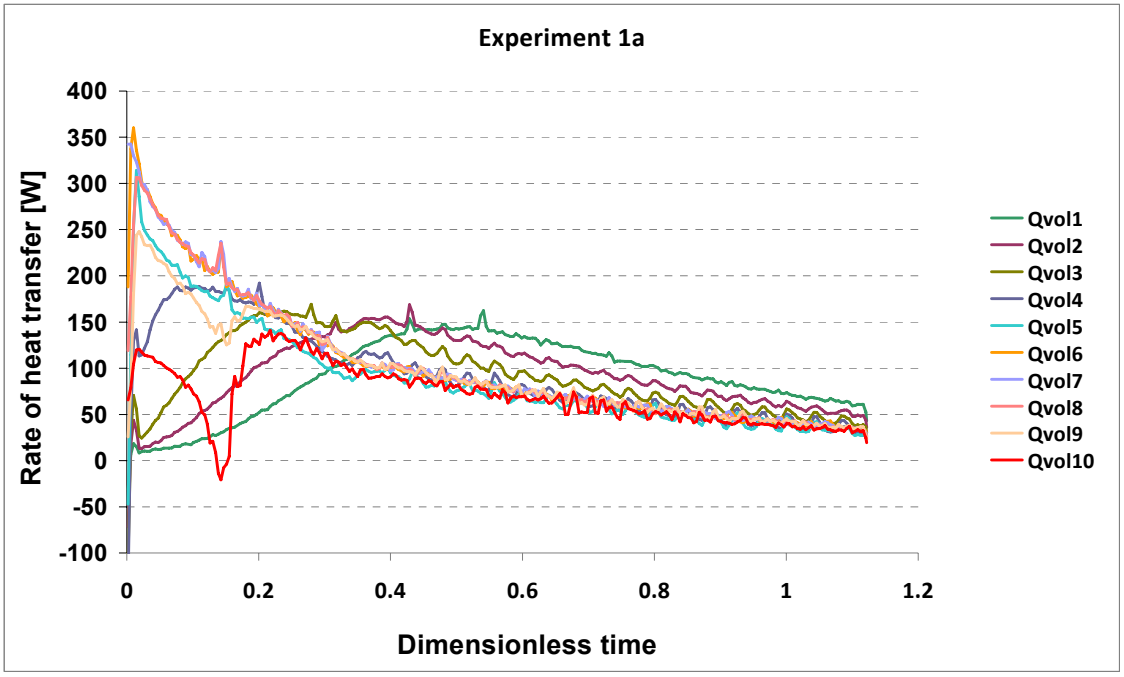

Fig. 2-11a. Heat transfer from each tank volume in Experiment 1a with a volume flow rate of 0.5 l/min.

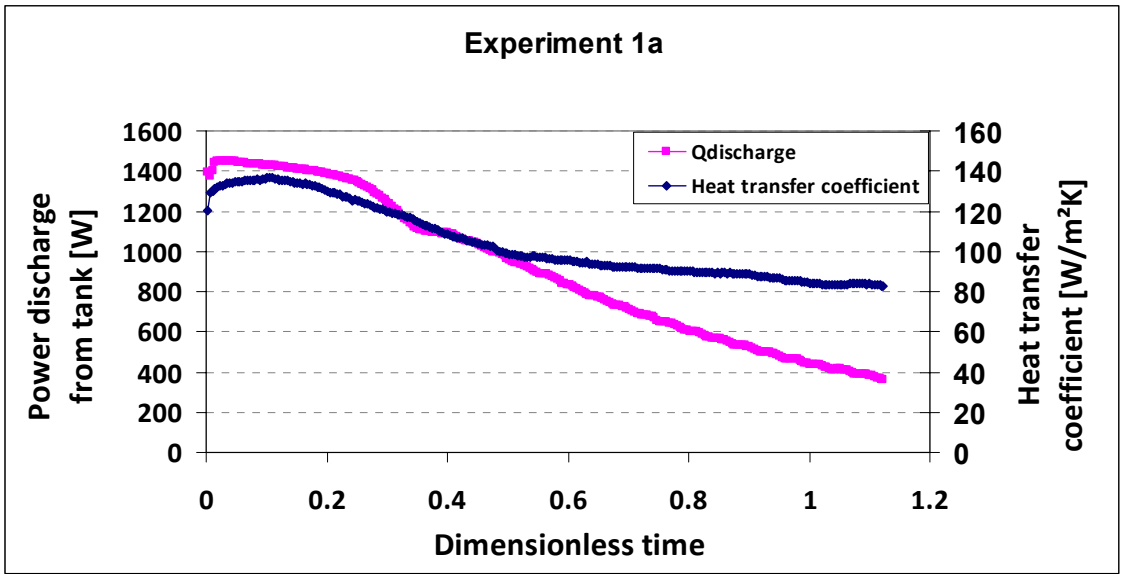

Fig. 2-11b. Power discharge from tank and the heat transfer coefficient for Experiment 1a with a volume flow rate of 0.5 l/min.

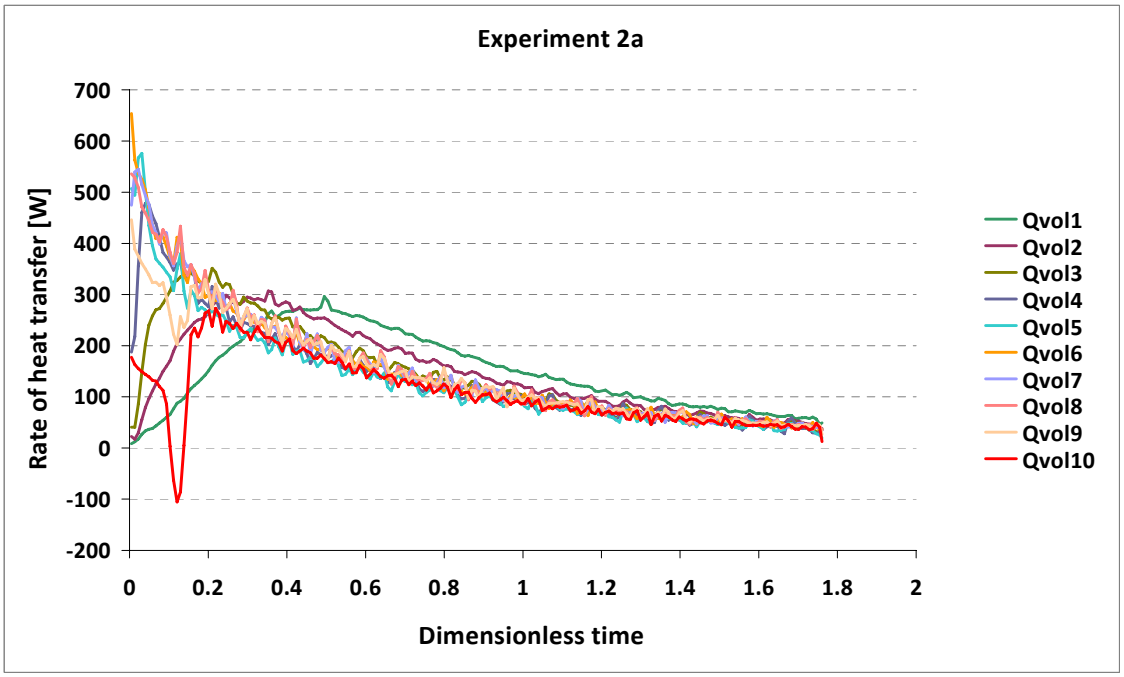

Fig. 2-12a. Heat transfer from each tank volume in Experiment 2a with a volume flow rate of 1 l/min.

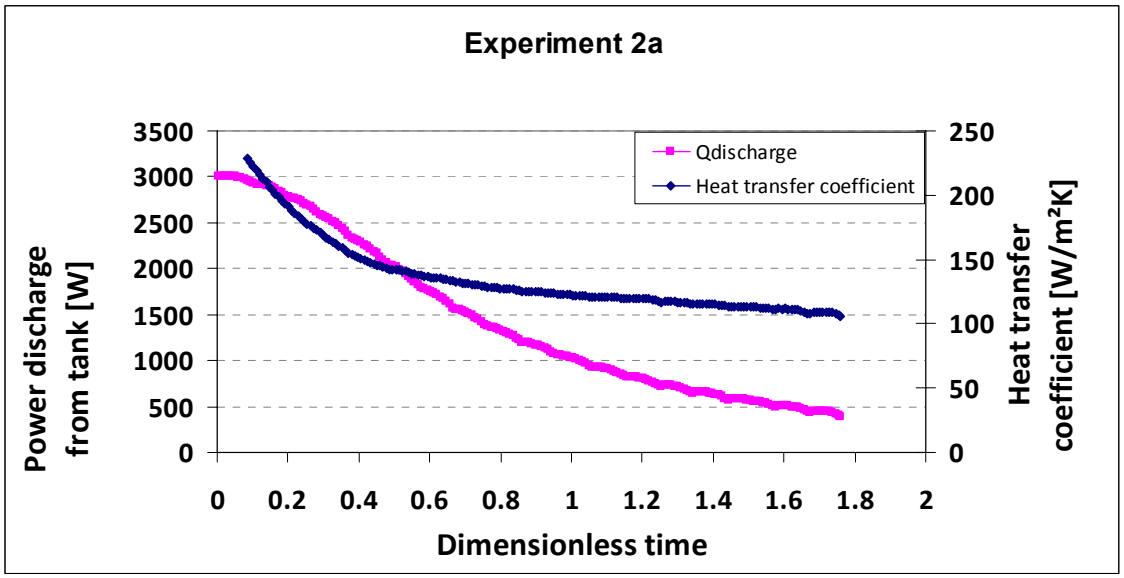

Fig. 2-12b. Power discharge from tank and the heat transfer coefficient for Experiment 2a with a volume flow rate of 1 l/min.

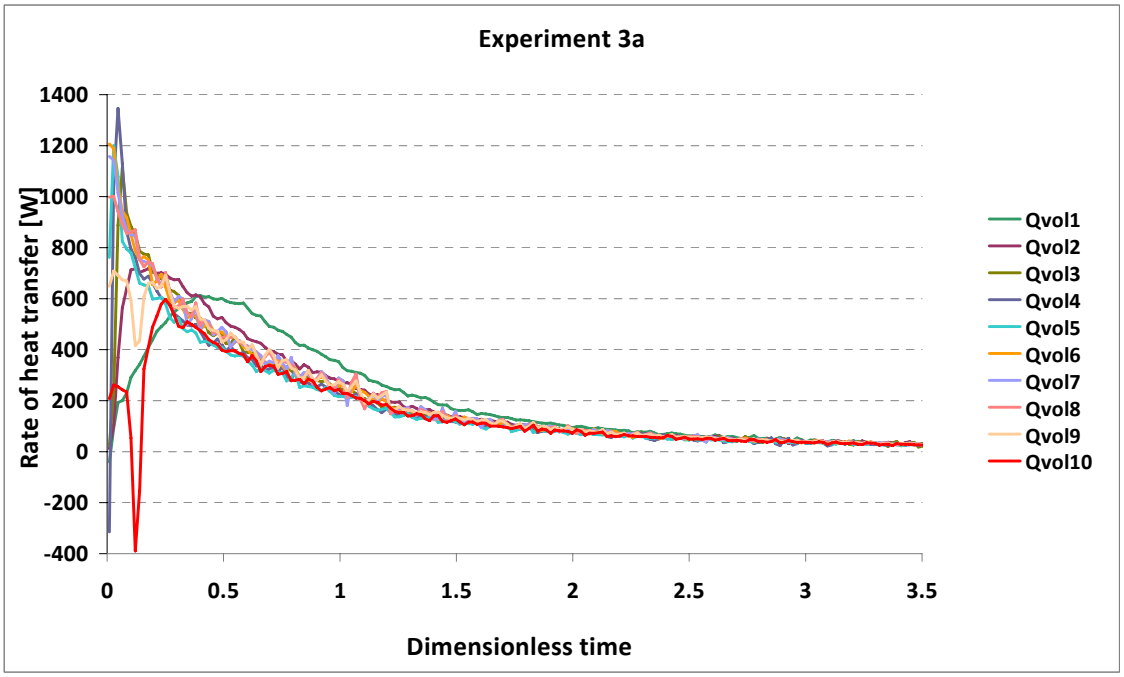

Fig. 2-13a. Heat transfer from each tank volume in Experiment 3a with a volume flow rate of 2 l/min.

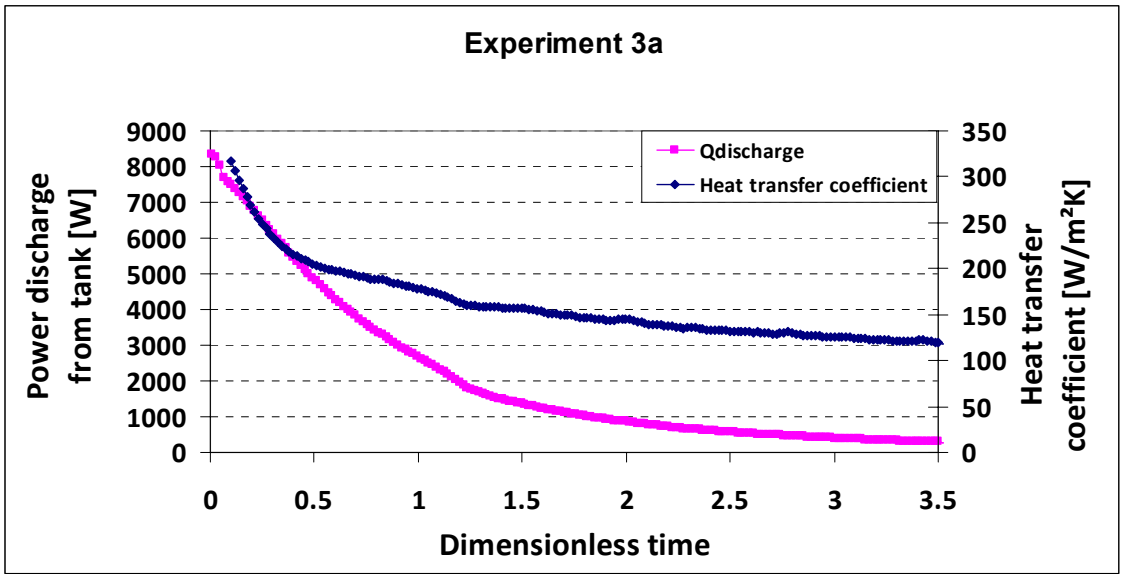

Fig. 2-13b. Power discharge from tank and the heat transfer coefficient for Experiment 3a with a volume flow rate of 2 l/min.

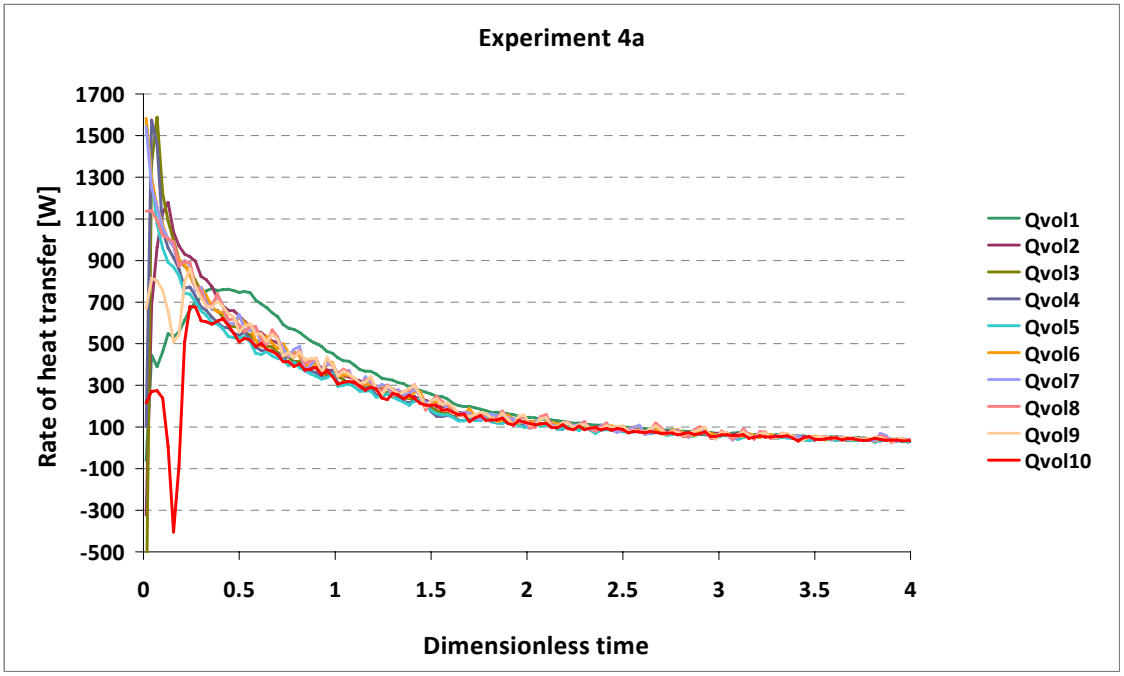

Fig. 2-14a. Heat transfer from each tank volume in Experiment 4a with a volume flow rate of 3 l/min.

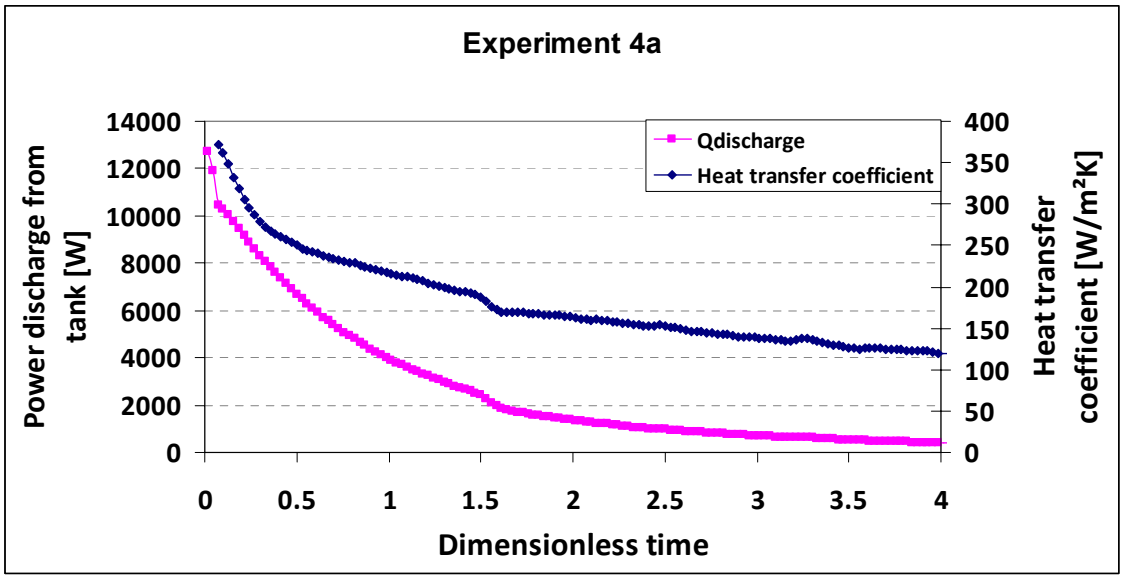

Fig. 2-14b. Power discharge from tank and the heat transfer coefficient for Experiment 4a with a volume flow rate of 3 l/min.

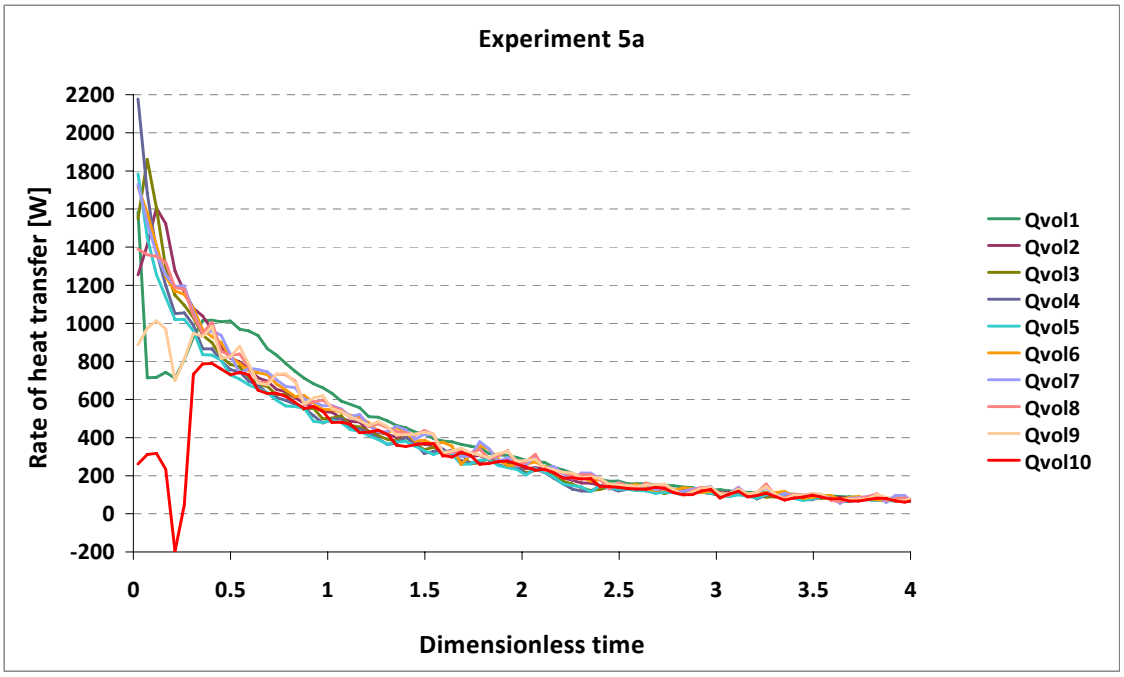

Fig. 2-15a. Heat transfer from each tank volume in Experiment 5a with a volume flow rate of 5 l/min.

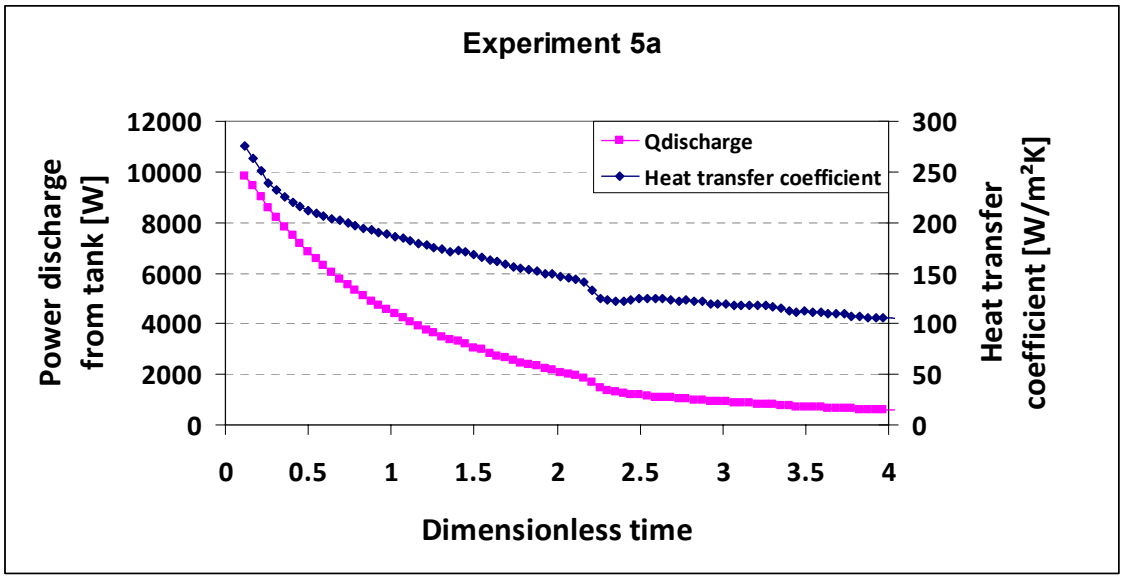

Fig. 2-15b. Power discharge from tank and the heat transfer coefficient for Experiment 5a with a volume flow rate of 5 l/min.

‘‘Experiment 1b-5b’’ [Initially mixed (45-60°C), Inlet temperature (20-22°C)]

The measured temperatures inside the tank, inlet and outlet temperatures for the upper mantle for experiments 1b, 2b, 3b, 4b and 5b for different mantle volume flow rates and initially mixed condition of the tank with around 50°C are shown in Fig. 2-16a, Fig. 2-16b, Fig. 2-17a, Fig. 2-17b, Fig. 2-18a, Fig. 2-18b, Fig. 2-19a, Fig. 2-19b, Fig. 2-20a and Fig. 2-20b. The mantle inlet temperature is between 20-22°C for all experiments.

In experiment 1b, with a volume flow rate of 0.5 l/min, the tank temperatures decrease. Thermal stratification is in the start of the discharge built up in the upper part of the tank surrounded by the upper mantle (T1-T7), while in the lower part a little thermal stratification is built up inside the tank. At the end of the experiment almost no stratification is seen inside the tank. It can also be seen that the outlet temperature from the upper mantle is very high between T1 and T2. The thermal stratification is similar to the thermal stratification in experiment 1a and the initially mixed temperature level does not have any significant influence on the thermal stratification.

In experiment 2b, the volume flow rate is 1 l/min. The thermal stratification in the tank is somewhat smaller than in experiment 1b. The outlet temperature from the upper mantle is close to T2. In experiment 3b with a volume flow rate of 2 l/min, the thermal stratification in the tank is much lower than in experiments 1b and 2b. The outlet temperature from the upper mantle is higher than T5 in the first 50 min of the test period, dimensionless time of 0.21. However, the outlet temperature behaves differently from experiment 3a where the outlet temperature is higher than T3 in the first 80 min of the test period, dimensionless time of 0.23. During the test, the outlet temperature decreases below the tank bottom temperature. In experiment 4b with a volume flow rate of 3 l/min, thermal stratification is lower than for the lower flow rates and the outlet temperature from the upper mantle is now lower than the lowest tank temperature, similar to the behavior of experiment 4a. The same result is

obtained for experiment 5b with a volume flow rate of 5 l/min. The reason for the low outlet temperature from the upper mantle for the high volume flow rates is the short time it takes the water to pass through the upper mantle. In all experiments 1b-5b, thermal stratification is similar to experiments 1a-5a even though some differences are seen in the outlet temperature in some tests.

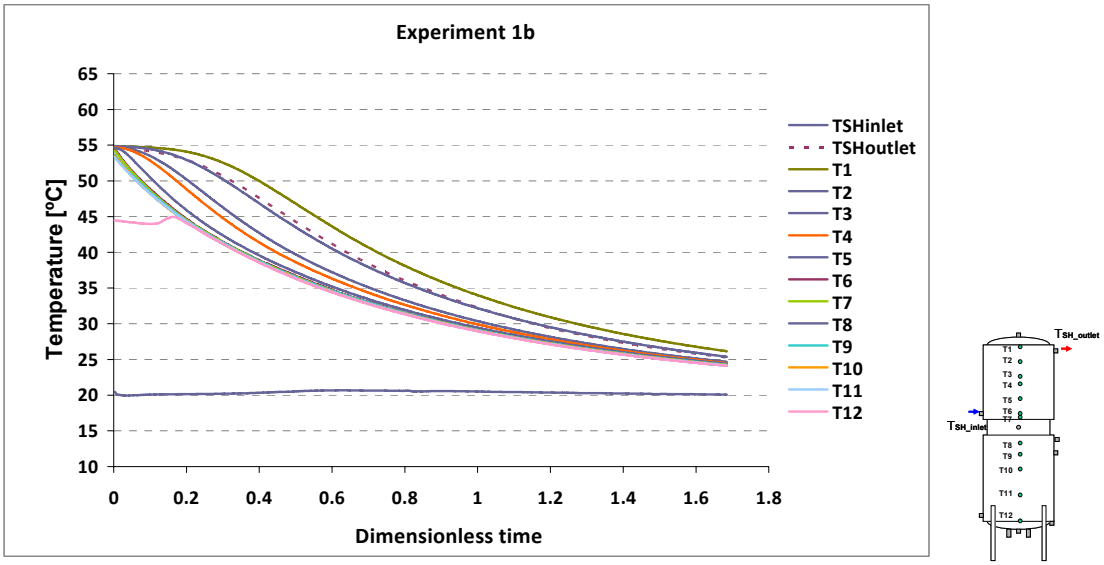

Fig. 2-16a. Measured temperatures with a volume flow rate of 0.5 l/min, experiment 1b.

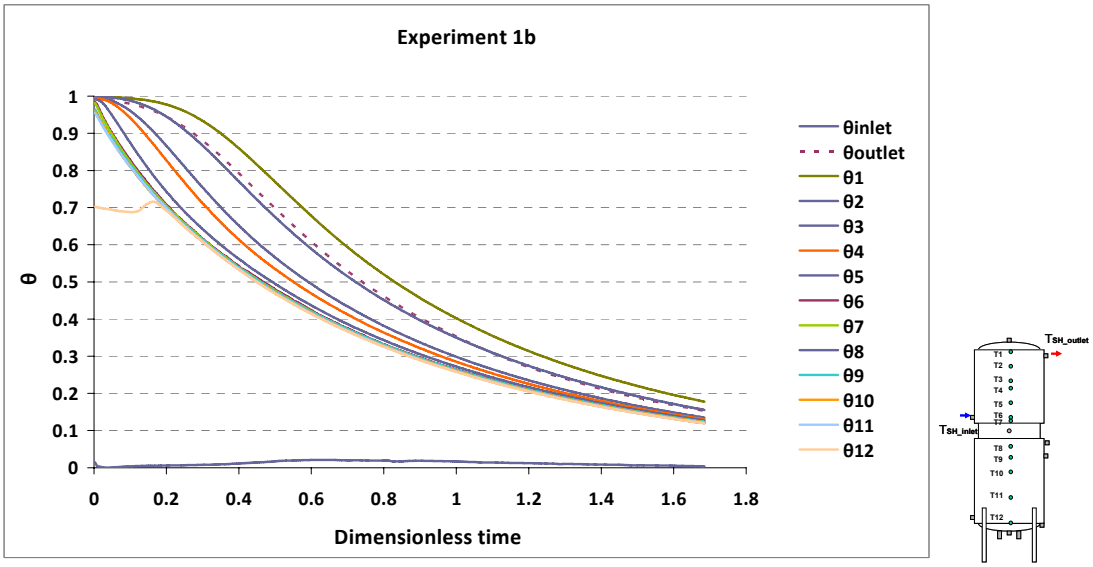

Fig. 2-16b. Dimensionless temperatures for experiment 1b with a volume flow rate of 0.5 l/min.

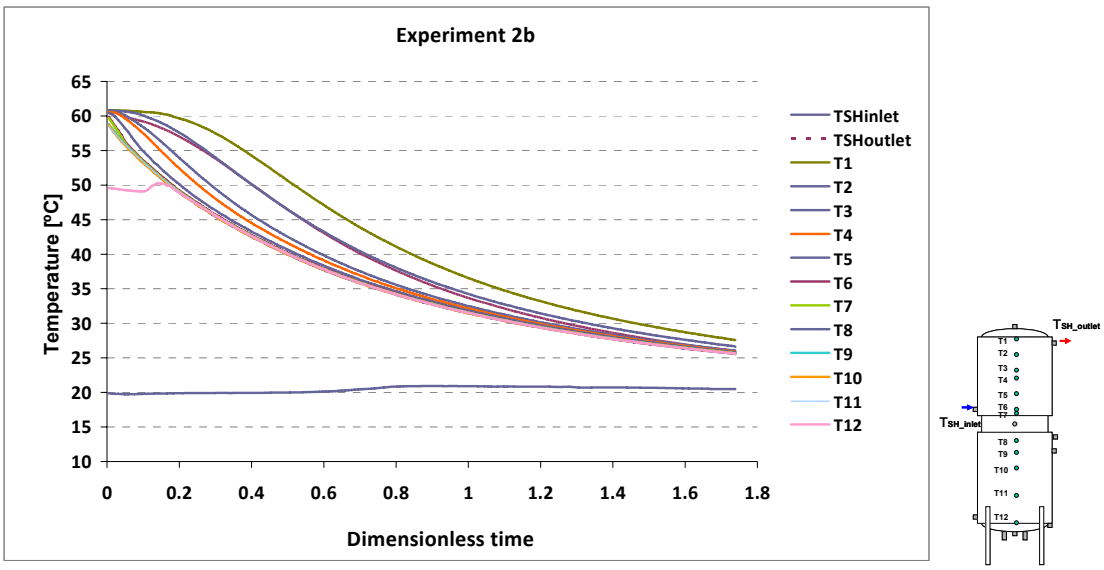

Fig. 2-17a. Measured temperatures with a volume flow rate of 1 l/min, experiment 2b.

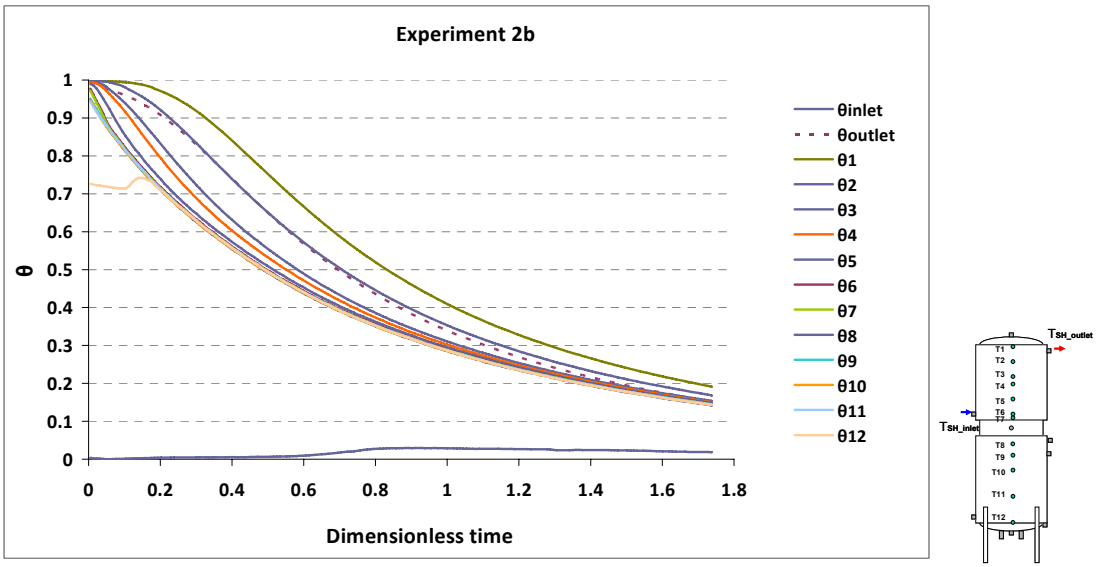

Fig. 2-17b. Dimensionless temperatures for experiment 2b with a volume flow rate of 1 l/min.

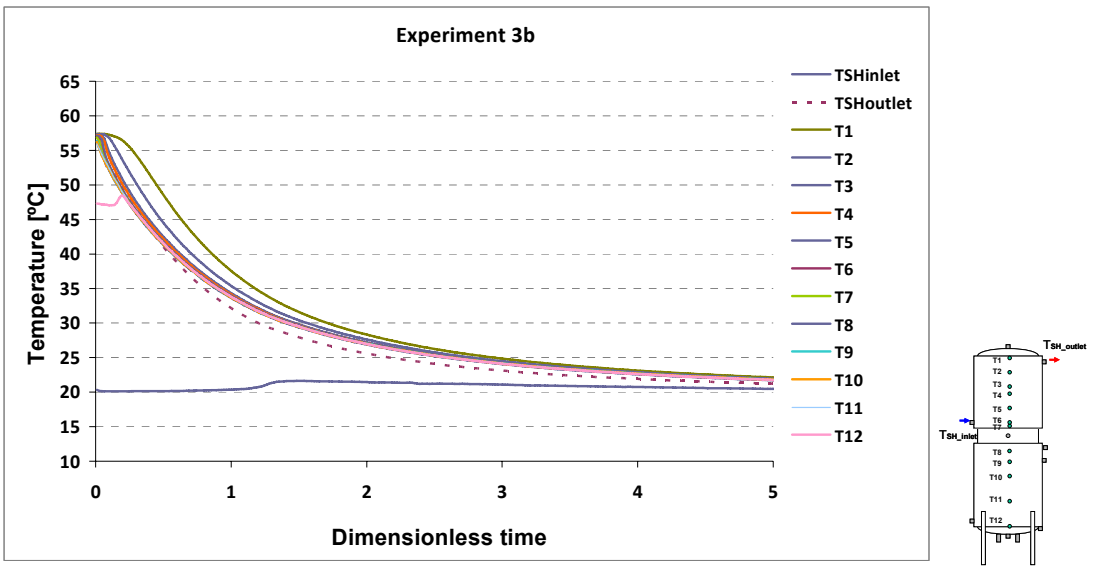

Fig. 2-18a. Measured temperatures with a volume flow rate of 2 l/min, experiment 3b.

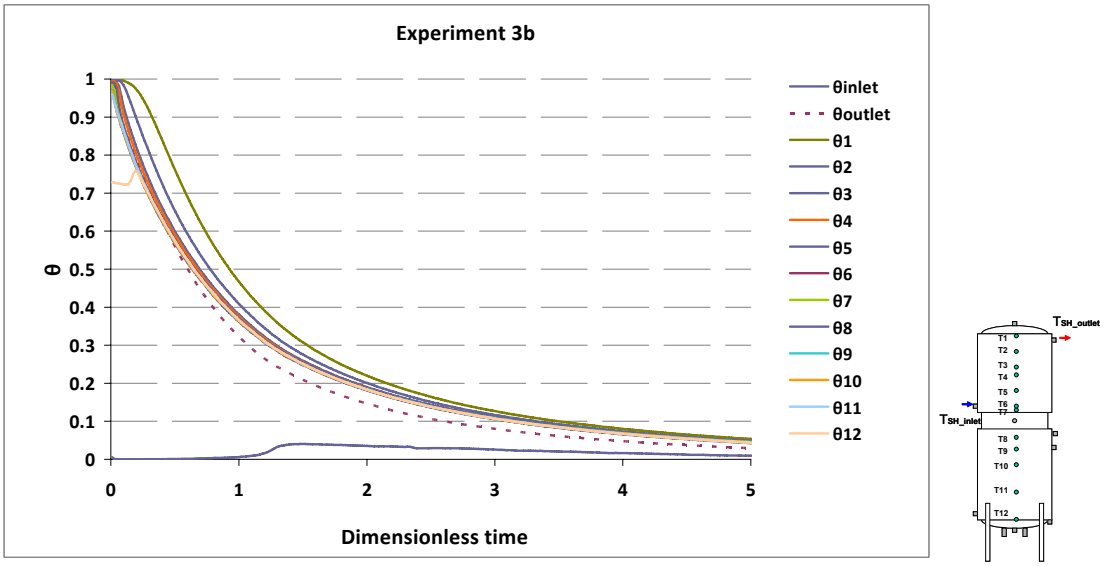

Fig. 2-18b. Dimensionless temperatures for experiment 3b with a volume flow rate of 2 l/min.

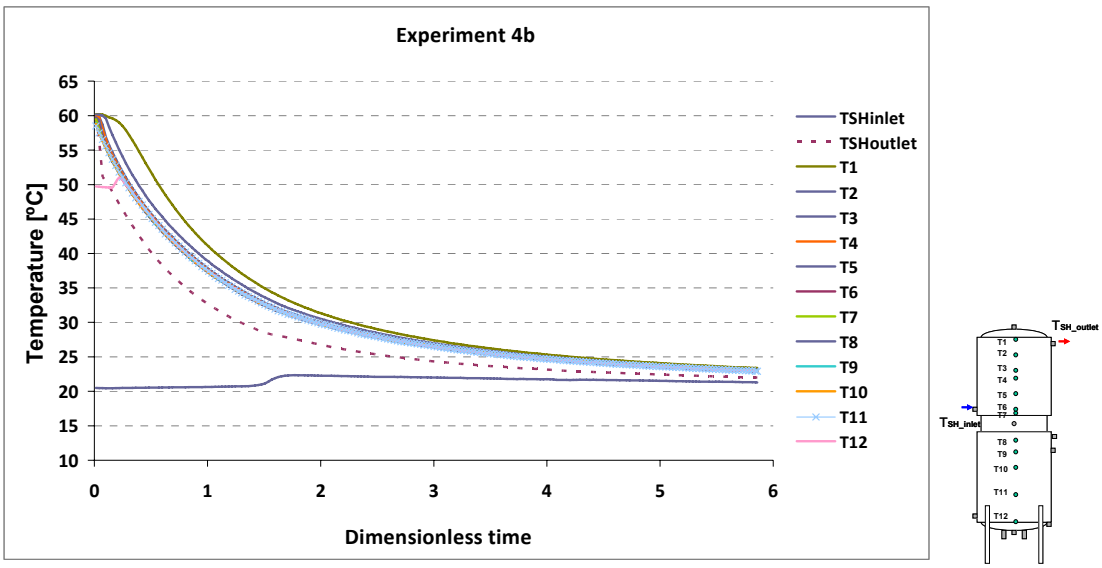

Fig. 2-19a. Measured temperatures with a volume flow rate of 3 l/min, experiment 4b.

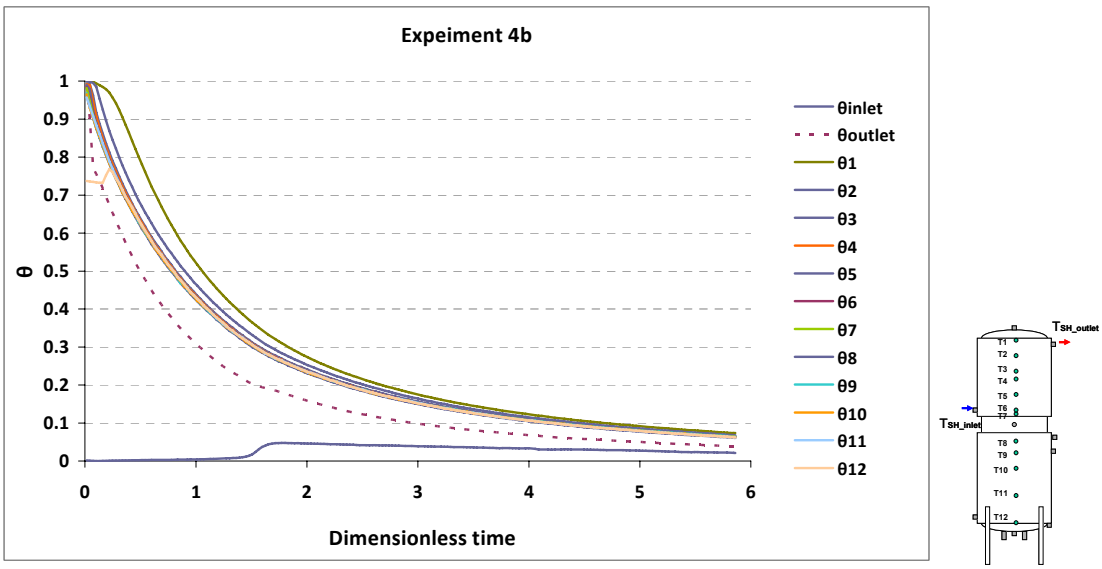

Fig. 2-19b. Dimensionless temperatures for experiment 4b with a volume flow rate of 3 l/min.

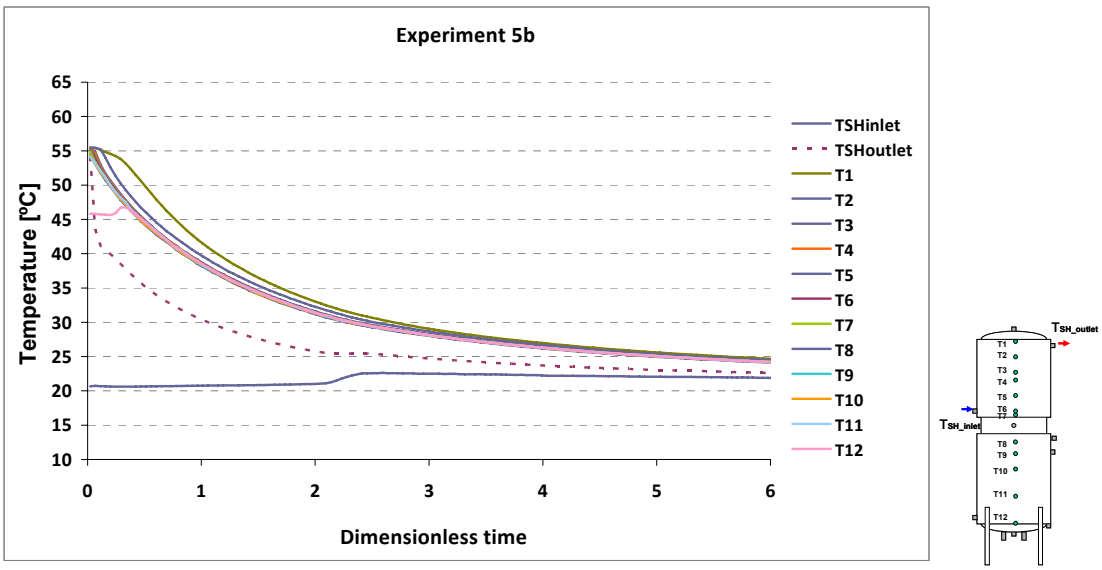

Fig. 2-20a. Measured temperatures with a volume flow rate of 5 l/min, experiment 5b.

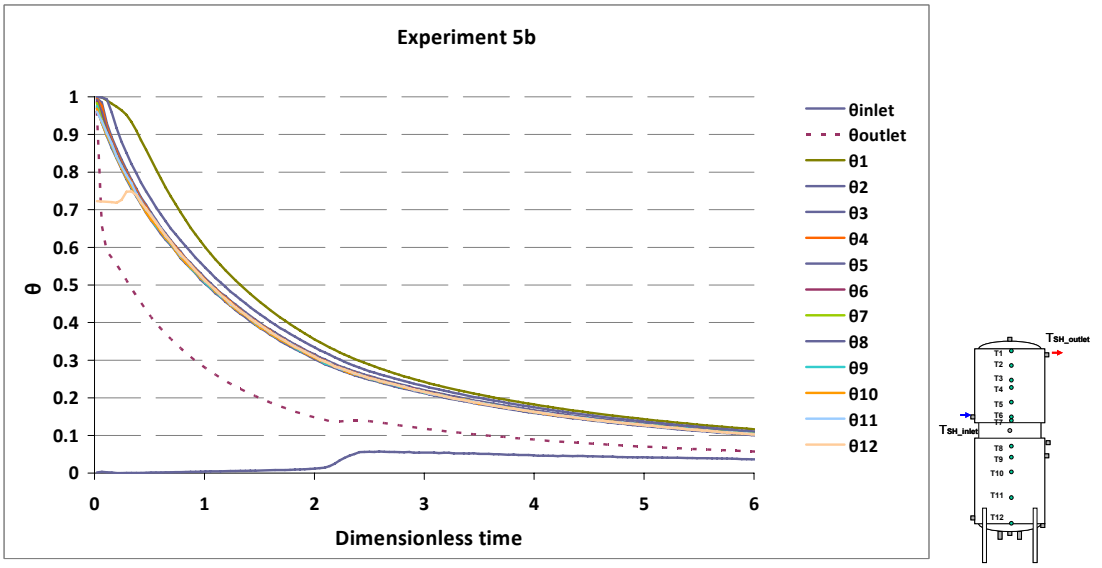

Fig. 2-20b. Dimensionless temperatures for experiment 5b with a volume flow rate of 5 l/min.

The heat transfer coefficient of the upper mantle and the discharge power are shown for the five different discharge tests in Fig. 2-21b till Fig. 2-25b. The test period can be divided to three main parts for analyzing the results, the first part is the time period when by discharge, heat is mainly taken from the lower part of the tank and in the very start of the test from the hot water in the upper mantle. The second part is a period where the heat discharge level changes from the lower part to the upper part of the tank. And the third part is where more heat is taken from the upper part than from the lower part of the tank.

In experiment 1b with a volume flow rate of 0.5 l/min, heat is in the first period of the test mostly discharged from Volume 6, then from Volume 7, followed by Volumes 8, 5, 9, 4, 10, 3, 2 and 1 which is desirable for creating thermal stratification. The peak power is about 350 W from one tank volume. In the second part of the test, the discharge powers from volumes 9 and 10 decreases to a minimum value so that after

80 min, dimensionless time of 0.17, heat is supplied to volume 10. Therefore, mixing occurs somewhat at the bottom part of the tank and it disturbs somewhat the thermal stratification. Further, the power discharge from volumes 8, 7, 6 and 5 decreases all the time, and the power discharge from volumes 4, 3, 2 and 1 increases and then decreases. In the third period of the test, most heat is taken from volume 1, second most from volume 2, third most from volume 3 followed by volumes 4, 5, 6, 7, 8, 9 and 10. In Fig. 2-21b, the power discharge from the tank and the heat transfer coefficient of the upper mantle is shown. The power discharge is about 200-1600 W and the heat transfer coefficient is about 80-180 W/m²K.

In experiment 2b with a volume flow rate of 1 l/min, heat is in the first period of the test mostly discharged from volume 6, second most from volume 7, third most from volume 8 followed by volumes 5, 9, 4, 10, 3, 2 and 1. Therefore, like in experiment 1b, heat in the start is mostly taken from the lower part of the tank which is desirable for creating thermal stratification. However, this situation exists only for a short period of about 50 min, dimensionless time of 0.16. For the second period of the test, power discharge from volumes 9 and 10 decreases and energy is supplied to volume 10 as experiment 1b. The power discharge from volumes 5, 6, 7 and 8 decreases and the power discharge from volumes 1, 2 and 3 increases and then decreases in the second period. In the third period of the test, most heat is taken from volume 1, second most from volume 2, third most from volume 3 followed by volumes 4, 5, 6, 7, 8, 9 and 10. The peak power is 550 W from one tank volume which is higher than in experiment 1b due to the fact that the volume flow rate is higher. The power discharge and heat transfer coefficient is also increased to 400-2700 W and 100-250 W/m²K.

In experiment 3b with a volume flow rate of 2 l/min, heat is in the first period of the test mostly discharged from volume 7, second most from 6, third most from volume 5 followed by volumes 8, 9, 4, 10, 3, 2 and 1. It can be seen that heat is taken from the tank at a somewhat higher level than in experiment 1b and 2b. For the second period of the test, power discharge from volumes 9 and 10 decreases and energy is supplied to volume 10 as in experiments 1b and 2b. The power discharge from volumes 5, 6, 7 and 8 decreases and the power discharge from volumes 1, 2 and 3 increases and decreases. In the third period of the test, most heat is taken from volume 1, second most from volume 2, third most from volume 3 followed by volumes 4, 5, 6, 7, 8, 9 and 10. The peak power is about 650 W from one tank volume which is higher than experiments 1b and 2b due to the higher volume flow rate. The power discharge is 200-5500 W and the heat transfer coefficient is 80-270 W/m²K.

In experiment 4b, the flow rate is 3 l/min. Heat is in the first period of the test mostly discharged from volume 4, second most from volume 6, third most from volume 5 followed by volumes 7, 3, 8, 9, 2, 1 and 10. The period of desirable building up the stratification is short, about 30 minutes, dimensionless time of 0.10 for this experiment, shorter than for experiments 1b, 2b and 3b. For the second period of the test, power discharge from volumes 9 and 10 decreases and energy is supplied to volume 10 as in experiments 1b, 2b and 3b. The power discharge from volumes 5, 6, 7 and 8 decreases and the power discharge from volumes 1, 2 and 3 increases and then decreases. In the third period of the test, most heat is taken from volume 1, second most from volume 2, third most from volume 3 followed by volumes 4, 5, 6, 7, 8, 9 and 10. The peak power is 1200 W from one tank volume. The discharge power is about 500-10000 W and the heat transfer coefficient is between 100-350 W/m²K.

In experiment 5b with a volume flow rate of 5 l/min, heat is in the first period of the test with a duration of 25 min, dimensionless time of 0.10 mostly discharged from volume 4, second most from volume 5 followed by volumes 6, 7, 3, 8, 9, 2, 10 and 1. For the second period of the test, power discharge from volumes 9 and 10 decreases and energy is supplied to volume 10 as in experiments 1b, 2b, 3b and 4b. The power discharge from volumes 5, 6, 7 and 8 decreases and the power discharge from volumes 1, 2 and 3 increases and decreases. In the third period of the test, most heat is taken from volume 1, second most from volume 2, third most from volume 3 followed by volumes 4, 5, 6, 7, 8, 9 and 10. The peak power is 1300 W from one tank volume. The discharge power is about 1100-6200 W and the heat transfer coefficient is between 150-250 W/m²K.

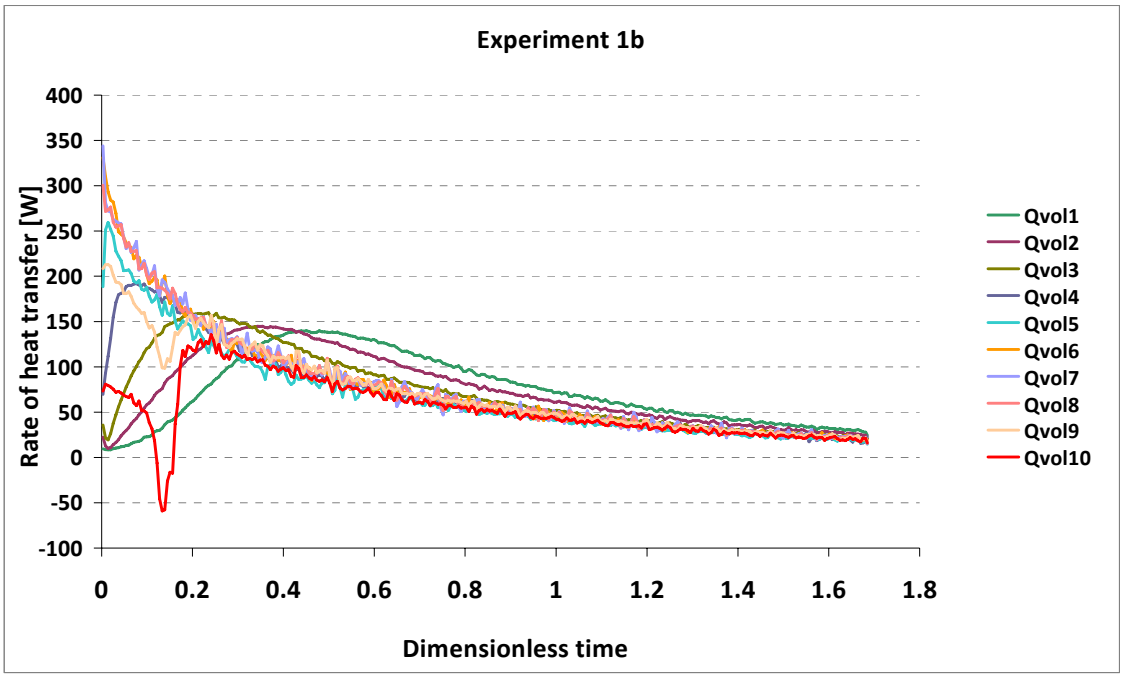

Fig. 2-21a. Heat transfer from each tank volume in Experiment 1b with a volume flow rate of 0.5 l/min.

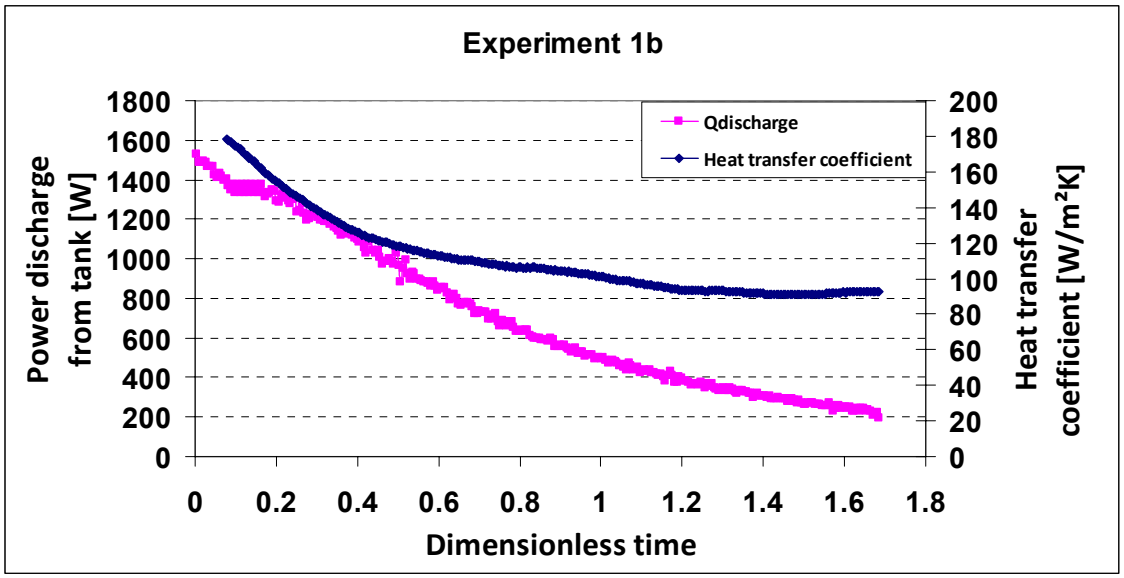

Fig. 2-21b. Power discharge from tank and the heat transfer coefficient for Experiment 1b with a volume flow rate of 0.5 l/min.

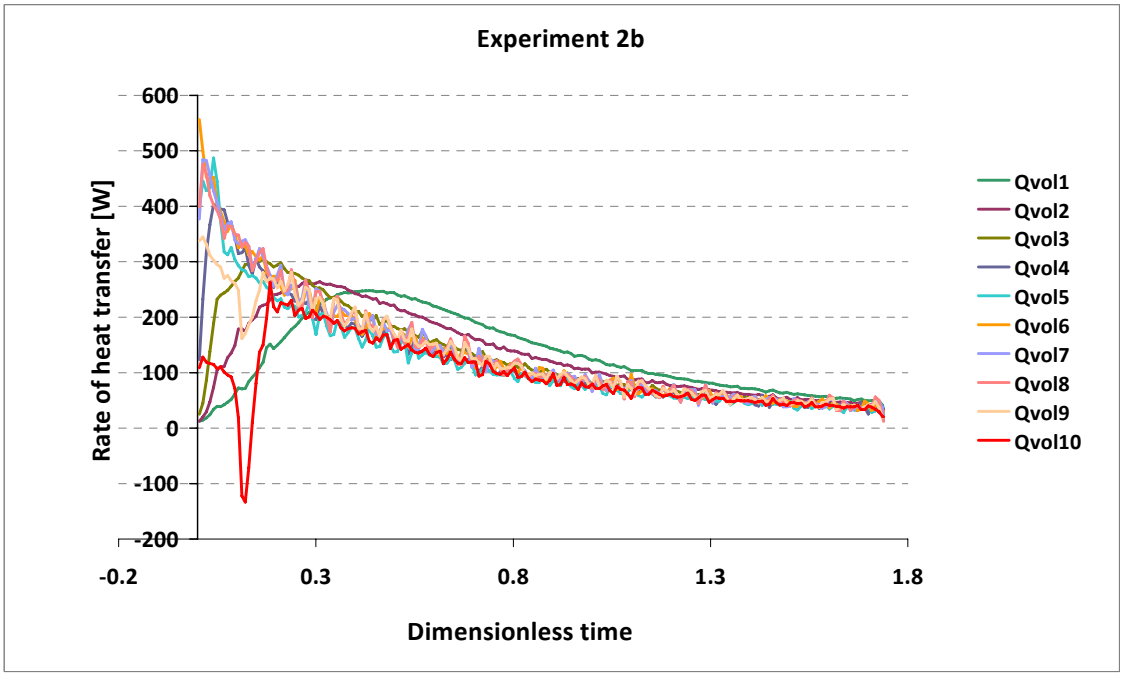

Fig. 2-22a. Heat transfer from each tank volume in Experiment 2b with a volume flow rate of 1 l/min.

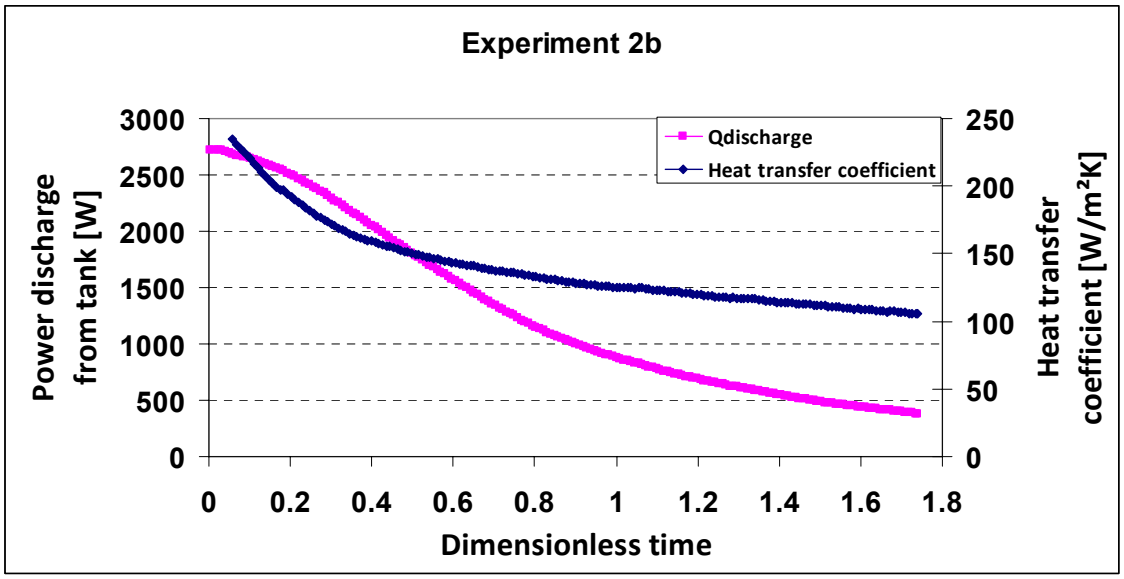

Fig. 2-22b. Power discharge from tank and the heat transfer coefficient for Experiment 2b with a volume flow rate of 1 l/min.

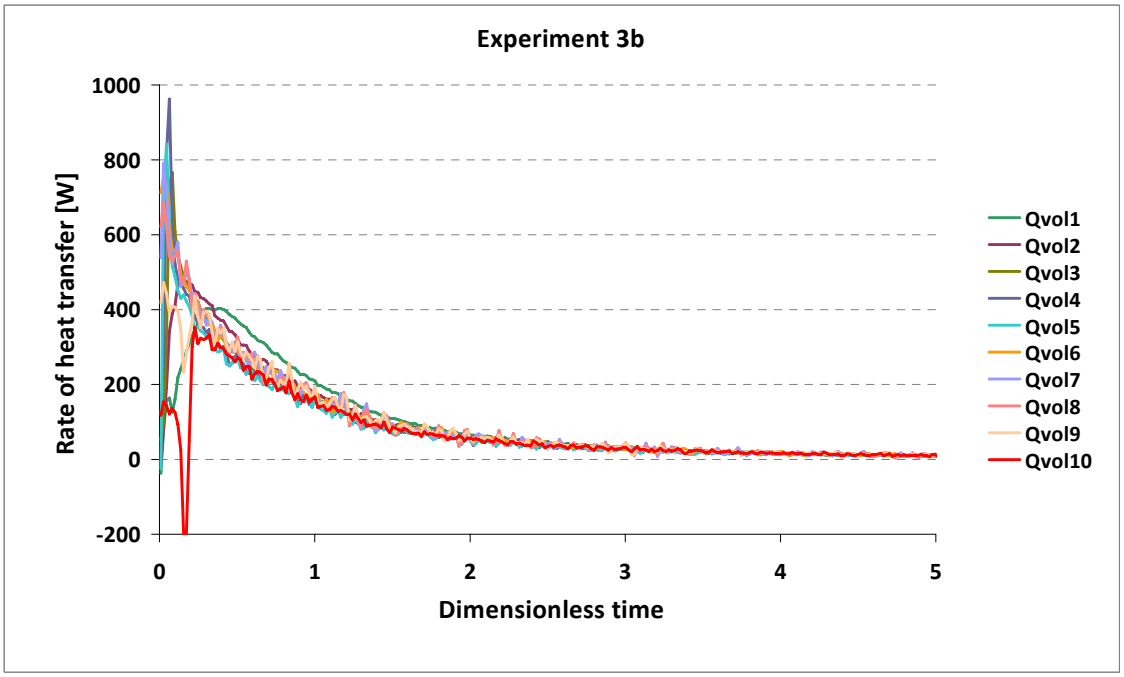

Fig. 2-23a. Heat transfer from each tank volume in Experiment 3b with a volume flow rate of 2 l/min.

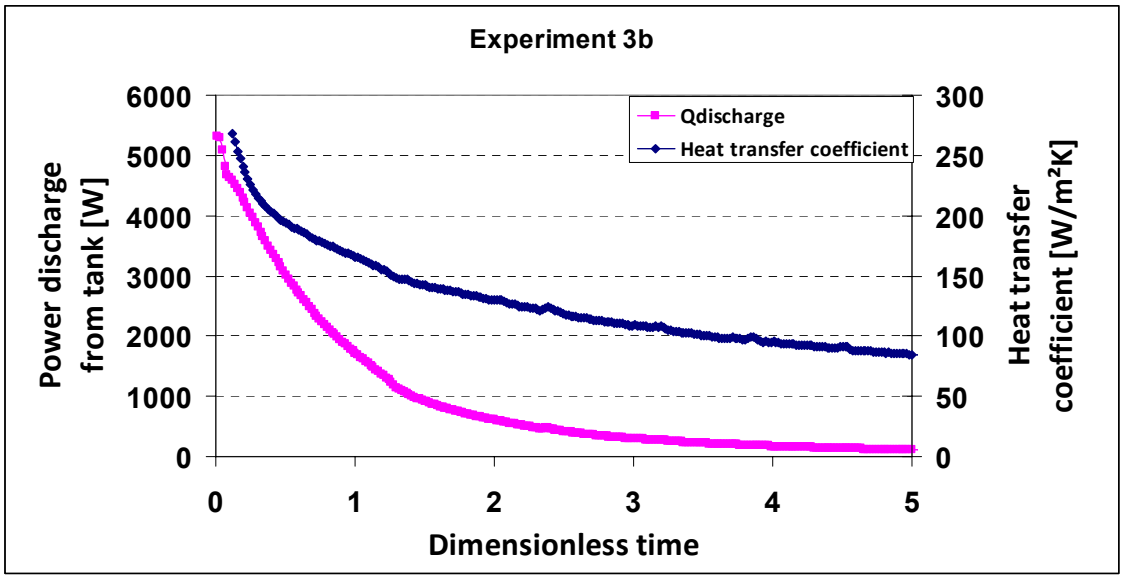

Fig. 2-23b. Power discharge from tank and the heat transfer coefficient for Experiment 3b with a volume flow rate of 2 l/min.

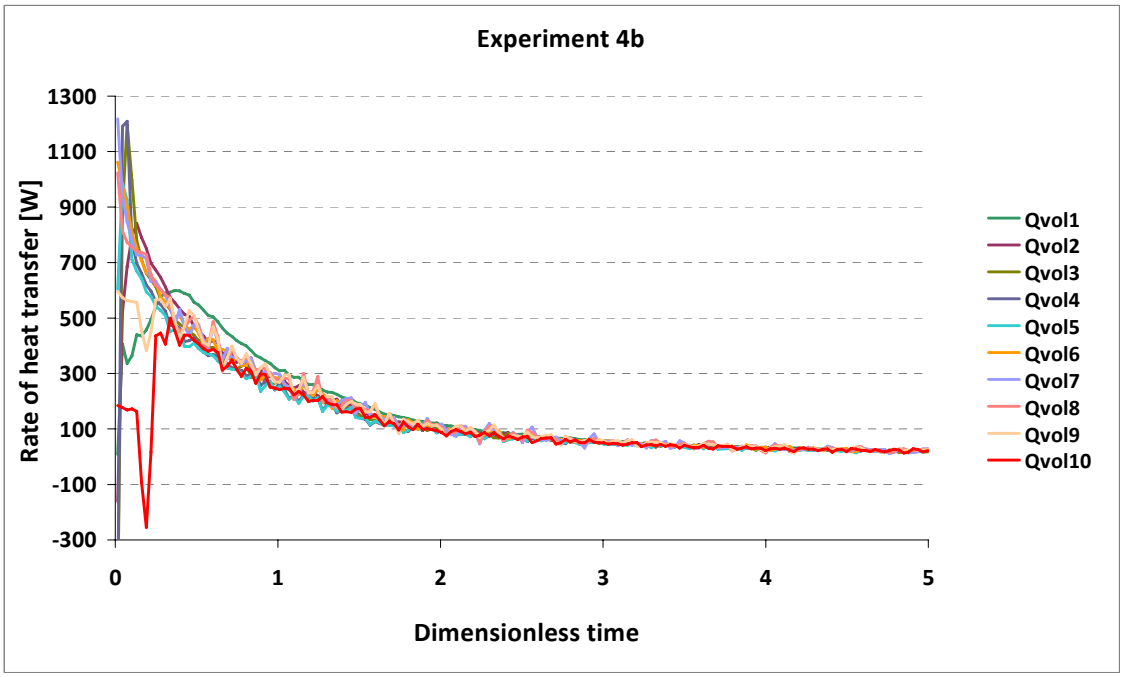

Fig. 2-24a. Heat transfer from each tank volume in Experiment 4b with a volume flow rate of 3 l/min.

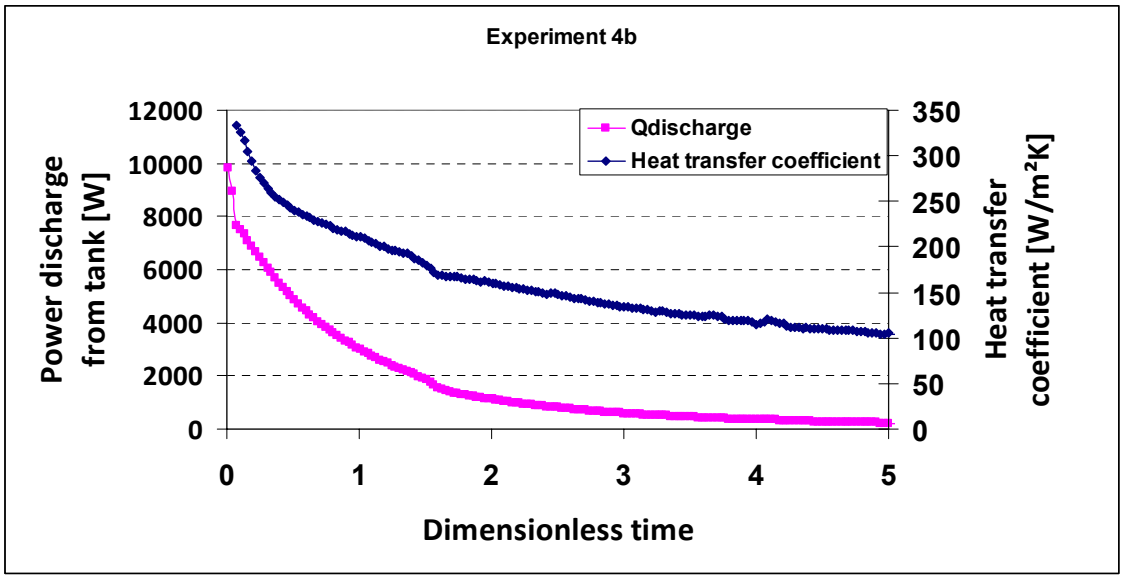

Fig. 2-24b. Power discharge from tank and the heat transfer coefficient for Experiment 4b with a volume flow rate of 3 l/min.

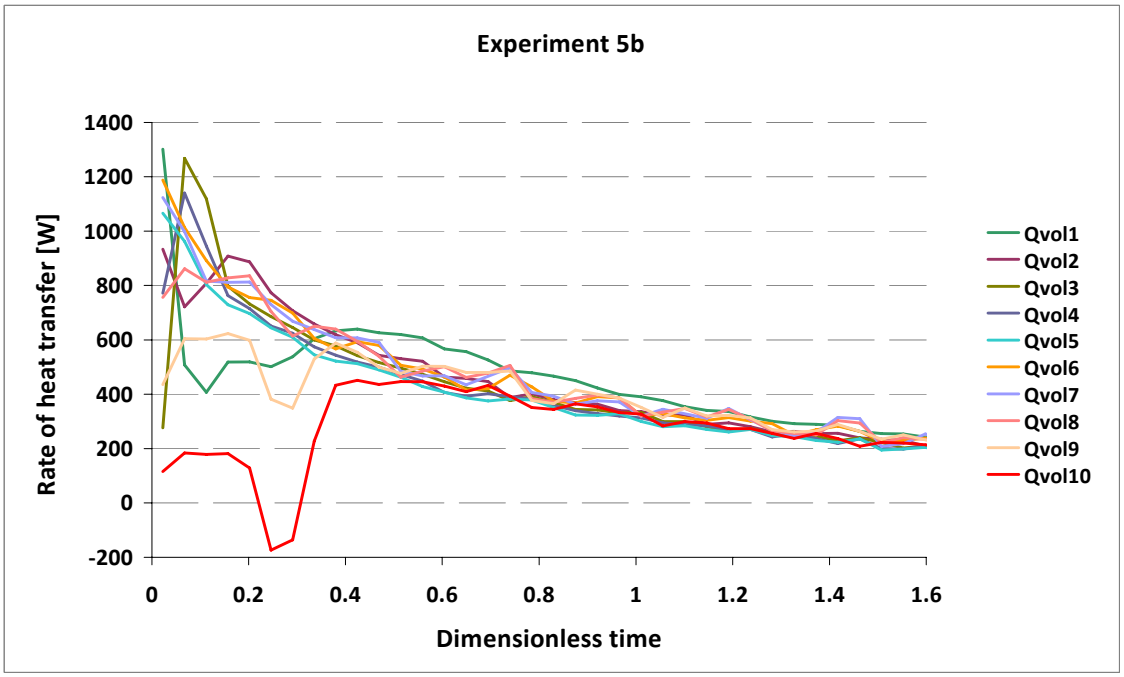

Fig. 2-25a. Heat transfer from each tank volume in Experiment 5b with a volume flow rate of 5 l/min.

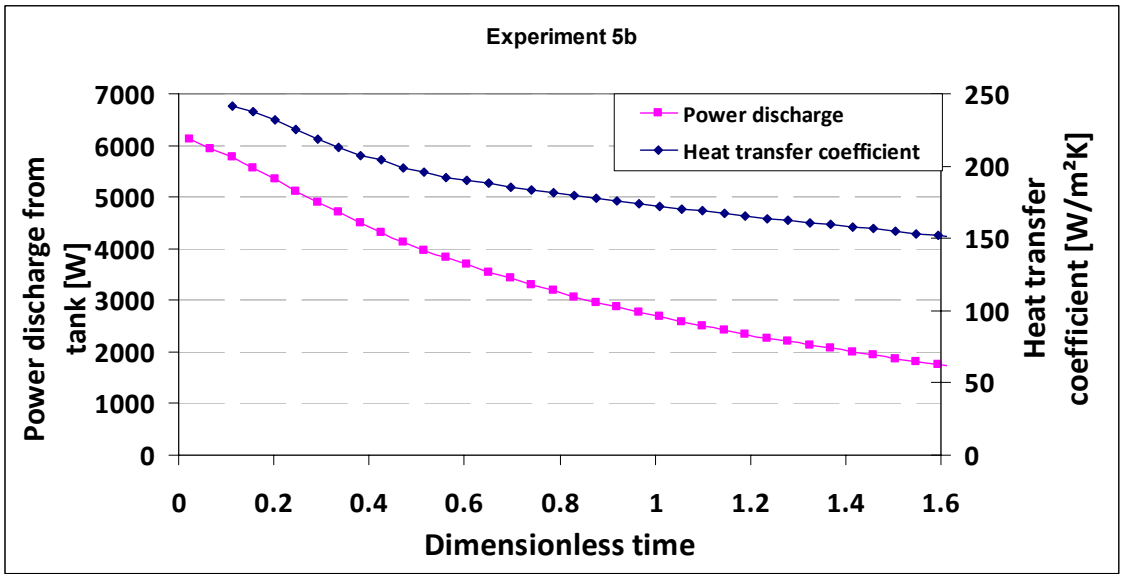

Fig. 2-25b. Power discharge from tank and the heat transfer coefficient for Experiment 5b with a volume flow rate of 5 l/min.

<u>''Experiment 1c-5c'' [Initially stratified (72-25°C), Inlet temperature (21-22°C)]</u>

The temperature distribution inside the tank, inlet and outlet temperatures for the upper mantle for experiments 1c, 2c, 3c, 4c and 5c for five different volume flow rates and with an initially stratified tank are shown in Fig. 2-26a, Fig. 2-26b, Fig. 2-27a, Fig. 2-27 b, Fig. 2-28a, Fig. 2-28b, Fig. 2-29a, Fig. 2-29b, Fig. 2-30a and Fig. 2-30b. The mantle inlet temperature is between 21 and 22°C for all experiments.

In experiment 1c, with a volume flow rate of 0.5 l/min, the tank temperature is initially stratified between 25°C and 72°C. The tank temperature T1-T7 which is located at the upper part of the tank decreases continuously during the discharge. T8 is constant for the first 20 minutes, dimensionless time of 0.03, of the test and then decrease. The same result is observed for T9 that is constant for the first 75 min of the test, dimensionless time of 0.11 and after that decreases. T10 is constant for the first 138 minutes of the test, dimensionless time of 0.21, and then decreases. T11 increases from 28.7°C to 29.5°C in the first 307 minutes of the test, dimensionless time of 0.47, and decreases to 27.2°C. The first increase is due to the heat conduction from the upper part of the tank and after some time the temperature decrease is due to the heat loss from the tank bottom and due to the discharge. T12 increases from 25.2°C to 26.7°C. The outlet temperature from the upper mantle is between T1 and T2. It can also be seen that the thermal stratification will vanish during the discharge.

In experiment 2c, the initially stratified temperatures are between 25°C and 70°C and the volume flow rate is 1 l/min. T1-T7 decrease continuously during the discharge. Like in experiment 1c, T8 is constant for about 14 minutes, dimensionless time of 0.04, and then decreases during the test. T9 is also constant for about 44 minutes, dimensionless time of 0.14, which is shorter than experiment 1c. T10 is constant for 83 minutes, dimensionless time of 0.25, which is shorter than for experiment 1c, and T10 then decreases during the test. The short period is due to the higher flow rate which discharges the tank faster than in experiment 1c. T11 increases from 29.4°C to 30°C, then decreases to 26.2°C. T12 increases from 25.9°C to 26.6°C and decreases to 26.2°C at the end of the test. The increase and decrease is due to the heat

conduction from the top and the heat loss from the tank bottom and the discharge. The outlet temperature is between T1 and T2 and close to T2. Thermal stratification is vanished during the discharge.
In experiment 3c with a volume flow rate of 2 l/min, the initial stratified temperatures are between 26°C and 70°C. T1-T7 decrease during the discharge. T8 is constant for 11 minutes, dimensionless time of 0.08, T9 for 32 minutes, dimensionless time of 0.21, T10 for 59 minutes, dimensionless time of 0.39, T11 for 122 minutes, dimensionless time of 0.80 and then decreasing. The outlet temperature from the upper mantle is between T2 and T3 which is higher than the outlet temperature of experiment 3a. Thermal stratification vanishes like in experiment 1c and 2c.
In experiment 4c, the volume flow rate is 3 l/min and the initially stratified temperatures are 25°C-70°C. T1-T7 decrease during the discharge. T8 is constant for about 19 minutes dimensionless time of 0.18, T9 for 41 minutes, dimensionless time of 0.37, T10 for 64 minutes, dimensionless time of 0.60 and T11 for 109 minutes, dimensionless time of 1 and then T11 is decreasing. T12 is almost constant. The outlet temperature is between T5 and T6 in the first 85 minutes of the test, dimensionless time of 0.78, and then decreases to be lower than the minimum tank temperature. Thermal stratification will be destroyed during the test.
In experiment 5c, the volume flow rate is 5 l/min and the initial stratified temperatures are 26-71°C. T1-T7 decrease continuously during the discharge. T8 is constant for about 10 minutes, dimensionless time of 0.16, T9 for 28 minutes, dimensionless time of 0.43, T10 for 53 minutes, dimensionless time of 0.79 and T11 for 95 minutes, dimensionless time of 1.40. T12 is also almost constant during the test. The outlet temperature is lower than the minimum tank temperature during the whole discharge period. The reason is the short time used for the water to pass the mantle.

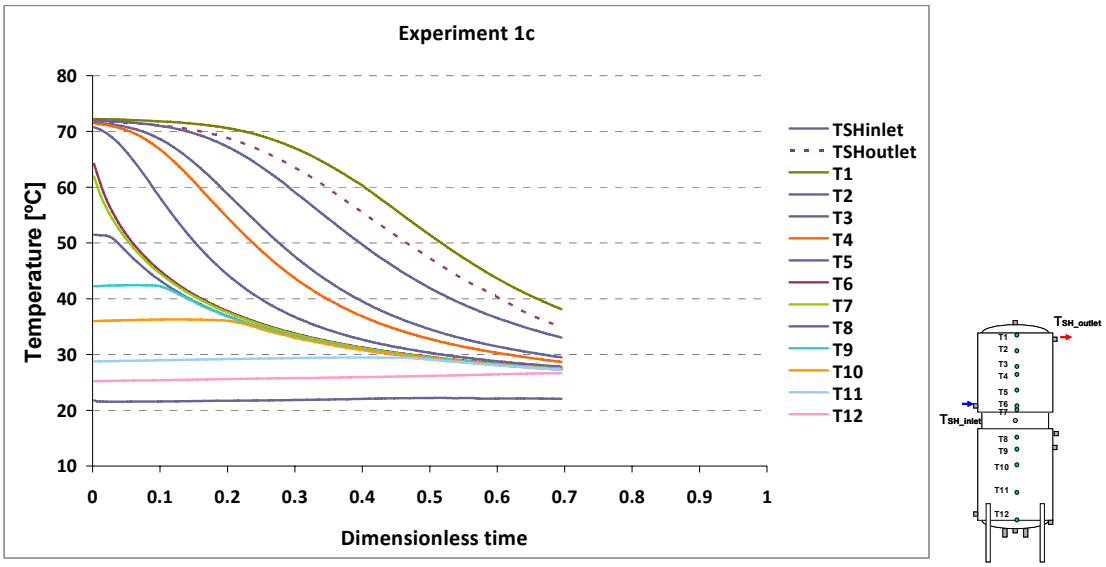

Fig. 2-26a. Measured temperatures with a volume flow rate of 0.5 l/min, experiment 1c.

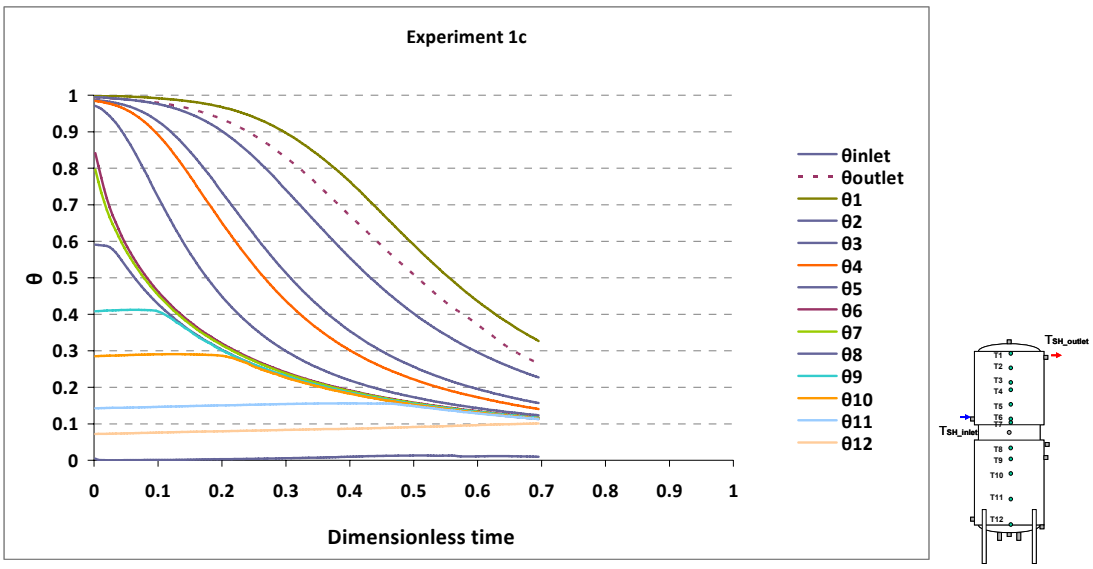

Fig. 2-26b. Dimensionless temperatures for experiment 1c with volume a flow rate of 0.5 l/min.

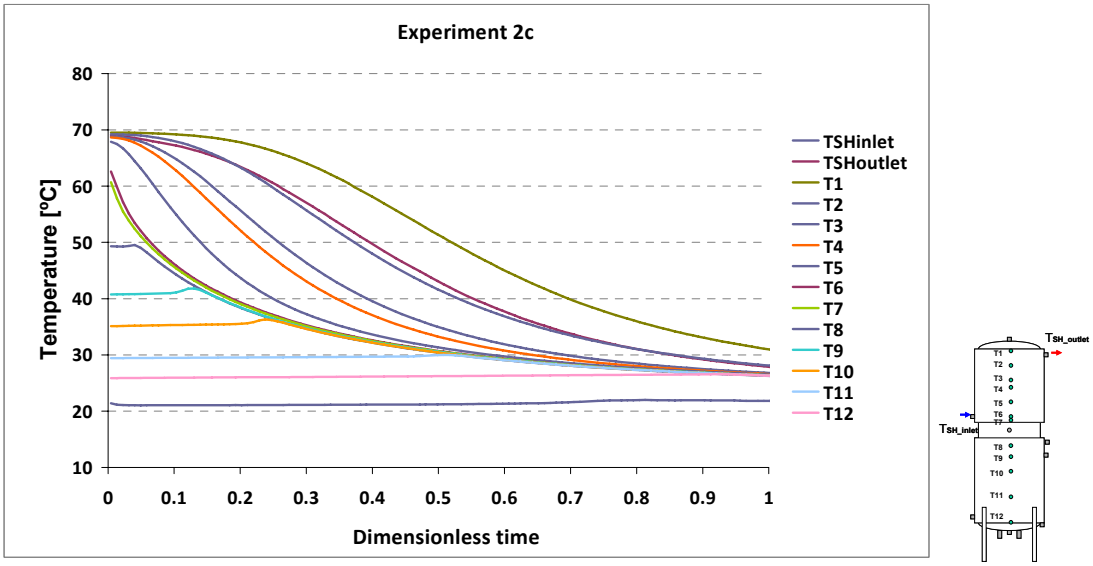

Fig. 2-27a. Measured temperatures with a volume flow rate of 1 l/min, experiment 2c.

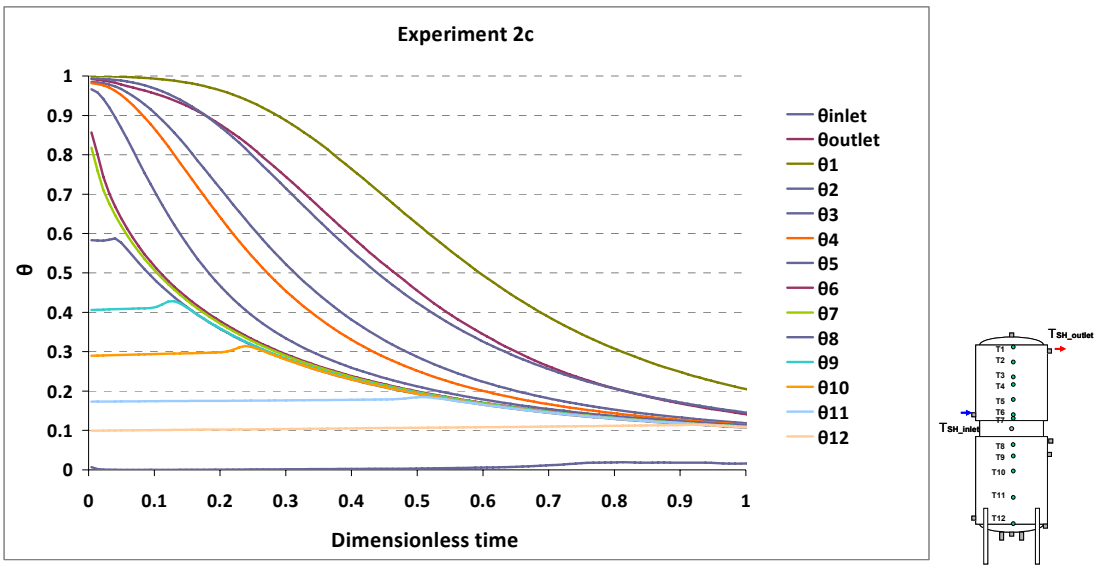

Fig. 2-27 b. Dimensionless temperatures for experiment 2c with a volume flow rate of 1 l/min.

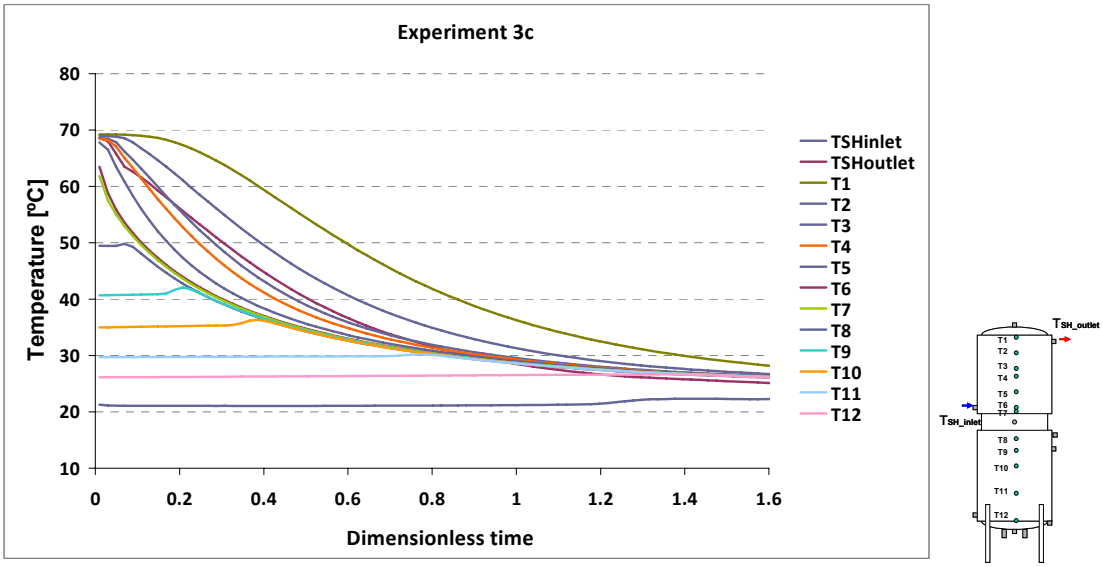

Fig. 2-28a. Measured temperatures with a volume flow rate of 2 l/min, experiment 3c.

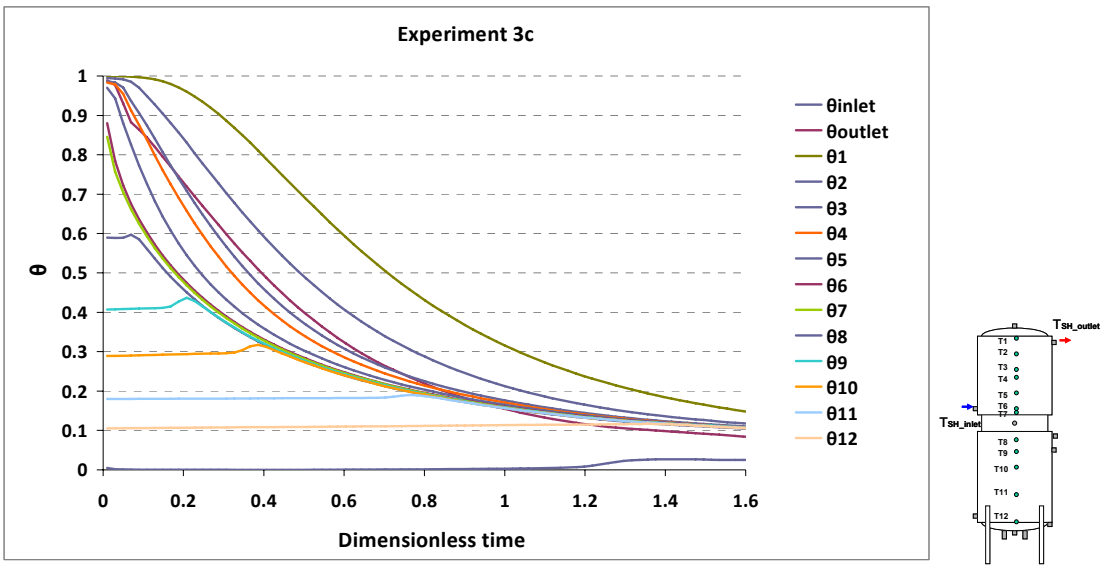

Fig. 2-28b. Dimensionless temperatures for experiment 3c with a volume flow rate of 2 l/min.

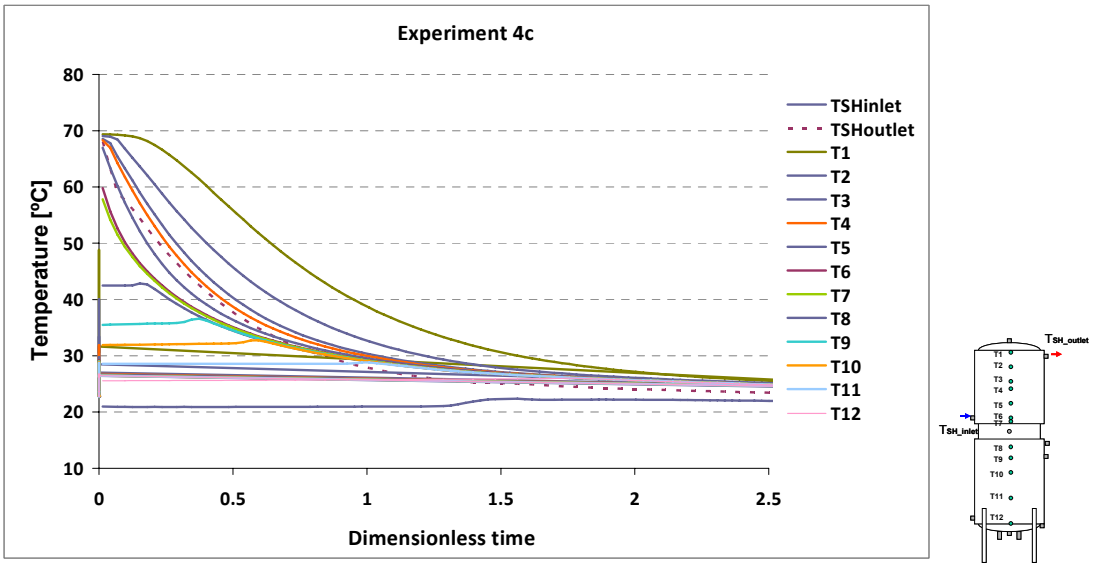

Fig. 2-29a. Measured temperatures with a volume flow rate of 3 l/min, experiment 4c.

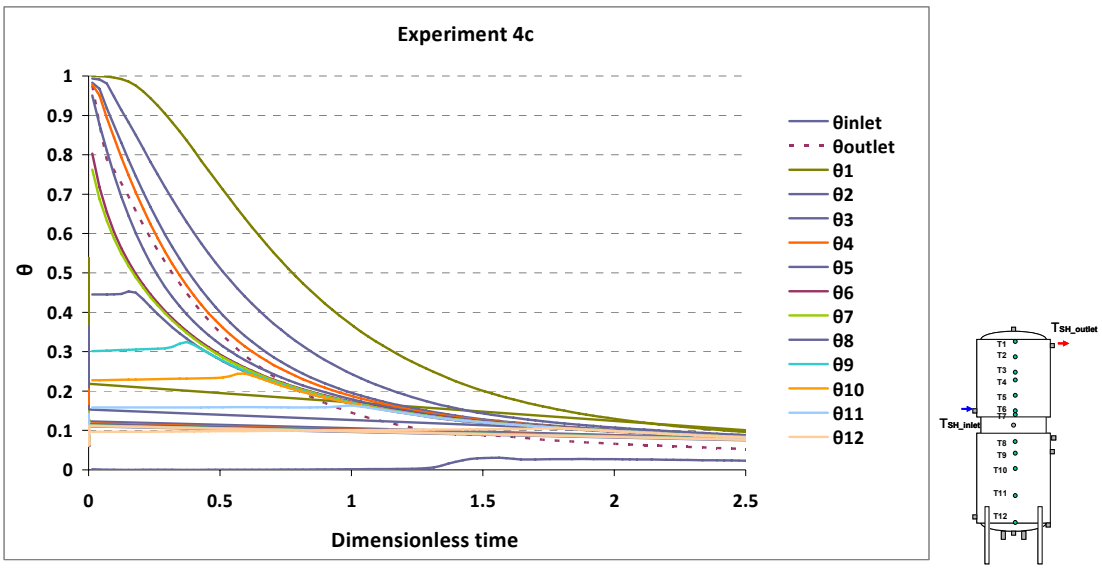

Fig. 2-29b. Dimensionless temperatures for experiment 4c with a volume flow rate of 3 l/min.

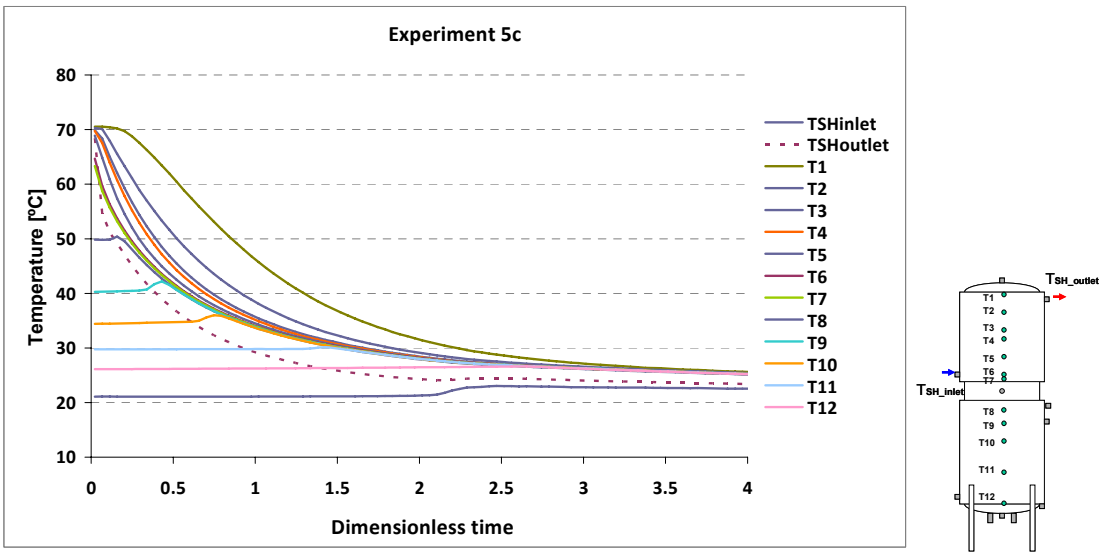

Fig. 2-30a. Measured temperatures with a volume flow rate of 5 l/min, experiment 5c.

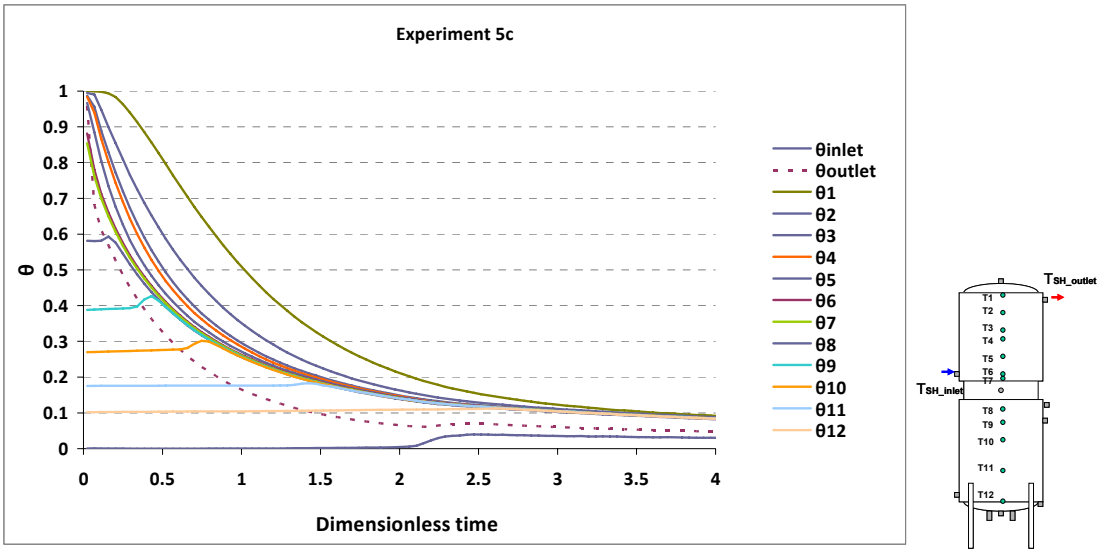

Fig. 2-30b. Dimensionless temperatures for experiment 5c with a volume flow rate of 5 l/min.

The discharge heat transfer from each ten volumes inside the tank is shown in Fig. 2-31a till Fig. 2-35a. The heat transfer coefficient of the upper mantle and the discharge power is shown in Fig. 2-31b till Fig. 2-35b. The test period can be divided into three main parts for analyzing the results; the first part is the time period when heat is mainly taken from the lower part of the tank. The second part is a period where the heat discharge level changes from the lower part to the upper part of the tank. And the third part is where more heat is taken from the upper part than from the lower part of the tank.

In experiment 1c with a volume flow rate of 0.5 l/min, heat is in the first part of the test mostly discharged from Volume 5, second most from Volume 4, followed by volumes 6, 3, 2, 1, 9, 8, 7 and 10 which is desirable for keeping thermal stratification. The peak power is about 920 W from one tank volume. For the second period of the test, the power discharge from volume 5 decreases all the time, and the power discharge from volumes 9, 8, 4, 3, 2 and 1 increases and then decreases. The power discharge from volume 6, first decreases, increases and then decreases. Heat is not discharged from or charged to volume 10. In the third period of the test, most heat is taken from volume 1, second most from volume 2, third most from volume 3 followed by volumes 4, 5, 6, 7, 8, 9 and 10. Heat is discharged from the top to the bottom of the tank. That is why stratification will diminish during discharge. In Fig. 2-31b, the power discharge from the tank and the heat transfer coefficient of the upper mantle is shown. The power discharge is about 400-1750 W and the heat transfer coefficient is about 90-225 W/m²K.

In experiment 2c with a volume flow rate of 1 l/min, heat is in the first part of the test mostly discharged from volume 5, second most from volume 4, third most from volume 6 followed by volumes 3, 2, 1, 9, 8, 10 and 7. Therefore, like in experiment 1c, heat in the start is mostly taken from the lower part of the tank which is desirable for keeping thermal stratification. However, comparing experiment 2c with 2a and 2b, more heat is discharged from the upper volumes for initially stratified condition than for the initially mixed condition at the beginning of the test. For the second period of the test, the power discharge from volume 5 decreases all the time, and the power discharge from volumes 4, 3, 2 and 1 increases and then decreases. The power discharge from volume 6, first decreases, then increases and again decreases. Power

discharge from volume 9 and 10 is constant during the test. However, the power discharge from volumes 7 decreases first and heat is supplied to volume 7 and then increases and decreases again. The power discharge from volume 8 has a decrease in its value, and then increases and decreases again. This increase and decrease of power discharge for volumes 7 and 8 is due to mixing occurring at that time period. In the third period of the test, most heat is taken from volume 1, second most from volume 2, third most from volume 3 followed by volumes 4, 5, 6, 7, 8, 9 and 10. The peak power is 1440 W from one tank volume which is higher than in experiment 1c due to the fact that the volume flow rate is higher. The power discharge and heat transfer coefficient is also increased to 390-3250 W and 85-325 W/m²K.

In experiment 3c with a volume flow rate of 2 l/min, heat is in the first part of the test mostly discharged from volume 5, second most from 4, third most from volume 6 followed by volumes 2, 9, 8, 10, 7, 3 and 1. It can be seen that heat is taken from the tank at a somewhat higher level than in experiment 1c and 2c. For the second period of the test, the power discharge from volume 5 decreases all the time, and the power discharge from volumes 4, 3, 2 and 1 increases and then decreases. The power discharge from volume 6, first decreases, then increases and again decreases. Power discharge from volume 9 and 10 is constant during the test. The power discharge from volumes 7 decreases first and heat is supplied to volume 7 and then increases and decreases again. The power discharge from volume 8 decreases, then increases and decreases again. In the third period of the test, most heat is taken from volume 1, second most from volume 2, third most from volume 3 followed by volumes 4, 5, 6, 7, 8, 9 and 10. The peak power is 3000 W from one tank volume which is higher than in experiment 1c and 2c due to the fact that the volume flow rate is higher. The power discharge and heat transfer coefficient is also increased to 420-7500 W and 100-400 W/m²K.

In experiment 4c with a volume flow rate of 3 l/min, heat is in the first part of the test mostly discharged from volume 5, second most from 4, third most from volume 6 followed by volumes 1, 3, 2, 9, 8, 10 and 7. For the second period of the test, the power discharge from volumes 4 and 5 decreases all the time, and the power discharge from volumes 3, 2 and 1 increases and then decreases. The power discharge from volume 6, first decreases, then increases and again decreases. Power discharge from volume 9 and 10 is close to 0 during the test. The power discharge from volumes 7 decreases first and heat is supplied to volume 7 and then increases and decreases again. The power discharge from volume 8 decreases, then increases and decreases again. In the third period of the test, most heat is taken from volume 1, second most from volume 2, third most from volume 3 followed by volumes 4, 5, 6, 7, 8, 9 and 10. The peak power is 2600 W from one tank volume which is higher than in experiment 1c, 2c and 3c due to the fact that the volume flow rate is higher. The power discharge and heat transfer coefficient is also increased to 240-8250 W and 90-420 W/m²K.

In experiment 5c with a volume flow rate of 5 l/min, heat is in the first part of the test mostly discharged from volume 5, second most from 4, third most from volume 3 followed by volumes 1, 2, 6, 9, 10, 8 and 7. For the second period of the test, the power discharge from volumes 4 and 5 decreases all the time, and the power discharge from volumes 3, 2 and 1 increases and then decreases. The power discharge from volume 6, first decreases, then increases and again decreases. Power discharge from volume 9 and 10 is close to 0. The power discharge from volume 7 decreases first and then increases and decreases again. The power discharge from volume 8 decreases, then increases and decreases again. In the third period of the test, most heat is taken from volume 1, second most from volume 2, third most from volume 3

followed by volumes 4, 5, 6, 7, 8, 9 and 10. The peak power is 2760 W from one tank volume which is higher than in experiment 1c, 2c, 3c and 4c due to the fact that the volume flow rate is higher. The power discharge and heat transfer coefficient is also increased to 230-10630 W and 90-340 W/m²K.

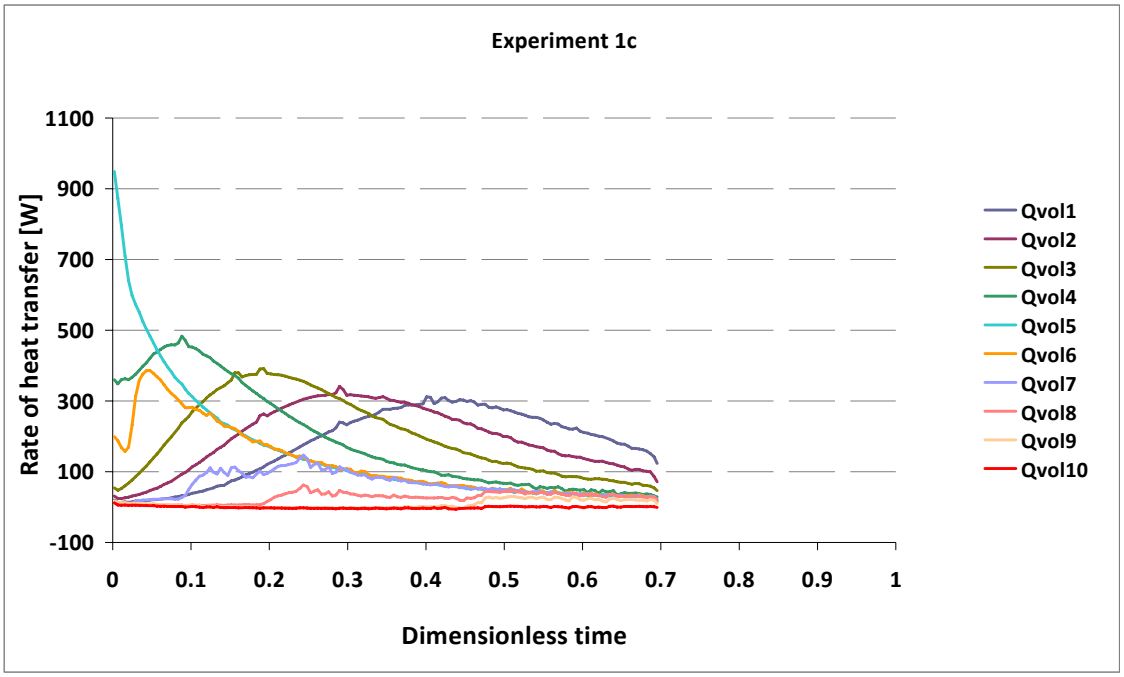

Fig. 2-31a. Heat transfer from each tank volume in Experiment 1c with a volume flow rate of 0.5 l/min.

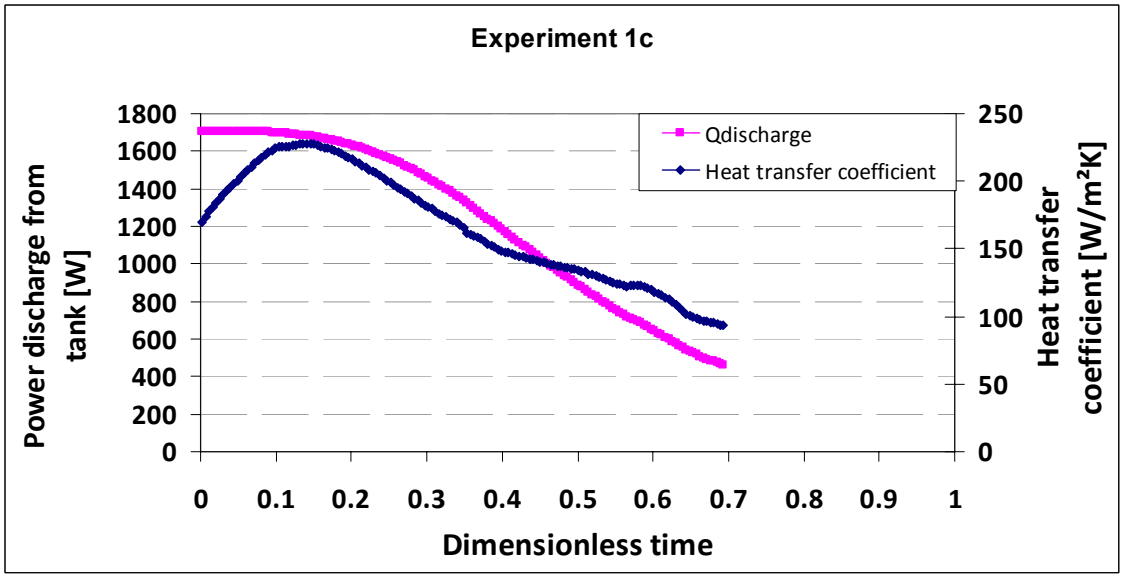

Fig. 2-31b. Power discharge from tank and the heat transfer coefficient for Experiment 1c with a volume flow rate of 0.5 l/min.

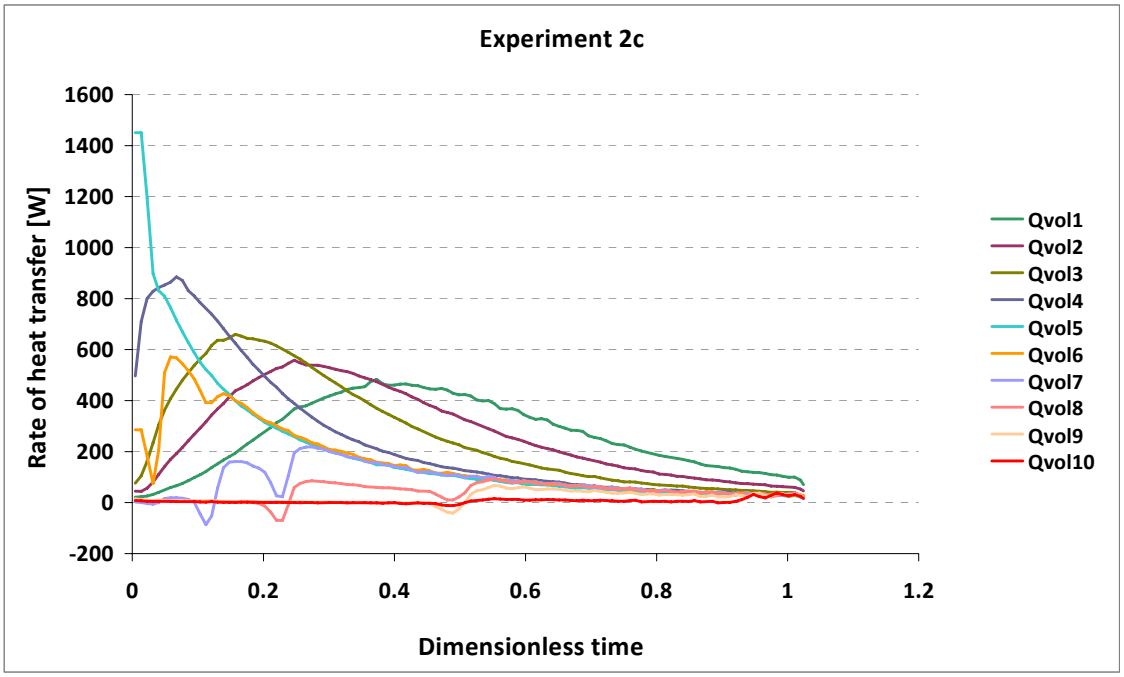

Fig. 2-32a. Heat transfer from each tank volume in Experiment 2c with a volume flow rate of 1 l/min.

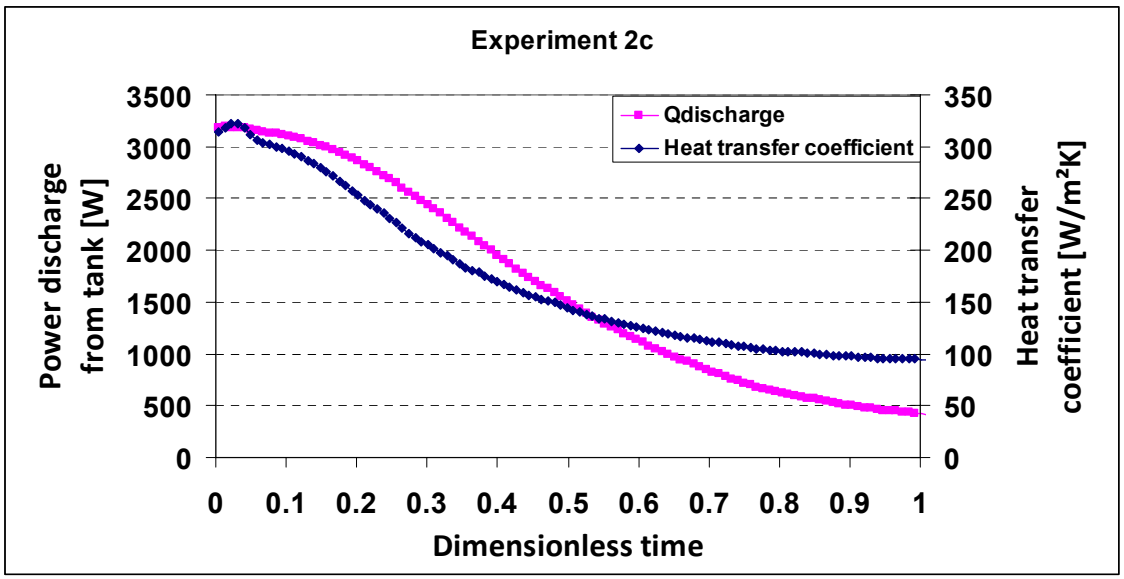

Fig. 2-32b. Power discharge from tank and the heat transfer coefficient for Experiment 2c with a volume flow rate of 1 l/min.

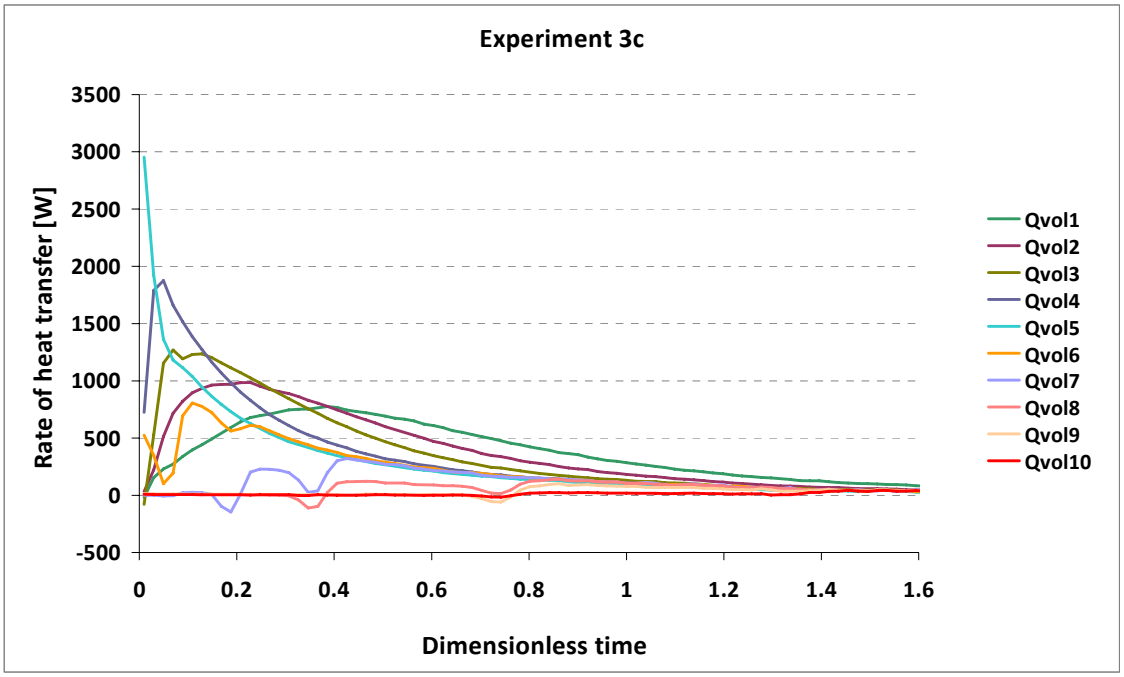

Fig. 2-33a. Heat transfer from each tank volume in Experiment 3c with a volume flow rate of 2 l/min.

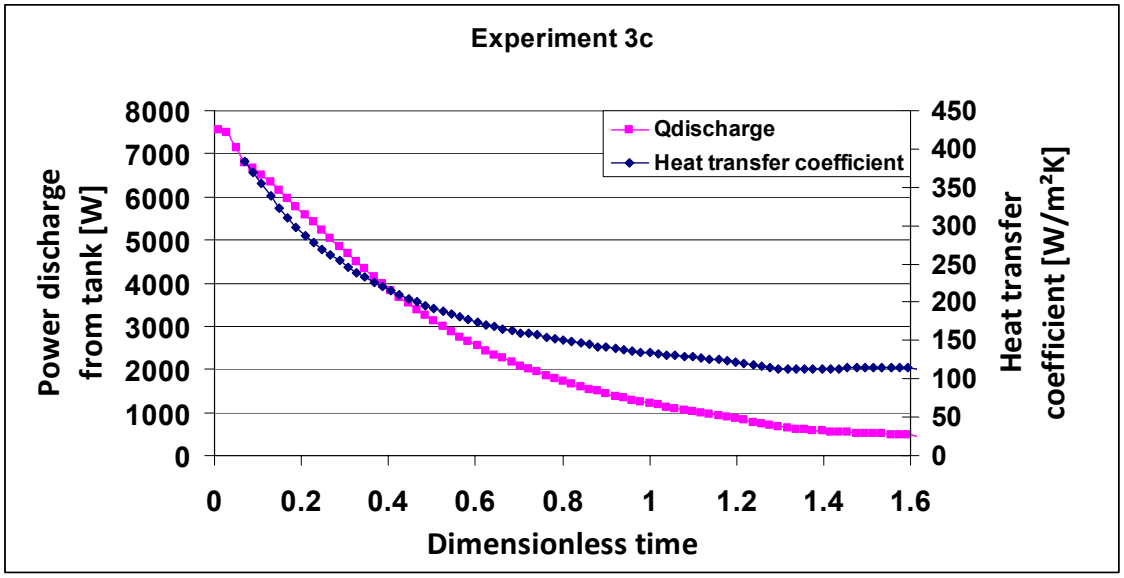

Fig. 2-33b. Power discharge from tank and the heat transfer coefficient for Experiment 3c with a volume flow rate of 2 l/min.

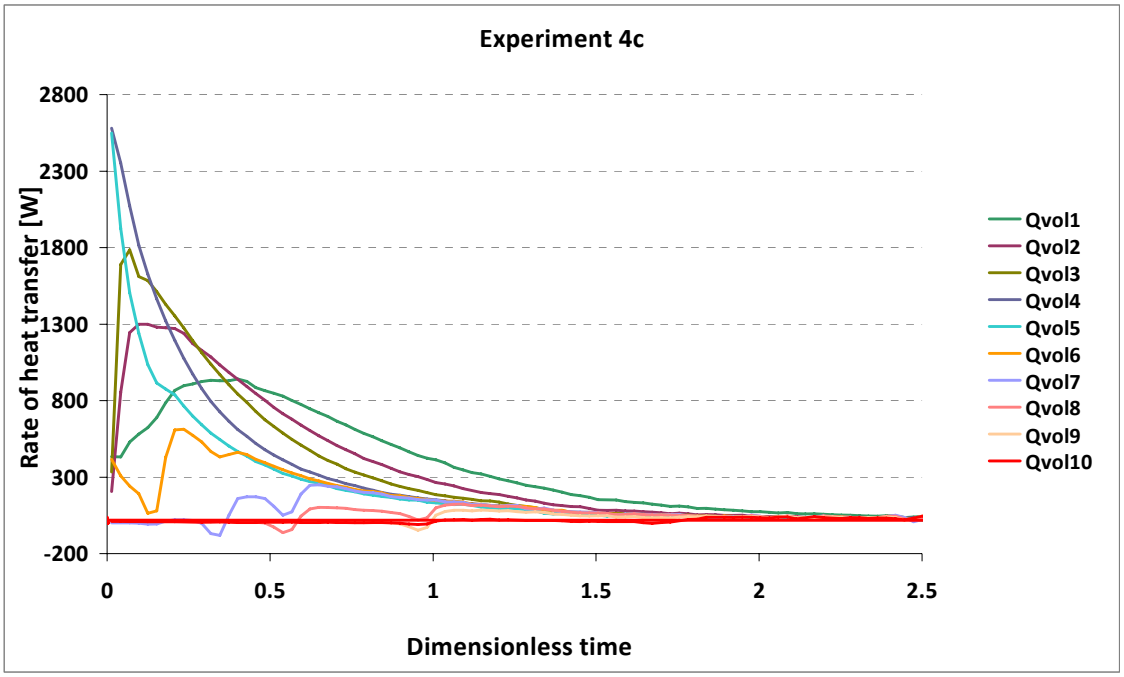

Fig. 2-34a. Heat transfer from each tank volume in Experiment 4c with a volume flow rate of 3 l/min.

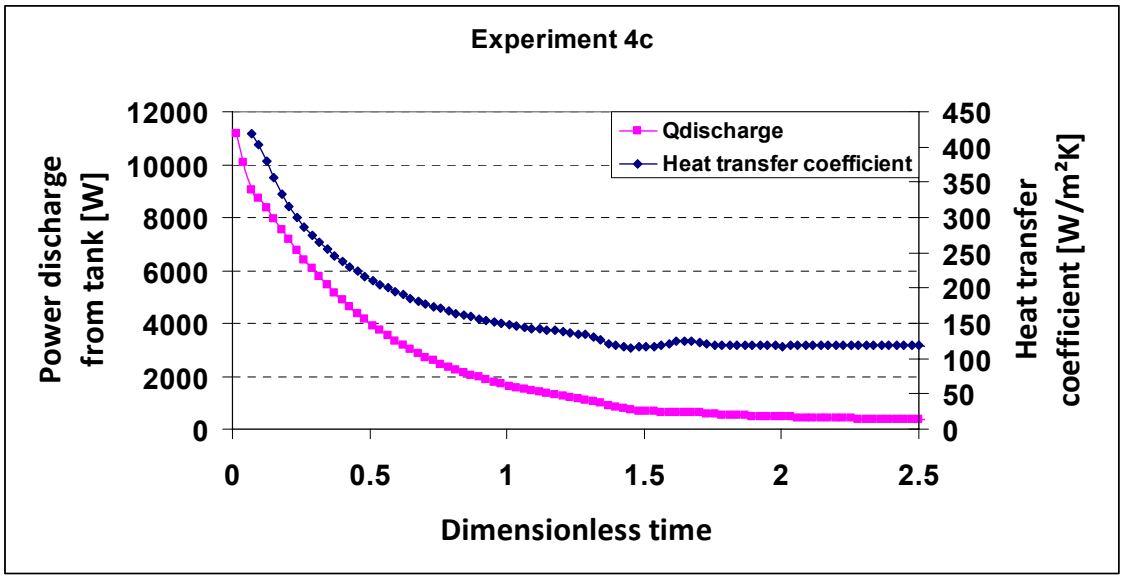

Fig. 2-34b. Power discharge from tank and the heat transfer coefficient for Experiment 4c with a volume flow rate of 3 l/min.

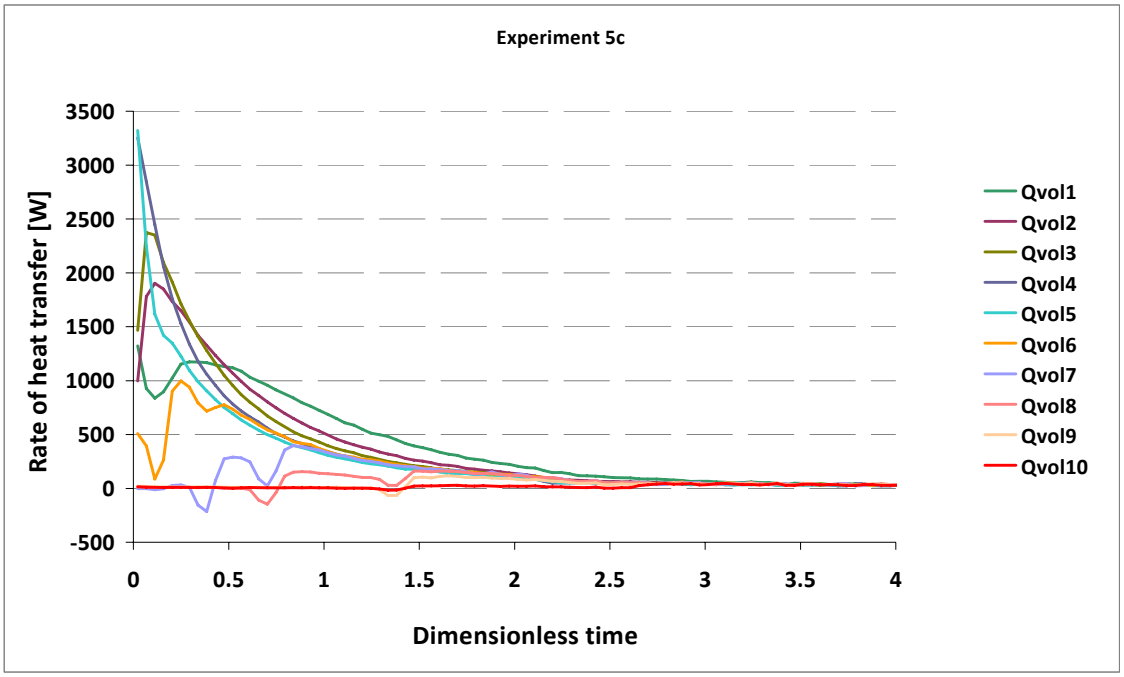

Fig. 2-35a. Heat transfer from each tank volume in Experiment 5c with a volume flow rate of 5 l/min.

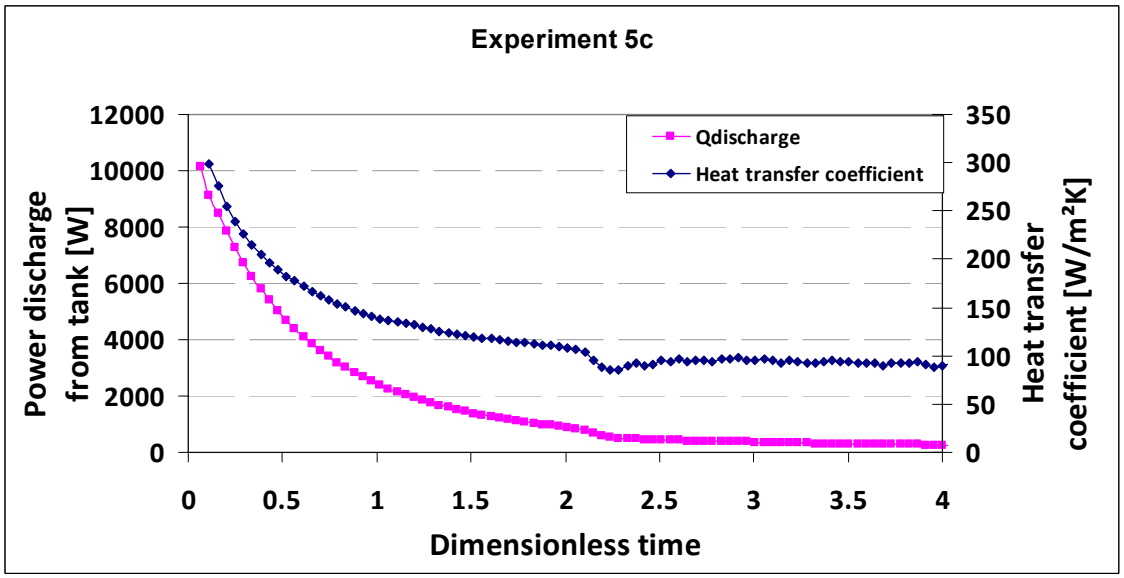

Fig. 2-35b. Power discharge from tank and the heat transfer coefficient for Experiment 5c with a volume flow rate of 5 l/min.

‘‘Experiment 1d-2d’’ [Initially stratified (25-59°C), Inlet temperature (21°C)]

The temperature distribution inside the tank, inlet and outlet temperatures for the upper mantle for experiments 1d and 2d for two volume flow rates of 0.5 l/min and 1 l/min for initially stratified condition are shown in Fig. 2-36a, Fig. 2-36b, Fig. 2-37a and Fig. 2-37b. The mantle inlet temperature is about 21°C for both experiments.

In experiment 1d, with the volume flow rate of 0.5 l/min, the tank temperatures are initially stratified between 25-59°C. The tank temperature T1-T7 which is located at the half upper part of the tank decreases continuously during the discharge. T8 is constant for the first 28 minutes of the test, dimensionless time of 0.05, and then decrease. The same result is observed for T9 that is constant for the first 80 min of the test, dimensionless time of 0.14 and after that decreases. T10 is constant for the first 131 minutes of the test, dimensionless time of 0.23, and then decreases. T11 and T12 are constant during the test. The outlet temperature from the upper mantle is between T1 and T2. The thermal stratification is almost the same as for experiment 1c. The thermal stratification vanish during the discharge.
In experiment 2d, the initially stratified tank temperatures are between 55°C and 25°C with a volume flow rate of 1 l/min. T1-T7 decrease continuously during the discharge. However, T8 is constant for about 25 minutes, dimensionless time of 0.07, and then decreases during the test. T9 is also constant for about 62 minutes, dimensionless time of 0.18 which is shorter than experiment 1d. The same result is seen for T10 that is constant for 92 minutes, dimensionless time of 0.28 which is shorter than experiment 1c, and then decreases during the test. The short period is because of the higher flow rate which discharges the heat faster than experiment 1c. T11 is constant at 32°C until dimensionless time of 0.47, and decreases to 27°C at the end of the test. T12 is almost constant during the test. The outlet temperature from the upper mantle is between T2 and T3, close to T2. Thermal stratification is also vanished during the discharge.

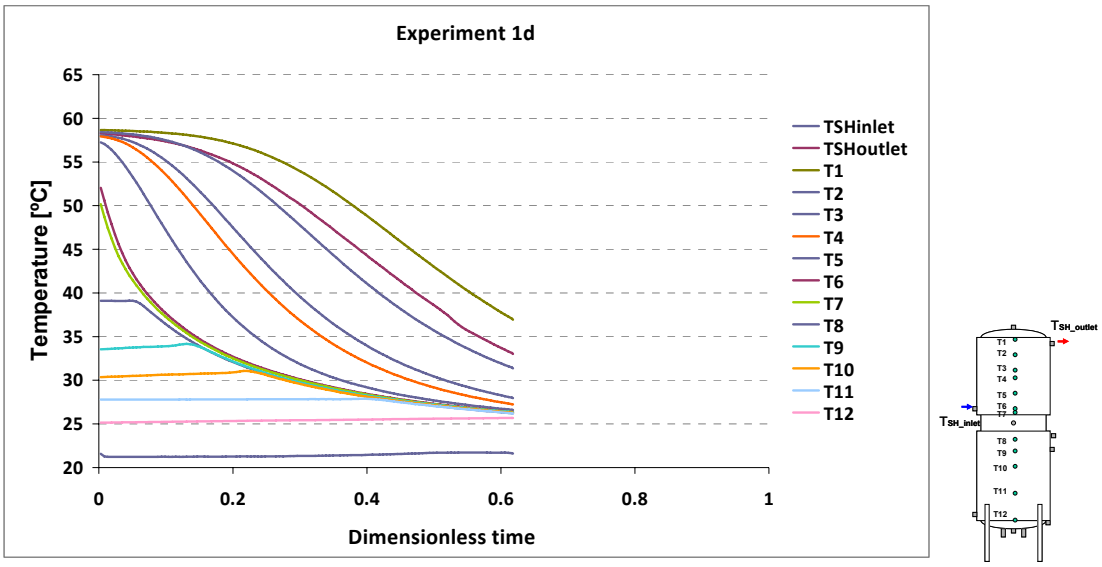

Fig. 2-36a. Measured temperatures with a volume flow rate of 0.5 l/min, experiment 1d.

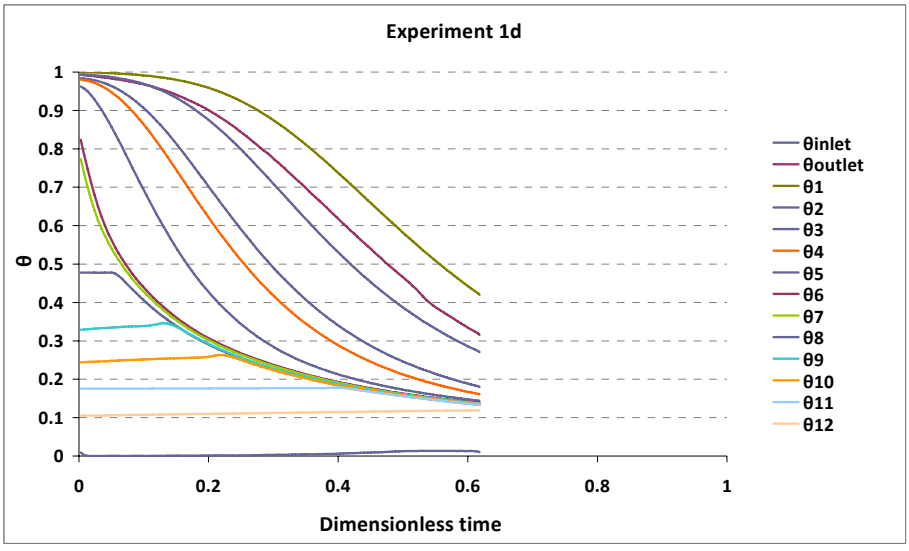

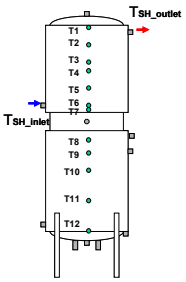

Fig. 2-36b. Dimensionless temperatures for experiment 1d with a volume flow rate of 0.5 l/min.

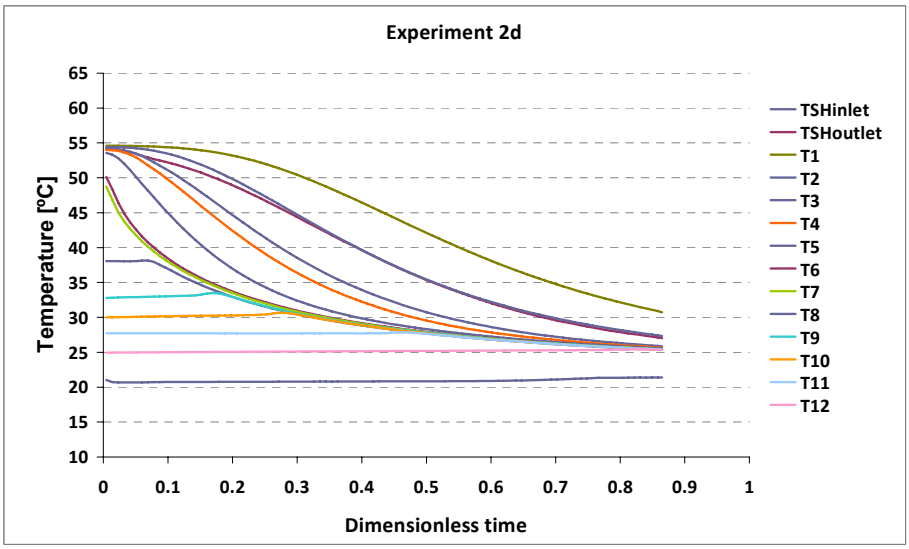

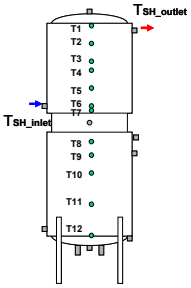

Fig. 2-37a. Measured temperatures with a volume flow rate of 1 l/min, experiment 2d.

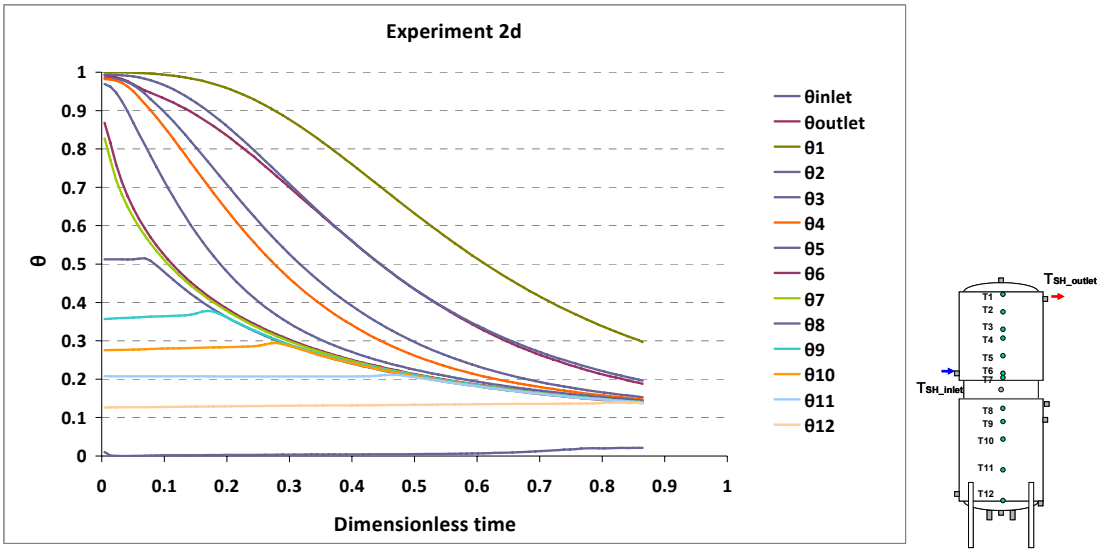

Fig. 2-37b. Dimensionless temperatures for experiment 2d with a volume flow rate of 1 l/min.

The heat transfer from each tank volume during the two experiments is shown in Fig. 2-38a and Fig. 2-39a. The discharge heat transfer from each ten volumes inside the tank is shown in Fig. 2-38a and Fig. 2-39a. The heat transfer coefficient of the upper mantle and the discharge power are shown in Fig. 2-38b and Fig. 2-39b. The test period can be divided into three main parts for analyzing the results; the first part is the time period where, heat is mainly taken from the lower part of the tank. The second part is a period where the heat discharge level changes from the lower part to the upper part of the tank. And the third part is where more heat is taken from the upper part than from the lower part of the tank.

In experiment 1d with a volume flow rate of 0.5 l/min, heat in the first part of the test is mostly discharged from Volume 5, second most from Volume 4, third most from Volume 6 followed by Volumes 3, 2, 9, 8, 1, 10 and 7 which is desirable for keeping thermal stratification. The peak power is about 800 W from one tank volume. For the second period of the test, the power discharge from volume 5 decreases all the time, and the power discharge from volumes 4, 3, 2 and 1 increases and then decreases. The power discharge from volume 6, first decreases, increases and then decreases. Power discharge from volumes 9 and 10 is close to 0. The power discharge from volumes 7 and 8 decreases first and heat is supplied to volumes 7 and 8 and then increases and decreases again. In the third period of the test, most heat is taken from volume 1, second most from volume 2, third most from volume 3 followed by volumes 4, 5, 6, 7, 8, 9 and 10. Furthermore, it can be seen that at the end of the test, heat is discharged from the top to the bottom of the tank. That is why stratification will diminish during discharge. In Fig. 2-38b, the power discharge from the tank and the heat transfer coefficients of the upper mantle is shown. The power discharge is about 400-1500 W and the heat transfer coefficient is about 90-225 W/m²K.

In experiment 2d with a volume flow rate of 1 l/min, heat in the first part of the test is mostly discharged from volume 5, second most from volume 4, third most from volume 6 followed by volumes 3, 2, 1, 9, 8, 10 and 4. For the second period of the test, the power discharge from volume 5 decreases all the time, and the power discharge from volumes 4, 3, 2 and 1 increases and then decreases. The power discharge from volume 6, first decreases, then increases and again decreases. The power discharge from volume 9 and 10 is close to 0. The power discharge from volume 7 decreases first and then increases and decreases again. The power discharge

from volume 8 decreases, then increases and decreases again. This increase and decrease of power discharge for volumes 7 and 8 is due to the mixing occurring at that time period. In the third period of the test, most heat is taken from volume 1, second most from volume 2, third most from volume 3 followed by volumes 4, 5, 6, 7, 8, 9 and 10. The peak power is 1000 W from one tank volume which is higher than in experiment 1d due to the fact that the volume flow rate is higher. The power discharge and heat transfer coefficient is also increased to 400-2300 W and 80-335 W/m²K.

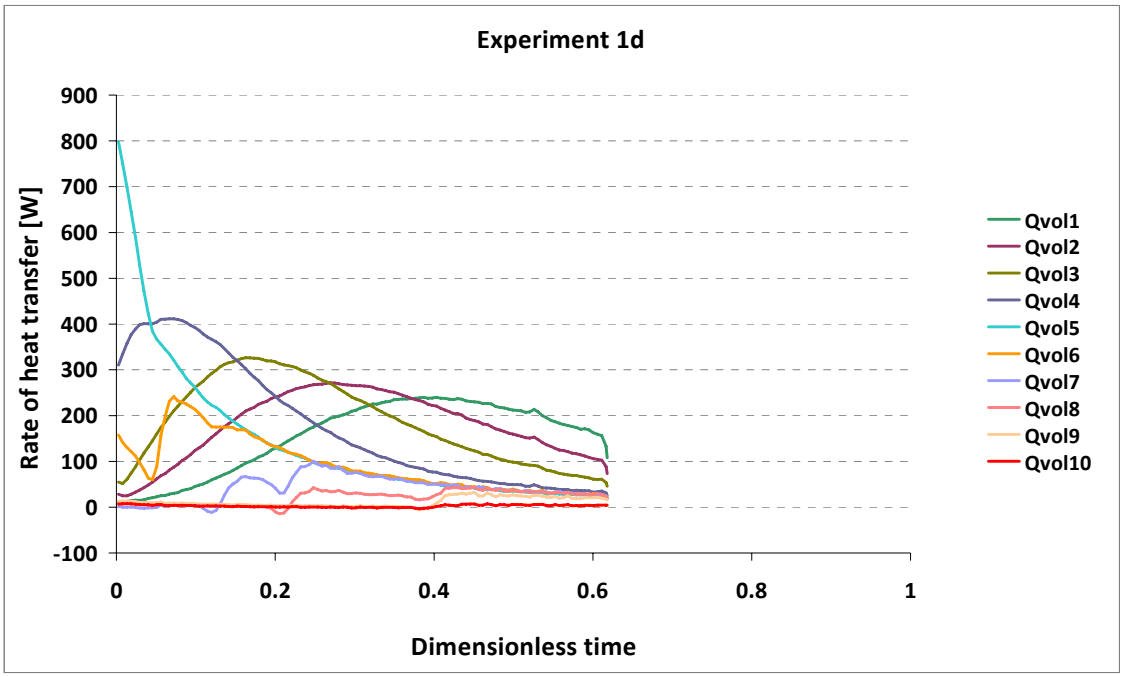

Fig. 2-38a. Heat transfer from each tank volume in Experiment 1d with a volume flow rate of 0.5 l/min.

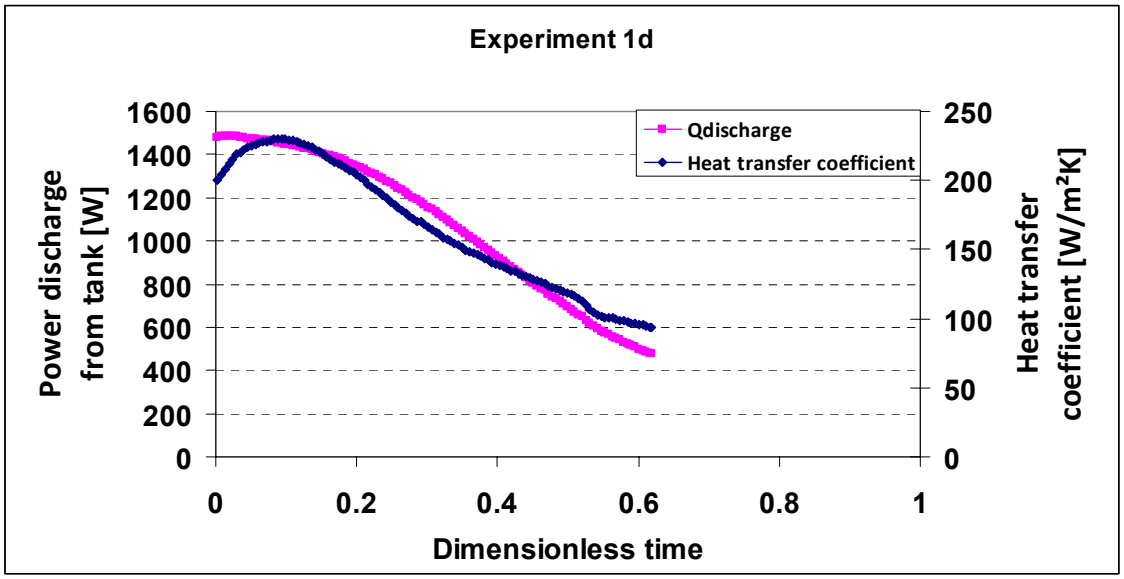

Fig. 2-38b. Power discharge from tank and the heat transfer coefficient for Experiment 1d with a volume flow rate of 0.5 l/min.

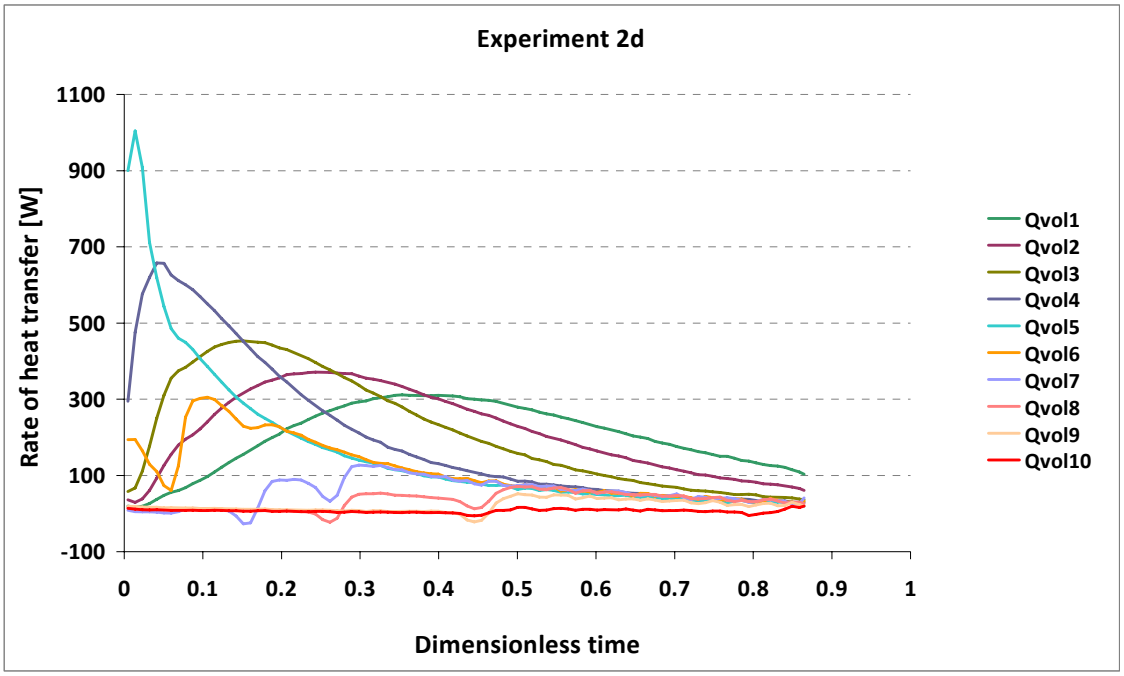

Fig. 2-39a. Heat transfer from each tank volume in Experiment 2d with a volume flow rate of 1 l/min.

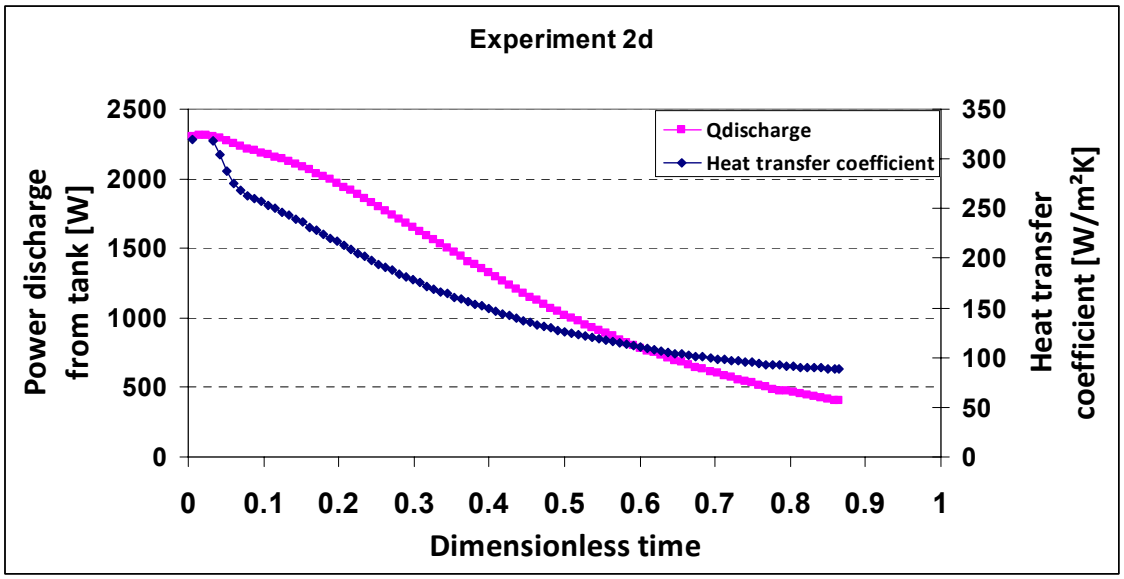

Fig. 2-39b. Power discharge from tank and the heat transfer coefficient for Experiment 2d with a volume flow rate of 1 l/min.

‘‘Experiments 1e-2e’’ [Initially mixed (51-61°C), Inlet temperature (31-36°C)]

In these experiments, the inlet temperature to the upper mantle is high in order to study the inlet temperature’s effect on the thermal stratification inside tank. Fig. 2-40a and Fig. 2-40b show the thermal stratification in the tank for the initially mixed condition of 51°C-57°C for a volume flow rate of 0.5 l/min for experiment 1e. The inlet temperature is 31°C. Thermal stratification is built up in the upper part of the

tank surrounded by the upper mantle (T1-T7), while in the lower part a little thermal stratification is built up inside the tank. It can also be seen that the outlet temperature from the upper mantle is very high between T1 and T2. The thermal stratification is similar to the thermal stratification in experiment 1b with a volume flow rate of 0.5 l/min and an inlet temperature of about 23°C. The thermal stratification diminishes a bit during discharge at the end of the test. However, comparing to experiment 1b, the increase in inlet temperature to the upper mantle does not have any significant effect on thermal stratification.

Fig. 2-41a and Fig. 2-41b show the thermal stratification in the tank for the initially mixed condition of 55°C-61°C for a volume flow rate of about 0.5 l/min. The inlet temperature is 36°C.

Thermal stratification is built up in the upper part of the tank surrounded by the upper mantle (T1-T7), while in the lower part a little thermal stratification is built up inside the tank. It can also be seen that the outlet temperature from the upper mantle is very high between T1 and T2. The thermal stratification is similar to the thermal stratification in experiment 1b and 1e with a volume flow rate of 0.5 l/min and an inlet temperature of about 23°C and 31°C. It can be seen that the increase in inlet temperature to the upper mantle does not have any significant effect on thermal stratification.

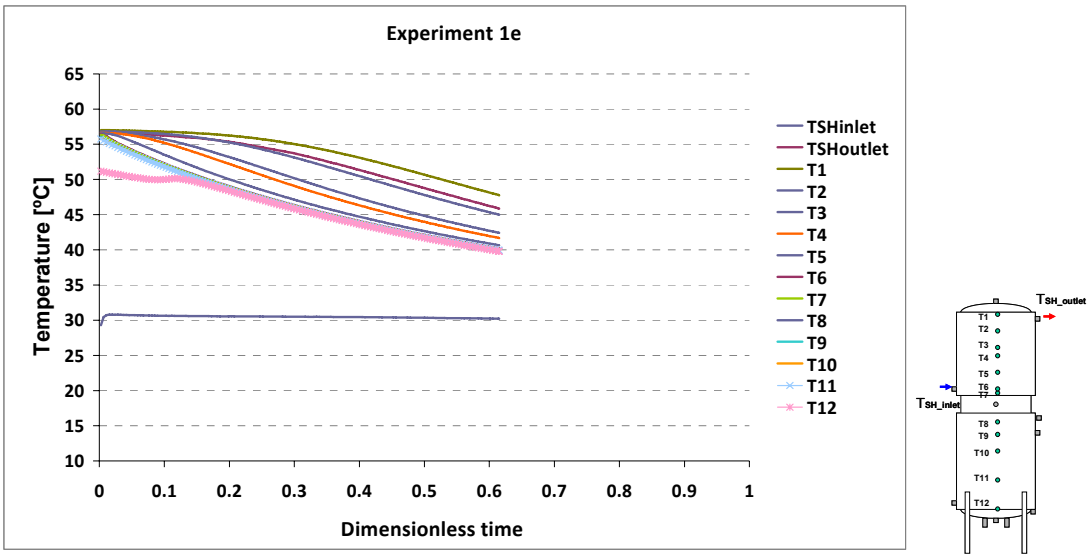

Fig. 2-40a. Measured temperatures with a volume flow rate of 0.5 l/min, experiment 1e.

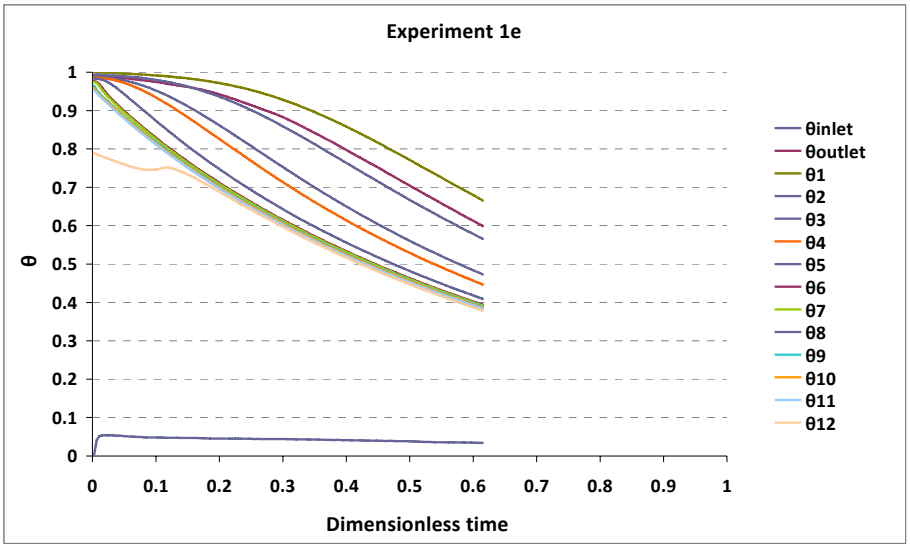

Fig. 2-40b. Dimensionless temperatures for experiment 1e with a volume flow rate of 0.5 l/min.

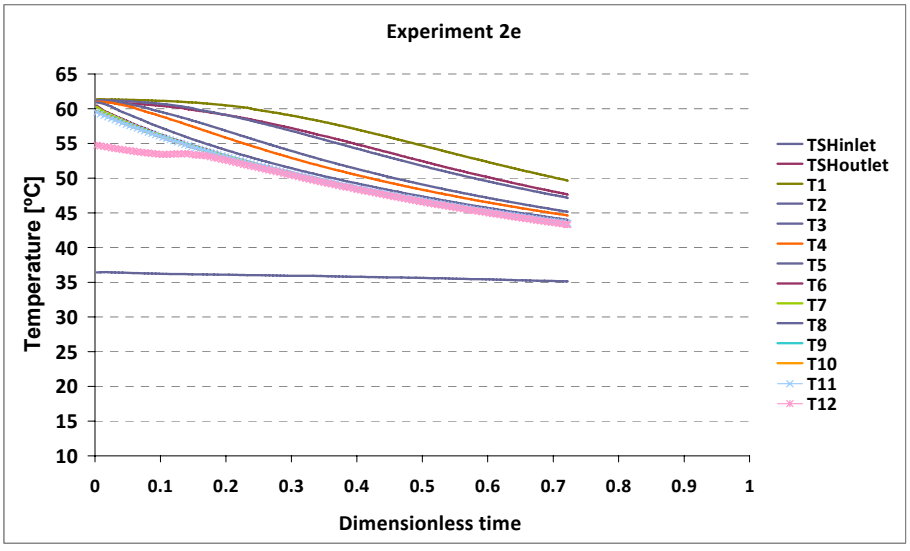

Fig. 2-41a. Measured temperatures with a volume flow rate of 0.5 l/min, experiment 2e.

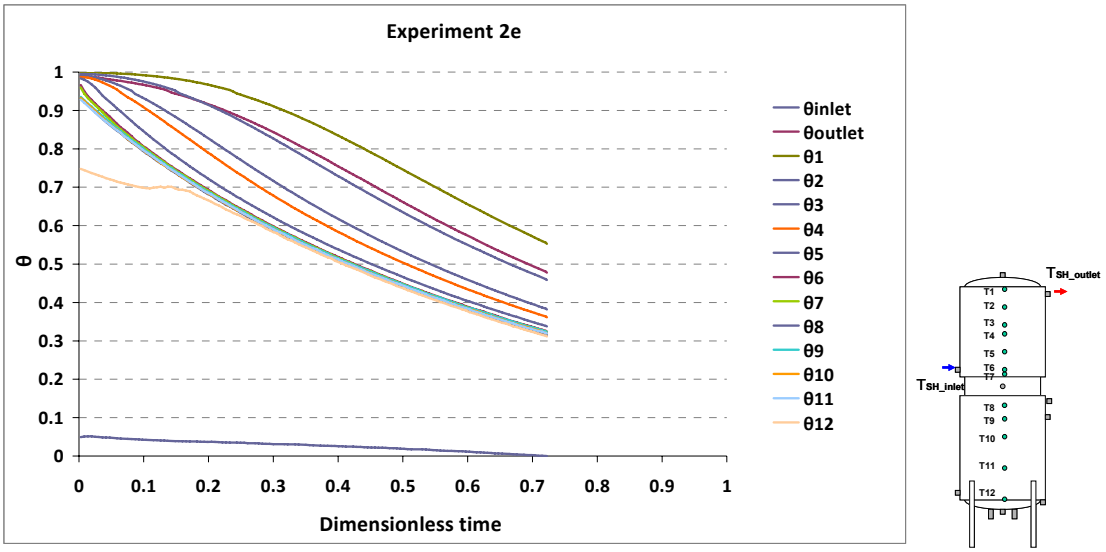

Fig. 2-41b. Dimensionless temperatures for experiment 2e with a volume flow rate of 0.5 l/min.

The discharge heat transfer from each ten volumes inside the tank is shown in Fig. 2-42a and Fig. 2-43a. The heat transfer coefficient of the upper mantle and the discharge power are shown in Fig. 2-42b and Fig. 2-43b. The test period can be divided into three main parts for analyzing the results; the first part is the time period when heat is mainly taken from the lower part of the tank. The second part is a period where the heat discharge level changes from the lower part to the upper part of the tank. And the third part is where more heat is taken from the upper part than from the lower part of the tank.

In experiment 1e with a volume flow rate of 0.5 l/min, heat is in the first part of the test mostly discharged from Volume 6, second most from Volume 7, third most from volume 8 followed by Volumes 9, 5, 10, 4, 3, 2 and 1 which is desirable for creating thermal stratification. The peak power is about 260 W from one tank volume. In the second part of the test, the discharge powers from volumes 9 and 10 decreases to the minimum value so that after 80 min dimensionless time of 0.10, heat is supplied to volume 10. Therefore, mixing occurs somewhat at the bottom part of the tank and it disturbs somewhat the thermal stratification. Further, the power discharge from volumes 8, 7 and 6 decreases all the time, and the power discharge from volumes 5, 4, 3, 2 and 1 increases and then decreases. In the third period of the test, most heat is taken from volume 1, second most from volume 2, third most from volume 3 followed by volumes 4, 5, 6, 7, 8, 9 and 10. In Fig. 2-42b, the power discharge from the tank and the heat transfer coefficients of the upper mantle is shown. The power discharge is about 500-900 W and the heat transfer coefficient is about 80-130 W/m²K.

In experiment 2e with a volume flow rate of 0.5 l/min, heat is in the first part of the test mostly discharged from Volume 5, second most from Volume 6, third most from volume 7 followed by Volumes 8, 9, 4, 10, 3, 2 and 1 which is desirable for creating thermal stratification. The peak power is about 190 W from one tank volume. In the second part of the test, the discharge powers from volumes 9 and 10 decreases to the minimum value so that after 60 min, dimensionless time of 0.13, heat is supplied to volume 10. Therefore, mixing occurs somewhat at the bottom part of the tank and it disturbs somewhat the thermal stratification. Further, the power discharge from volumes 8, 7, 6 and 5 decreases all the time, and the power discharge from volumes 4, 3, 2 and 1 increases and then decreases. In the third period of the test, most heat is

taken from volume 1, second most from volume 2, third most from volume 3 followed by volumes 4, 5, 6, 7, 8, 9 and 10. In Fig. 2-43b, the power discharge from the tank and the heat transfer coefficient of the upper mantle is shown. The power discharge is about 500-1100 W and the heat transfer coefficient is about 90-160 W/m²K.

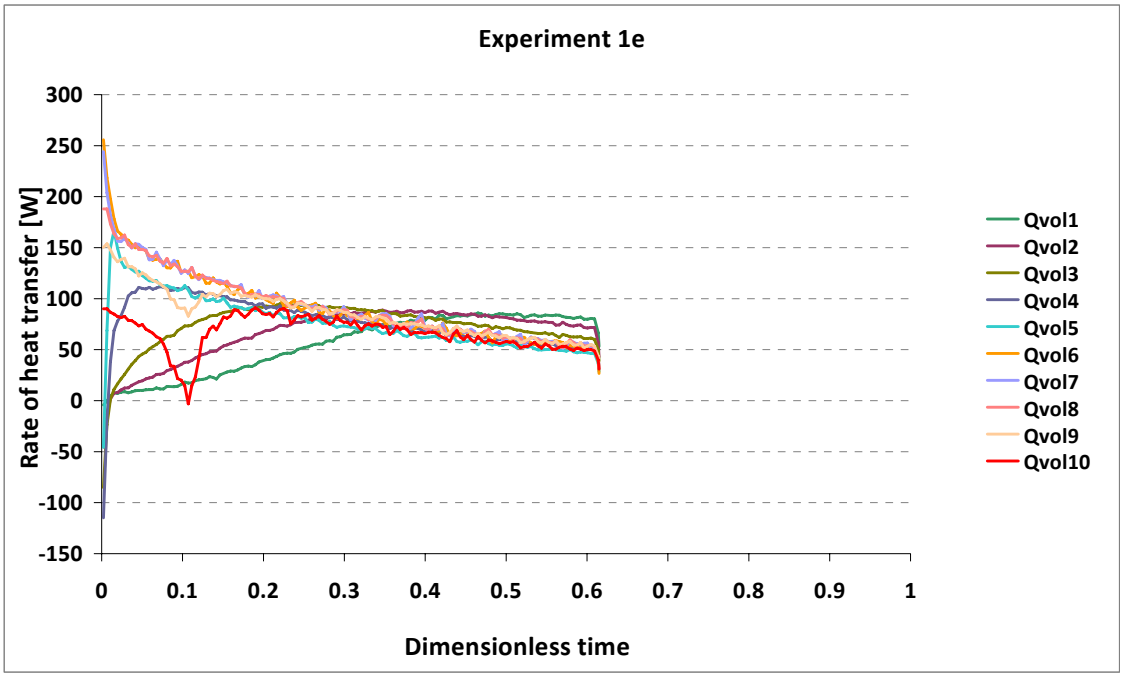

Fig. 2-42a. Heat transfer from each tank volume in Experiment 1e with a volume flow rate of 0.5 l/min.

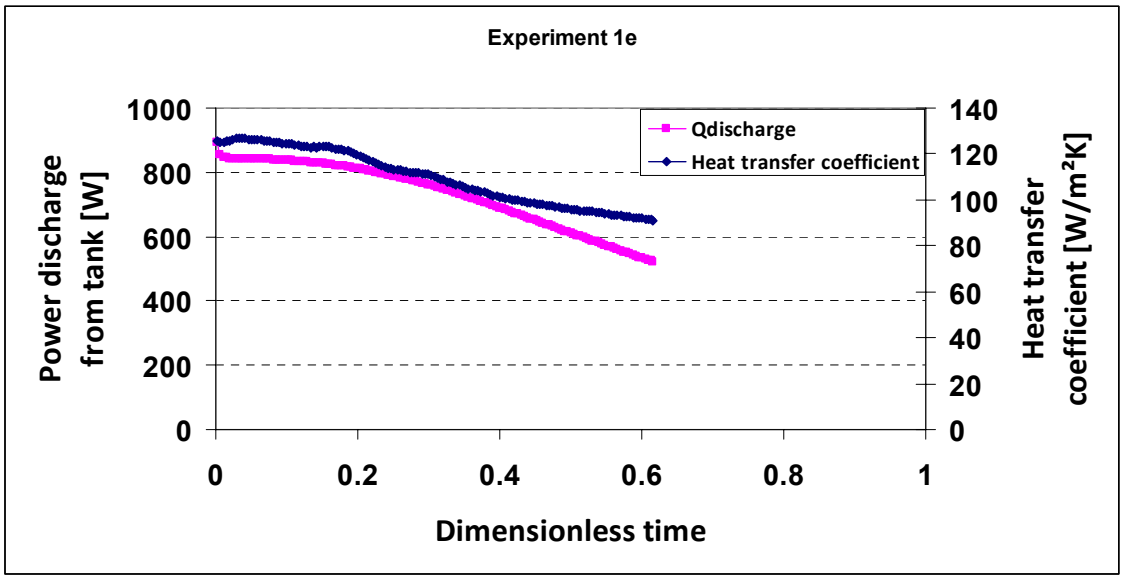

Fig. 2-42b. Power discharge from tank and the heat transfer coefficient for Experiment 1e with a volume flow rate of 0.5 l/min.

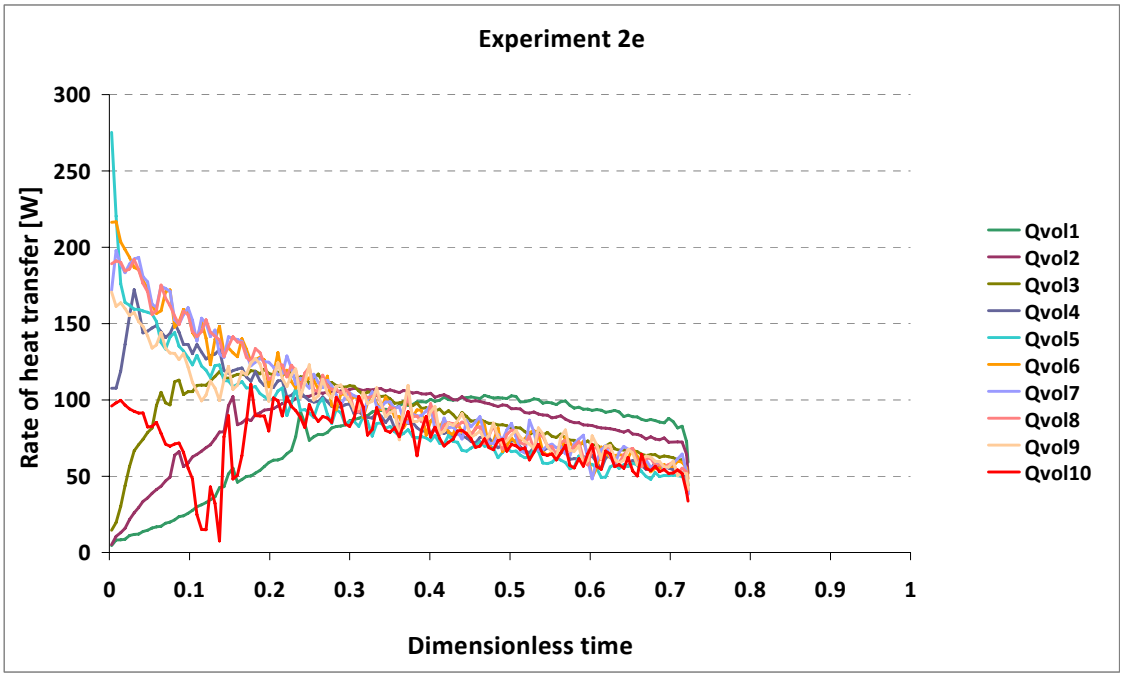

Fig. 2-43a. Heat transfer from each tank volume in Experiment 2e with a volume flow rate of 0.5 l/min.

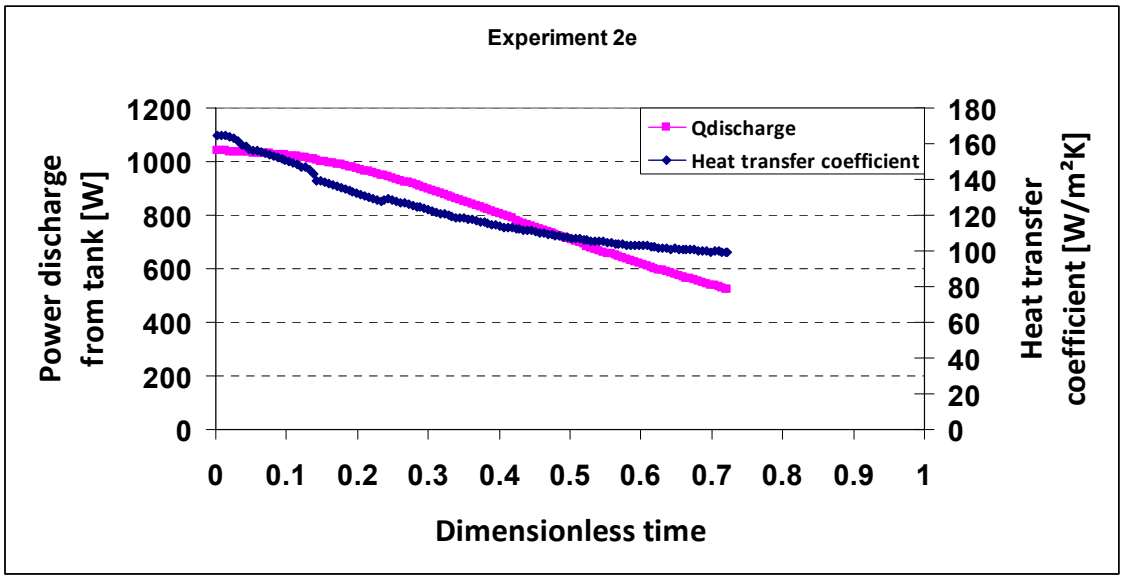

Fig. 2-43b. Power discharge from tank and the heat transfer coefficient for Experiment 2e with a volume flow rate of 0.5 l/min.

2.1.6. Discharge efficiency

By means of the measured inlet and outlet temperatures and the flow rate in the upper mantle, the actual energy amount discharged from the tank Q_1 and the maximum possible discharged energy amount, Q_2 are obtained by Eqs. (2.3) and (2.4), and the discharge efficiency is determined by Eq. (2.6). Ideal discharge efficiency is at dimensionless time or dimensionless volume of 1 equal to 1. Even though the duration of each test is not the same, the influence of the heat loss on the discharge efficiency is low because the tank is well insulated. The discharge efficiency at different discharged volumes are compared for different volume flow rates.
Fig. 2-44 shows the discharge efficiencies as a function of the dimensionless volume discharged from the tank for five different tests: 1a, 2a, 3a, 4a and 5a with volume flow rates of 0.5 l/min, 1 l/min, 2 l/min, 3 l/min and 5 l/min and initially mixed condition of 59-75°C.
It can be seen that for a specific dimensionless volume, the higher the volume flow rate, the lower the discharge efficiency. The decrease of discharge efficiency for higher volume flow rate is due to the worse thermal stratification inside the tank.

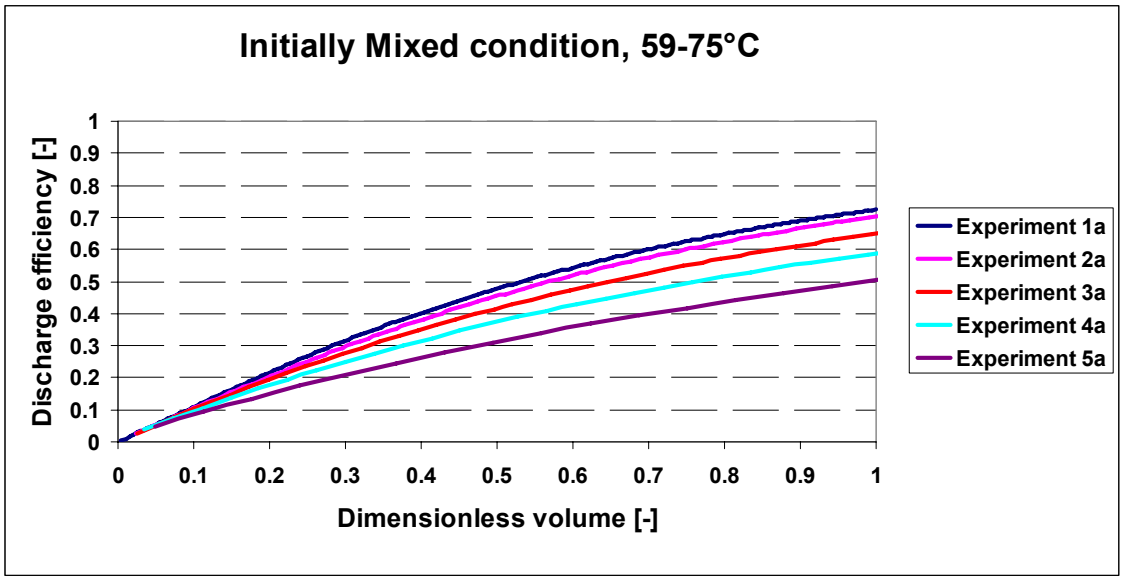

Fig. 2-44. Discharge efficiency as a function of dimensionless volume for five volume flow rates of 0.5 l/min, 1 l/min, 2 l/min, 3 l/min, and 5 l/min.

Fig. 2-45 shows the discharge efficiencies as a function of the dimensionless volume discharged from the tank for five different tests 1b, 2b, 3b, 4b and 5b with the volume flow rates of 0.5 l/min, 1 l/min, 2 l/min, 3 l/min and 5 l/min and initially mixed condition of 45-60°C.
It can be seen that for a specific dimensionless volume, the higher the volume flow rate, the lower the discharge efficiency. The decrease of discharge efficiency for high volume flow rates is due to the worse thermal stratification inside the tank.
From Fig. 2-44 and Fig. 2-45, it is seen that the discharge efficiency is not strongly influenced by the temperature level at the start of discharge.

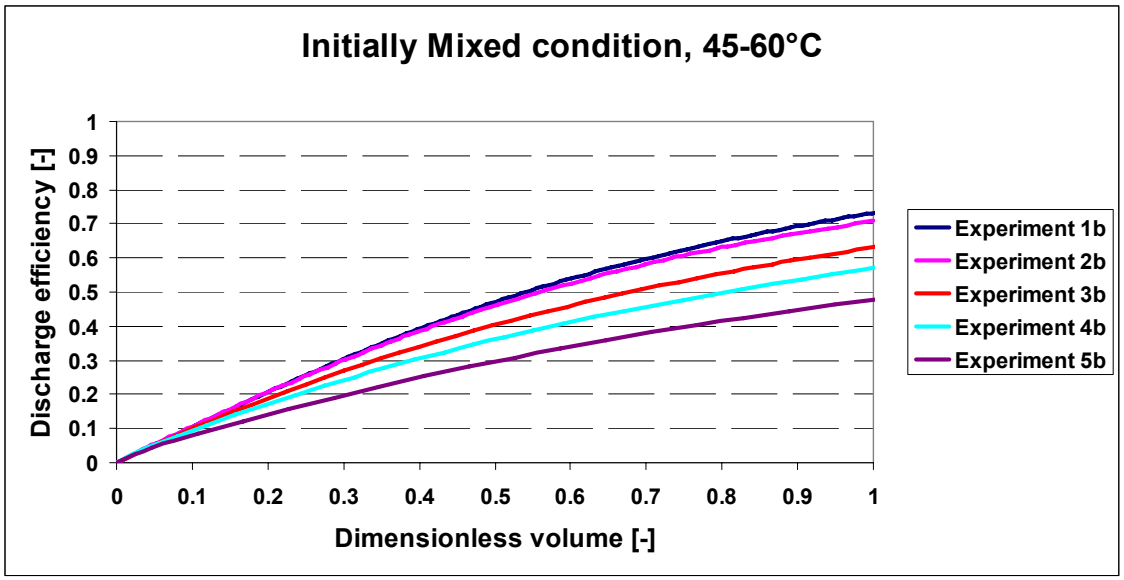

Fig. 2-45. Discharge efficiency as a function of dimensionless volume for five volume flow rates of 0.5 l/min, 1 l/min, 2 l/min, 3 l/min, 5 l/min.

2.2 Thermal experiments of the tank-in-tank heat store

2.2.1 Experimental set up

Fig. 2-46 is a photo of the tested tank-in-tank heat store including dimensions. The data of the tank-in-tank are also given in Table 2-3. A hot loop is used in the experiments connected to the top of the space heating tank. In this way, the store can be heated to the required temperature. The hot loop is by means of a counter flow heat exchanger heated by 27 kW electric heating elements. A cold loop is connected to another open loop which pumps water to the bottom of the DHW tank. The volume flow rate and the inlet temperature of the water, both the hot and the cold are controlled and regulated in a precise way. Fig. 2-47 shows the heating loop and cold water draw off.

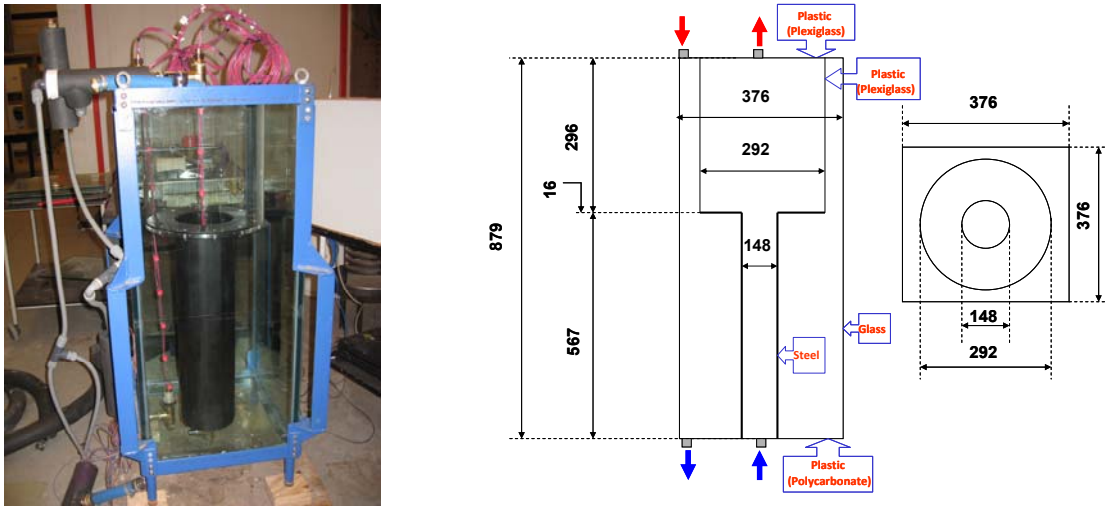

Fig. 2-46. Tank-in-tank heat store photo and inner dimensions.

Table 2-3. Data for the tested tank-in-tank heat store.

Total tank volume, l	124.5
Lower DHW tank volume, l	9.7
Upper DHW tank volume, l	19.8
Space heating volume, l	95
Outside glass thickness, mm	12
Plexiglass thickness, mm	4
Steel thickness, mm	4
Insulation material	Polystyrene
Insulation thickness top, mm	50
Insulation thickness side, mm	50
Insulation thickness bottom, mm	0

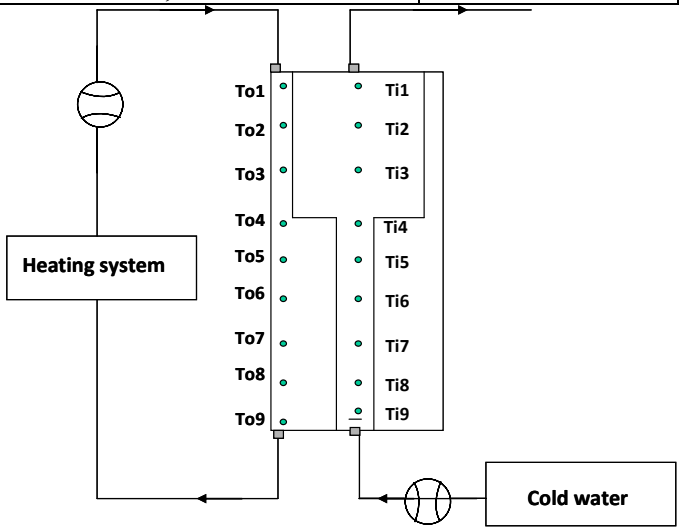

Fig. 2-47. Hot water loop and cold water draw off.

The ambient temperature and the temperatures of the water in the inner and outer tank are measured at eighteen measuring points inside the tank-in-tank heat store by means of copper/constantan thermocouples, Type TT placed in the tank through the top to the bottom of the tank. The temperatures of the water to and from the outer and inner

tank are also measured by means of copper/constantan thermocouples, type TT. The temperature differences between inlet and outlet are measured by copper/constantan thermopiles.
The eighteen temperature sensor positions in the tank and their distance from the bottom of the tank is shown in Fig. 2-48. The accuracy of the measuring thermocouples is estimated to be about ± 0.5 K and for the thermopiles about ± 0.03 K (Ellehauge(1993)).
The cold and hot loop flow rates are measured with two vortex flow meter, type VFS 1-20 from Grundfos. The flow meter has an accuracy of about ± 1.5 %. The data are logged by PC (using the software: IMPVIEW) and two Schlumberger IMP measuring cards (Type 35951C and Type 35952A).

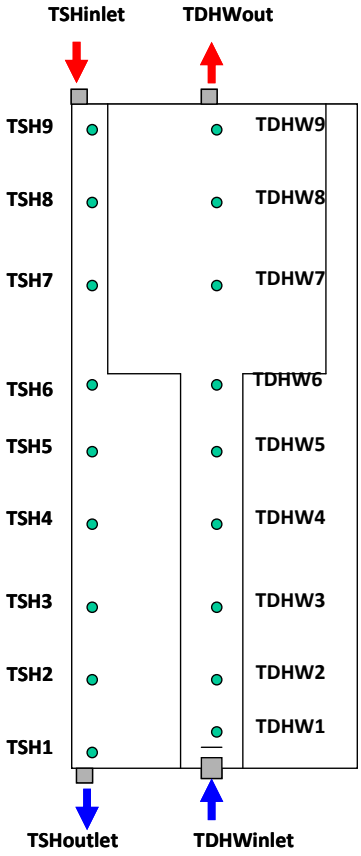

TSH9	84.4	TDHW9	84.4
TSH8	74.4	TDHW8	74.4
TSH7	64.4	TDHW7	64.4
TSH6	54.4	TDHW6	54.4
TSH5	44.4	TDHW5	44.4
TSH4	34.4	TDHW4	34.4
TSH3	24.4	TDHW3	24.4
TSH2	14.4	TDHW2	14.4
TSH1	4.4	TDHW1	6.4

Fig. 2-48. Thermal measuring points and their position in cm from the bottom of tank.

2.2.2 Test conditions

Tests are carried out with three different flow rates of 2.3, 4.0 and 6.5 l/min for the domestic hot water draw off with an inlet temperature of about 20°C to the lower inlet of the DHW tank. These three flow rates corresponds to about 5, 10 and 15 l/min DHW flow rates which are usually tapped in real systems. That is: The upward velocity is the same in the lower part of the inner tank of a typical marketed heat store during a DHW discharge with volume flow rates of 5, 10 and 15 l/min as the upward velocity in the lower part of the inner tank, for the tested heat store with DHW flow rates of 2.3, 4.0 and 6.5 l/min has been used.
The tank is tested with and without insulation material. The store is heated to around 50°C and the domestic hot water discharge tests started after steady state conditions

have been reached. DHW tank discharge tests are carried out; one test with the whole DHW volume discharged and one test with the lower part of the DHW tank discharged, 9.7 l. After the discharge, the tank remains stand still and the measurements are continued. The measured data is logged every one second.
The duration of the test is different from test to test due to the different flow rates. The test conditions are shown in Table 2-4.

Table 2-4. Description of 8 tests.

Test number	Insulation?	Flow rate [l/min]	Volume discharged [l]	Inlet temperature [°C]	Start store temperatures [°C]
1a	Yes	2.3	29.5	20	50
2a	Yes	4.0	29.5	20	50
3a	Yes	6.5	29.5	20	50
1b	No	2.3	29.5	20	50
2b	No	4.0	29.5	20	50
3b	No	6.5	29.5	20	50
1c	Yes	4.0	9.7	20	50
2c	No	4.0	9.7	20	50

2.2.3 Effect of different flow rates

‘‘Experiment 1a-3a’’ [With insulation]

The measured temperatures inside the DHW tank, the space heating tank, the inlet and outlet temperatures for the DHW tank and space heating tank for experiments 1a, 2a, 3a for three different volume flow rates of 2.3, 4.0 and 6.5 l/min and for a tank with insulation are shown in Fig. 2-49a, Fig. 2-49b and Fig. 2-49c.
In experiment 1a, the store is heated to 50°C and after constant temperatures are reached, 29.5 l is discharged through the DHW tank with a volume flow rate of 2.3 l/min. As it is seen from Fig. 2-49a, the temperatures TDHW1-TDHW9 decrease from 50°C to 21-32°C during the discharge. Therefore, thermal stratification is established at the end of the discharge. During the discharge, heat is transferred from the outer tank to the inner tank through the DHW tank wall.
After the whole DHW tank volume is discharged, the tank remains without charge or discharge. The temperatures in the DHW tank increase dramatically in the first period of the stand by period. However, the sharp increase in the temperature profile decreases when the time passes. TDHW1 increases to 39°C and after 4 hr, it decreases to 37.6°C, TDHW2 increases to its maximum temperature of 41°C and after 4 hr, it is 39.7°C, TDHW3 increases to its maximum temperature of 41°C and after 4 hr, it is 41.7°C, TDHW4 increases to its maximum temperature of 43°C and after 4 hr, it is 42.8°C. TDHW5 increases to its maximum temperature of 43.9°C and after 4 hr, it is

43.6°C. TDHW6-TDHW9 increase to their maximum temperatures of about 44°C and after 4 hr, the temperatures remain at about 44°C.
The temperature in the outer tank decreases dramatically during the discharge and during the stand by, the sharp decrease is reduced. At the end of the test TSH1 decreases to its minimum temperature of 34°C, TSH2 decreases to 38°C, TSH3 decreases to 41°C, TSH4 decreases to 42°C, TSH5 decreases to 43.6°C and TSH6-TSH9 remains at 44°C. As seen in Fig. 2-49a, TSH9 fluctuates a lot. It is due to the heat loss through the inlet pipe of the space heating loop. Due to the heat loss from the outer tank, after 3 hr, the DHW temperatures are higher than the temperatures in outer tank in the higher level of the tank.
In experiment 2a, the store is heated to 50°C and after constant temperatures are reached, 29.5 l is discharged through the DHW tank with a volume flow rate of 4.0 l/min. As it is seen from Fig. 2-49b, the temperatures TDHW1-TDHW9 decrease from 50°C to 21-29°C during discharge. Thermal stratification is established during the discharge. During the discharge, heat is transferred from the outer tank to inner tank through the DHW tank wall.
After the whole DHW tank volume is discharged; the tank remains stand still. The temperatures in DHW tank increase dramatically in the first period of the stand by period. However, the sharp increase in the temperature profile decreases when the time passes. TDHW1 increases to 39°C and after 4 hr, it decreases to 37°C, TDHW2 increases to its maximum temperature of 40.6°C and after 4 hr, it is 39.5°C, TDHW3 increases to its maximum temperature of 41.9°C and after 4 hr, it is 41.4°C, TDHW4 increases to its maximum temperature of 42.6°C and after 4 hr, it is 42.3°C. TDHW5 increases to its maximum temperature of 43.2°C and after 4 hr, it is 42.9°C. TDHW6-TDHW9 increase to their maximum temperatures of about 43°C and after 4 hr, the temperatures remain at about 43°C.
The temperature in the outer tank decreases dramatically during the discharge like in experiment 1a and during the stand by, the sharp decrease is lowered down. At the end of the test, TSH1 decreases to its minimum temperature of 35.2°C, TSH2 decreases to 39.4°C, TSH3 decreases to 41.4°C, TSH4 decreases to 42.3°C, TSH5 decreases to 42.9°C and TSH6-TSH9 remains at 43°C. TSH9 fluctuates a lot, due to the heat loss through the inlet pipe of the space heating loop. Due to the heat loss from the outer tank, after 3 hr, the DHW temperatures are higher than the temperatures in the outer tank in the higher level of the tank.
In experiment 3a, the store is heated to 50°C and after constant temperatures are reached, 29.5 l is discharged through the DHW tank with a volume flow rate of 6.5 l/min. As it is seen from Fig. 2-49c, the temperatures TDHW1-TDHW9 decrease from 50°C to 21.4-26.5°C during discharge. Thermal stratification is established during the discharge. During the discharge, heat is transferred from the outer tank to the inner tank of DHW tank through the DHW tank wall.
After the whole DHW tank volume is discharged, the tank remains stand still. The temperature in the DHW tank increases dramatically in the first part of the stand by period. However, the sharp increase in the temperature profile decreases when the time passes. TDHW1 increases to 39.9°C and after 4 hr, it decreases to 38.4°C, TDHW2 increases to its maximum temperature of 41.1°C and after 4 hr, it is 40.2°C, TDHW3 increases to its maximum temperature of 41.9°C and after 4 hr, it is 41.7°C, TDHW4 increases to its maximum temperature of 42.3°C and after 4 hr, it is 42.5°C. TDHW5 increases to its maximum temperature of 42.4°C and after 4 hr, it is 43.1°C. TDHW6-TDHW9 increase to their maximum temperatures of about 43.6°C and after 4 hr, the temperatures are about 43.2°C.

The temperature in the outer tank decreases dramatically during the discharge like in experiment 1a and experiment 2a and after that the sharp decrease is lowered down during the stand by period. At the end of the test TSH1 decreases to its minimum temperature of 36.6°C, TSH2 decreases to 40.1°C, TSH3 decreases to 41.8°C, TSH4 decreases to 42.5°C, TSH5 decreases to 43°C and TSH6-TSH9 remains at 43.1°C. TSH9 fluctuates a lot due to the heat loss through the inlet pipe of the space heating loop. Due to the heat loss of the outer tank, after 3 hr, the DHW temperatures are higher than the SH temperatures in the outer tank in the higher level of the tank.

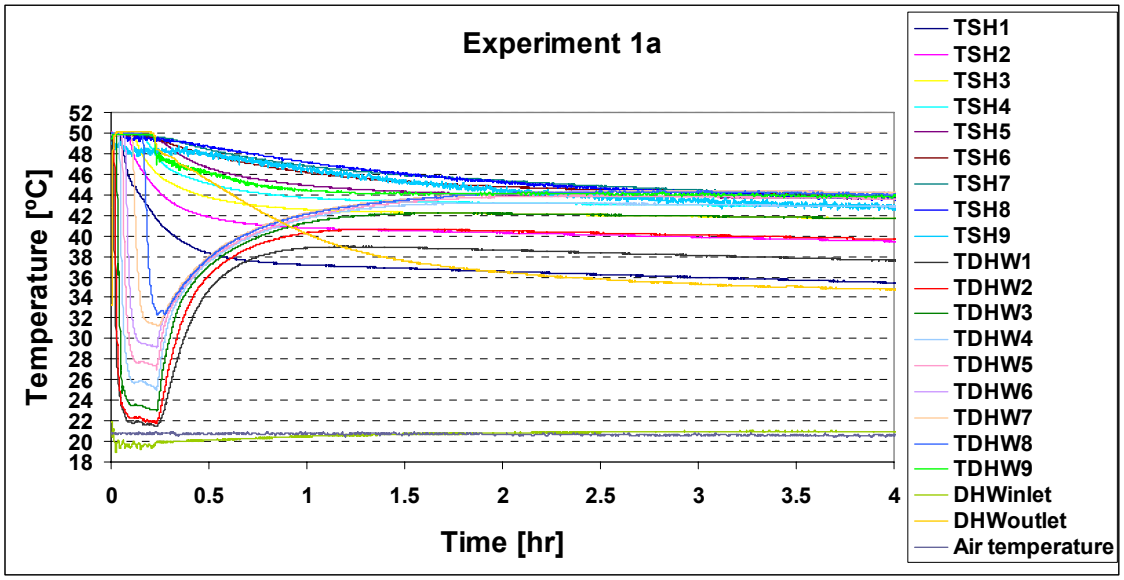

Fig. 2-49a. Temperatures for experiment 1a with a DHW volume flow rate of 2.3 l/min and tank insulation.

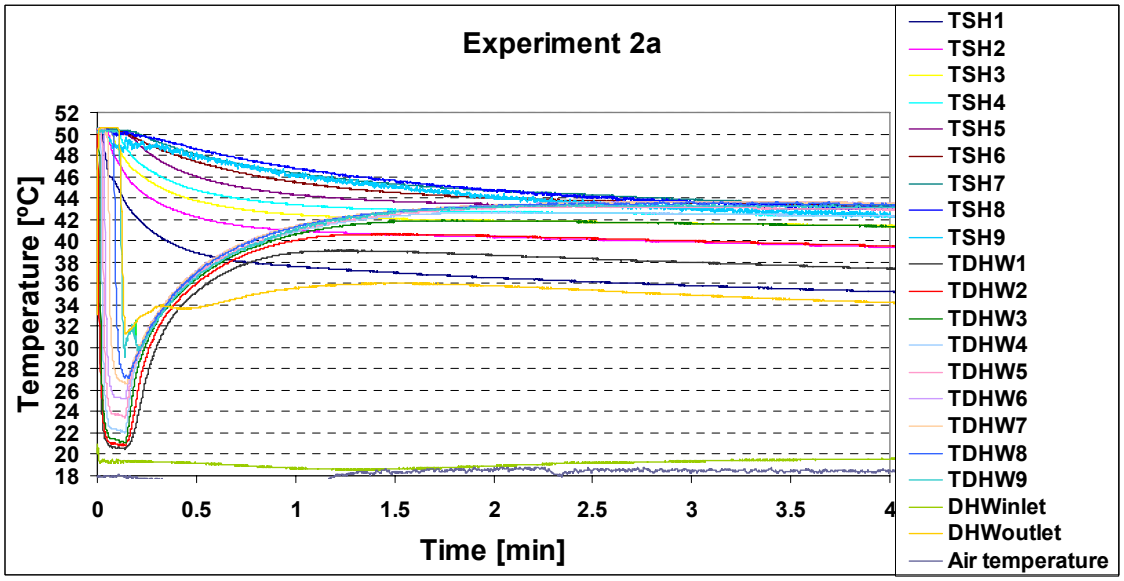

Fig. 2-49b. Temperatures for experiment 2a with a DHW volume flow rate of 4 l/min and tank insulation.

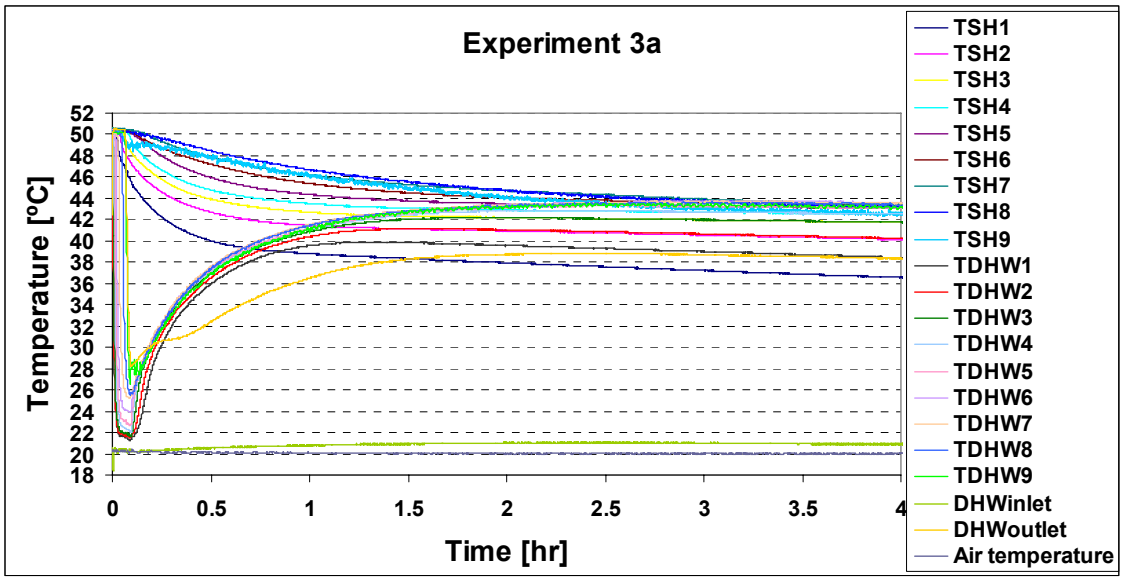

Fig. 2-49c. Temperatures for experiment 3a with a DHW volume flow rate of 6.5 l/min and tank insulation.

Comparing the tests with three flow rates of 2.3, 4.0 and 6.5 l/min during discharge show that the temperatures in the outer tank is a little bit higher for experiment 3a than experiments 2a and 1a. The difference between TSH1 and TSH9 is higher for experiment 1 than experiment 2a and 3a after four hours. Consequently, there is higher thermal stratification in the outer tank in experiment 1a than in experiments 2a and 3a. The reason for higher thermal stratification is due to the fact that the lower inlet flow rate to the tank is, the lower is the mixing in the inner tank and the more even is the heat transfer from the outer side resulting in a higher thermal stratification.

‘‘Experiment 1b-3b’’ [Without insulation]

The measured temperatures inside the DHW tank, the space heating tank, the inlet and outlet temperatures for the DHW tank and space heating tank for experiments 1b, 2b, 3b for three different volume flow rates of 2.3, 4.0 and 6.5 l/min and for a tank without insulation are shown in Fig. 2-50a, Fig. 2-50b and Fig. 2-50c.
In experiment 1b, like experiment 1a, 2a and 2c, the store is heated to 50°C and after constant temperatures are reached, 29.5 l is discharged from the DHW tank with volume flow rate of 2.3 l/min.
As it is seen from Fig. 2-50a, the temperatures TDHW1-TDHW9 decrease from 50°C to 22.4-36.6°C during the discharge. Thermal stratification is established during the discharge. Heat is transferred from the outer tank to the inner tank through the DHW tank wall.
After the whole DHW tank volume is discharged, the tank remains stand still. The temperatures in the inner tank increase dramatically in the first part of the stand by period. However, the sharp increase in the temperature profile decreases when the time passes. TDHW1 increases to 36.8°C and after 4 hr, it decreases to 33°C, TDHW2 increases to its maximum temperature of 38.2°C and after 4 hr, it is reduced to 34.5°C, TDHW3 increases to its maximum temperature of 39.2°C and after 4 hr, it is 36°C, TDHW4 increases to its maximum temperature of 39.6°C and after 4 hr, it is 36.7°C. TDHW5 increases to its maximum temperature of 40°C and after 4 hr, it is

37°C. TDHW6-TDHW9 increase to their maximum temperatures of about 38°C and after 4 hr, the temperatures remain at about 38°C.
The temperature in the outer tank decreases dramatically during the discharge and after that the sharp decrease is lowered down during the stand by period. At the end of the test TSH1 decreases to its minimum temperature of 31.4°C, TSH2 decreases to 34.1°C, TSH3 decreases to 35.7°C, TSH4 decreases to 36.3°C, TSH5 decreases to 36.6°C and TSH6-TSH9 remains at 36.8°C. TSH9 fluctuates a lot. It is due to the heat loss from the inlet pipe of the space heating loop. Due to the heat loss of the outer tank, after 3 hr, the DHW temperatures are higher than the temperatures in the outer tank in the higher level of the tank. The temperatures in the outer and inner tank are lower than experiment 1a which is because the tank is not insulated.
In experiment 2b, as it is seen from Fig. 2-50b, the temperatures TDHW1-TDHW9 decrease from 50°C to 21.4-29.6°C during the discharge. Thermal stratification is established during the discharge.
After the whole DHW tank volume is discharged, the tank remains stand still. The temperatures in the inner tank increase dramatically in the first part of the stand by period. However, the sharp increase in the temperature profile decreases when the time passes. TDHW1 increases to 37.7°C and after 4 hr, it is decreased to 33.8°C, TDHW2 increases to its maximum temperature of 38.8°C and after 4 hr, it is 35.2°C, TDHW3 increases to its maximum temperature of 39.5°C and after 4 hr, it is 36.5°C, TDHW4 increases to its maximum temperature of 39.7°C and after 4 hr, it is 37.1°C. TDHW5 increases to its maximum temperature of 39.8°C and after 4 hr, it is 37.4°C. TDHW6-TDHW9 increase to their maximum temperatures of about 40.1°C and after 4 hr, the temperatures remain at about 38.2°C.
The temperatures in the outer tank decrease dramatically during the discharge and after that the sharp decrease is lowered down during the stand by period. At the end of the test TSH1 is decreased to its minimum temperature of 32.3°C, TSH2 decreases to 34.8°C, TSH3 decreases to 36.2°C, TSH4 decreases to 36.6°C, TSH5 decreases to 36.9°C and TSH6-TSH9 remains at 37.1°C. TSH9 fluctuates a lot due to the heat loss through the inlet pipe of the space heating loop. Due to the heat loss from the outer tank, after 3 hr, the DHW temperatures are higher than the SH temperatures in the outer tank in the higher level of the tank. The temperatures in the outer and inner tank are lower than in experiment 2a because the tank is not insulated.
In experiment 3b, as it is seen from Fig. 2-50c, the temperatures at TDHW1-TDHW9 decrease from 50°C to 21.5-35.6°C during the discharge. Thermal stratification is established during the discharge.
After the whole DHW tank volume is discharged, the tank remains stand still. The temperatures in the DHW tank increases dramatically in the first part of the stand by period. However, the sharp increase in the temperature profile decreases when the time passes. TDHW1 increases to 39°C and after 4 hr, it decreases to 34.8°C, TDHW2 increases to its maximum temperature to 40°C and after 4 hr, it reduces to 36.1°C, TDHW3 increases to its maximum temperature of 40.6°C and after 4 hr, it is 37.2°C, TDHW4 increases to its maximum temperature of 40.8°C and after 4 hr, it is 37.7°C. TDHW5 increases to its maximum temperature of 40.9°C and after 4 hr, it is 38°C. TDHW6-TDHW9 increase to their maximum temperatures of about 41.1°C and after 4 hr, the temperatures are about 39.1°C.
The temperatures in the outer tank decrease dramatically during the discharge and after that the sharp decrease is lowered down during the stand by period. At the end of the test TSH1 decreases to its minimum temperature of 33.3°C, TSH2 decreases to 35.7°C, TSH3 decreases to 36.9°C, TSH4 decreases to 37.3°C, TSH5 decreases to

37.5°C and TSH6-TSH9 remains at 37.5°C. TSH9 fluctuates a lot due to the heat loss from the inlet pipe of the space heating loop. Due to the heat loss from the outer tank, after 3 hr, the DHW temperatures are higher than the temperatures in the outer tank in the higher level of the tank.

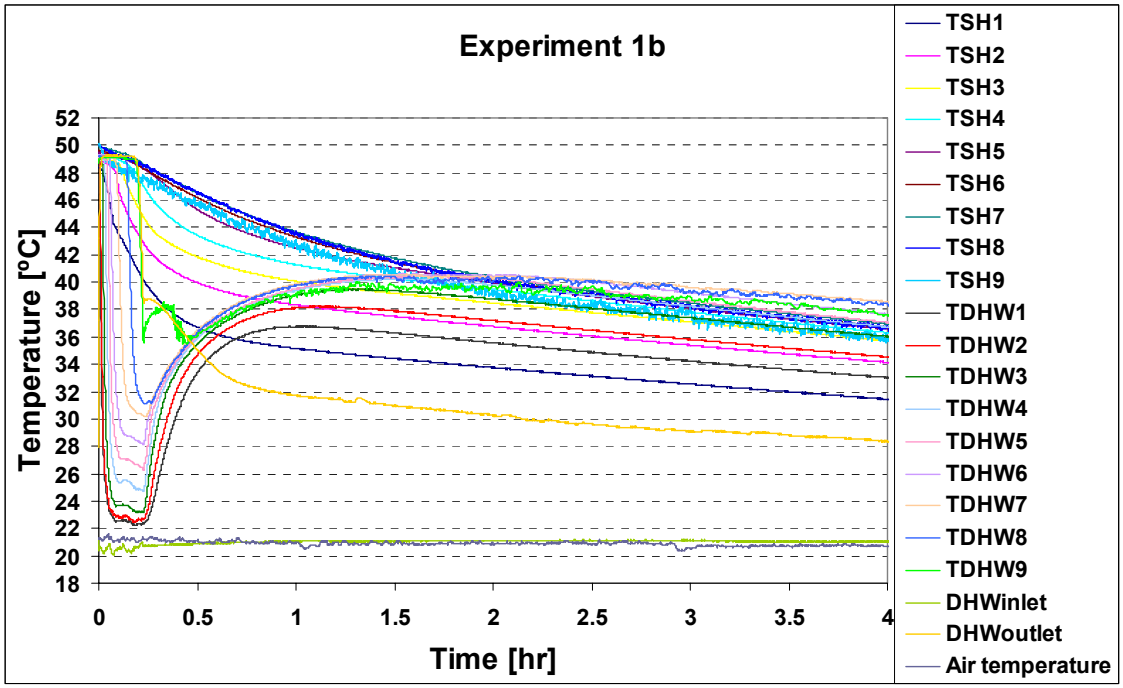

Fig. 2-50a. Temperatures for experiment 1b with a DHW volume flow rate of 2.3 l/min and uninsulated tank.

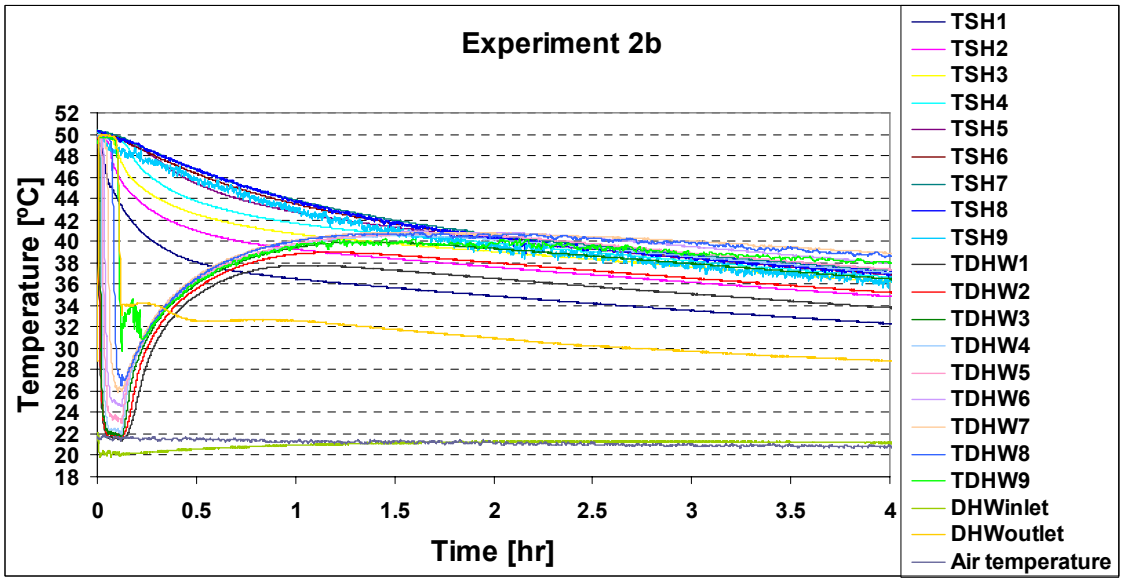

Fig. 2-50b. Temperatures for experiment 2b with a DHW volume flow rate of 4 l/min and uninsulated tank.

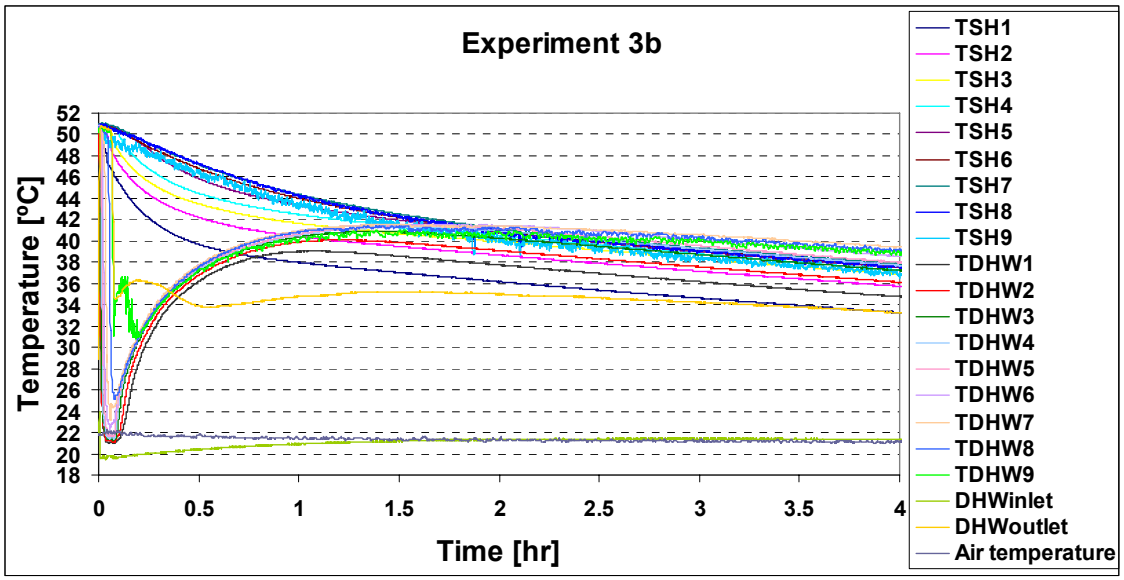

Fig. 2-50c. Temperature for experiment 1b with a DHW volume flow rate of 6.5 l/min and uninsulated tank.

The temperature level in the outer and inner side of the tank are lower in experiments 1b, 2b and 3b than in experiment 1a, 2a and 3a which due to the uninsulated tank. The tests show that less insulation causes lower degree of thermal stratification in the tank.

''Experiment 1c-2c'' [With and without insulation]

Two tests were carried out with a domestic hot water draw off volume flow rate of 4 l/min and a total hot water draw-off of 9.7 lit. The tank was with and without insulation.
In experiment 1c, the tank is heated up to 50°C and the tank is insulated. As it is seen from Fig. 2-51a, the temperatures TDHW1-TDHW6 decrease from 50.3°C to 22°C, 22.2°C, 23°C, 26°C, 30°C and 39.4°C during discharge. TDHW7-TDHW9 remains more or less at the same temperature at about 50.3°C. That is the temperature at the upper part of the DHW tank remains at 50.3°C and in the lower part of DHW tank, thermal stratification is built up.
After discharge, the tank remains stand still. It can be seen that TDHW1-TDHW6 increases dramatically in the first part of the stand by period. However, the sharp increase in the temperature profile decreases when the time passes. TDHW1 increases to 43.2°C and after 4 hr, it is decreased to 41.4°C, TDHW2 increases to its maximum temperature of 45°C and after 4 hr, it is reduced to 43.8°C, TDHW3 increases to its maximum temperature of 46.8°C and after 4 hr, it is 46°C, TDHW4 increases to its maximum temperature of 48.2°C and after 4 hr, it is 47.5°C. TDHW5 increases to its maximum temperature of 49.2°C and after 4 hr, it is 48.2°C. TDHW6 increases to its maximum temperature of 49.7°C and after 4 hr, it is 48.6°C. TDHW7-TDHW9 remains during the whole test at high level. After 4 hr, the temperatures are about 48.8°C.
The temperature in the outer tank decreases dramatically during the discharge and after that the sharp decrease is lowered down during the stand by period. At the end of the test TSH1 is decreased to its minimum temperature of 39.1°C, TSH2 decreases to 43.6°C, TSH3 decreases to 46.1°C, TSH4 decreases to 47.5°C, TSH5 decreases to

48.2°C, TSH6 decreases to 48.2°C and TSH7-TSH9 remains at 48.3°C. TSH9 fluctuates a lot due to the heat loss from the inlet pipe of the space heating loop. Due to the heat loss in the space heating tank, after 3 hr, the DHW temperatures are higher than the temperatures in the outer tank in the higher level of the tank.
In experiment 2c, the insulated tank is heated up to 50°C. As it is seen from Fig. 2-51b, the temperatures TDHW1-TDHW6 decrease from 50.3°C to 23.1°C, 23.6°C, 25.2°C, 28.6°C, 34.6°C and 49.5°C during the discharge. TDHW7-TDHW9 remains more or less at the same temperature of about 50.5°C. That is the temperature at the upper part of the DHW tank remains at 50.5°C and in the lower part of the DHW tank, thermal stratification is built up.
After the discharge, the tank remains stand still. TDHW1-TDHW6 increases dramatically in the first part of the stand by period. The sharp increase in the temperature profile decreases when the time passes. TDHW1 increases to 42.5°C and after 4 hr, it decreases to 37.1°C, TDHW2 increases to its maximum temperature to 44.4°C and after 4 hr, it is 38.9°C, TDHW3 increases to its maximum temperature to 46.5°C and after 4 hr, it is 40.6°C, TDHW4 increases to its maximum temperature to 47.7°C and after 4 hr, it is 41.3°C. TDHW5 increases to its maximum temperature to 48.3°C and after 4 hr, it is 41.7°C. TDHW6 increases to its maximum temperature to 49.2°C and after 4 hr, it is 42.4°C.However, TDHW7-TDHW9 remains at about 50°C and after 4 hr, the temperatures are about 44°C.
The temperatures in the outer tank decrease dramatically during the discharge and after that the sharp decrease is lowered down during the stand by period. At the end of the test TSH1 decreases to its minimum temperature of 35.2°C, TSH2 decreases to 38.5°C, TSH3 decreases to 40.2°C, TSH4 decreases to 40.8°C, TSH5 decreases to 41.2°C, TSH6 decreases to 41.3°C and TSH7-TSH9 remains at 41.5°C. TSH9 fluctuates a lot due to the heat loss from the inlet pipe of the space heating loop. Due to the heat loss of the outer tank, after 3 hr, the DHW temperatures are higher than the temperatures in the outer tank in the higher level of the tank.

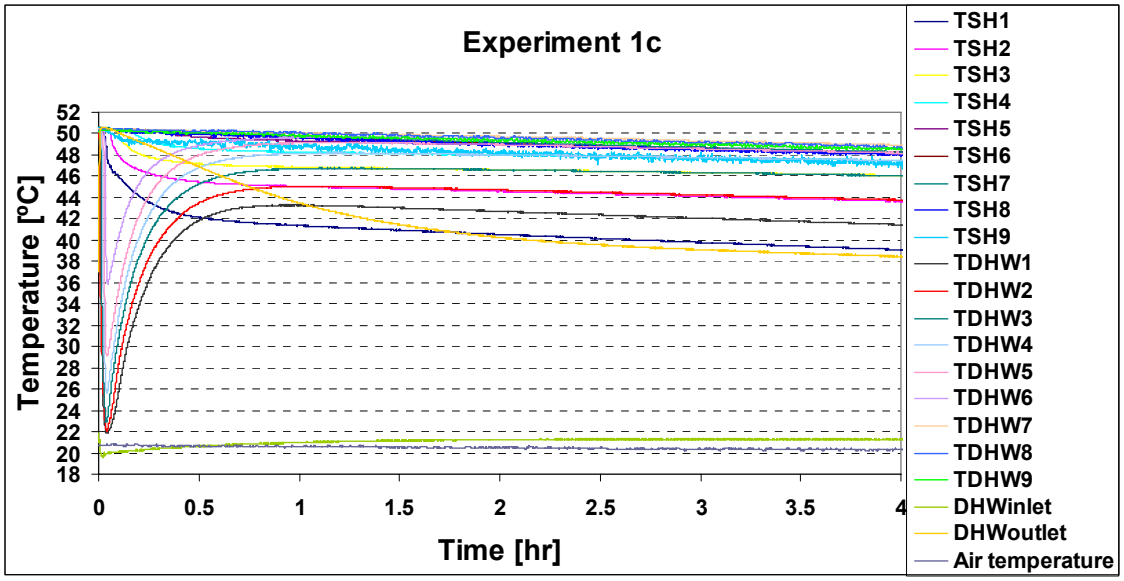

Fig. 2-51a. Temperatures for experiment 1c with a DHW volume flow rate of 4 l/min, a volume discharge of 9.7 l, and an insulated tank.

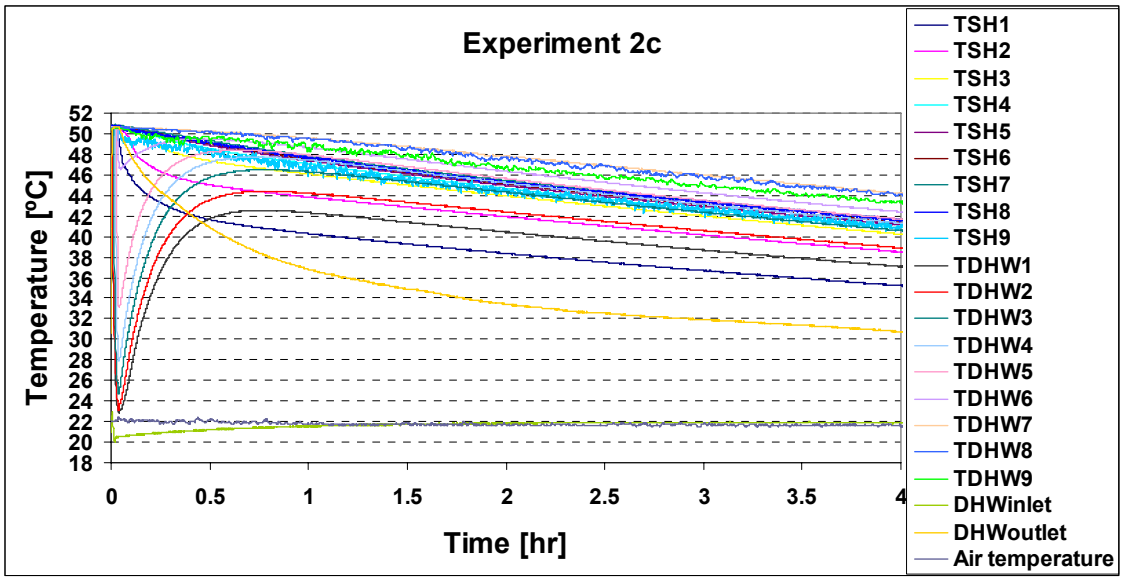

Fig. 2-51b. Temperatures for experiment 2c with a DHW volume flow rate of 4 l/min, a volume discharge of 9.7 l and an uninsulated tank.

The temperature levels in experiment 1c are higher than in experiment 2c because the tank is insulated in experiment 1c. The thermal stratification in the inner tank is slightly higher for test 1c than 2c after 4 hours. The temperature difference between TDHW1 and TDHW9 is about 6.5 K for the tank without insulation while it is about 7.3 K for the insulated tank. However for the outer tank, there is a somewhat higher thermal stratification in experiment 2c than in experiment 1c, even though the temperature level in the tank without insulation is lower than for the tank with insulation. The temperature difference between TSH1 and TSH9 is about 8.1 K for the tank without insulation while it is about 5.7 K for the tank with insulation. This is caused by the higher heat loss for the uninsulated tank which makes a higher thermal stratification possible in the tank.

2.3 Summary

In this chapter, it was investigated how different discharge volume flow rates through the upper mantle influence the thermal stratification and the thermal behavior of a bikini tank. A wide range of discharge tests was carried out in a heat storage test facility. The experiments showed that when the discharge volume flow rate through the upper mantle is high, thermal stratification inside the tank is destroyed. For low volume flow rates, thermal stratification can be created at the beginning of the test but thermal stratification is destroyed at the end of the test. The duration of the period in which thermal stratification is created is increasing for decreasing volume flow rates. The thermal behavior of the bikini tank during the discharge through the upper mantle is not strongly influenced by the temperature level of the tank and of temperature level of the water flowing into the upper mantle.
The discharge efficiencies of the bikini tanks are also measured for two different initially mixed conditions. It is shown that the discharge efficiencies for both temperature levels are similar to each other. The discharge efficiency is influenced by

the volume flow rate. The higher the volume flow rate, the lower the discharge efficiency.
A tank-in-tank store was also investigated with different DHW discharge volume flow rates of 2.3, 4.0 and 6.5 l/min. The thermal stratification of the tank was also investigated after the discharge. The results showed that thermal stratification is higher for lower DHW discharge volume flow rates compared to higher volume flow rates. The temperature level in the tank is of course lower for the tank without insulation than for a tank with insulation.

3 CFD calculations and PIV measurements on tank-in-tank heat store

3.1 Introduction

Theoretical investigations of a tank-in-tank heat storage for a solar combisystem have been carried out. The investigated combi store is designed for PIV measurement studies. The theoretical investigations are carried out by means of the Computational Fluid Dynamics CFD code Fluent 6.1 (2003). A schematic picture of the heat storage is shown in Fig. 3-1. The tank-in-tank heat storage is a tank where the domestic hot-water (DHW) tank is placed in the space heating storage tank. The space heating storage tank is heated by the solar heat by circulating water through the outer tank. Heat is transferred from the space heating storage tank to the DHW tank through the tank wall of the DHW tank.

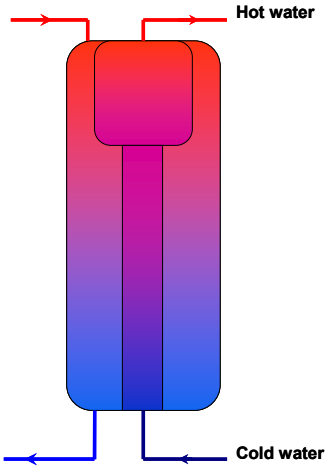

Fig. 3-1. Schematic picture of the tested tank-in-tank heat store

A model of the heat storage tank used for experimental studies has been built up in the CFD program. The fluid motion and the thermal conditions for the heat store have been investigated during different operation conditions. It has been analyzed how the thermal stratification in the space-heating storage and DHW tank during periods with hot water consumption is influenced by different flow rates during hot water draw-off.

3.2 Investigated tank-in-tank store

In Fig. 3-2, a picture of the investigated tank-in-tank heat store is shown. Three different materials are used for the tank-in-tank heat store. The upper part of the DHW tank is made from plastic. The lower part with smaller diameter is made of steel. The outer wall of the tank is made of glass. The store is heated up from the top to the bottom in the outer tank and can be discharged from the inner tank (DHW tank).

Fig. 3-2. Picture of the tank-in-tank heat store. The inner tank is for domestic hot water, whereas the outer tank is for water for space heating.

Table 3-1 shows the volume of space heating, domestic water in the heat store and the total volume respectively.

Table 3-1. The volume of domestic water and water for space heating in the tank.

	Volume [l]
Domestic water, upper level	9.7
Domestic water, lower level	19.8
Water for space heating	94.8
Total	124.3

The tank-in-tank heat store dimensions are shown in Fig. 3-3 at a vertical and a horizontal section, respectively. All dimensions are the inside diameter. The outside glass thickness is 12 mm and the inside plastic thickness is 4 mm.

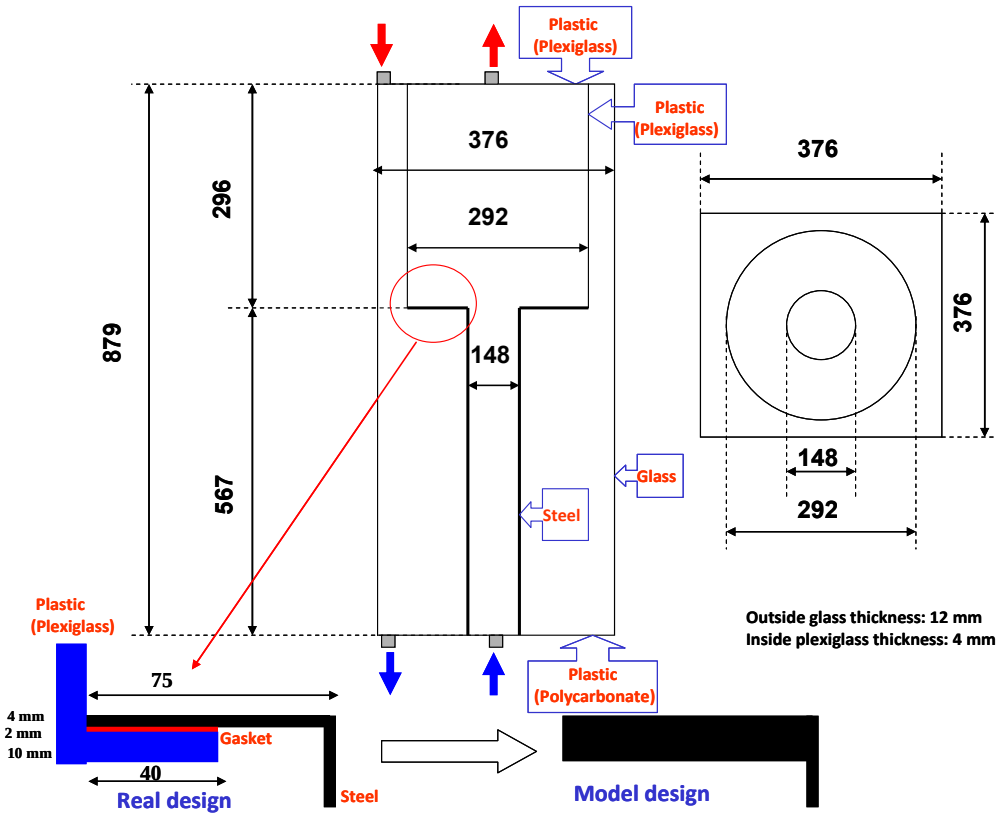

Fig. 3-3. Tank-in-tank heat storage dimensions. The dimensions are inside diameter.

3.3 CFD model of tank-in-tank

A model of the heat store has been built in Gambit. A number of simplifications have been made so that in FLUENT the final model of the heat store is somewhat simpler than the real heat store.

The contact between the lower and upper wall material is in the CFD model simplified to a simpler geometry. Therefore, the thermal property of such a geometry is obtained and used for the simulations. Table 3-2 shows the thermal properties of the materials used in the model.

The model contains the water in the tank with the space heating section and the water in the inner domestic hot water tank. With the model it is possible to investigate how thermal stratification both in the inner and outer tank are established, and how the heat transfer into the domestic water will be during different operation conditions. Further, it is possible to investigate the natural convection in both tanks.

Table 3-2. Thermal properties of the used material in the model.

Material	Density [kg/m³]	Cp [J/kg·K]	Thermal conductivity [W/m·K]
Glass	840	2250	1
Plastic (Polycarbonate)	1200	1170	0.21
Plastic (Plexiglass)	950	1880	0.43
Steel	7830	434	64
Steel-plastic combined	2682	1070	0.67

3.3.1 Grid distribution of model

In FLUENT the model of the heat store is divided into a computational mesh composed of small cells. One forth of the tanks is selected for the simulations because the geometry is symmetrical and it reduces the computational time. Fig. 3-4 shows the geometry of the model made in Gambit.

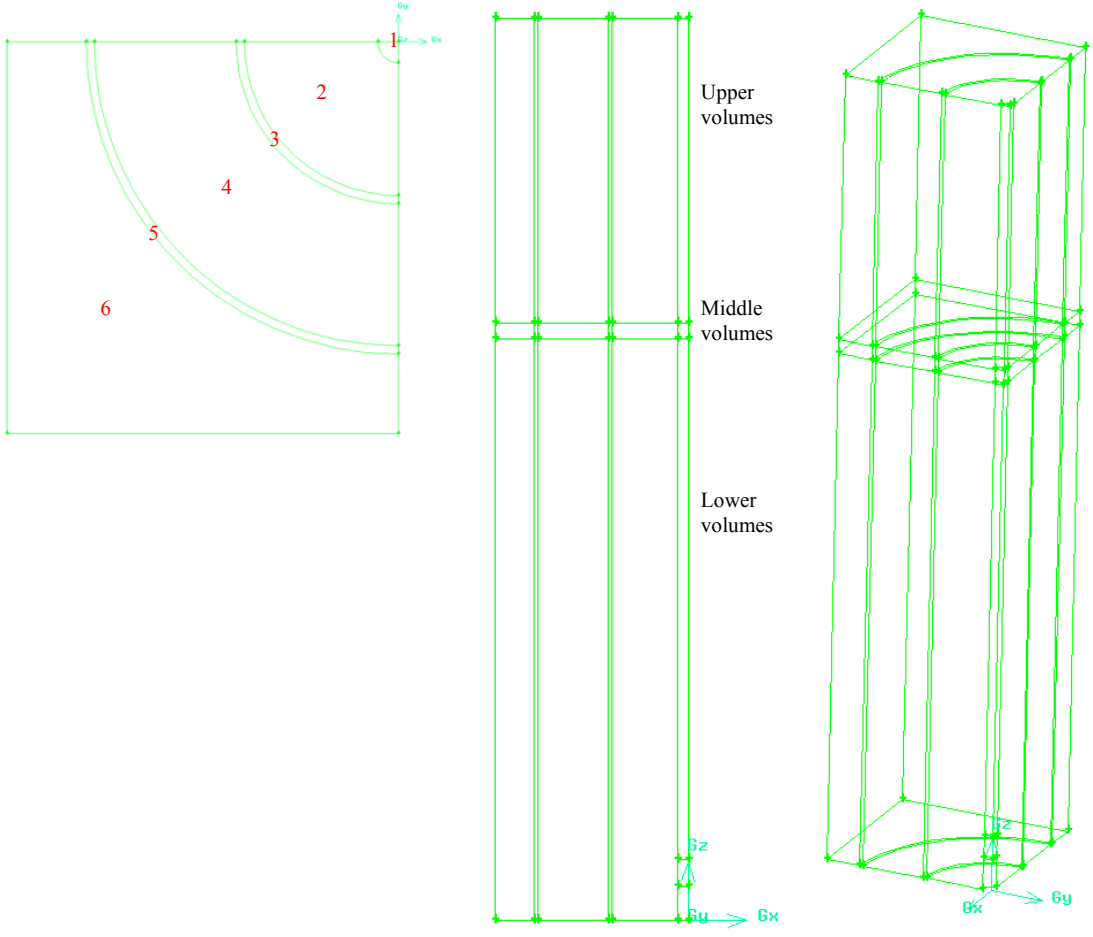

From the top | From side | Three dimensional geometry

Fig. 3-4. The tank geometry made in Gambit.

The inlet and outlet to and from the DHW tank is located exactly at the middle of the DHW tank. The store volume is divided to many other volumes, so that the Cooper

method that is used for meshing the geometry is applicable to the tank and also for defining the three different tank materials which are used for the tank. The inner and outer tanks as well as the tank materials are included in the model.
As it is seen from the top in Fig. 3-4, there are 6 faces that are meshed. The inlet and outlet to the tank has denser mesh than the other parts of the tank. Boundary layers are first applied to the inner and outer wall of the inner tank with first row of 0.2 mm and growth rate of 1.2 due to having denser mesh close to the tank walls. The inlet, face 1, is first meshed with the Pave scheme with the interval size of 4 mm. Face 2 is meshed with the Pave scheme and interval size of 2mm. Face 3 which is a wall thickness is meshed with Map scheme with the interval size of 5 mm. Face 4 is meshed with the Pave scheme and interval size of 1 mm. Face 5 which is a wall, is meshed with Map scheme with the interval size of 5 mm. And finally Face 6 which is an outer surface is meshed with the Pave method with the interval size of 4 mm. All Faces 1 to 6 are located at middle volume part shown in Fig. 3-4. Therefore, the Cooper method is used to mesh the middle, the lower and the upper volume. First the middle volume is meshed, then the lower and finally the upper volume with the Hex-Cooper method with the interval size of 4 mm. Totally, 1167859 cells are used and checked in Gambit as shown in Fig. 3-5. The worst meshed element is found to have a skewness angle of 0.44. The skewness angle is a criteria that is between 0 to 1 and the lower this value is, the better the quality of mesh will be. Therefore the mesh quality is determined to be good enough for the CFD calculations in FLUENT.

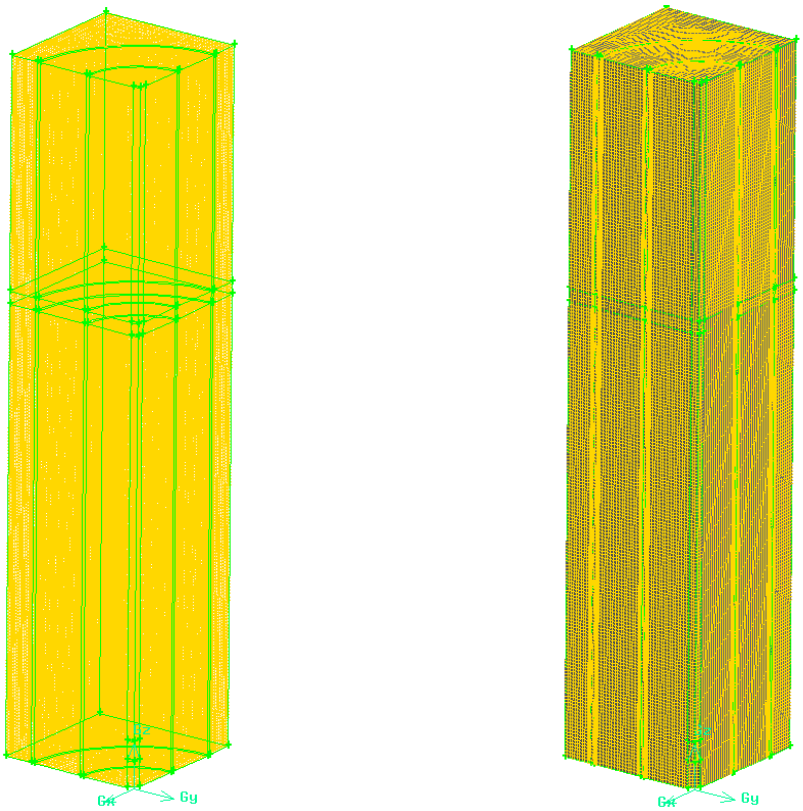

Fig. 3-5. Model with the built mesh

3.3.2 Boundary conditions

The inlet water of the DHW tank which is located at the bottom of the tank is chosen as a velocity inlet and for the outlet, the outflow option is chosen as shown in Fig. 3-6.

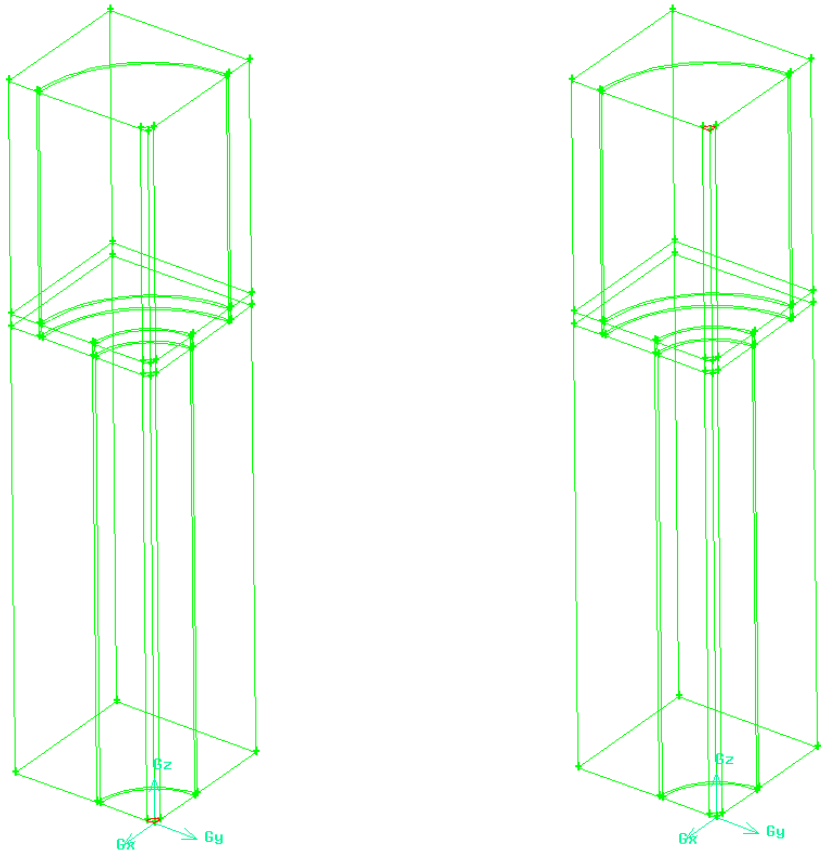

Fig. 3-6. Inlet as velocity inlet(left) and outlet as outflow (right)

Since the model is ¼ of the real geometry, it is needed to define some surfaces in Gambit as interface so that in FLUENT, periodic condition could be applied. The tank surfaces are divided into some interfaces named as the innertank_water, outertank_water, lower wall_steel, upperwall_plastic and middlewall_plastic_steel as shown in Fig. 3-7. It should also be mentioned that the same boundary condition is selected for the same symmetric geometry on the other side of the tank named number 2. Both 1 and 2 symmetric interfaces are connected together by making a periodic condition in FLUENT to simulate the whole tank. Therefore, the symmetric interfaces are rotated 270 degrees to make a model of a real tank.

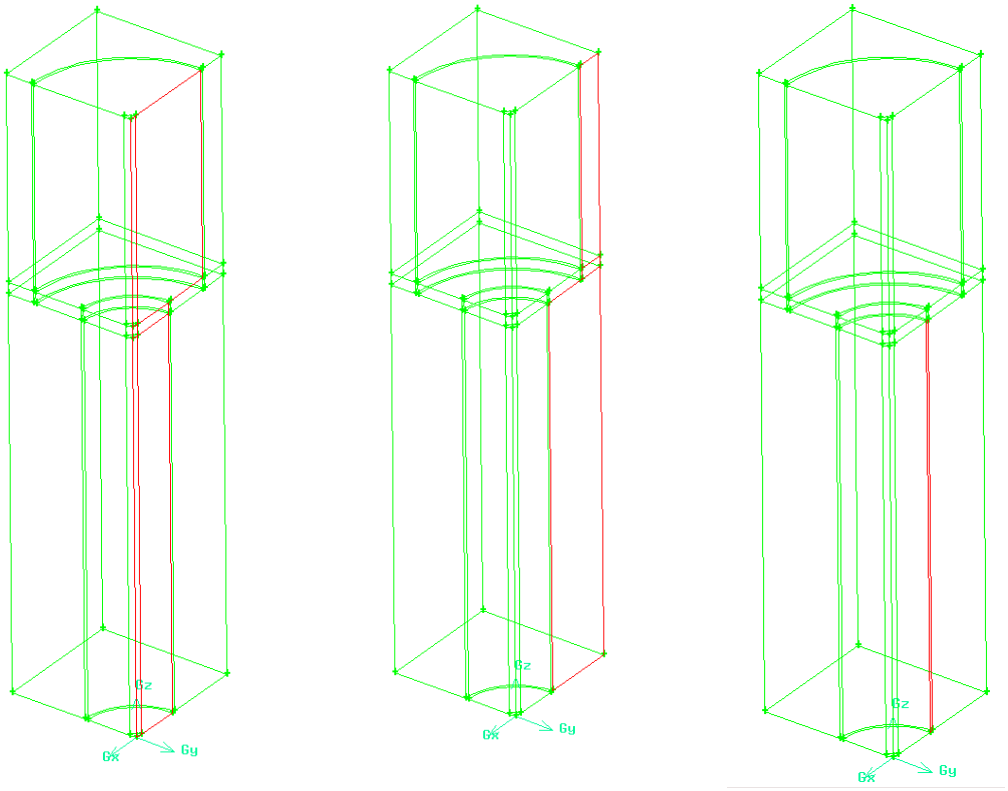

a. innertank_water b. Outertank_water c. lowerwall_steel

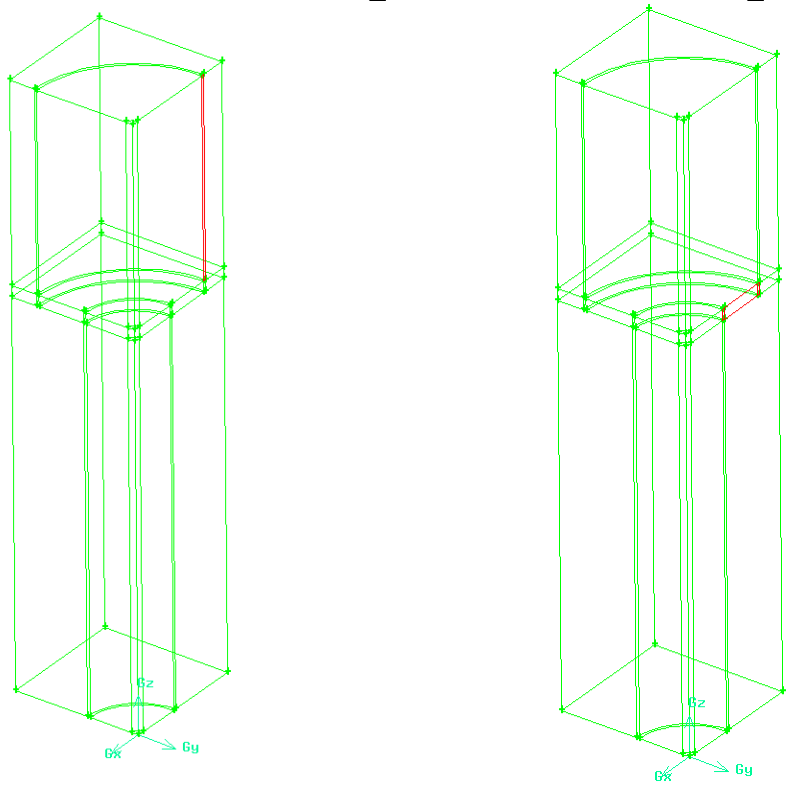

c. upperwall_steel d. middlewall_plastic_steel

Fig. 3-7. Tank interfaces

The bottom, top and side walls are defined separately as a wall as shown in Fig. 3-8.

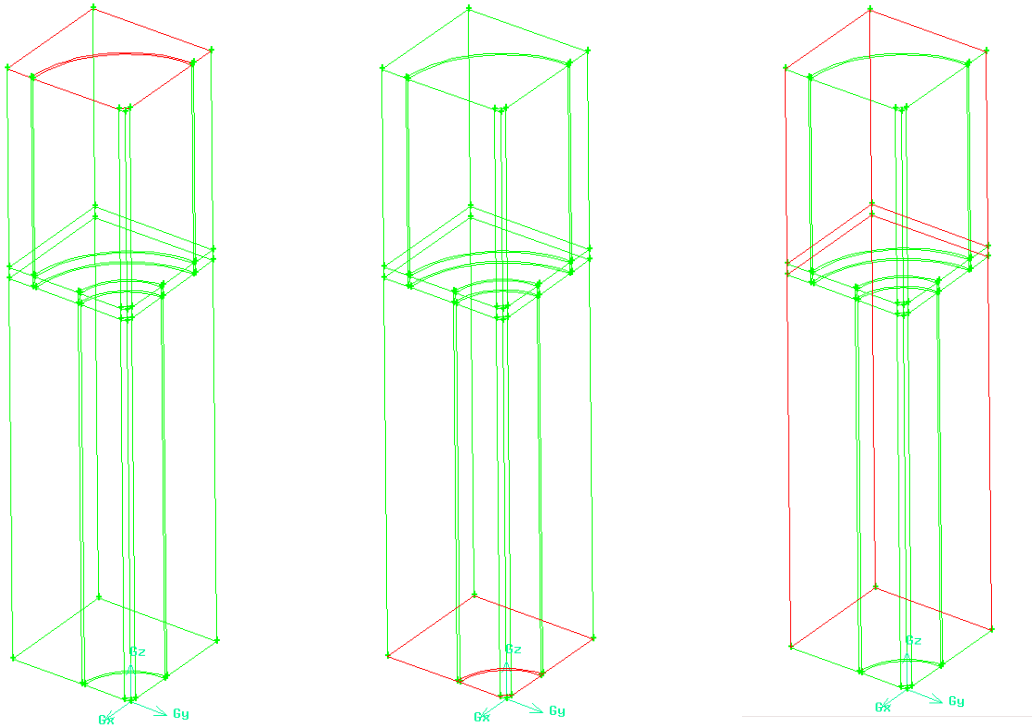

Fig. 3-8. Top wall (left), bottom wall (middle) and side wall (right)

The upper wall is divided to two inner and outer surfaces, the lower wall is also divided to two inner and outer surfaces and the middle wall is shown as unique surface as shown in Fig. 3-9.

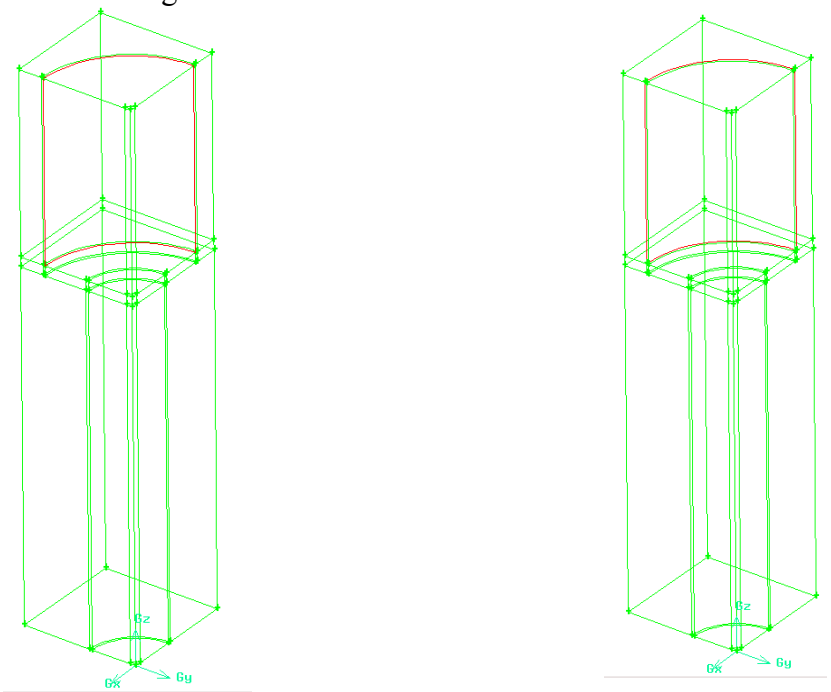

a. Upperwall_plastic_in

b. Upperwall_plastic_out

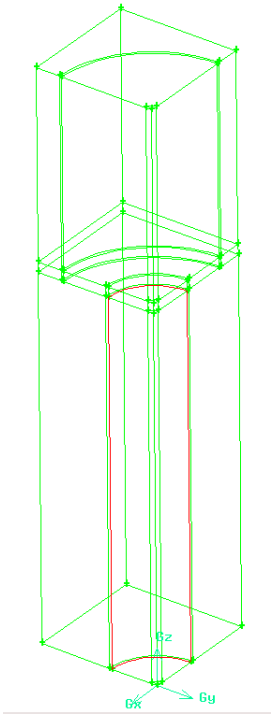

c. lowerwall_steel_in

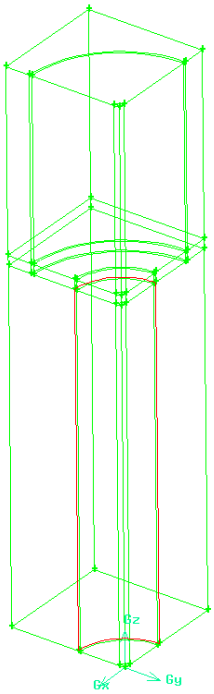

d. lowerwall_steel_out

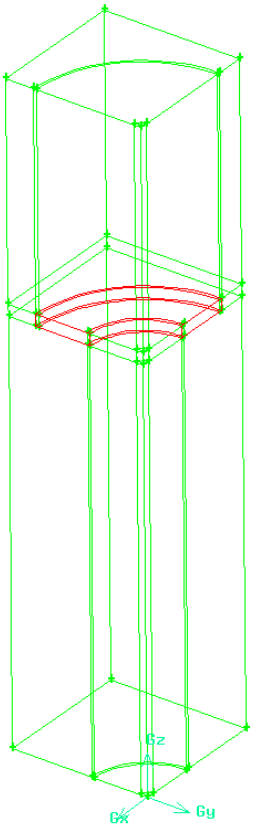

e. middlewall_plastic_steel

Fig. 3-9. tank information and their materials

The material types also needed to be specified and separated in Gambit so that it could be easy for material definitions. In Fig. 3-9, the material types are shown and the properties of such materials are shown Table 3-1.

In FLUENT, for the boundary conditions, the ambient temperature is set to 20°C. The heat transfer coefficients through the upper, side and bottom walls are set to 15.5, 10.77 and 5 W/m²K for the tank without insulation and to 3.56, 2.47 and 1.15 W/m²K for the tank with insulation. This corresponds to the measured tank heat loss. Water is a working fluid in the model which is calculated by Boussinesq's buoyancy approximation, which is good for simulating flows caused by comparatively small temperature differences (Kays and Crawford (1993)).
Boussinesq's buoyancy approximation calculates the differences in density by the following equation:

$$\Delta\rho = \rho \cdot \beta \cdot \left(T - T_{ref}\right) \tag{3.1}$$

where
T is variable temperature [K]
T_{ref} is reference temperature [K]
β is thermal expansion coefficient [K^{-1}]
ρ is density at the reference temperature [kg/m³]
$\Delta\rho$ is difference in density (difference from reference condition) [kg/m³]

The solver is pressure based and implicit method is used to solve the set of equations. Unsteady state condition is chosen so that it could be possible to study the fluid flow and heat transfer in different time steps. Energy equation is also chosen to be solved together with Navier-Stokes equation. In the operating condition, the gravity is set to 9.806 m/s² and operating temperature is set to 35°C which is a mean temperature inside the tank.
The governing equations for laminar fluid flow and heat transfer are summarised in this section. They are called Navier-Stokes equations.
The basic set of equations necessary for solving laminar fluid flow and heat transfer includes the continuity equation, the momentum equation and the energy equation. The equations are given in tensor notation where x_i (i=1,2,3) or (x,y,z) are the Cartesian coordinates and u_i or (u_x, u_y, u_z) are the Cartesian components of the velocity vector $\boldsymbol{v}$. Repeated indices in a term of an equation imply summation of the term over the three values of k (summation convention). The Kronecker delta is $\delta_{ij} = 0$, i #j, and $\delta_{ij} = 1$, i =j.
The continuty equation is:

$$\frac{\partial \rho}{\partial t} + \frac{\partial}{\partial x_i}(\rho u_i) = 0 \tag{3.2}$$

The momentum equestion is:

$$\frac{\partial}{\partial t}(\rho u_i) + \frac{\partial}{\partial x_i}(\rho u_j u_i) = -\frac{\partial P}{\partial x_i} + \frac{\partial \tau_{ij}}{\partial x_j} + \rho g_i \tag{3.3}$$

where τ_{ij} is the stress tensor:

$$\tau_{ij} = \mu\left[\left(\frac{\partial u_i}{\partial x_j} + \frac{\partial u_j}{\partial x_i}\right) - \left(\frac{2}{3}\frac{\partial u_k}{\partial x_k}\right)\delta_{ij}\right] \tag{3.4}$$

The energy equation is:

$$\frac{\partial}{\partial t}(\rho H) + \frac{\partial}{\partial x_i}(\rho u_i H) = \frac{\partial}{\partial x_j}\left[\lambda \frac{\partial T}{\partial xj}\right] + \frac{\partial P}{\partial t} \quad (3.5)$$

g_i	is the gravity, $g_i = (g_x, g_y, g_z)$, [m/s²]
H	is the total enthalpy, $H = h + \frac{1}{2}u_i^2$, [J/kg]
h	is the thermodynamic enthalpy, h = h(T,p), [J/kg]
λ	is the thermal conductivity, [W/(m·K)]
P	is the pressure, [kg/(m·s²)]
T	is the temperature, [K]
t	is the time, [s]
u_i	is the fluid velocity, $u_i = (u,v,w)$, [m/s]
μ	is the dynamic viscosity, [kg/(m·s)]
ρ	is the density, [kg/m³]

It was found out that a turbulent model is suitable for the natural convection inside the DHW tank and a laminar flow model is suitable in the outer tank (space heating tank). k-epsilon (k-ε) model for turbulence is used for modeling of turbulence in the tank. Turbulence, flow and energy equations are solved together with the SIMPLE algorithm for pressure-velocity coupling equations. Body forced weighted method which is suitable for buoyancy driven flow is used for interpolation scheme for discretization of the face pressure. First order upwind interpolation method is used for discretization of momentum, turbulent kinetic energy, turbulent dissipation rate and energy equations. Under relaxation factor of different parameters is shown in Table 3-3. Under relaxation factors makes the solutions get converge. The lower the relaxation factor is, the longer the calculation will be but it can guarantee that the solution can be converged.

Table 3-3. Under relaxation factors set for the control solution.

	Pressure	Density	Body force	Momentum	Turbulent kinetic energy	Turbulent dissipation rate	Turbulent viscosity	Energy
Under relaxation factor	0.3	1	1	0.7	0.8	0.8	1	0.9

The initial condition for the tank temperature is 50°C with the turbulent kinetic energy of 1.848e-4 m²/s² and turbulent dissipation rate of 2.808e-4 m²/s³. The convergence criterion for the residual of energy, velocities, continuity, k and epsilon is shown in Table 3-4.

Table 3-4. Residual values for the convergence.

	Continuity	X velocity	y velocity	z velocity	energy	k	epsilon
Residual	0.0001	0.0001	0.0001	0.0001	10e-7	0.001	0.001

The property conservation is also checked. The mass flow rate imbalance is calculated as -2.79e-9 kg/s.

A time step of 2 sec is used for the simulation and the maximum number of iterations per time step is 20 for the unsteady state condition. Number of time steps is chosen depending on the test period.

3.4 Comparison of thermal experiments and CFD results

Simulations have been carried out with the built CFD-model of the tank-in-tank heat store. The aim of the simulations is to investigate the fluid motion and heat transfer in the tank during a number of typical operation conditions.
To begin with, during domestic hot water draw-off, the development of thermal stratification in the space heating storage tank and DHW tank and the development of the outlet temperature from the DHW tank are investigated. In addition, investigations are made of fluid motion in the store.
The tank is divided to 19 different layers in the CFD model and nine locations correspond to nine temperature sensor measurement point in the tank. The temperature sensor locations are shown in Fig. 3-10.

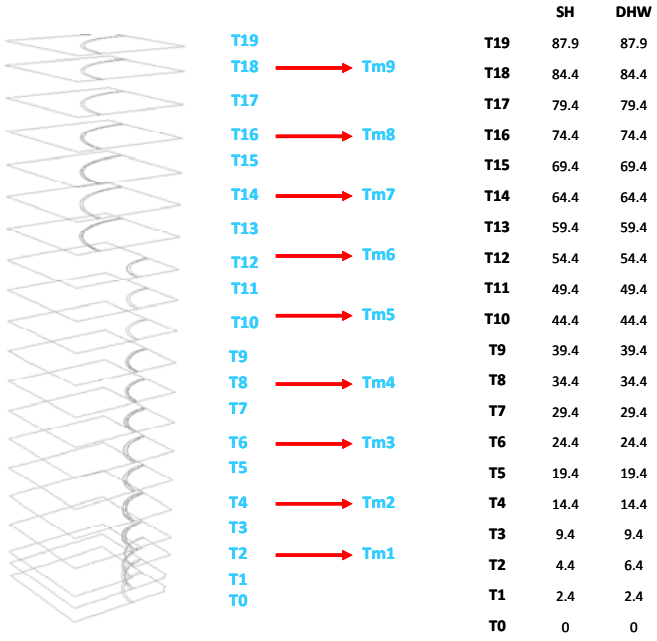

	SH	DHW
T19	87.9	87.9
T18	84.4	84.4
T17	79.4	79.4
T16	74.4	74.4
T15	69.4	69.4
T14	64.4	64.4
T13	59.4	59.4
T12	54.4	54.4
T11	49.4	49.4
T10	44.4	44.4
T9	39.4	39.4
T8	34.4	34.4
T7	29.4	29.4
T6	24.4	24.4
T5	19.4	19.4
T4	14.4	14.4
T3	9.4	9.4
T2	4.4	6.4
T1	2.4	2.4
T0	0	0

Fig. 3-10. Temperature sensor locations inside space heating and DHW tank in the CFD model and the measured tank.

In the investigations, the starting temperatures of 50ºC for both DHW and space heating tank are used, and the DHW tank is discharged with a flow of about 2, 4 and 6 l/min, and an inlet temperature to the DHW tank of about 20ºC. Of course, the flow rates and the inlet temperatures are set to the exact values of the measurements. The glass tank is with and without insulation. In one case the total DHW tank volume is discharged and in another case, the whole lower part of the tank with the small diameter is discharged. The thermal stratification is investigated after the discharge.

3.4.1 Grid and time independency analysis

In any CFD modeling or numerical modeling, it is very important to establish grid and time independent results. Grid independence is achieved when further refinement or expansion of the grid does not result in significant changes to the converged CFD solutions. In unsteady state conditions, time independence is important. The governing equations in CFD are descretised and solved by a discrete grid of cells called mesh or grid. The number of grids should be as low as possible in order to save computational time while the mathematical error should be below a certain acceptable rate.

In this study three different mesh numbers of 0.8, 1.2 and 1.4 million have been investigated. Fig. 3-11 shows tank height versus the temperature distribution of DHW tank during discharge. The temperatures are averaged temperatures for the levels in question in the tank. The discharge flow rate is 2.3 l/min and the cold water inlet temperature is 20 ºC. The temperature distribution is for three different grid numbers. The simulation runs till the whole DHW tank volume is discharged corresponding to 12.83 min.

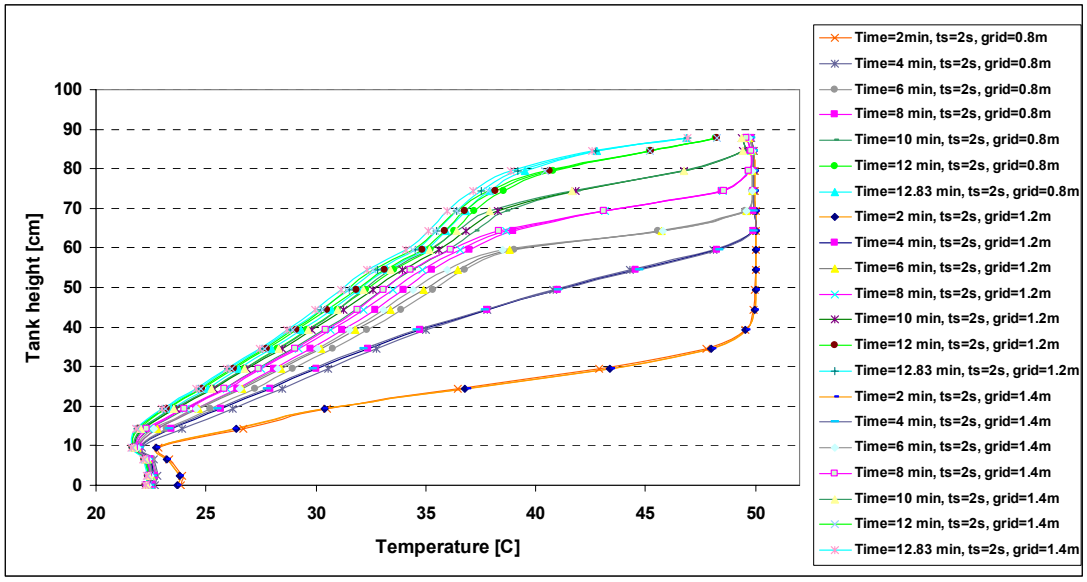

Fig. 3-11. Temperature distribution inside the DHW tank for different grid numbers, discharge flow rate=2.3 l/min.

Fig. 3-12 shows the tank height versus the temperature in the space heating tank. The temperature in the space heating tank decreases by the time. The result is for three different grid numbers.

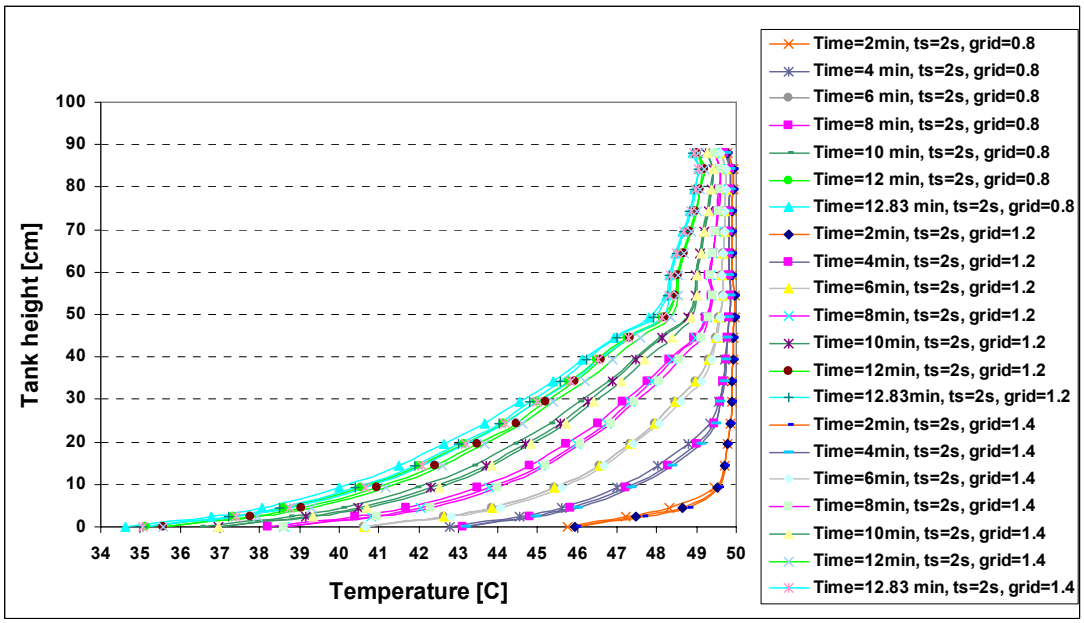

Fig. 3-12. Temperature distribution inside the space heating tank for different grid numbers, discharge flow rate=2.3 l/min.

Based on Fig. 3-11 and Fig. 3-12, showing the temperature distribution in the inner and outer tank it is concluded that grid number of 1.2 million is suitable for the CFD simulations while grid number of 0.8 million showed that it is not capable of modeling the flow and heat transfer well and grid number of 1.4 millions increases the computational time, without resulting in improved accuracy.

The time independency analysis was also carried out with three different time steps of 1, 2 and 5 seconds. The results of the time indecency are shown in Fig. 3-13 and Fig. 3-14.

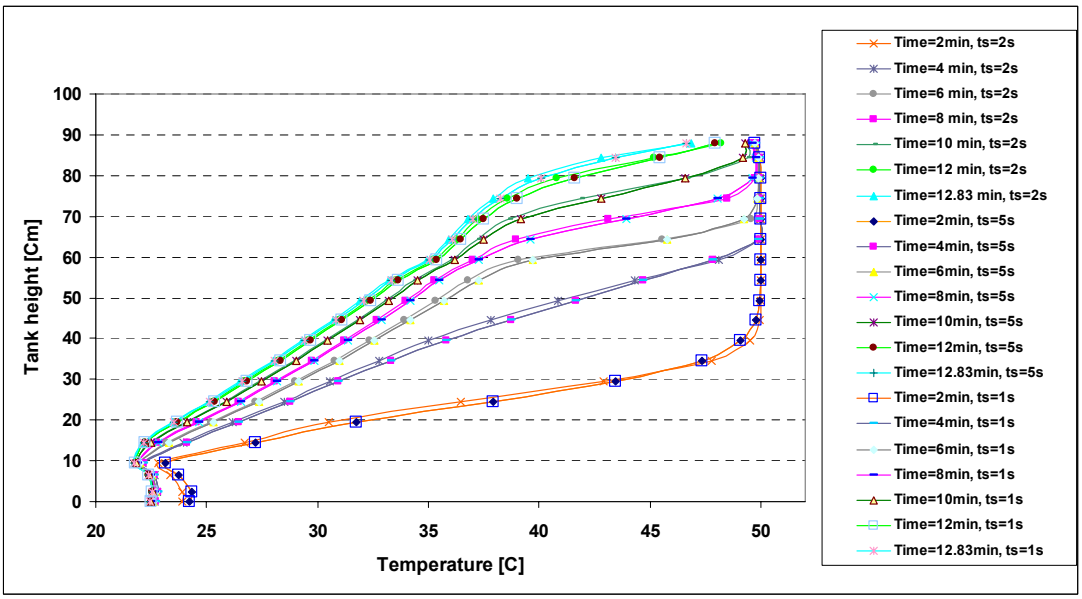

Fig. 3-13. Temperature distribution inside the DHW tank for different time steps, discharge flow rate=2.3 l/min.

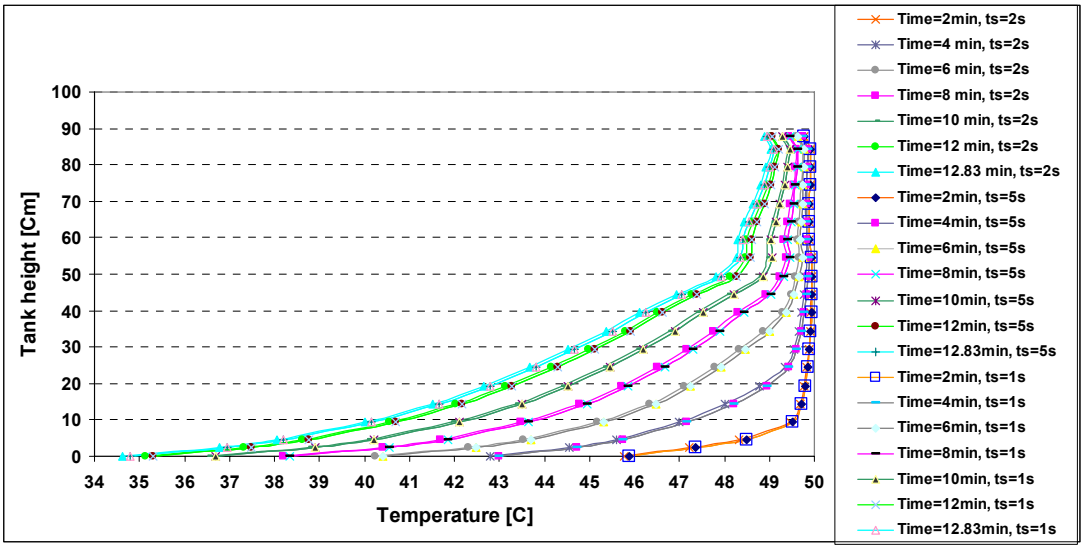

Fig. 3-14. Temperature distribution inside the space heating tank for different time steps, discharge flow rate=2.3 l/min.

The results with time steps of 1 and 2 second are close to each other, while a time step of 5 second is not suitable for the simulation since the temperature prediction is not the same as for 1 and 2 second. Therefore, a time step of 2 second is chosen as the best time step where a good accuracy and a short computational time will be achieved.

3.4.2 Comparison between measurements and calculations

Case 1. Insulated tank-discharge with volume flow rate of 4 l/min

The test is carried out with an initial temperature of 50ºC, a volume flow rate of 4 l/min and an inlet temperature of about 20ºC for the insulated tank. The whole DHW tank volume is discharged. Fig. 3-15 shows the temperature distribution inside the DHW tank. The temperature inside the tank is decreasing when the discharge is started and continues decreasing till 505 sec. After the discharge, the tank remains stand still without any discharge and the temperature inside DHW tank starts increasing due to heat transfer from the outer tank. Due to the time consumption of the CFD work, only 1 hour of the test has been calculated. The calculated temperatures are temperatures where the temperature sensors are placed. There is a good agreement between measured and calculated temperatures inside the DHW tank.

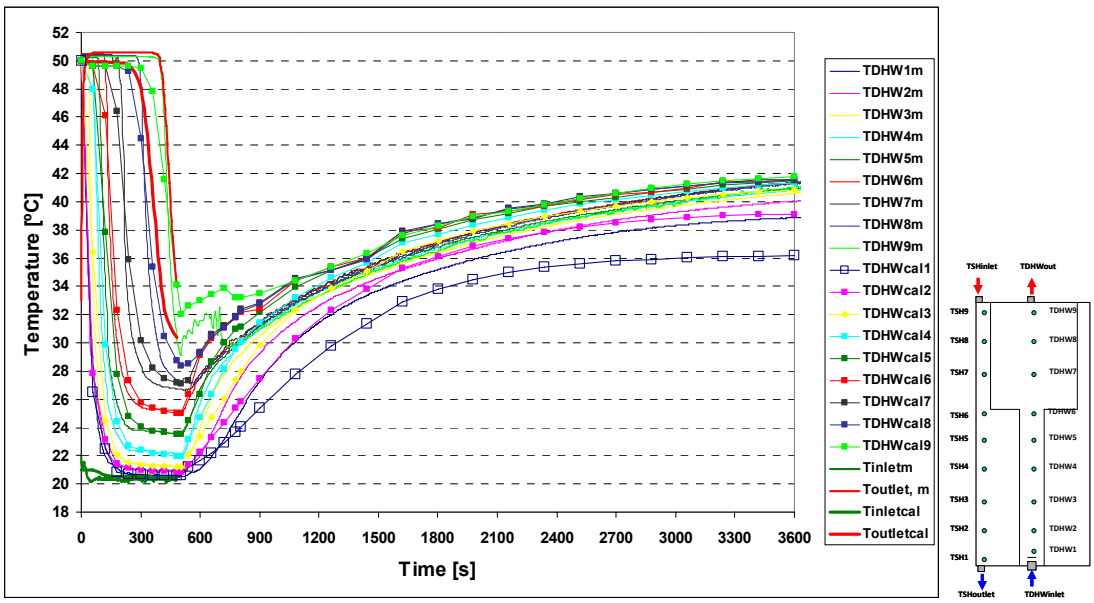

Fig. 3-15. Calculated and measured temperature distribution inside the DHW tank for discharge flow rate of 4 l/min and insulated tank.

The temperature distribution of the outer space heating store is shown in Fig. 3-16. The agreement between calculated and measured temperatures is better for the bottom of the tank than for the upper level of the tank. The temperature sensor TSH9 is located close to the inlet to the space heating tank. This temperature fluctuates due to the high heat loss of the pipe connection.

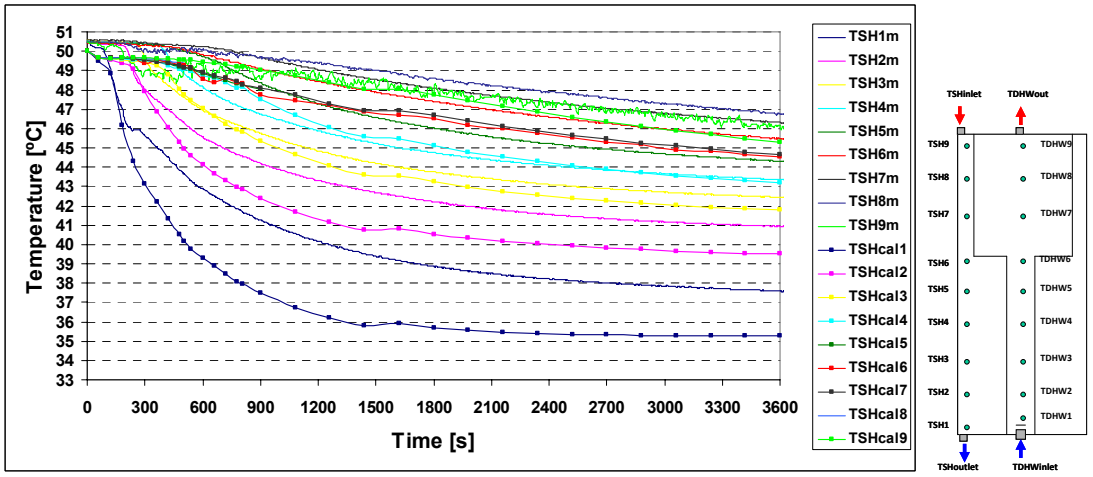

Fig. 3-16. Calculated and measured temperature distribution inside the space heating tank for discharge flow rate of 4 l/min and insulated tank.

Fig. 3-17 shows the measured and calculated temperature distribution along the DHW tank height for the test after 1 min, 8.43 min, 9 min, 13 min, 18 min, 30 min and 60 min. After 1 min, the calculated temperatures inside the lower part of the tank are a little bit higher than the measured temperatures. After 8.43 min where the DHW discharge stops, there is a good agreement between calculated and measured temperatures at the lower level of the tank, while in the upper part of the tank, the calculated temperatures are higher than the measured temperatures. It can be explained by the high thermal bridge caused by the pipe connection at the space

heating inlet. The thermal bridge is not considered in the CFD calculations. Therefore, the upper level temperatures are overestimated by the calculations. During stand by after the discharge, at 9 min, 13 min, 18 min and 30 min, the calculated temperatures are lower than the measured temperatures at the lower level, while in the upper level it is the other way around. But as the time passes, the calculated temperatures are higher than the measured temperatures. All in all, it is concluded that there is a reasonable agreement between measured and calculated temperatures.

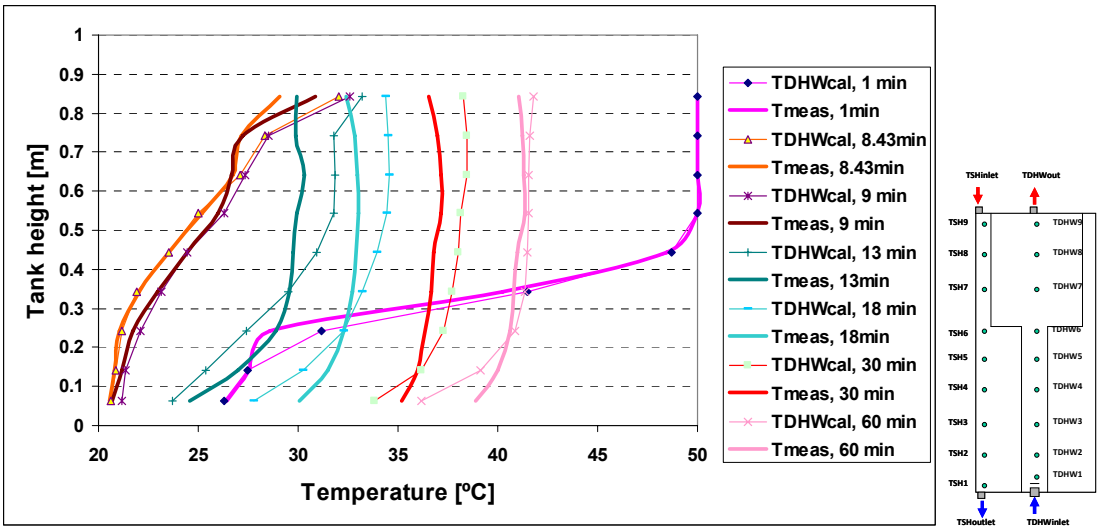

Fig. 3-17. Measured and calculated temperature distribution inside the DHW tank for discharge flow rate of 4 l/min and insulated tank.

Fig. 3-18 shows the temperature distribution inside the space heating tank along the tank height for the test after 1 min, 8.43 min, 9 min, 13 min, 18 min, 30 min and 60 min. After 1 minute, the measured temperatures are higher than the calculated temperatures. At 8.43 min, the same situation exists. During the stand by, the calculated temperatures are lower than the measured temperatures at the lower and upper level, while in the middle level the calculated temperatures are higher than the measured temperatures.

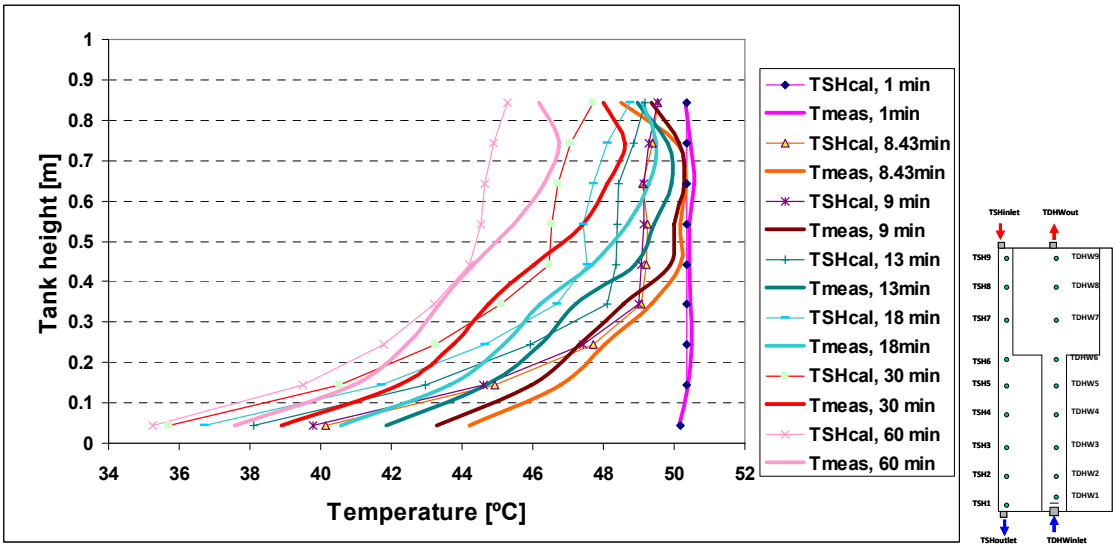

Fig. 3-18. Measured and calculated temperature distribution inside the space heating tank for discharge flow rate of 4 l/min and insulated tank.

It is concluded that there is a good agreement between measured and calculated temperatures.

Case 2. Uninsulated tank-discharge with volume flow rate of 4 l/min

Measured and CFD calculated tank temperatures are also compared for a test for the tank without insulation. The discharge test is carried out with a volume flow rate of 4 l/min, the initial temperature of 50ºC and an inlet temperature of about 20ºC. Fig. 3-19 shows the temperature distribution inside the DHW tank. The temperatures inside the tank are decreasing when the DHW discharge is started and continues decreasing till 445 sec. After the discharge, the tank remains stand still without any discharge and the temperatures inside the DHW tank starts increasing. The measured and calculated temperatures are in a good agreement during and after discharge. The calculated temperatures during the stand by are lower than measured temperatures at the bottom of tank (TDHWcal1 and TDHWcal2). TDHW9 which is located close to outlet is influenced by the flow and the thermal bridge/the outlet pipe. It is obvious that the temperature rise during the stand by is higher for the insulated tank than for the uninsulated tank due to the higher heat loss of the uninsulated tank.

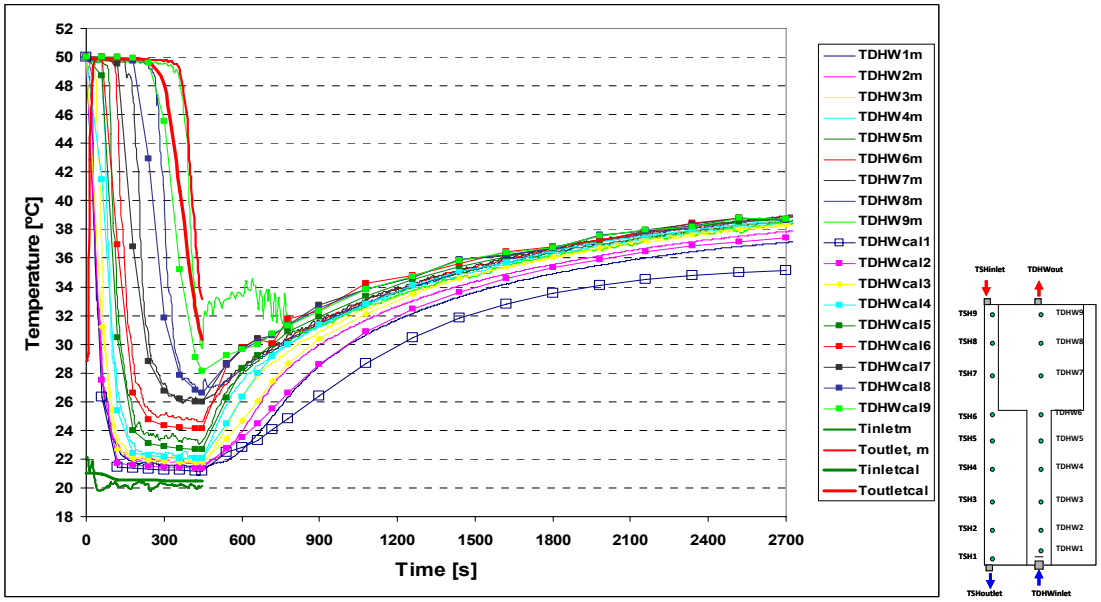

Fig. 3-19. Temperature distribution inside the DHW tank for discharge flow rate of 4 l/min and uninsulated tank.

Fig. 3-20 shows the temperature distribution in the outer space heating tank. The bottom measured and calculated temperatures (TSH1 and TSH2) do not fit well at the end of the test. However, in the other parts of the tank, there is a good agreement between measured and calculated temperatures.

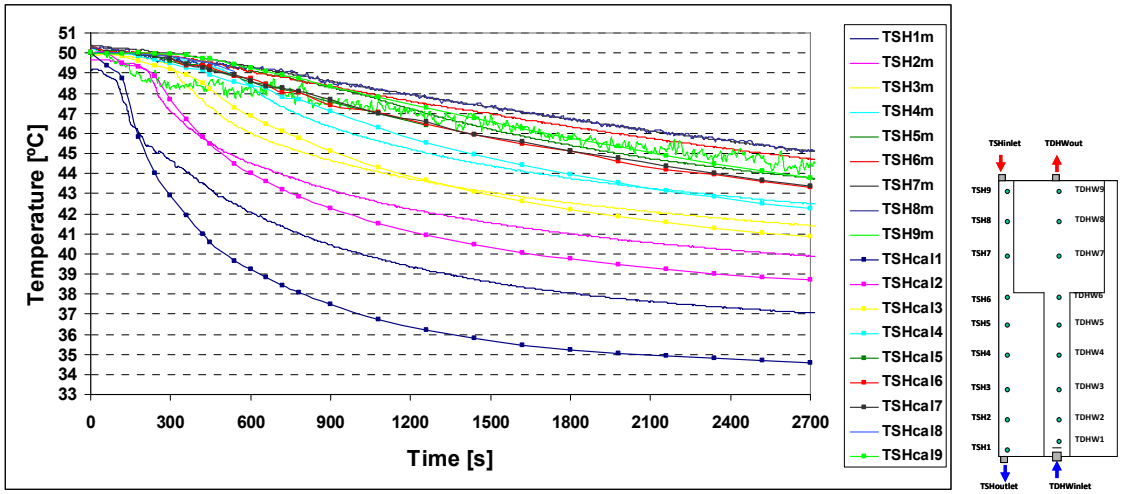

Fig. 3-20. Temperature distribution inside the space heating tank for discharge flow rate of 4 l/min and uninsulated tank.

Case 3. Insulated tank-lower tank part discharged with volume flow rate of 4 l/min

The insulated tank is heated up to 50ºC and the discharge test is carried out with a volume flow rate of 4 l/min and an inlet temperature of about 20ºC. The tank is discharged only in the lower level (9.7 lit) which is similar to a small hot water draw-off in practice. Fig. 3-21 shows the temperature distribution inside the DHW tank. The temperatures inside the DHW tank (TDHW1-TDHW6) are decreasing till the discharge ends. TDHW7-TDHW9 remains constant at 50ºC since the cold water level does not reach the upper level. When the discharge stops, the temperature inside the DHW tank (TDHW1-TDHW6) increases due to heat transfer from the outer space heating tank. However, TDHW7-TDHW9 remains more or less 49-50ºC during the stand by.

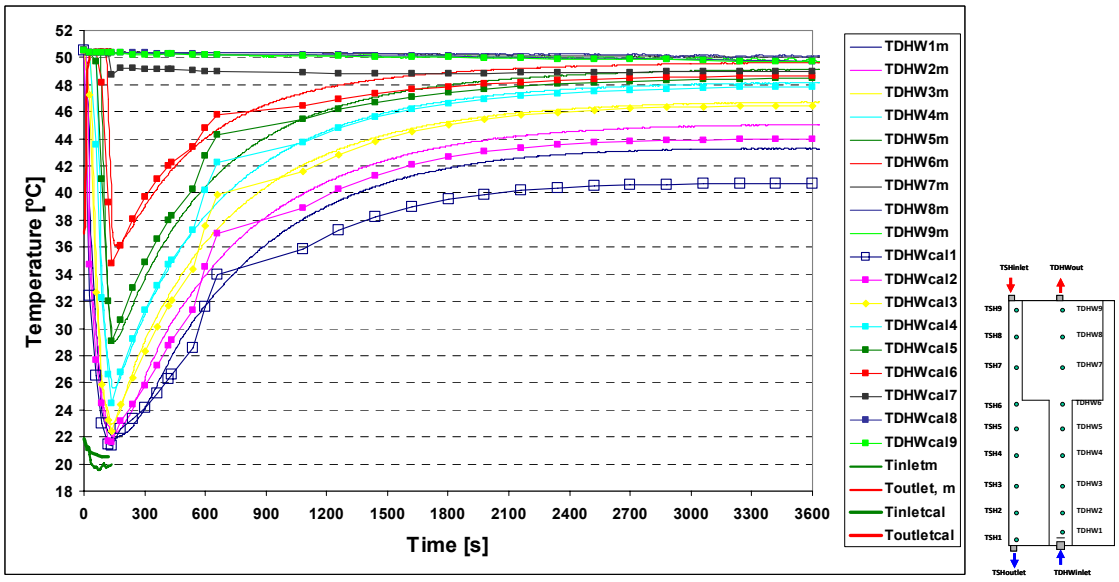

Fig. 3-21. Temperature distribution inside the DHW tank for lower DHW volume discharge, a volume flow rate of 4 l/min and insulated tank.

Fig. 3-22 shows the temperature distribution in the outer space heating tank. The bottom measured and calculated temperatures (TSH1) do not fit well at the end of the test. However, in the other parts of the tank, there is a very good agreement between measured and calculated temperatures.

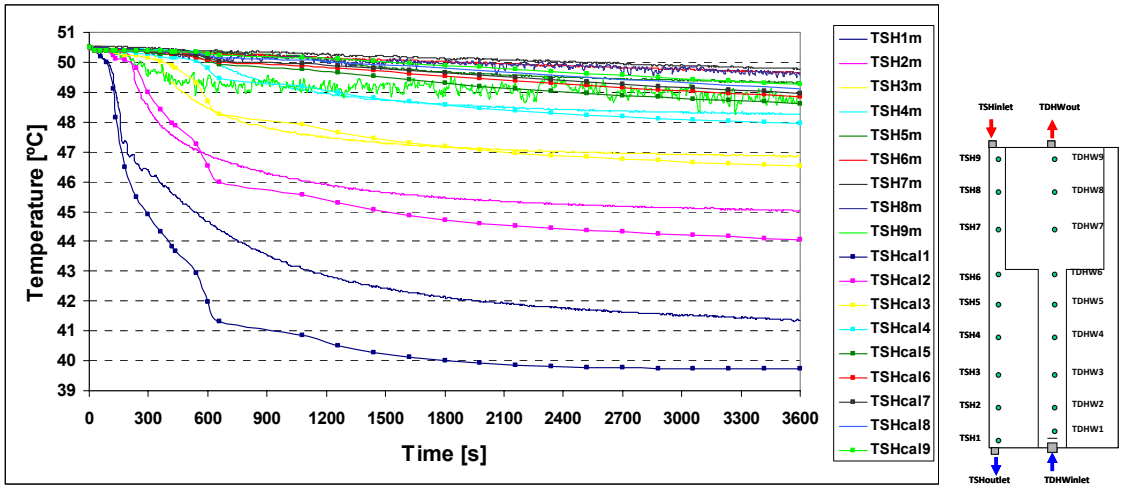

Fig. 3-22. Temperature distribution inside the space heating tank for lower DHW volume discharge, a volume flow rate of 4 l/min and insulated tank.

Case 4. Insulated tank-discharge with volume flow rate of 2 l/min

The insulated tank with an initial temperature of 50ºC is discharged with a volume flow rate of 2 l/min and an inlet temperature of about 20ºC. Fig. 3-23 shows the temperature distribution inside the DHW tank. TDHW1-TDHW9 decreases when the discharge starts and continues decreasing till 835 sec when the discharge stops. Then the inside temperatures start to increase due to heat transfer from the outer space heating tank to the inside DHW tank. After one hour, the temperature in the DHW tank in CFD is between 35-48ºC while in the experiment temperatures are between 38-45 ºC.

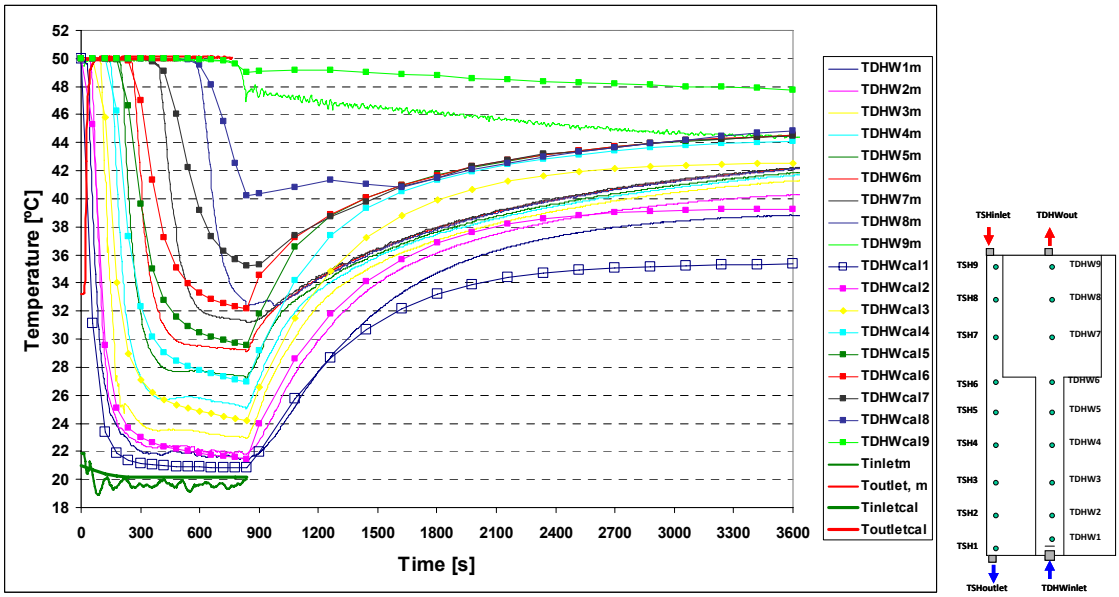

Fig. 3-23. Temperature distribution inside the DHW tank for lower tank part discharge, a volume flow rate of 2 l/min and insulated tank.

Fig. 3-24 shows the temperature distribution in the outer space heating tank. The inside temperatures decrease all the time during the discharge and stand by test. The decrease trend in temperatures is sharper for the first 900 sec and then the decrease trend decreases due to lower heat transfer. The bottom measured and calculated temperatures (TSH1) do not fit well at the end of the test. However, in the other parts of the tank, there is a very good agreement between measured and calculated temperatures.

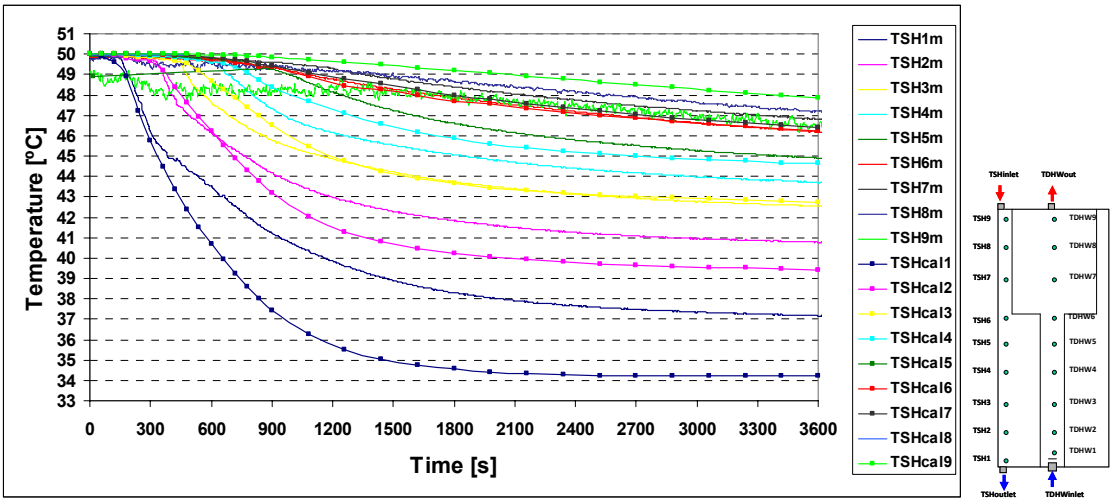

Fig. 3-24. Temperature distribution inside the space heating tank for lower tank part discharge, a volume flow rate of 4 l/min and insulated tank.

3.5 Comparison of PIV measurements and CFD calculations

3.5.1 PIV technique

Particle Image Velocimetry is a technology by which a flow pattern visualization for a certain object can be made so that a comparison with simulations can be made. PIV relies on seeding particles, mixed in the fluid or gas that is being analyzed, which have approximately the same density as the surrounding materials so the velocity of each seed particle could be considered to be the same as the fluid velocity.
A laser sheet is sent through the fluid or gas, and the seeding particles scatter the light. A high-speed camera is set up exactly perpendicular to the laser sheet and records an image frame at the same time as the laser emits light. This is done by a control system which times the laser pulses and the frame capturing of the camera to occur with 1 ns precision. At a certain time after the first frame, a second laser pulse and image frame are generated. An analysis system can, when it knows how big the area in the picture frame is in reality, accurately calculate the flow rate at any point in the analyzed area by matching the two frames together and analyzing where the particles in the first frame moved to in the second frame, and dividing the calculated distance with the difference in time of recording. This technique is called cross-correlation. Normally only one high-speed camera is used, but then any flows perpendicular to the laser sheet (the z-axis) are not taken into account and might actually cause some noise in the flow rates calculated for the x- and y- directions. When it is expected that flows in the z-plane occur, it is possible to use two high-speed cameras at an angle of 90

degrees from each other and an angle of 45 degrees from the laser sheet. The flow in z-direction can then be derived from the difference in calculated flow in x- and y-direction between the two camera angles. A graphical explanation of the PIV technology is shown in Fig. 3-25.

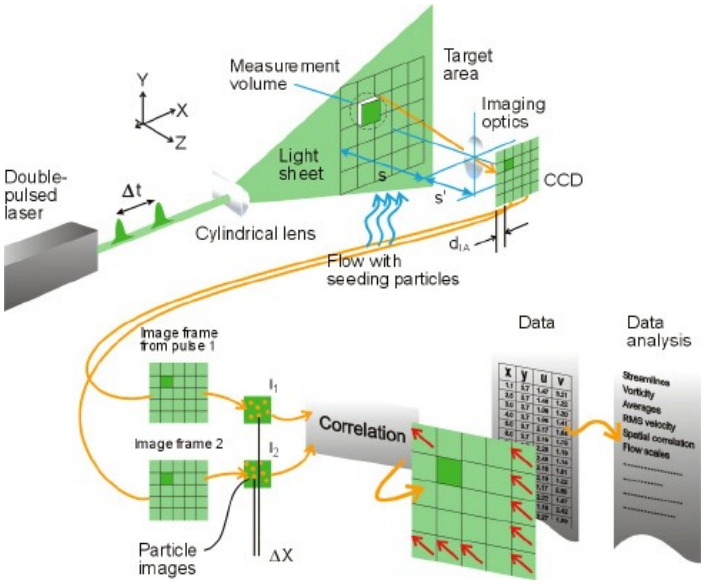

Fig. 3-25. Particle Image Velocimetry technique.

3.5.2 PIV experiments procedure

In order to validate the CFD model, the tank-in-tank system is experimentally investigated by means of PIV (Particle Image Velocimetry).
The experimental set-up is shown in Fig. 3-26. The heating system consisted of a heater which provides the required heat to adjust the inlet temperature to the tank. The water is pumped to the inlet of the SH tank at the top and returned back to the heater from the bottom of the tank to ensure that the whole tank volume is heated to the required temperature. After charging the tank, cold water enters to the DHW tank from the bottom with a low inlet temperature. Warm water from the top of the DHW tank goes back to the cooling loop in which the water is cooled to the required inlet temperature. The heat store described in section 3.2 is used for the PIV measurements. The data of the tank-in-tank heat storage dimensions is given in Fig. 3-3. The PIV equipment consists of a laser, a camera and a processing unit system for analysing the pictures taken by the camera. The PIV measurements analyzed here are performed with a PIV system supplied by Dantec Dynamics. The Solo II PIV 15 system produced by New Wave is used in this investigation, and is equipped with a double-pulsed class IV Nd:YAG-laser with a maximum pulse rate of 15 Hz. The high-speed camera is also produced by new wave. Dantec Dynamics produces the processing and synchronization unit, the Flow Map system hub, themselves.

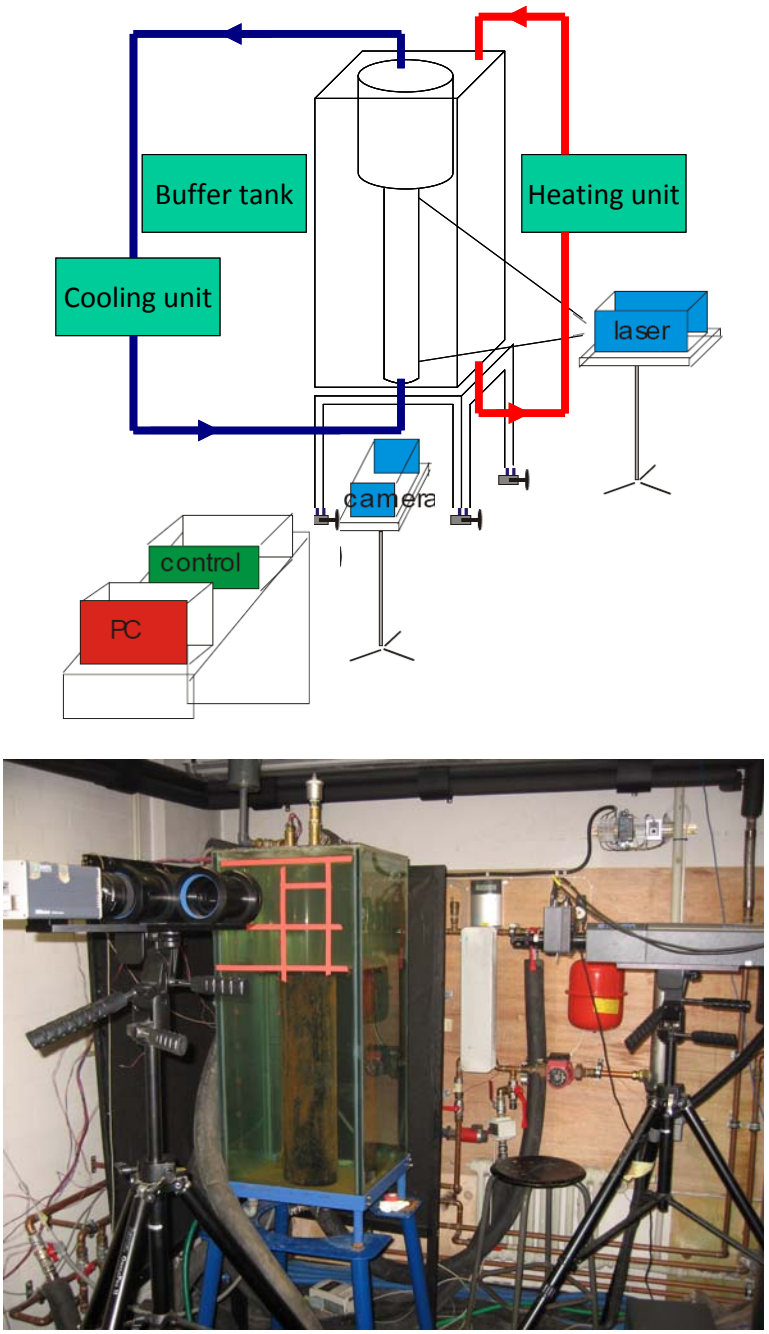

Fig. 3-26. Experimental setup for PIV measurements.

The time between measurements has to be chosen in such a way that the seeding particles in the analyzed field do not move too far between the two frames, otherwise the system will not be able to calculate in which direction the particles have moved. The required separation time between the two laser pulses depends on the fluid velocity to be measured. If the velocities are high, a short time interval between the two laser pulses is needed, and if the velocities are small, a longer time interval is needed.

The seeding particles also should be big enough for the camera to be able to capture the laser light scattered by them. When the particles are too small, they can't be detected from the camera images. Care has to be taken that there are not too few and not too many seeding particles per volume. When there are not enough, the system

will not detect enough particles and can not accurately detect the velocity field. When there are too many particles, the system will have trouble identifying which particles in one frame should be matched with which particles in the other frame. Another problem with a too high amount of particles in the analyzed fluid is that the scattered light could be scattered again and not reach the camera, which makes the image blurry and unreliable for analysis.

The camera has to be properly calibrated so its point of focus is located exactly at the laser sheet. The size of the camera image has to be measured with a ruler positioned exactly in the laser sheet, and this information has to be stored in the system that calculates the flow rates.

As part of this investigation, PIV measurements have been made of the flow pattern created in the outer and inner tank of the tank-in-tank store, during and after a discharge period in which the entire inner tank volume and lower part of DHW volume is replaced with cold water. The obtained flow pattern is compared to CFD simulations for the same tank.

The tank-in-tank store is charged to a uniform temperature level of 50°C by water circulating through the heating loop and the outside part of heat storage from top to bottom. Once the temperature is high enough, all circulation is stopped five minutes before measurements are made. This will allow the store temperature to stabilize and will minimize the effect of the charging circulation on the PIV measurements. Thereafter the measurement cycle starts, with 5 cross-correlation images created per measurement.

The same measurement is repeated 4 times, each time a different section of the outer tank was measured. The results of the four measurements are joined together with MatLab and compared with the FLUENT simulation model and the store temperature data.

The camera had a resolution of 1280×1024 pixels. In order to get sufficient resolution with the PIV system, the inner and outer tank were divided into smaller sections, and images of particle tracks from each section were assembled to get the full flow field in the area of interest. In the inner tank, the fluid velocity was measured above the upper part of the DHW tank with a large tank diameter. The measurement area in the inner tank was divided into 2 sections and in the outer tank; it is divided to 4 sections as shown in Fig. 3-27.

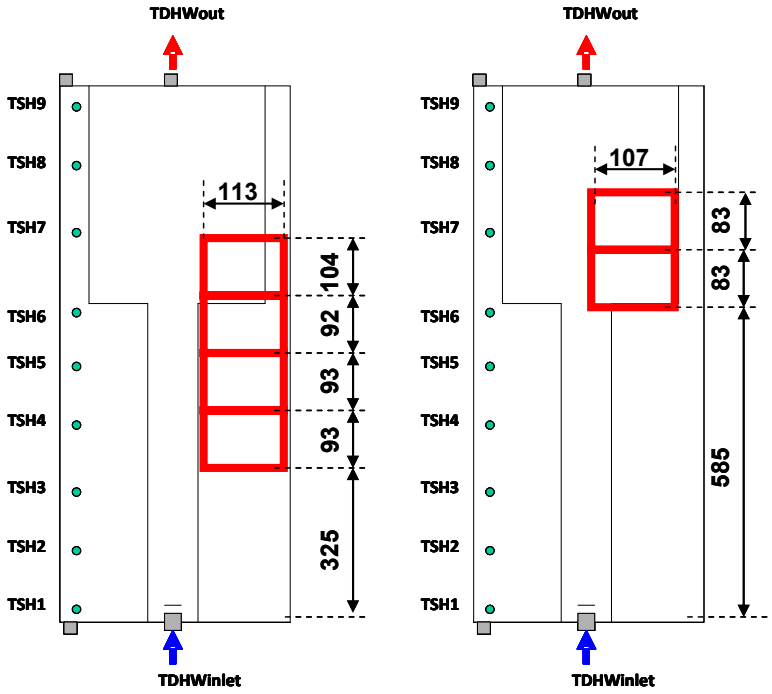

Fig. 3-27. The measurement area in the inner tank (to the right) and outer tank (to the left).

3.5.3 Results: Flow distribution in outer tank

The uninsulated tank is first charged to 50ºC and after reaching stability, the discharge test is started with an inlet temperature of 20ºC and a volume flow rate of 4.5 l/min for about 6.5 minutes. CFD calculations and PIV results are compared during and after the discharge. Fig. 3-28 shows the measured flow field in the outer tank in 4 different sections which are glued together after 2 minutes of discharge. Velocity vectors are shown for different times during and after discharge. There is a downward flow close to the steel wall at lower levels of the tank. This downward flow can be visualized better in CFD than PIV. The downward flow close to the steel wall can not be seen well in the PIV measurements because the steel tank wall reflects the laser lights which cause that the camera could not take a good quality picture close to the steel tank wall.

There is a downward flow in the narrow upper level of the outer tank and it is higher close to the glass tank than the middle of the tank. This higher velocity close to the glass tank wall is due to the higher heat loss that causes higher downward flow. There is upward flow shown in both CFD and PIV at the middle of the narrow upper level of the tank. In the region where the diameter of the lower and upper tank is changed, the flow structure is slightly different from the rest of the tank. In this region, the upward flow coming from the lower part of the tank meets the downward flow caused by heat loss. Therefore some flows go upward at the middle of the narrow region and some flow back to the lower tank. Consequently at this region, a rotating region appears which is due to the sudden change in diameter and the upward and downward flow. This appears clearly from the PIV measurements. The result for the discharge after 2 minutes shows quite a good prediction by CFD simulations. The velocity range in the tank is from 0 to 30 mm/s.

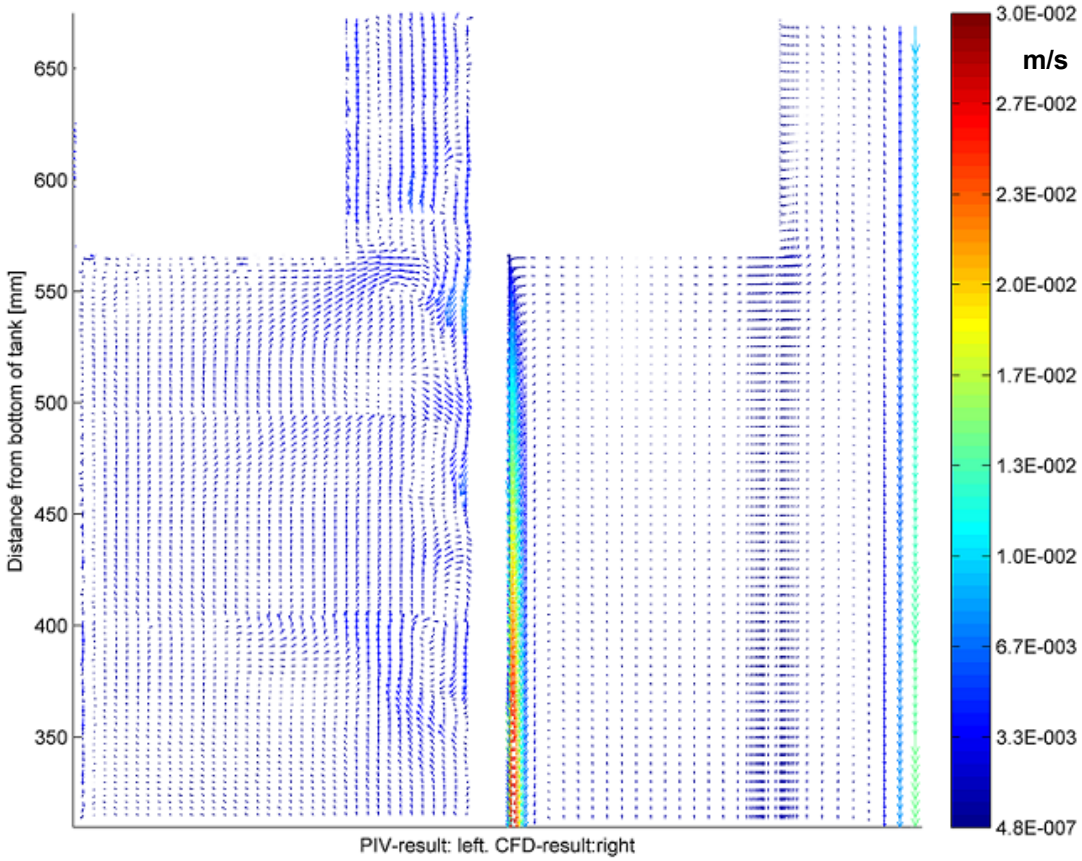

Fig. 3-28. Comparison of CFD and PIV flow field for the space heating tank during discharge after 2 minutes.

Fig. 3-29 shows the comparison between CFD and PIV during discharge after 5 min of the discharge test. It can be seen that during the discharge, in the narrow upper level of the tank, there are two downward flows close to the plexiglass tank wall and glass tank wall. This downward flows cross the upward flow coming from the lower tank and cause rotations around where the diameter of the tank changes. The flow velocities after 5 minutes are higher than flow velocities after 2 minutes. The downward flow close to the glass tank wall is caused by the heat loss. Again due to the high reflection of laser from the steel wall, the downward flow close to the steel wall can not be seen well in PIV. However, it is shown in CFD that due to the heat transfer to the inner tank, the downward flow is high. And the downward flow is higher close to the lower part of the tank than the upper part of tank.

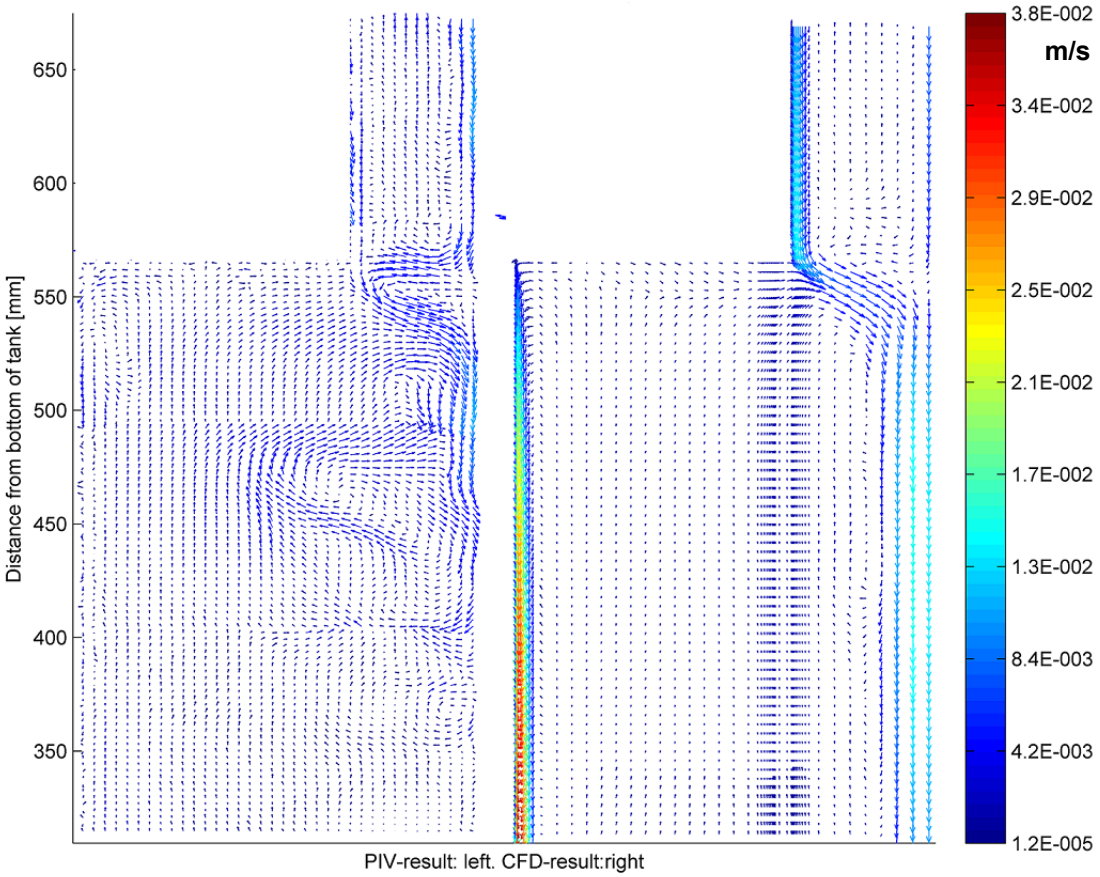

Fig. 3-29. Comparison of CFD and PIV flow field for the space heating tank during discharge after 5 minutes.

The comparison between PIV and CFD flow fields is shown in Fig. 3-30 after 30 seconds after the discharge. The flow pattern at this time is similar to after 2 and 5 minutes. However, the flow is stronger in this time step. Downward flow close to the glass tank wall caused by heat loss is lower in the upper level of the tank than the downward flow in the lower part of the tank. There is also a whirling part in where the tank diameter changes. This rotating region is due to the downward flow coming from both glass tank and plexiglass tank wall in the narrow region and upward flow from the lower tank. Downward flow from the heat loss in the lower part continues to the bottom of the tank.

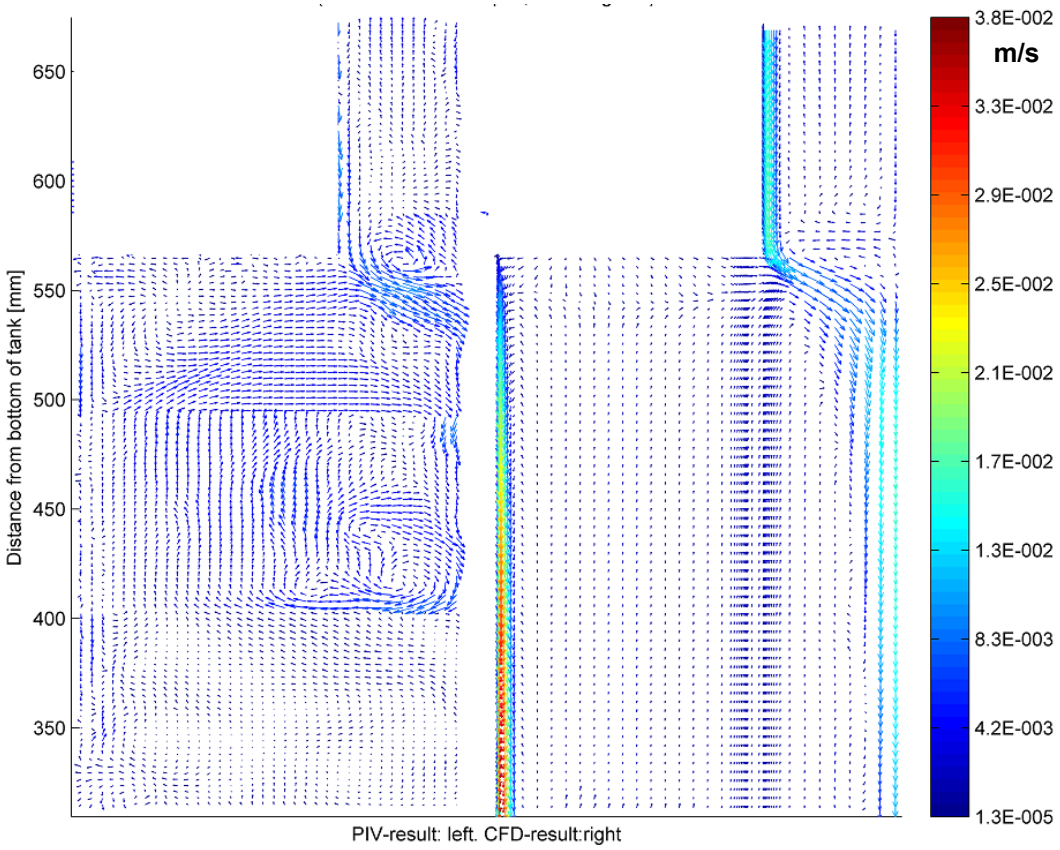

Fig. 3-30. Comparison of CFD and PIV flow field for the tank during stand by, 30 seconds of after the end of the discharge.

The measured flow field for the outer tank during stand by, 8.5 minutes after the end of the discharge is shown in Fig. 3-31. There are still strong downwards velocities close to glass and plexiglass walls in the upper part of the tank. Further, there is upward flow in the middle of the narrow region. Close to the horizontal wall there is downward flow. The rotating region still exists close to the narrow region. There is also a downward flow along the glass tank in the lower part of the store due to the heat loss. There is also an upward flow at the middle of the tank in the lower part of the store.

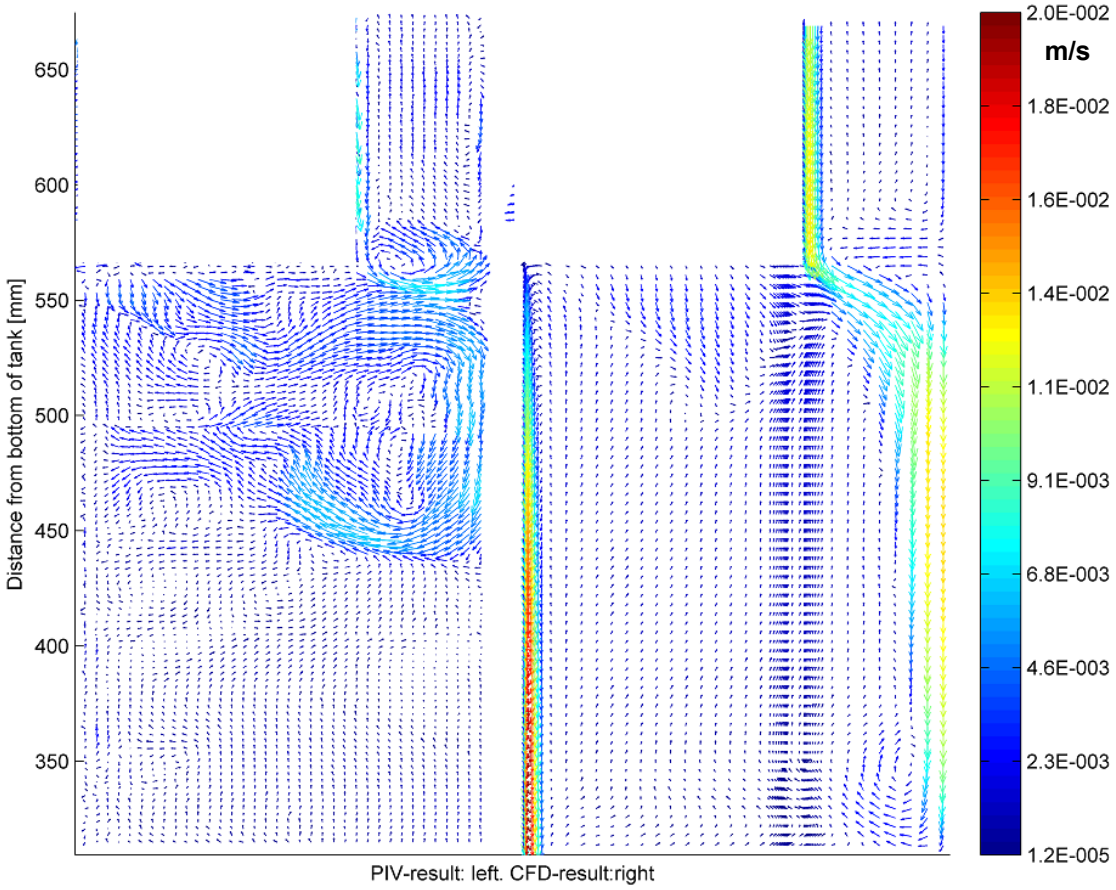

Fig. 3-31. Comparison of CFD and PIV flow field for the space heating tank during stand by, 8.5 minutes after the end of the discharge.

Fig. 3-32 shows the PIV and CFD flow measurement for the discharge test during stand by, 23.5 minutes after the end of the discharge. Two rotating regions appear in the PIV measurements. Similar regions can be seen from the CFD result. The rotating region is caused by the downward flow and upward flow caused by the heat transfer between two tanks and the heat loss to the ambient. All in all there is a good agreement between PIV measurements and CFD calculations of flow fields for the whole period of the test.

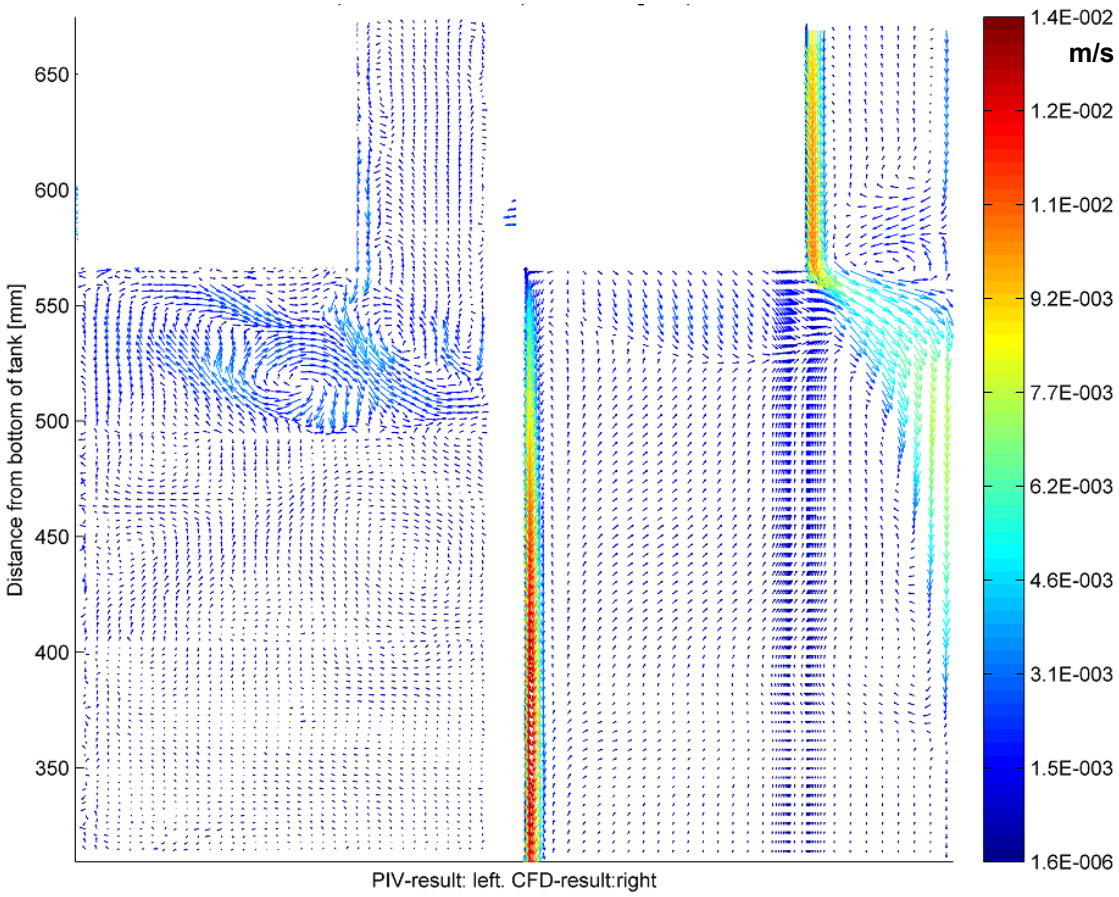

Fig. 3-32. Comparison of CFD and PIV flow field for the space heating tank during stand by, 23.5 minutes after the end of the discharge.

3.5.4 Results: Flow distribution in inner tank

The inner DHW tank flow field is also investigated by means of CFD and PIV as shown in Fig. 3-27. The main reason for choosing the region where the tank diameter is changing is to visualize how the fluid flow behavior is influenced by the change in diameter of the inner tank in the tank-in-tank heat store. Therefore the same experiments were carried out for the inner tank as well. Two sections are glued together as it is shown. Velocity vectors are shown for different times like for the outer tank experiments during and after discharge. The tank is first charged to 50ºC and after reaching stability, the discharge test is started with an inlet temperature of 20ºC and a volume flow rate of 4.5 l/min for about 6.5 minutes.
Fig. 3-33 shows the flow field of the inner tank 2 minutes after the discharge. There is an upward flow coming from the lower tank with smaller diameter to the upper tank with larger diameter. The upward flow when reaching the larger diameter turns to the right part of the tank and then it returns back from the corner of the tank to the center of the tank. The flow from the center of the tank then continues moving to the right and then center of the flow field again. And they finally reaches and points to the outlet located at the top of the investigated region. Average temperatures of all levels of the inner tank are shown in Fig. 3-34.

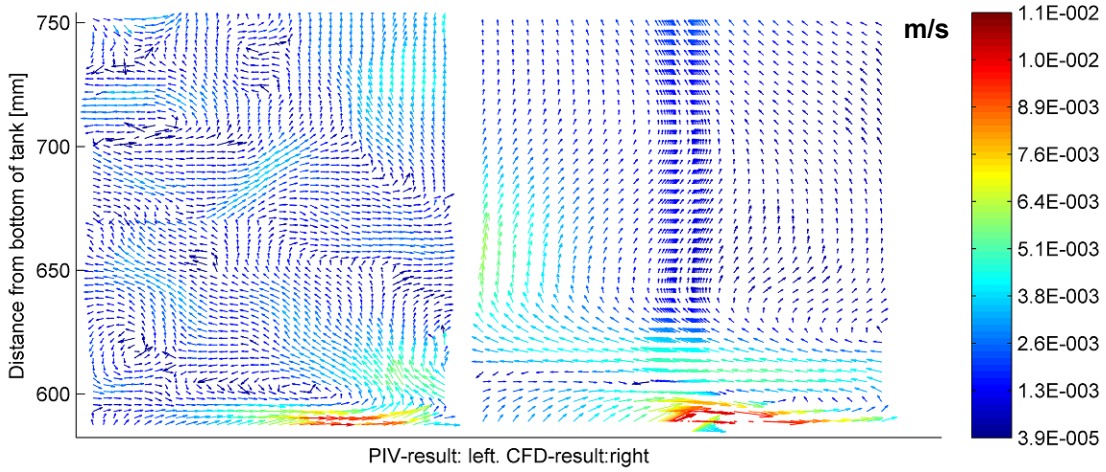

Fig. 3-33. Comparison of CFD and PIV flow field for the inner tank during discharge after 2 minutes.

The temperature distribution after 2 minutes shows that the bottom of the tank is 26ºC while the top of the tank is 50 ºC. There is an overall upward flow inside the DHW tank.

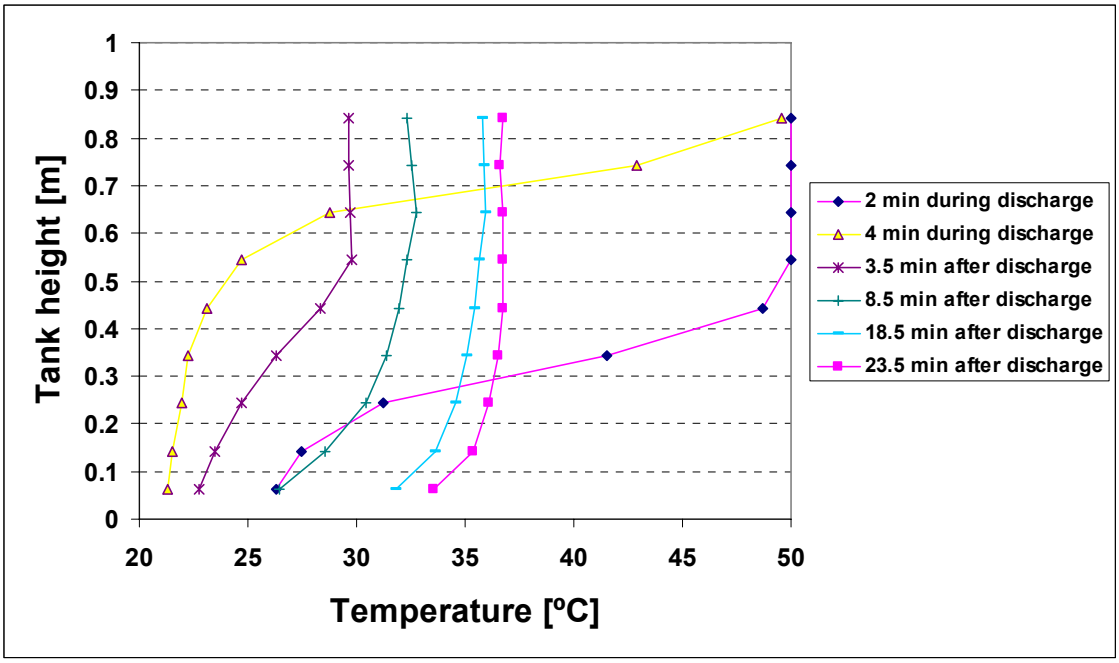

Fig. 3-34. Temperature distribution of the inside tank 2 and 4 minutes during discharge and 3.5, 8.5, 18.5 and 23.5 minutes after discharge.

The flow field in the inner tank after 4 minutes is shown Fig. 3-35. The cold water enters to much higher DHW tank level as shown in Fig. 3-34. There is a strong thermal stratification in the investigated part of the inner tank water after 4 minutes. The fluid flow first goes upward and then when it reaches to the relatively high level of the large diameter tank, the flow turn to the right of the tank and some turn back to the center of the tank and goes upward and then back again to the right part of the flow field. The velocity is lower at higher levels than at lower levels.

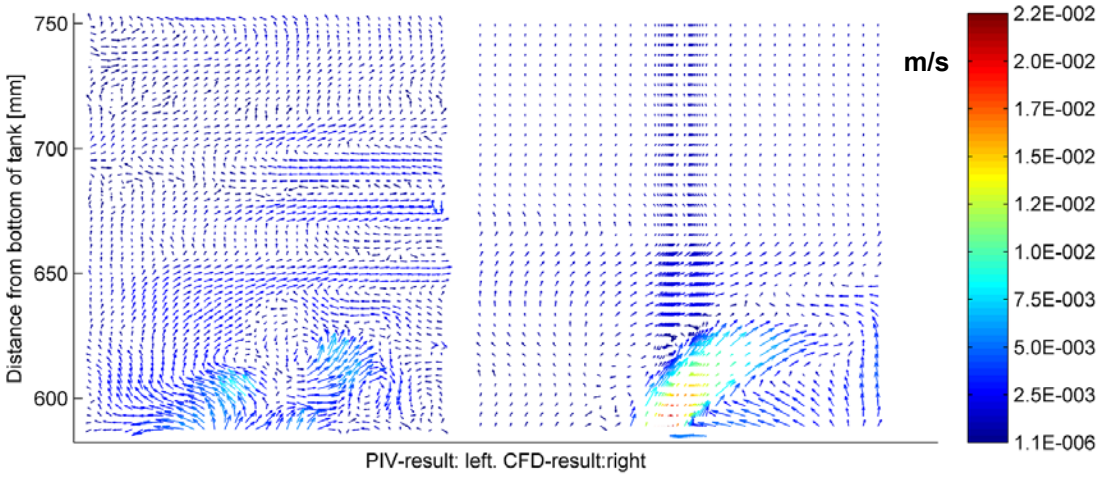

Fig. 3-35. Comparison of CFD and PIV flow field for the inner tank during discharge after 4 minutes.

Fig. 3-36 shows the flow field for the tank during stand by after 3.5 minutes of discharge. The full discharge of the inner tank ended at 6.5 minutes. The inner tank is heated by heat transfer from the outer tank. There is a strong upward flow coming from the lower part of the tank resulting from the high heat transfer between the inner and outer tank through the steel wall. The temperature distribution after 10 minutes in Fig. 3-34 shows that the temperature increases from the bottom of the tank till 0.56 m where the diameter of the DHW tank changes. From 0.56 m to the top of the tank, the temperature slightly decreases. This is because the lower tank part is heated up faster that the upper tank part. This reverse thermal stratification will result in a strong upward water flow from the lower to the upper part of the tank. The upward flow from the lower part of tank to the higher part of the tank goes to the left hand side of the tank, that is to the center of the tank while during discharge it goes to the right. The fluid velocity at the center of the tank is higher as shown in red colors with high velocity of 18 mm/s. However, due to the thermal bridge through the outlet, water from the upper levels above the flow field region shown in the figure goes down to the flow field region, pushes the flow to the right side of the tank and causes whirling region. This whirling region has a little bit higher velocity in PIV than in CFD, because the thermal bridge is not considered completely in CFD. However, there is still overall a good agreement between CFD calculations and PIV measurements.

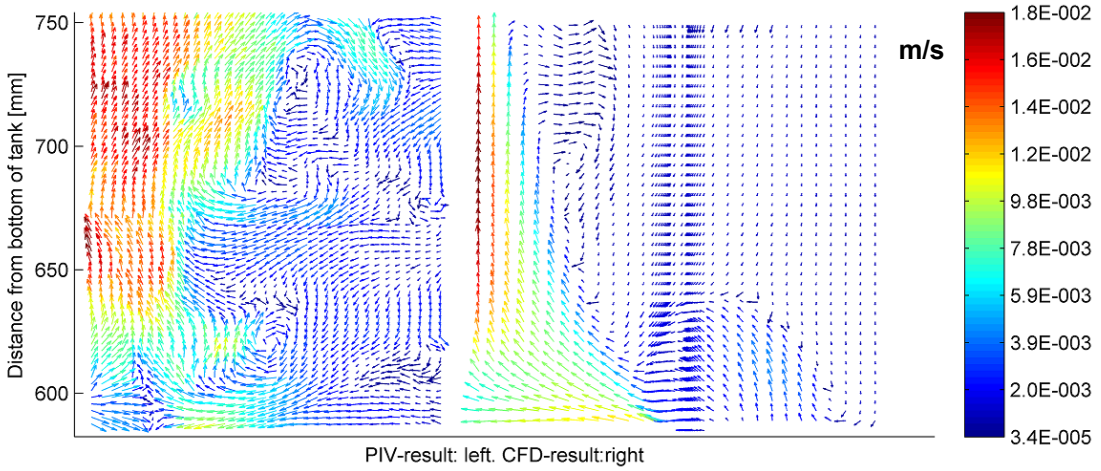

Fig. 3-36. Comparison of CFD and PIV flow field for the inner tank during stand by, 3.5 minutes after the end of the discharge.

Fig. 3-37 shows the flow field comparison between CFD and PIV 8.5 minutes after the end of the discharge during stand by. There is still an upward flow coming from the lower level to the upper center of the inner tank. The reason for this high velocity from the lower tank is due to the fact that the water is getting warm faster in the lower part than in the upper part. The temperature distribution from Fig. 3-34, shows that the temperature increases till 0.65 m in and then decreases slightly till top of the tank. The velocity is high at the center of the upper part of the tank or left side of the shown flow field, about 20 mm/s. There is also downward flow coming from the upper right of the tank resulting from the heat loss. This cold downward flow from the right region pushes the high velocity water coming from the lower part of the tank to the left causing a whirling region.

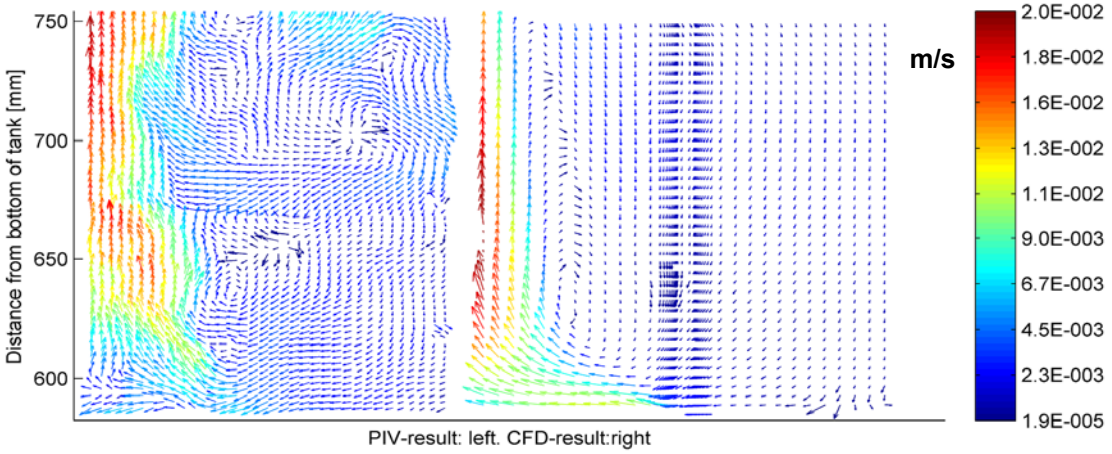

Fig. 3-37. Comparison of CFD and PIV flow field for the inner tank during stand by, 8.5 after the end of the discharge.

Fig. 3-38 shows the flow field region in the inner tank during stand by 18.5 minutes after the end of the discharge. The flow from the lower tank goes upward and some goes to the center of the tank or to the left side of the flow field region and some goes back to the lower level and goes downward. The flow is pushed by the flow going downward from the upper level right of the flow field region to the lower level left side of the flow field. There is a good agreement between PIV measurements and CFD calculations.

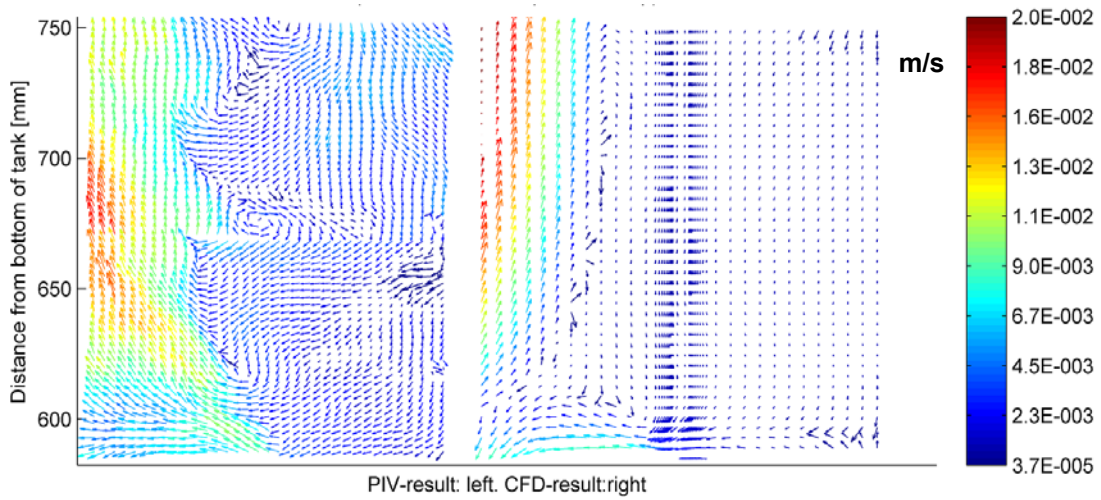

Fig. 3-38. Comparison of CFD and PIV flow field for the inner tank during stand by, 18.5 minutes after the end of the discharge.

Fig. 3-39 shows the flow field of the inner tank during stand by, 23.5 minutes after the end of the discharge. The flow pattern is similar to the flow pattern for 18.5 minutes after discharge. There is a strong upward flow close to the steel tank wall. When it reaches to the upper tank with a large diameter, it is pushed by the downward flow coming from the top tank. Therefore, some flow go back to the lower tank again. And some goes up to the center of the tank to the left side of the flow field region. All in all, under the whole test, there is a reasonable good agreement between flow patterns and flow velocities calculated with CFD calculations and measured with PIV measurements.

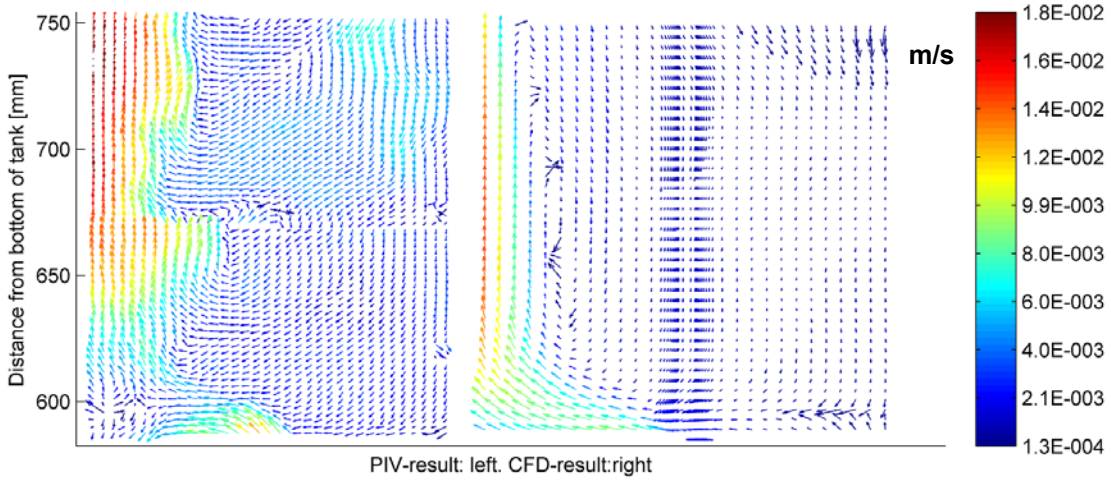

Fig. 3-39. Comparison of CFD and PIV flow field for the inner tank during stand by, 23.5 minutes after the end of the discharge.

3.6 Conclusions

The purpose of this chapter is to validate the CFD model of the tank-in-tank store during and after DHW discharge.
The discharge DHW tests are carried out by means of PIV measurements and thermal experiments. The CFD calculations show that during DHW discharge, turbulent model can be applied for modeling of the inner DHW tank and for the outer tank, laminar model can be used. When the DHW discharge is stopped, that is during stand by periods, laminar model can be applied in both the inner and the outer tank.
The comparison between the CFD and thermal experiments shows a good agreement between calculated and measured temperatures. And also there is a very good agreement between PIV measurements and CFD calculations on flow velocities.
Based on the theoretical and experimental investigations, it can be concluded that the CFD model has the capability to predict and simulate the heat transfer, flow velocities and temperature distribution in the tank-in-tank store in a reasonable way. In the following chapter, the CFD model of a real steel tank-in-tank heat store will be used for investigating the thermal stratification, heat transfer and flow structure for different geometries of the tank-in-tank heat store.

4 CFD calculations on tank-in-tank stores

4.1 Introduction

It was shown in chapter 3 that the CFD-model is able to model temperatures, fluid flow and heat transfer in tank-in-tank heat store in a reasonable way. In this chapter the flow in the inner DHW tank, the fluid flow in the outer space heating tank and the heat transfer at the DHW wall are analysed for a number of different mantle designs and different operation conditions.
The model used for the parameter variations use the same principles as described in chapter 3. A standard tank and standard boundary conditions are used.
A three-dimensional grid model of a steel tank-in-tank store was developed. Only one fourth of a tank was modelled as symmetry was assumed in the centre plane through the inlet and outlet to and from the DHW tank.
Fig. 4-1 shows the vertical grid distribution and Fig. 4-2 shows the horizontal grid distribution of the model. The mesh was concentrated in high gradient regions near the walls. The computational domain consists of the inner tank and the outer tank.
In FLUENT, the model of the tank-in-tank store is divided into a computational mesh composed of small cells. The computational mesh consists of boundary layers close to the tank walls, whereas it consists of larger mesh in the rest of the model. This means that the computational mesh is finer close to the tank walls, where large variations of flow and temperature may occur, and that it is coarser in the rest of the tank.
The numbers of cells are 1374002. In chapter 3, it was shown that this number of cells is capable of predicting the temperature and heat transfer very well. Moreover, a time step of 2 seconds is used.

Fig. 4-1. Vertical grid distribution of the CFD-model of the tank-in-tank heat store.

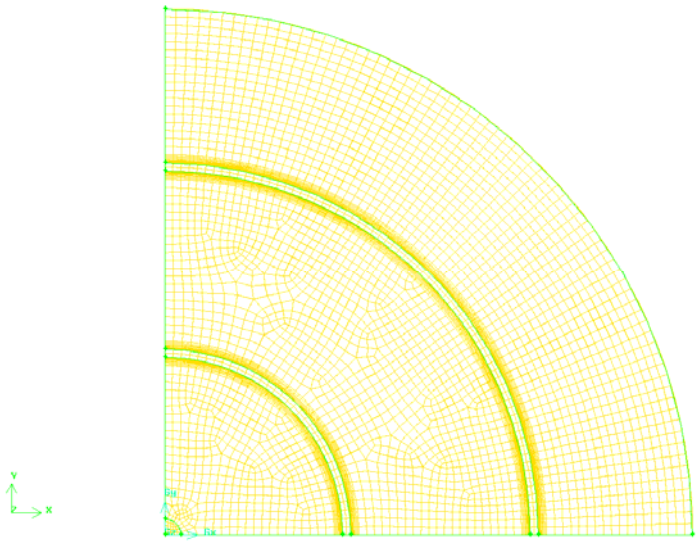

Fig. 4-2. Horizontal grid distribution of the CFD-model of the steel tank-in-tank store.

Two different geometries with different H/D ratio at the lower DHW tank are investigated in this study. Table 4-1 shows the volume of space heating, domestic water for the investigated reference tank-in-tank store inclusive the total volume.

Table 4-1. The volume of domestic water and water for space heating for the reference tank-in-tank store.

	Volume [l]
Domestic water, upper level	110.5
Domestic water, lower level	34.8
Water for space heating	393.9
Total	539.2

The investigated reference tank-in-tank heat store dimensions are shown in Fig. 4-3 for a vertical and a horizontal cross section, respectively. The tank wall thickness is 5 mm and the whole tank material is steel.

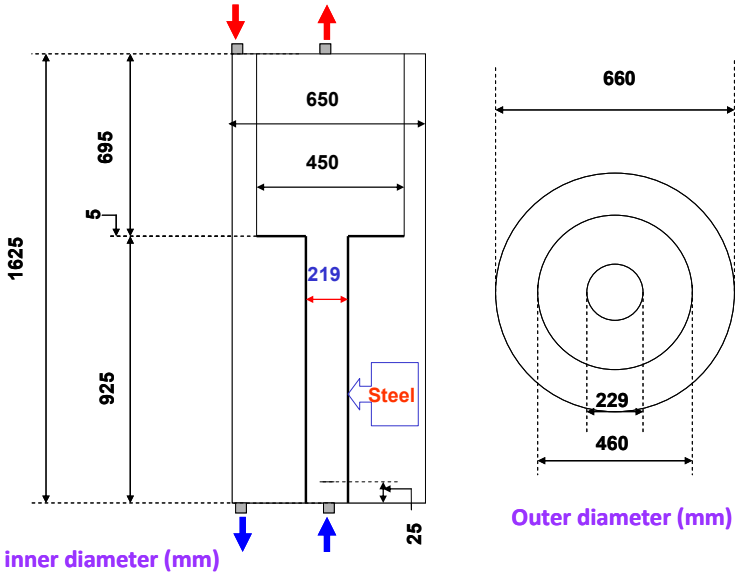

Fig. 4-3. Tank-in-tank heat storage dimensions.

A baffle plate at the cold water inlet of the DHW tank is used in order to prevent mixing in the tank. The baffle plate is located 25 mm at the top of the inlet to DHW tank.
Another geometry is considered for the CFD study. The geometry has higher H/D ratio at the lower DHW tank with the diameter of 150 mm. The whole tank volume is the same as the volume of the reference tank-in-tank store. The volume at the lower DHW tank is smaller than for the reference tank due to a higher H/D ratio. Table 4-2 shows the tank volume in the DHW and space heating tank.

Table 4-2. The volume of domestic water and water for space heating in the tank-in-tank store with higher H/D ratio.

	Volume [l]
Domestic water, upper level	110.5
Domestic water, lower level	16.3
Water for space heating	412.4
Total	539.2

Fig. 4-4 shows the dimension of the tank-in-tank store with higher H/D ratio. The same baffle plate is used for this geometry to prevent mixing in the tank.

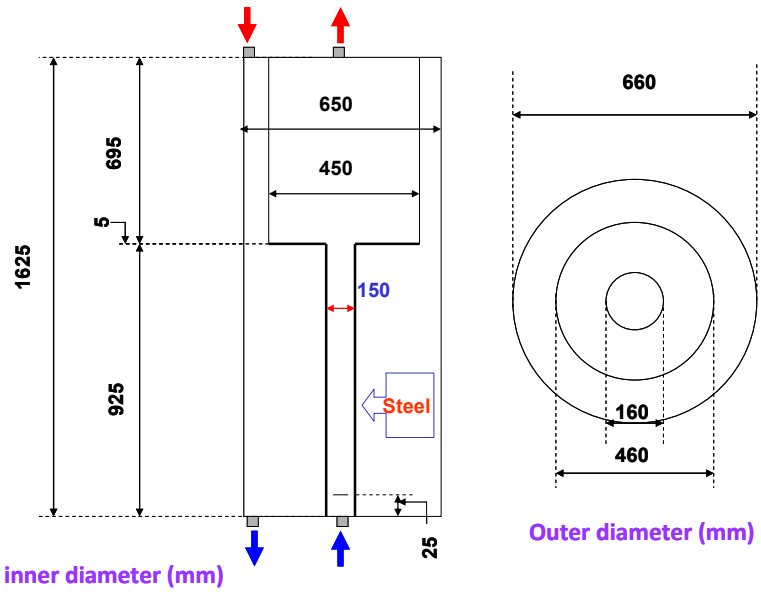

Fig. 4-4. Tank-in-tank heat store with higher H/D ratio dimensions.

The tank is made from steel. The material properties of the tank are shown in Table 4-3.

Table 4-3. The steel material properties.

Specific heat [J/kg·K]	434
Thermal conductivity [W/m·K]	64
Density [kg/m³]	8830

The insulation is not included directly in the computational domain but it is indirectly taken into account by applying U-values as boundary conditions for the steel tank. Heat loss coefficient for the top, sides and bottom of the tank is shown in Table 4-4. The values given in Table 4-4 are used for all CFD models in this chapter.

Table 4-4. Heat loss coefficient of the tank.

Top [W/m²·K]	0.12
Sides [W/m²·K]	0.55
Bottom [W/m²·K]	3.9

The boundary conditions for the simulations are based on the calculations made for the tank described in chapter 3. Three different kinds of DHW flow rates are assumed for the steel tank. The flow rates are 5, 10 and 15 l/min, corresponding to low, medium and high flow rates. The cold water temperature is assumed to be 20ºC. Like in the experiments explained in chapter 3, the whole store is first heated up to 50 ºC, before the hot water draw-off is started. The discharge volume from the DHW tank is 50 l. These simulations are applied for both the reference tank and the tank with a smaller diameter of the lower hot water tank.
Fig. 4-5 shows the temperature sensor locations assumed in the inner and outer tank. Twenty different locations in the tank are considered for the tank. The temperature locations are used to analyse the calculated temperatures in the store. The analyses are based on calculated average temperatures for the levels in question.

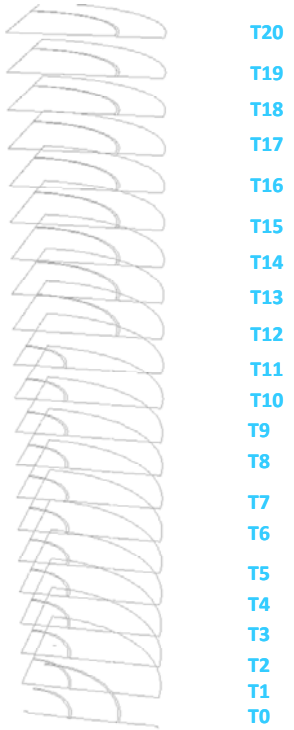

	SH	DHW
T20	1625	1625
T19	1543.75	1543.75
T18	1462.5	1462.5
T17	1381.25	1381.25
T16	1300	1300
T15	1218.75	1218.75
T14	1137.5	1137.5
T13	1056.25	1056.25
T12	975	975
T11	893.75	893.75
T10	812.5	812.5
T9	731.25	731.25
T8	650	650
T7	568.75	568.75
T6	487.5	487.5
T5	406.25	406.25
T4	325	325
T3	243.75	243.75
T2	162.5	162.5
T1	81.25	81.25
T0	0	0

Fig. 4-5. Temperature sensor locations inside space heating and DHW tank in the CFD model (in mm).

4.2 Method of analysing results

The outputs from a single CFD-simulation are numerous. For each control volume temperature, three velocity components, heat flux and heat transfer coefficient at surfaces etc. are indicated. Furthermore, it is possible to create virtual surfaces within the domains of the model and then either visualize the results at those surfaces or write selected results for the surfaces to a file for further analysis.

In this chapter absolute values of heat fluxes at tank walls are analysed along with water velocities in the inner and outer tank.

4.2.1 Heat flux

In this chapter the heat flux at the tanks wall is defined as the heat flux from the tank wall to the domestic water in the tank. Fig. 4-6 illustrates the heat flux at the tank wall.

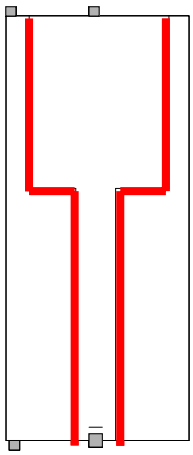

Fig. 4-6. Heat flux at the tank wall.

In order to evaluate the heat flux in the tank, the average heat flux at the tank wall is calculated by an area-weighted average of the heat flux. The calculation of the area-weighted average heat flux is performed within the CFD-programme, Fluent 6.1 (2003) by the equation given below:

$$q = \frac{1}{A_w} \sum_{i=1}^{n} q_i . A_{w,i} \tag{4.1}$$

where

A_w is the total area of the wall, [m²]

$A_{w,i}$ is the area of face number 'i' on the surface, [m²]

n is the total number of faces of the wall, [-]

q is the area-weighted average of the heat flux, [W/m²]

q_i is the heat flux at face number 'i', [W/m²]

In order to evaluate the temperature at different levels, the store is divided into small parts at different levels as shown in Fig. 4-5. The average temperature for each small part is calculated by calculating an area-weighted average of the temperatures. The calculations of the area-weighted average temperature at different horizontal levels are calculated by:

$$T = \frac{1}{A_h} \sum_{j=1}^{m} T_j . A_{h,j} \tag{4.2}$$

where

A_h is the total horizontal cross section area of the tank, [m²]
$A_{h,j}$ is the horizontal cross section area of face number 'j' of the tank, [m²]
m is the total number of faces on the horizontal cross section area of the tank, [-]
T is the area-weighted average of the temperature, [K]
T_j is the temperature of face number 'j', [K]

4.3 Results

4.3.1 Temperature distribution in the reference tank and the tank with smaller diameter

Temperature distributions for three different DHW flow rates for the reference tank are shown in Fig. 4-7-Fig. 4-12 during and after the hot water draw-off. In Fig. 4-7, the DHW flow rate is 5 l/min and the discharge is continued till 10 min when a volume of 50 l is discharged. Then the discharge is stopped and during stand by the tank remains stands still for 50 minutes. Fig. 4-7 shows that there is a good thermal stratification at the beginning of the test. After 2 minutes, the cold water goes up in DHW tank and the cold water continuing going up when 50 l water is tapped from DHW tank. The temperature decreases to 22.1ºC at 243.75 mm height of the tank. After 10 min, heat transfer from the outer tank to the inner tank heat up the inner side and the temperature in the lower level rise up. There is a sharp increase between 975 mm and 1100 mm which is located between the lower and higher diameter. There is a very good thermal stratification in the upper part of the DHW tank.

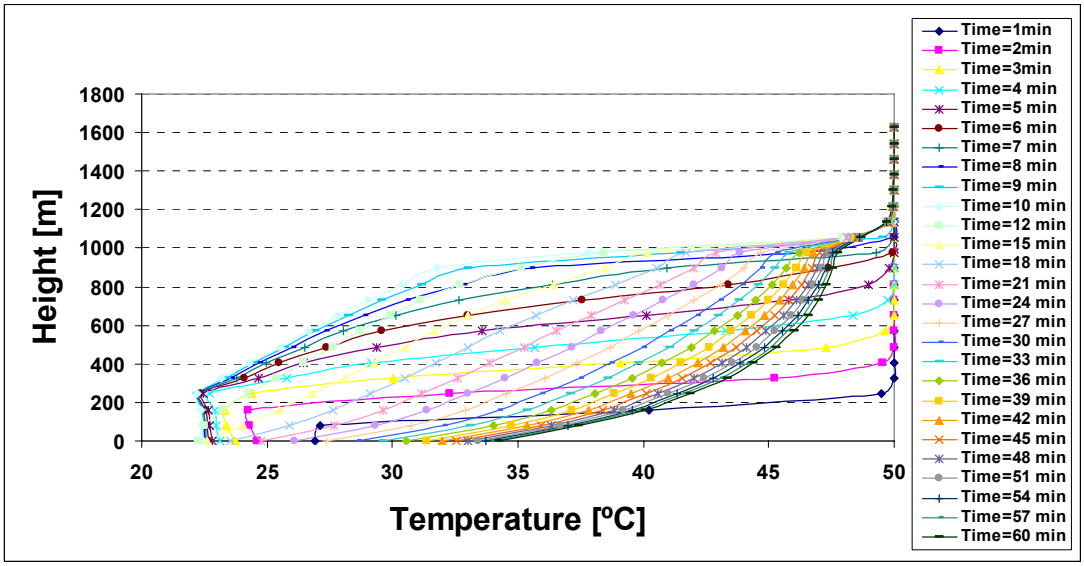

Fig. 4-7. Temperature distribution in the inner tank of the reference store during and after discharge for a hot water draw-off volume flow rate of 5 l/min.

In the outer side of the tank, the temperature decreases slightly by the time. The temperature decrease is relatively low in the upper part of the tank, that is 650 mm from the bottom and upwards.

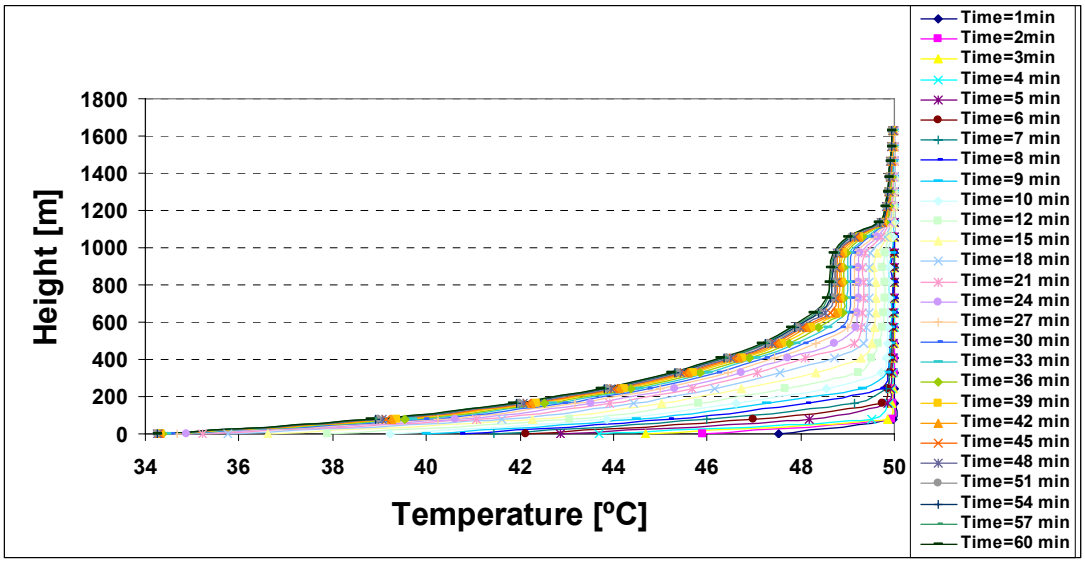

Fig. 4-8. Temperature distribution in the outer tank of the reference store during and after discharge for a hot water draw-off volume flow rate of 5 l/min.

Temperature distribution of the inner tank during and after discharge for a hot water draw-off volume flow rate of 10 l/min is shown in Fig. 4-9. Also here 50 l hot water is tapped from the inner tank. That is the draw-off is stopped after 5 minutes. After 1 minute, the temperature at the bottom of the tank is higher than the temperature in higher levels due to mixing during the draw-off. After 5 minutes when 50 l is discharged, the heat transfer from the outer to the inner tank increases the temperature in the inner tank.

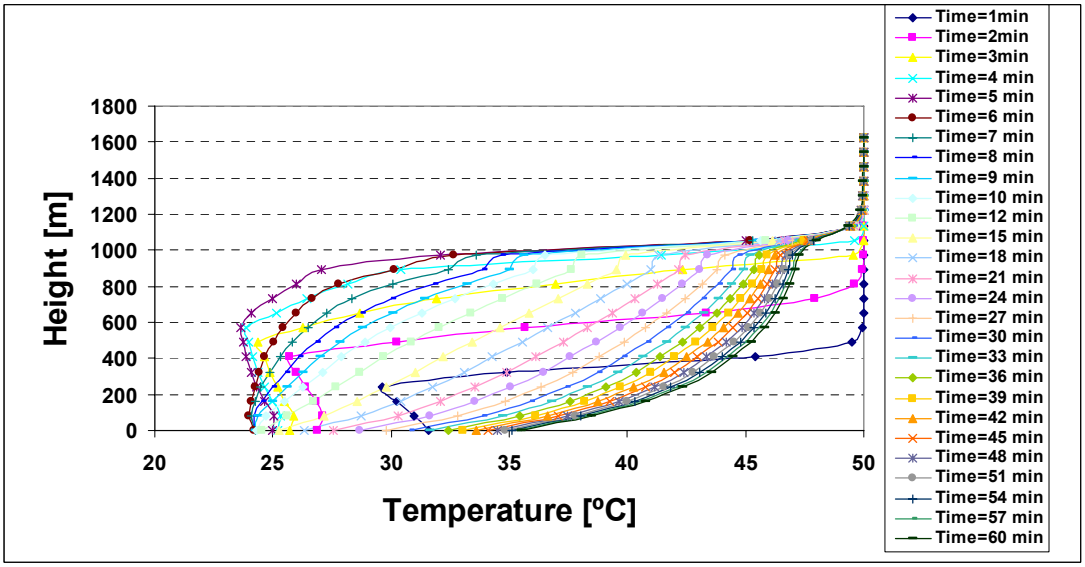

Fig. 4-9. Temperature distribution along the inner tank of the reference store during and after discharge for a hot water draw-off volume flow rate of 10 l/min.

After stand by period, the cold temperatures are placed somewhat higher in the tank than for the test with a hot water draw-off volume flow rate of 5 l/min.
The temperatures in the outer tank during and after the hot water draw-off are shown in Fig. 4-10. The temperature decreases, especially in the lower part of the tank.

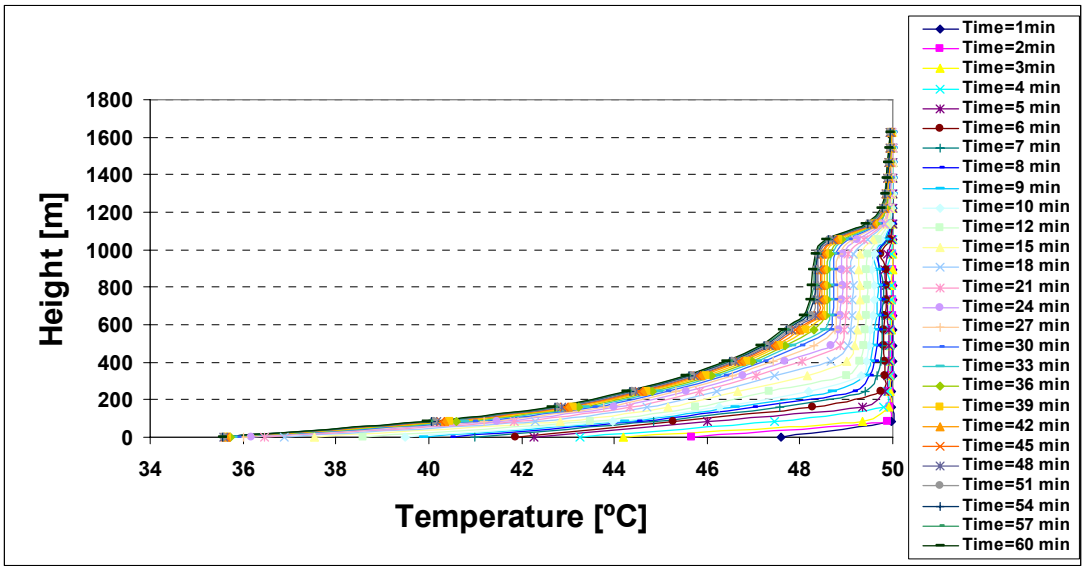

Fig. 4-10. Temperature distribution in the outer tank of the reference store during and after discharge for a hot water draw-off volume flow rate of 10 l/min.

Temperature distribution of the inner tank during and after discharge for a hot water draw-off volume flow rate of 15 l/min is shown in Fig. 4-11. 50 l is tapped from the inner tank after 3 minutes and 20 s. A strong mixing during the draw-off is obvious in the lower part of the tank.

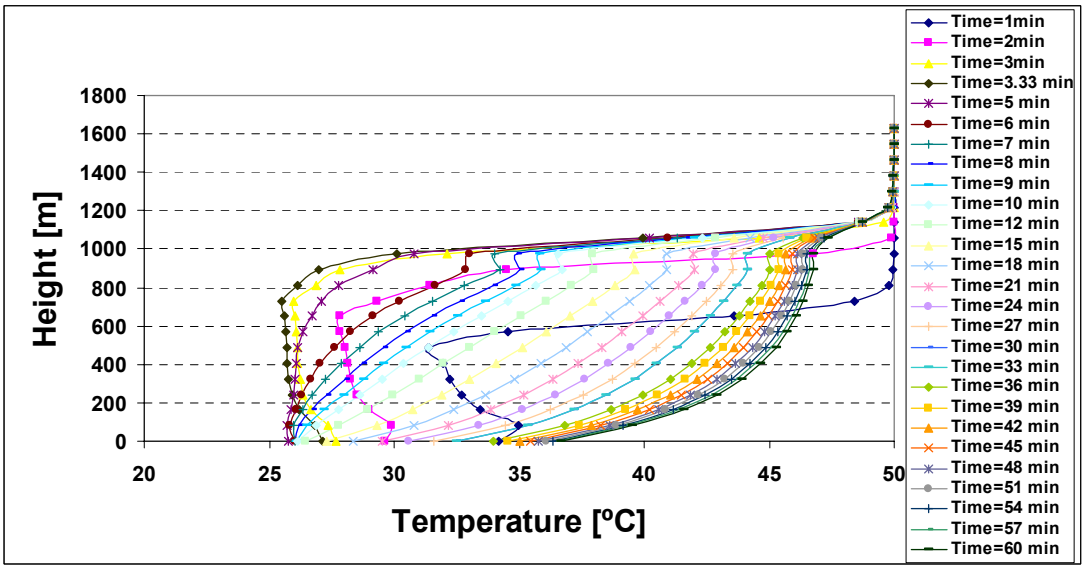

Fig. 4-11. Temperature distribution in the inner tank of the reference store during and after discharge for a hot water draw-off volume flow rate of 15 l/min.

After the stand by period, the cold temperatures are located at a higher level than for the tests with a hot water draw-off volume flow rate of 10 l/min. After 4 minutes, the temperature at 894 mm is higher than at 975 mm due to the fact that water is heated up faster in the lower level than at the higher level in the tank. This temperature difference increases after 7 minutes where the temperature difference is about 0.2 K. This temperature difference decreases till 60 minutes. The reason for such a temperature difference is that a small volume in the lower part of the tank is heated up faster than a large volume in the upper part of the tank. The inverse temperature stratification will accelerate the heating of the upper part of the tank due to natural

convection transferring heat upwards from the lower part of the inner tank with the small diameter to the upper part of the inner tank with the large diameter.
Fig. 4-12 shows the temperature distributions for the outer part of the tank during and after the hot water draw-off with a hot water draw-off with a volume flow rate of 15 l/min. Comparisons of Fig. 4-8 and Fig. 4-10 show that the low temperatures are placed somewhat higher in the tank than for lower hot water draw-off volume flow rates due to a stronger mixing during hot water draw-off.

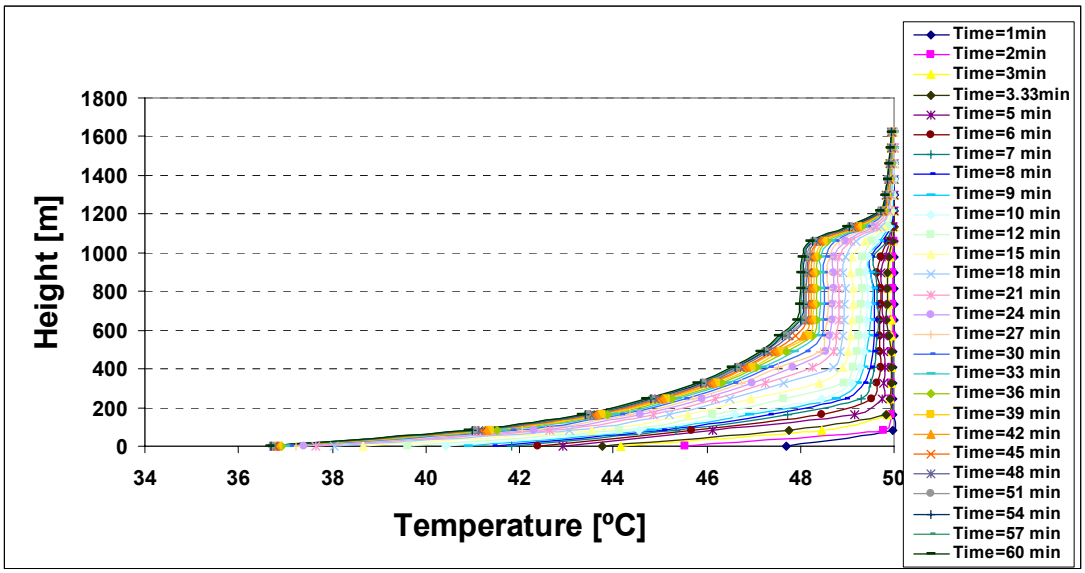

Fig. 4-12. Temperature distribution in the outer tank of the reference store during and after discharge for a hot water draw-off volume flow rate of 15 l/min.

4.3.2 Temperature distribution in the tank with a small inner tank diameter in the lower part of the store

Temperature distributions of three hot water draw-off volume flow rates of 5, 10 and 15 l/min for the store with a small DHW tank diameter have been investigated. The tank has a small diameter at the lower part of the DHW tank and the volume of the lower part of the hot water tank is about half of volume of the lower part of the hot water tank for the reference store. The upper parts of the two hot water tanks have the same volume.
In Fig. 4-13, the hot water draw-off volume flow rate is 5 l/min and the discharge is continued till 10 min when 50 l tank volume is discharged. After that, the discharge is stopped and during stand by the tank remains stands still for 50 minutes. Fig. 4-13 shows that there is a good thermal stratification at the beginning of the test. It is obvious that mixing occurs in the lower part of the inner tank during the hot water draw-off. The thermal stratification in the tank with smaller diameter is not as good as the thermal stratification in the reference store. This appears from Fig. 4-7 and Fig. 4-13.

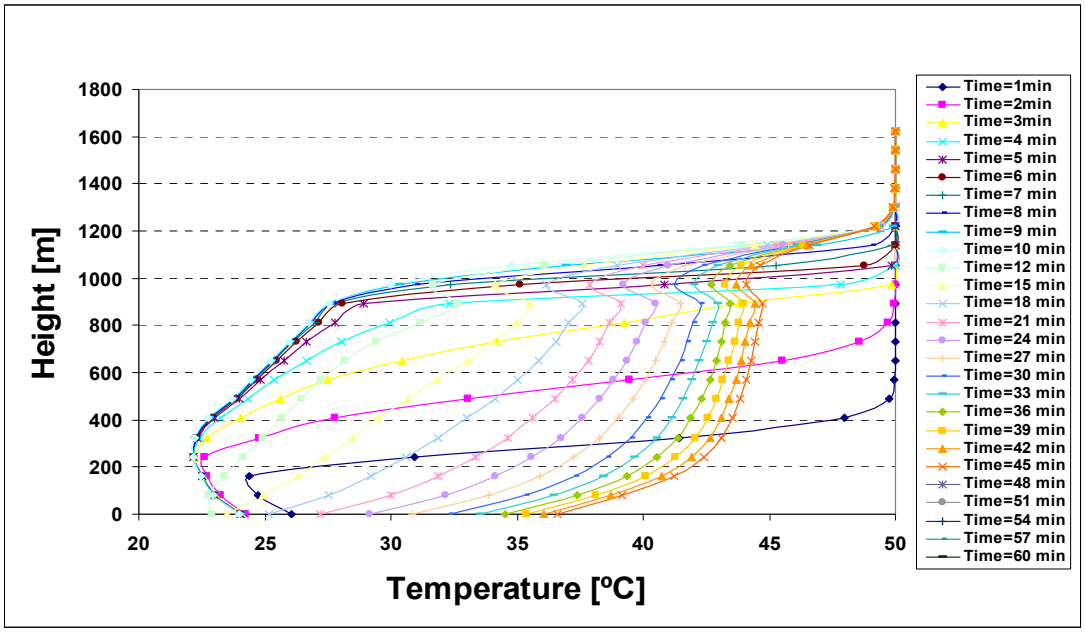

Fig. 4-13. Temperature distribution in the inner tank during and after discharge for a hot water draw-off volume flow rate of 5 l/min for the store with a small DHW tank diameter.

Fig. 4-14 shows the temperature distributions for the outer tank for a hot water draw-off volume flow rate of 5 l/min. In the outer side of the tank, the temperature decreases slightly by the time, especially in the lower part of the tank. The thermal stratification is better in the reference tank than in the tank with the small diameter of the lower part of the inner tank.

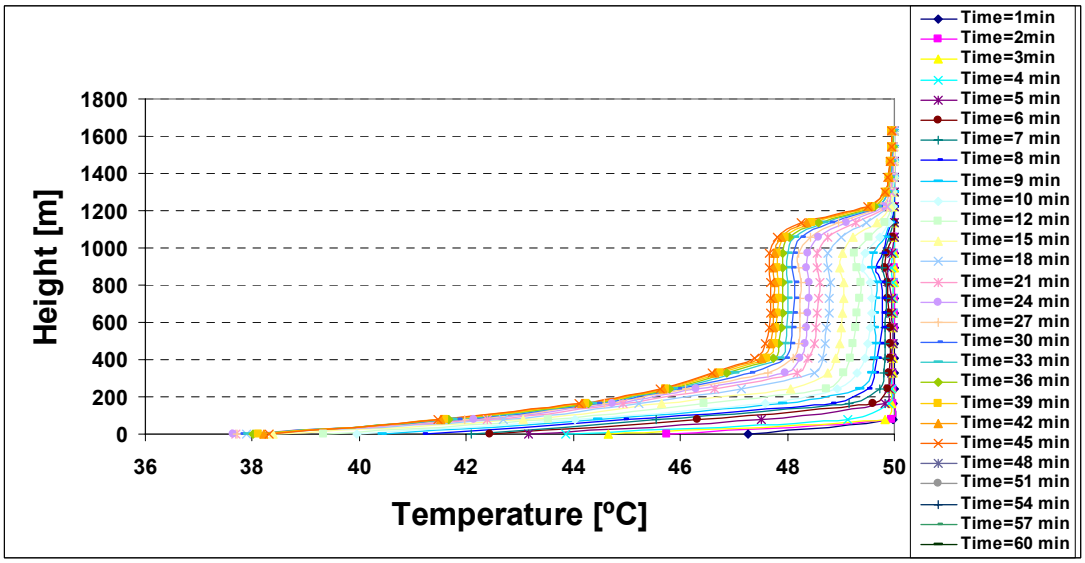

Fig. 4-14. Temperature distribution in the outer tank during and after discharge for a hot water draw-off volume flow rate of 5 l/min for the store with a small DHW tank diameter.

Fig. 4-15 shows the diagram of the height versus the temperature for the store with a small DHW tank diameter for a hot water draw-off volume flow rate of 10 l/min. The tank is discharged in 5 minutes, corresponding to a tapped volume of 50 l. After that the store stays stand still for 55 minutes. The results indicate a strong mixing in the lower part of the tank during the draw-off. After the discharge, the water at 894 mm

level is heated up faster than the water in the upper level. The reason is that a small water volume in the inner tank at the level with a small diameter is heated up faster than a great water volume in the inner tank at the level with a high tank diameter.

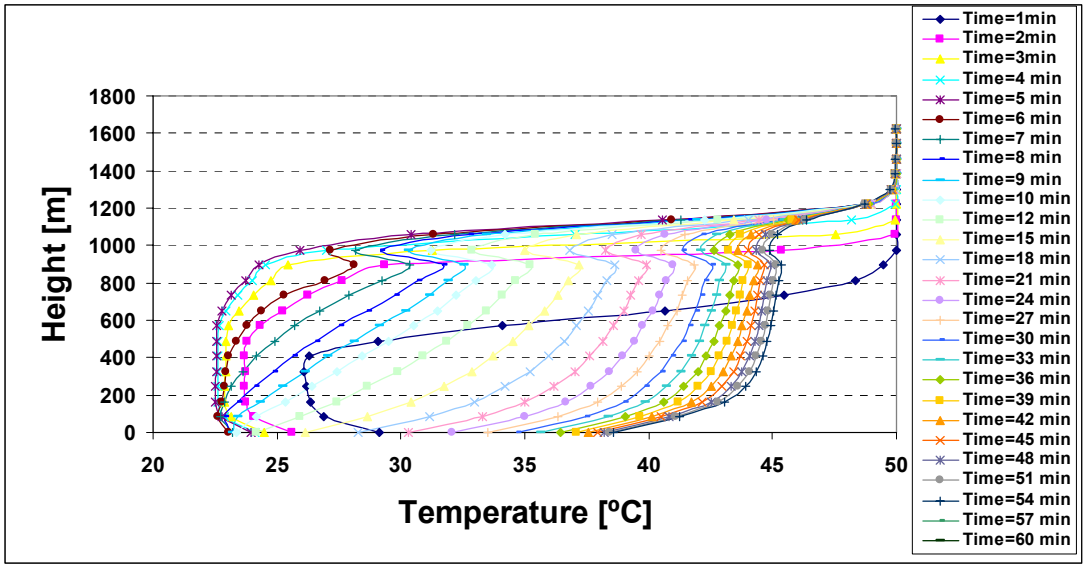

Fig. 4-15. Temperature distribution in the inner tank during and after discharge for a hot water draw-off volume flow rate of 10 l/min for the store with a small DHW tank diameter.

In the outer tank as shown in Fig. 4-16, temperatures are decreased, especially in the lower parts of the store. The thermal stratification in the reference tank is higher than in the tank with a small diameter.

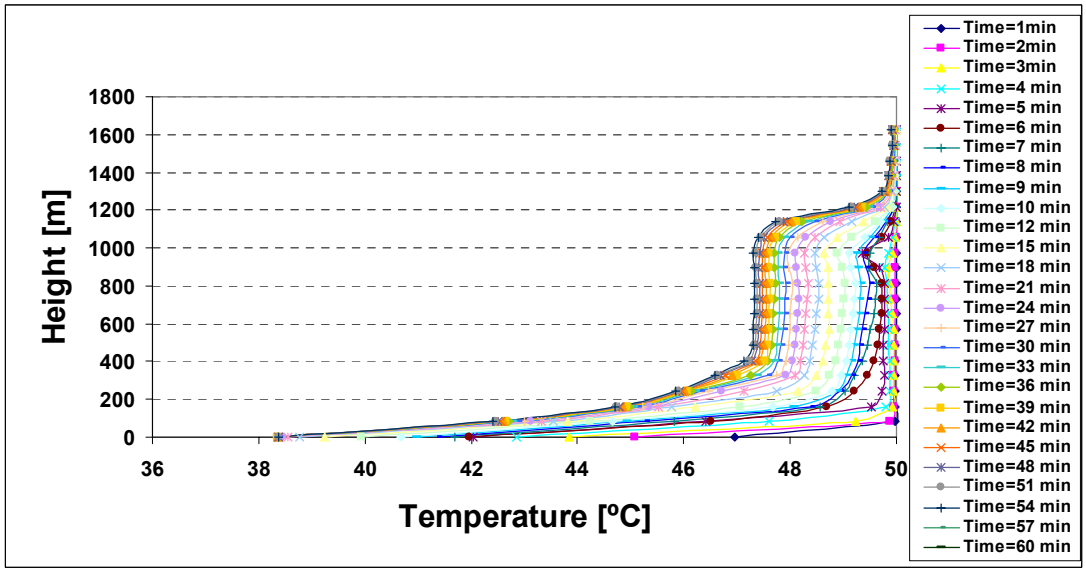

Fig. 4-16. Temperature distribution in the outer tank during and after discharge for a hot water draw-off volume flow rate of 10 l/min for the store with a small DHW tank diameter.

Temperature distributions for the DHW discharge of 15 l/min for the store with a small DHW tank diameter is shown in Fig. 4-17. The duration of the discharge is 3 minutes and 20 s, corresponding to a hot water draw-off of 50 l. During the draw-off mixing occur at the lower part of the tank. After 3 minutes and 20 s, the discharge is stopped. After 4 minutes, the temperature at the 894 mm level is higher than at the 975 mm level due to the fact that water is heated up faster in the lower level than at

the higher level of the tank. This temperature difference increases after 8 minutes to about 2.8 K. The temperature difference decreases during the remaining part of the stand by. The temperature difference is higher in the store with a small DHW tank diameter than in the reference tank, because the water volume heated in the lower part of the tank is small.

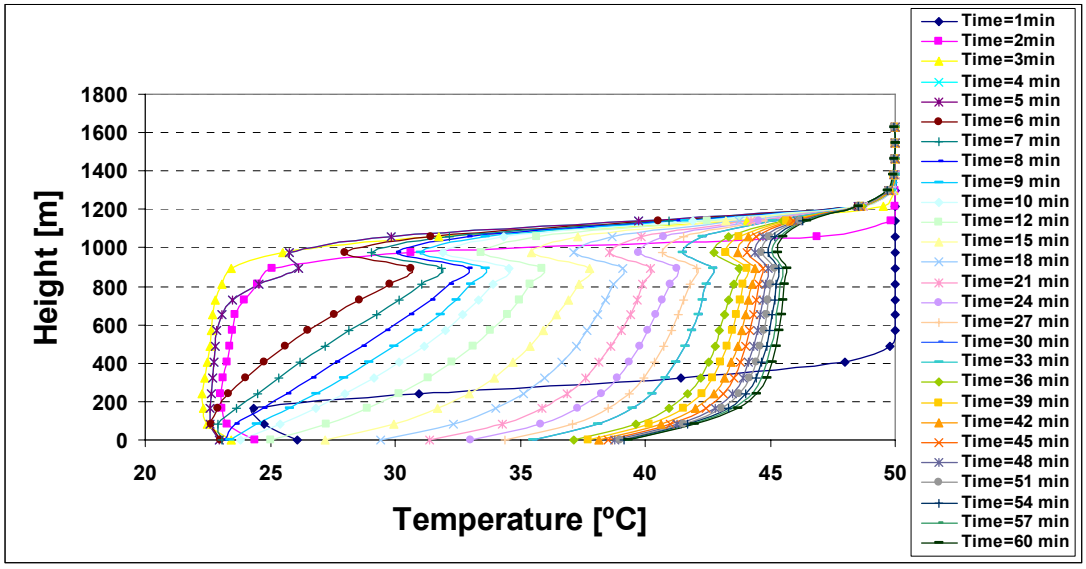

Fig. 4-17. Temperature distribution in the inner tank during and after discharge for a hot water draw-off volume flow rate of 15 l/min for the store with a small DHW tank diameter.

Fig. 4-18 shows temperature distributions for the outer part of the tank for a hot water draw-off volume flow rate of 15 l/min for the tank with small diameter. The temperatures decrease during the whole test period, especially in the lower part of the tank. The temperature stratification is lower for increasing draw-off volume flow rate during the discharge. The reason is the increased mixing for increasing draw-off volume flow rates.

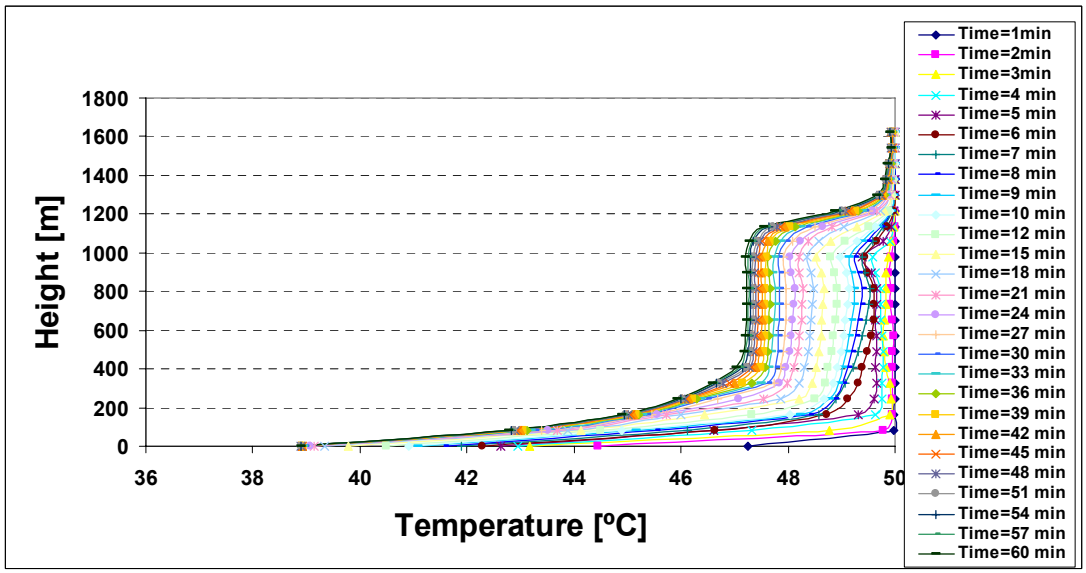

Fig. 4-18. Temperature distribution in the inner tank during and after discharge for a hot water draw-off volume flow rate of 15 l/min for the store with a small DHW tank diameter.

4.3.3 Heat flux and heat transfer for the reference tank and the tank with a small diameter

Fig. 4-19 shows the simulated total average heat flux for the DHW tank wall for 60 minutes of discharge and standby test for three different hot water draw-off volume flow rates of 5, 10 and 15 l/min.
The heat flux is increasing by the time till the discharge is stopped. The heat flux is highest at the time that the discharge test is stopped for both cases. During the stand by, the heat flux decreases. The heat flux is higher in the store with a small DHW tank diameter than in the reference tank during and shortly after the hot water draw-off. There is much less difference in heat flux during stand by for the reference tank and the tank with a small diameter.

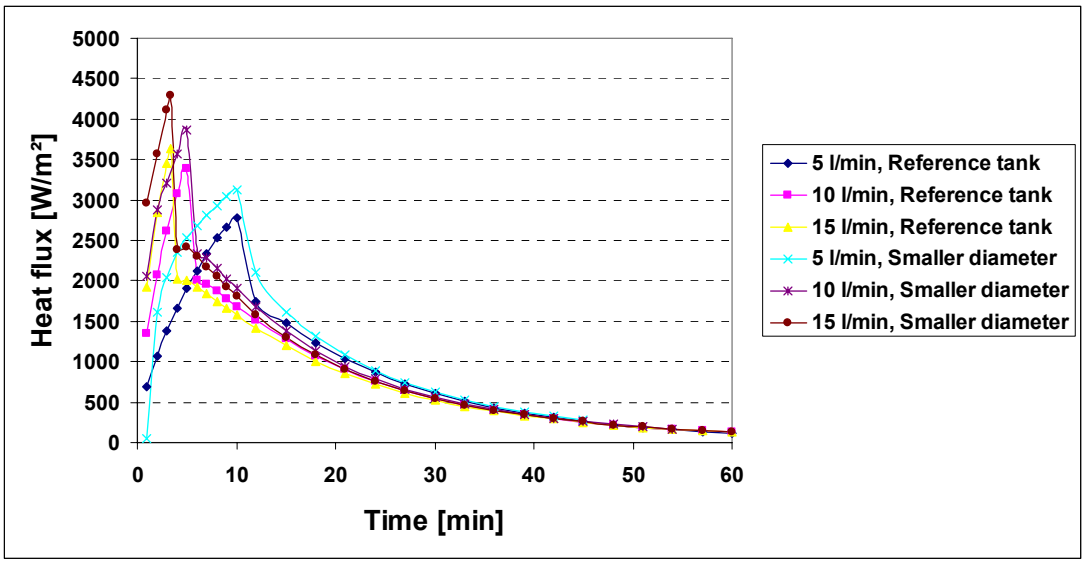

Fig. 4-19. Heat flux at the inner DHW tank wall in the reference store and in the store with a small DHW tank diameter.

Fig. 4-20 shows the total heat transfer for the DHW tank for 60 minutes of discharge and stand by test for three different hot water draw-off volume flow rates of 5, 10 and 15 l/min. The heat transfer is increasing by the time till the discharge is stopped. The heat transfer is highest at the time that the discharge test is stopped for both stores. The heat transfer is higher in the store with a small DHW tank diameter than in the reference store during and shortly after the hot water draw-off. The highest heat transfer is for the store with a small DHW tank diameter and for a draw-off volume flow rate of 15 l/min. The maximum heat transfer power is about 1150 W for the store with the small DHW tank diameter and it is around 990 W for the reference store. During the stand by, the heat transfer decreases. There is much less difference in heat transfers during stand by for the reference store and for the store with a small DHW tank diameter.

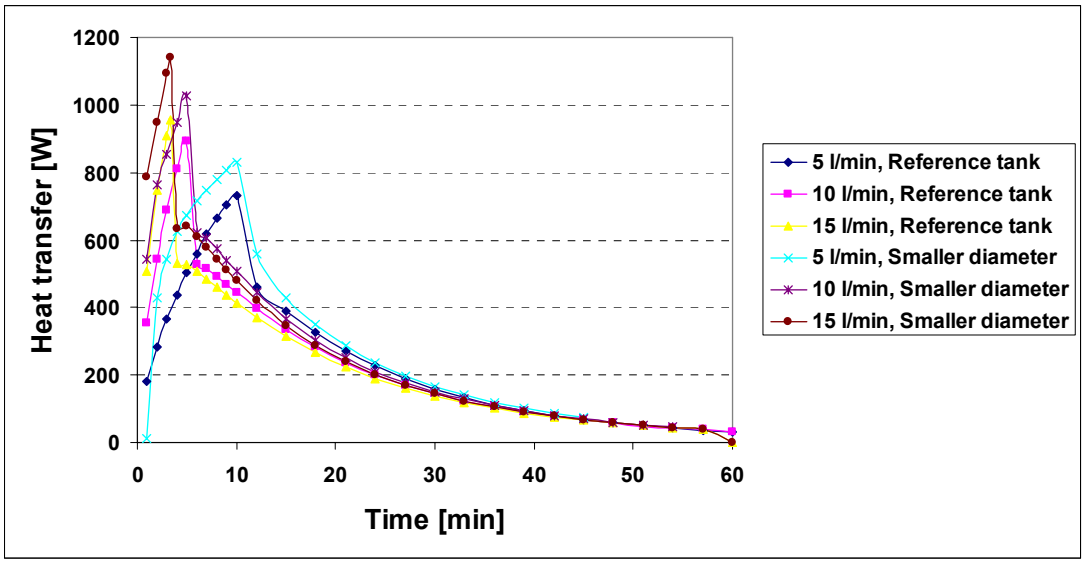

Fig. 4-20. Heat transfer at the inner DHW tank wall in the reference store and in the store with a small DHW tank diameter.

4.3.4 Heat transfer coefficient for the reference store and the store with a small DHW tank diameter

The average heat transfer coefficient from the inner tank wall to the inner water is determined by means of the CFD model. The average heat transfer coefficient increases from the beginning of the test till 50 litre of DHW is discharged from the tank. Fig. 4-21 shows the heat transfer coefficient of the DHW tank wall as a function of time for both the reference store and the store with a small DHW tank diameter. After the discharge and during stand by period, the heat transfer coefficient decreases. The highest peak heat transfer coefficient occurs at the time that the discharge is stopped for both stores. The highest average heat transfer coefficient is about 260 W/m²K for a draw-off volume flow rate of 15 l/min for the store with a small DHW tank diameter while it is about 200 W/m²K for the reference store. For 5 and 10 l/min hot water draw-off volume flow rates, the heat transfer coefficient is also higher for the store with a small DHW tank diameter than the reference store during discharge. However, there is not a significant difference in the heat transfer coefficient for the reference store and for the store with a small DHW tank diameter during stand by.

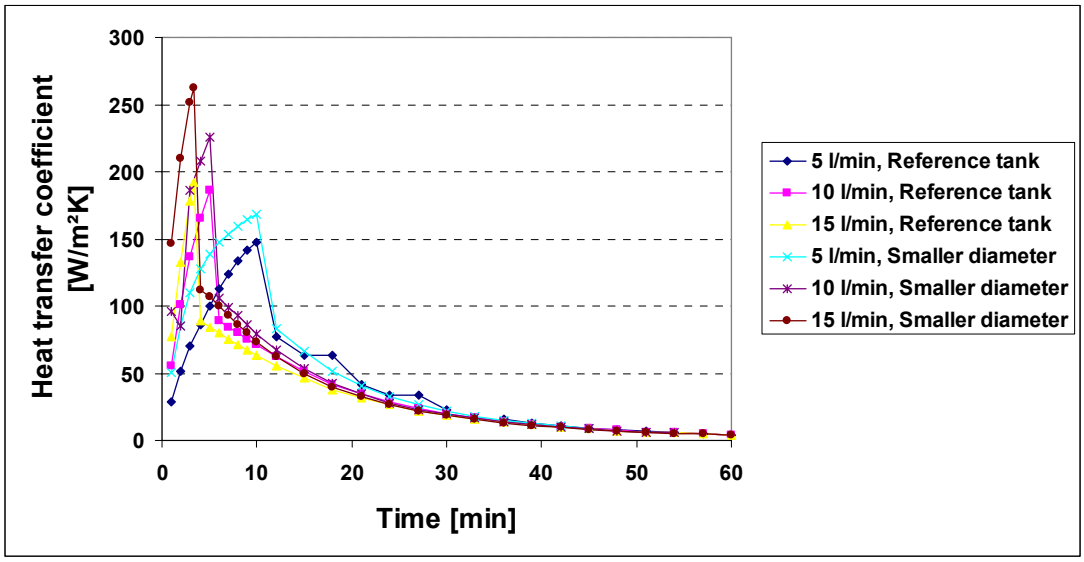

Fig. 4-21. Heat transfer coefficient at the inner DHW tank wall for the reference store and for the store with a small DHW tank diameter.

4.3.5 Fluid velocities in the reference tank

Velocity vectors for the inner and outer tank for a hot water draw-off volume flow rate of 5 l/min for the time after 5 minutes is illustrated in Fig. 4-22. 25 litre DHW volume is discharged from the tank. There is an upward flow in the inner side close to the tank wall and there is a downward flow on the outer side of the tank. There are not significant velocities in other parts of the tank.

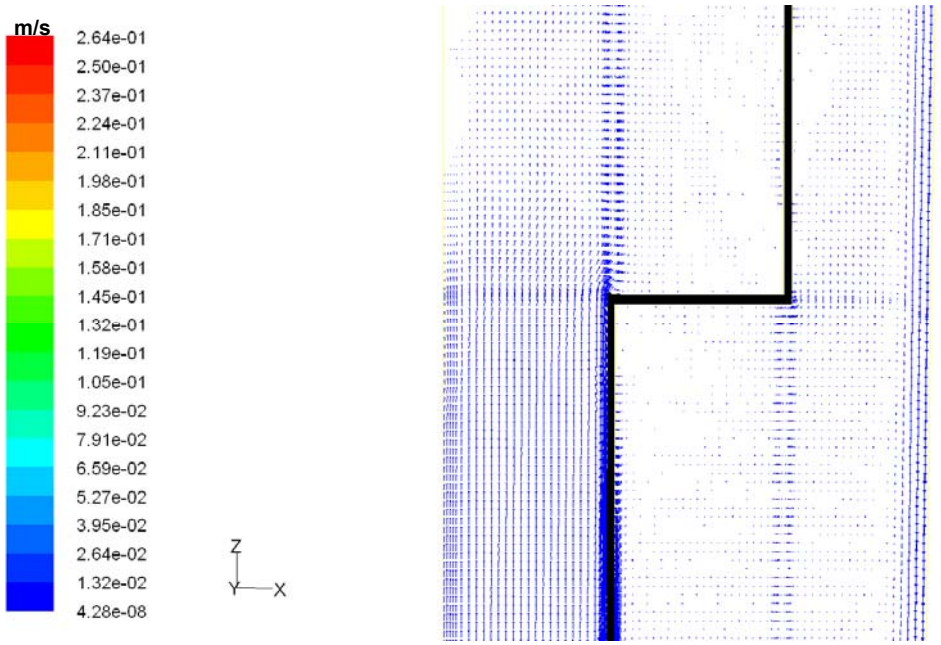

Fig. 4-22. Velocity vectors in the reference tank during discharge for 5 l/min DHW discharge and for 5 minutes.

Fig. 4-23 shows the velocity flow field for the inner and outer tank for the discharge time of 10 minutes, that is the time the discharge is stopped. The flow field shows that the inner tank velocity is higher close to the inner tank wall and when it goes up and reaches the upper DHW volume, it turns to right of the tank and the velocity decreases. At the upper part of the DHW tank wall, the velocity increases. On the other side of the tank, the outer side, there is a downward flow close to the narrow region, due to the heat transfer from the outer side to the inner side. Downward velocities increase at lower levels of the store. There is also a strong downward flow close to the outer tank wall in the lower level due to the heat loss. At the middle of the outer tank, there is an upward flow.

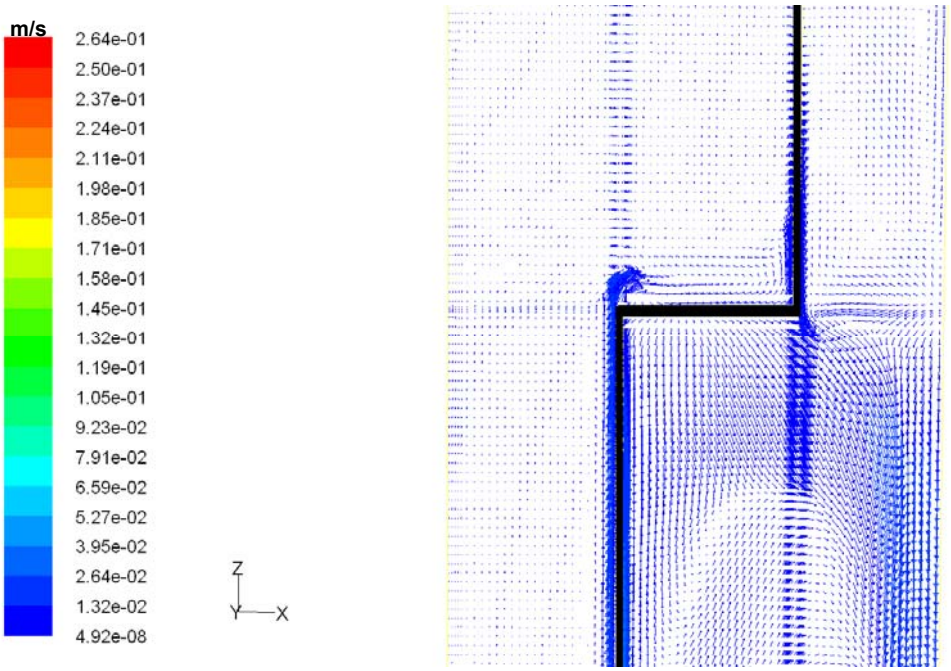

Fig. 4-23. Velocity vectors in the reference tank when discharge is stopped at 10 minutes.

Fig. 4-24 shows the flow field in the inner and outer tank during stand by after 30 minutes of the discharge test for a draw-off volume flow rate of 5 l/min. In the inner tank, there is a strong upward flow close to the inner tank wall and it goes up till it reaches the diameter change in the inner tank. The flow then divides into two parts, going to the right and to the left side of the tank. Here there is a whirling region resulting from the upward and a downward flow. Moreover, there is also a strong upward flow close to the tank wall in the upper part of the tank resulting from the heat transfer from the outer to the inner side.

On the outer side of the tank, there is a strong downward flow close to the tank wall in the narrow region. When this downward flow leaves the narrow region and continues to the larger part it mixes with the upward flow and causes a whirling region at the centre of the lower part of the tank. There is also a downward flow close to the tank wall of the outer part of the tank due to the heat transfer from the outer to the inner part of the tank. The downward flow resulting at the lower part of the store from the heat loss also causes a whirling region at the lower part of the store due the upward flow in the central part of the outer tank.

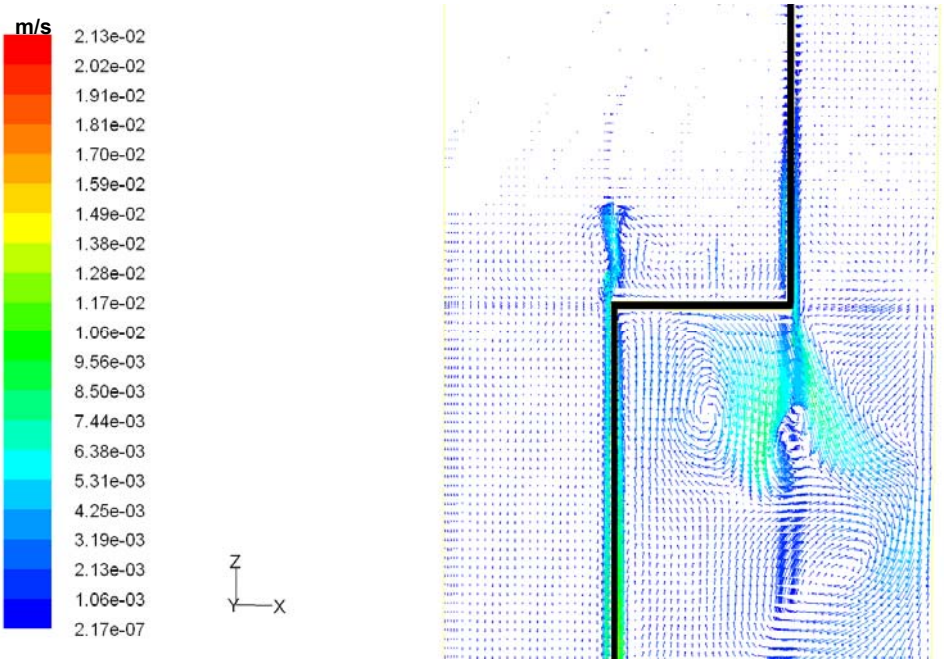

Fig. 4-24. Velocity vectors in the reference tank after discharge at 30 minutes.

Fig. 4-25 shows the flow field of the inner and outer side of the tank during stand by at 40 minutes. In the inner side, the velocity vectors are similar to the velocity vectors at 30 minutes. In the inner tank, the velocities are upward close to the walls of the lower part of the inner tank and when the water reaches the upper level with a large diameter, it continues upward and divides into two parts going to the right and to the left. On the outer side, there is a downward flow close to the tank wall in the narrow region and it combines with a downward flow close to the horizontal surface. The upward flow in the central part of the outer tank and the downward flows cause a whirling region close to the narrow region. The downward flow close to the outer tank wall is due to the heat loss.

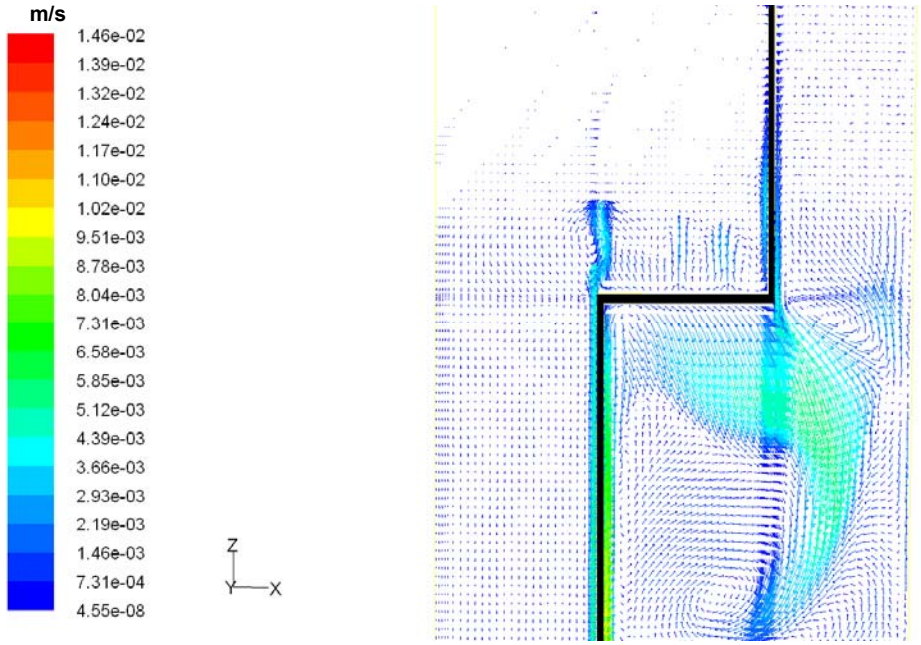

Fig. 4-25. Velocity vectors in the reference tank after discharge at 40 minutes.

4.3.6 Fluid velocities in the tank with the small diameter

Velocity vectors for the inner and outer tank for a draw-off volume flow rate of 5 l/min for the time after 5 minutes for the store with a small DHW tank diameter illustrated in Fig. 4-22. 25 litre DHW volume is discharged from the tank. There is an upward flow in the inner side close to the tank wall and there is a downward flow close to the tank wall at the outer side of the tank. The velocities are higher for the reference tank. The reason for that is the higher heat flux for the store with a small DHW tank diameterthan for the reference tank.

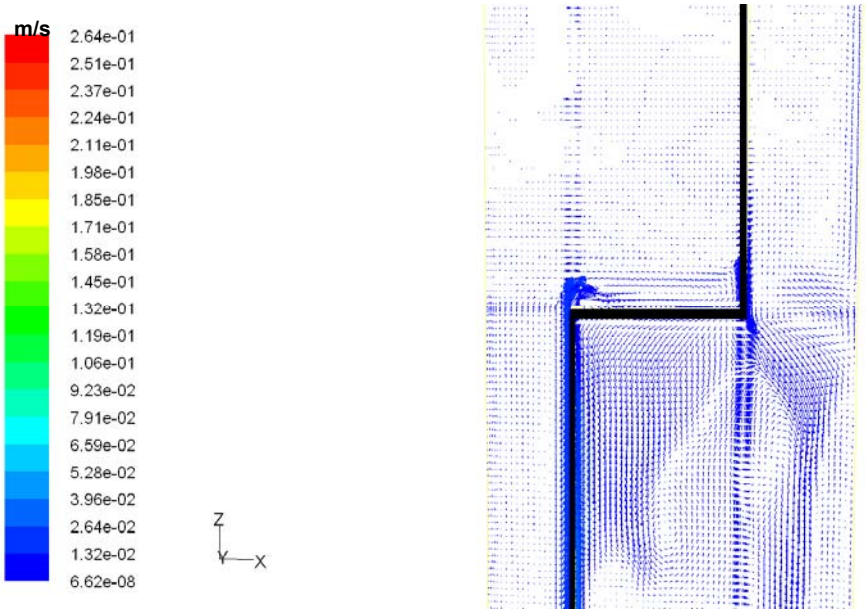

Fig. 4-26. Velocity vectors in the tank with small diameter after discharge for 5 minutes.

Fig. 4-27 shows the flow field for the inner and outer tank of the store with a small tank diameter for the DHW flow rate of 5 l/min for the time of 10 minutes, that is by the end of the draw-off period.
The water velocity is high close to the inner tank wall and when it goes up and reaches the upper DHW volume, it turns to right of tank and the velocity decreases. Close to the inner upper wall of the DHW tank, the velocity increases. On the other side of the inner tank, on the outer side, there is a downward flow close to the narrow region, due to the heat transfer from the outer to the inner side. When it goes downward and reaches the lower tank level, the downward velocity increases. There is also a strong downward flow close to the outer tank wall in the lower level due to the heat loss. At the middle of the outer tank, water is flowing upward replacing water going downward.

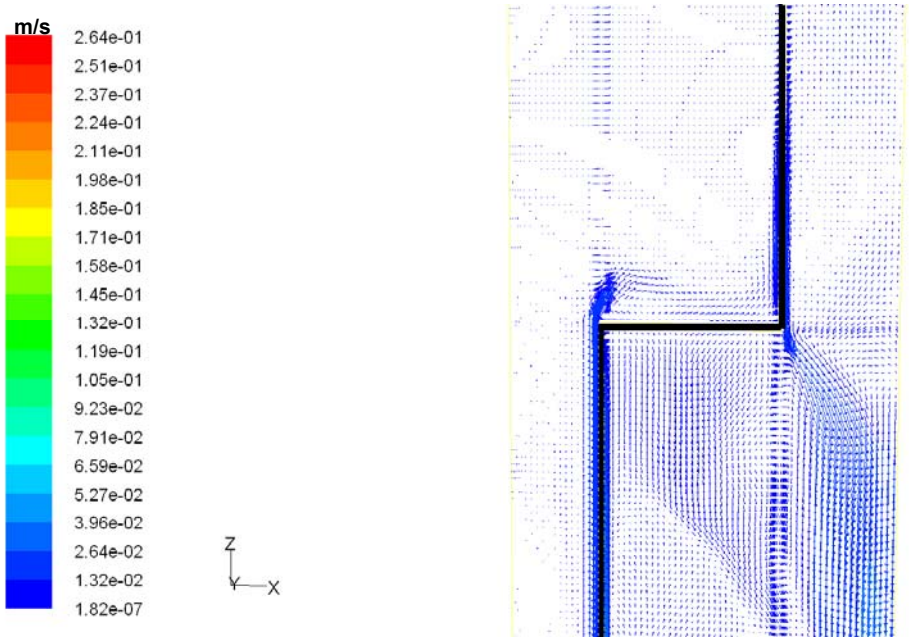

Fig. 4-27. Velocity vectors in the store with a small DHW tank diameter at 10 minutes.

Fig. 4-28 shows the velocity vectors for the store with a small DHW tank diameter during stand by at 30 minutes. The velocities are higher than in the reference tank due to a higher heat transfer. On the inner side, there is an upward flow close to the tank wall and when it reaches the upper level, it turn to the left and some goes down in the tank. On the outer side, there is a downward flow in the narrow region and it continues downward in the lower level in the outer tank. There is also a strong downward flow close to the outer wall due to the heat loss.

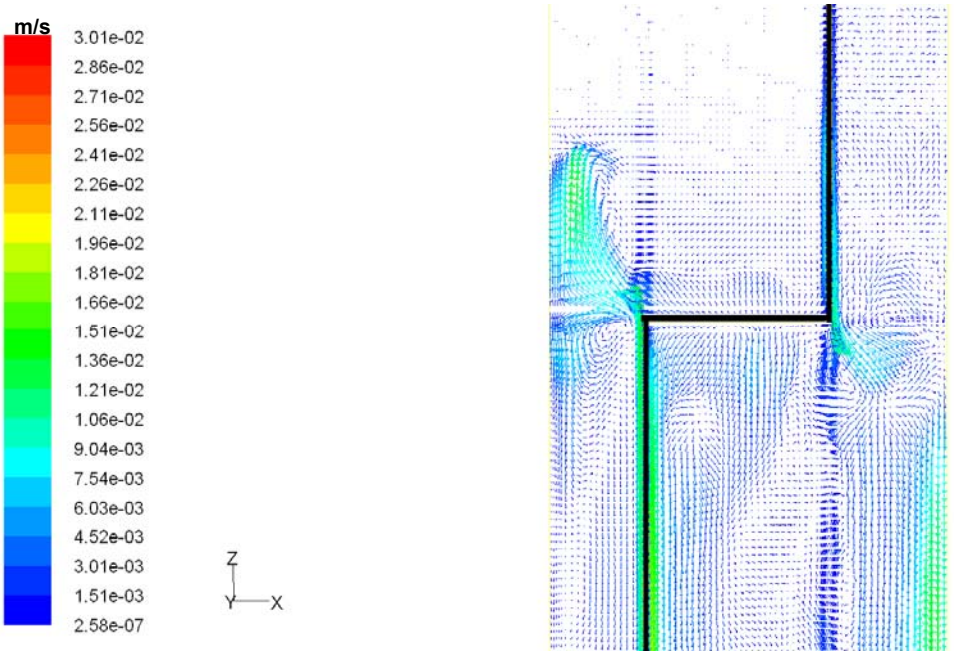

Fig. 4-28. Velocity vectors in the store with a small DHW tank diameter at 30 minutes.

Fig. 4-29 shows the flow field for the inner and outer side for the store with a small DHW tank diameter at 40 minutes. In the inner side, there is an upward flow close to the tank wall and when it reaches the upper wall, it divides to two parts. One goes

upward and one goes downward and causes a whirling region close to a location where the diameter of the inner tank changes. On the outer side, there is a downward flow in the narrow region and when the downward flow goes down in the tank and meets the upward flow in the central part of the outer tank a whirling region in the central part of the outer tank will appear. Again the velocity is higher for the store with a small DHW tank diameter than for the reference tank.

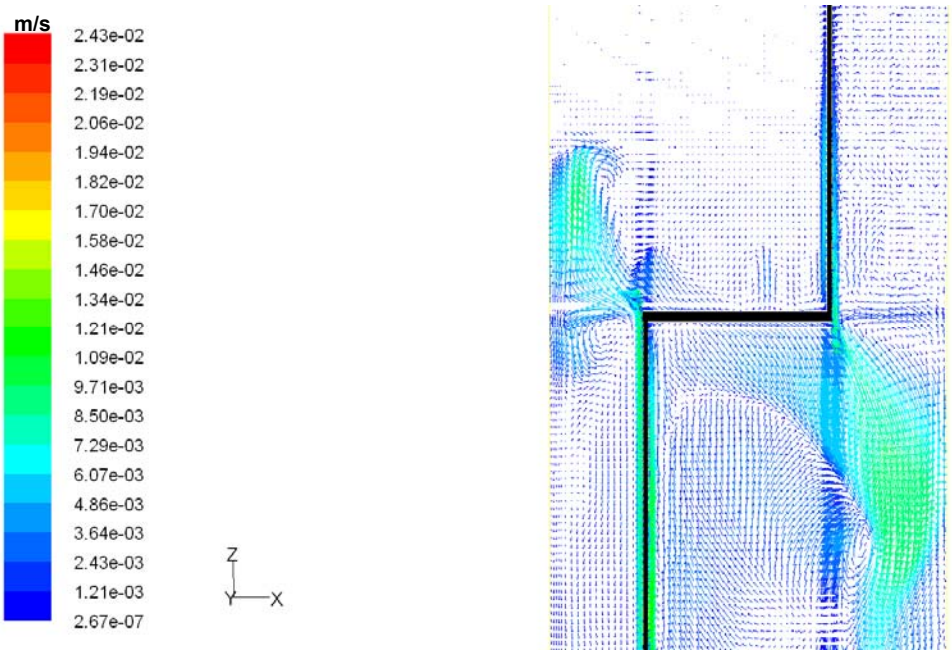

Fig. 4-29. Velocity vector in the store with a small DHW tank diameter at 40 minutes.

4.3.7 Comparison of flow behavior and heat transfer in the reference store and the store with a small DHW tank diameter

The temperature distribution of the tank wall for the reference store and for the store with a small DHW tank diameter during and after a hot water draw-off with a volume flow rate of 15 l/min are shown in Fig. 4-30 and Fig. 4-31. The duration of the hot water draw-off is 3 minutes and 20 sec. The temperatures are the area average temperature of the tank wall in the level in question. The wall temperatures in the reference store are higher than in the store with a small DHW tank diameter. Due to mixing during discharge and due to the heat stored in the bottom part of the DHW tank wall, the tank wall temperature at the lower part of the tank is higher than the temperature at higher levels during the discharge. After the discharge and during the stand by, the wall temperature from the bottom to the 894 mm level increases, then there is a decrease at level 975 mm. The diameter of the DHW tank changes between these two levels. The temperature difference between level 894 mm and level 975 mm is higher for the store with a small DHW tank diameter than for the reference tank. However, the temperature level is higher for the reference tank than for the store with a small DHW tank diameter.

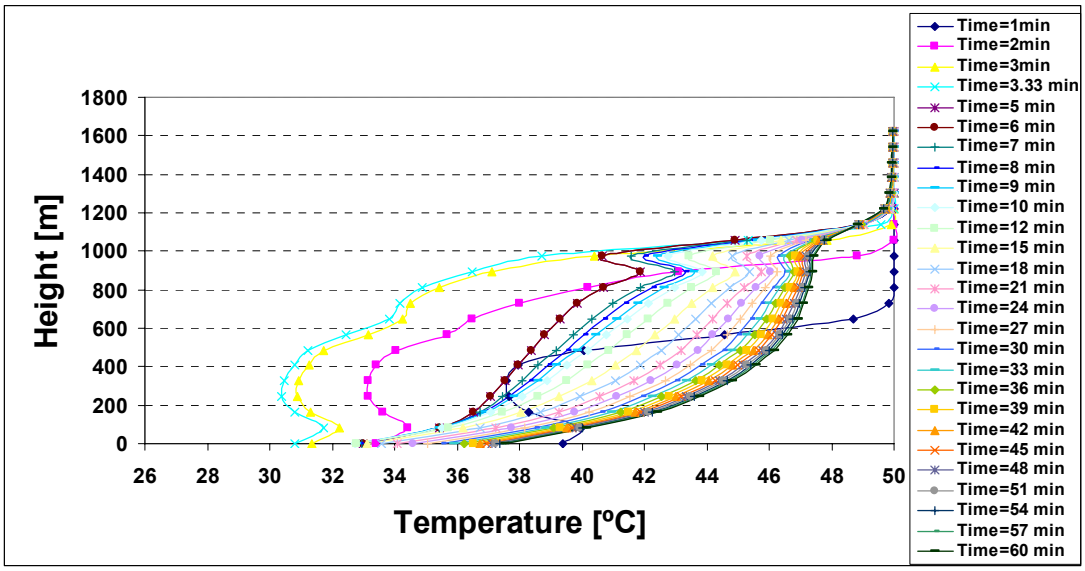

Fig. 4-30. Temperature distribution in the tank wall of the reference store during and after discharge for a hot water draw-off volume flow rate of 15 l/min.

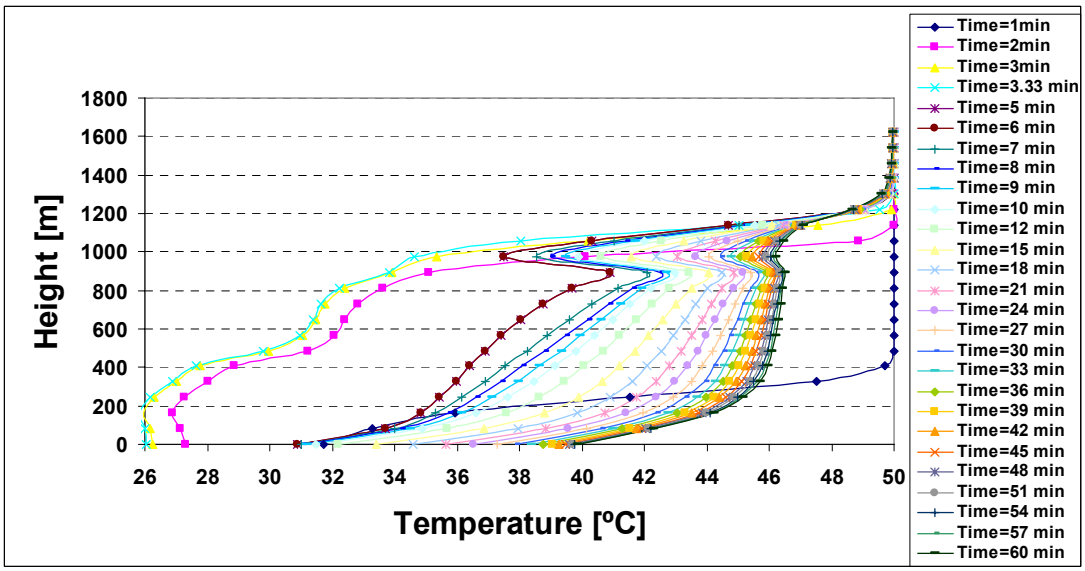

Fig. 4-31. Temperature distribution in the tank wall during and after discharge for a hot water draw-off volume flow rate of 15 l/min for the store with a small DHW tank diameter.

Two levels of the stores, level 894 mm and level 975 mm are used for comparisons of the flow behaviour and temperatures in the stores. The DHW tank diameter is changed between these two levels. The temperature distribution for both cross sections is shown after 7 minutes of the beginning of the test or 3 minutes and 40 sec after the discharge. Fig. 4-32 shows temperatures in a quarter of the inner DHW tank for level 894 mm and level 975 mm for the reference store. There are higher temperatures at the lower level than at the higher level. Close to the DHW tank wall, the temperature is highest due to the heat transfer from the outer tank to the inner tank. The reason for the higher temperatures in the lower level is that the small water volume is heated faster than the larger water volume by the heat transfer from the outer tank.

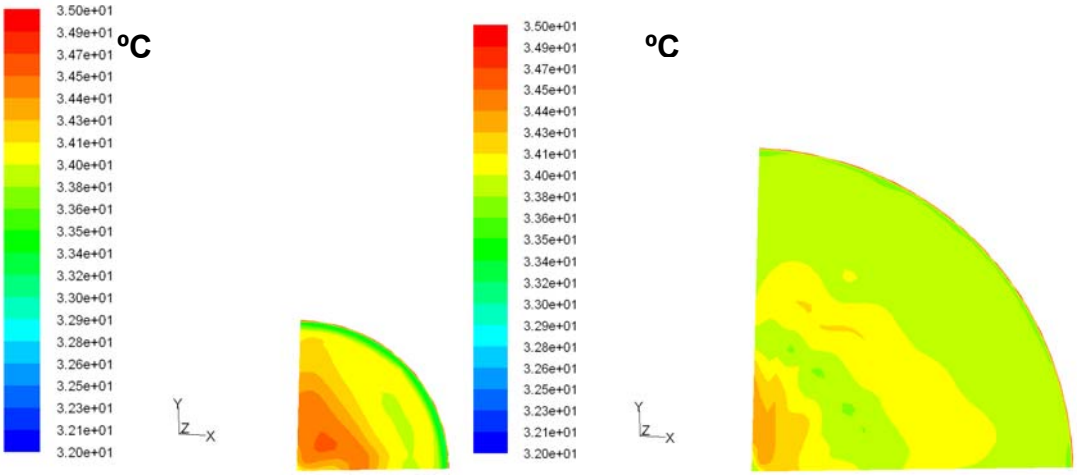

Fig. 4-32. Temperature distribution in a horizontal surface of the inner tank of the reference store for the height of 894 mm (to the left) and of 975 mm (to the right) from the bottom of the tank.

The temperatures in the outer tank for the reference store are shown in two levels at the same time as in Fig. 4-33. The left hand side image shows temperatures in the outer tank in the lower level while temperatures in the upper level are shown to the right. The temperature is coldest close to the DHW tank wall. However, cold temperatures are also found in other parts of the cross section area at the lower level.

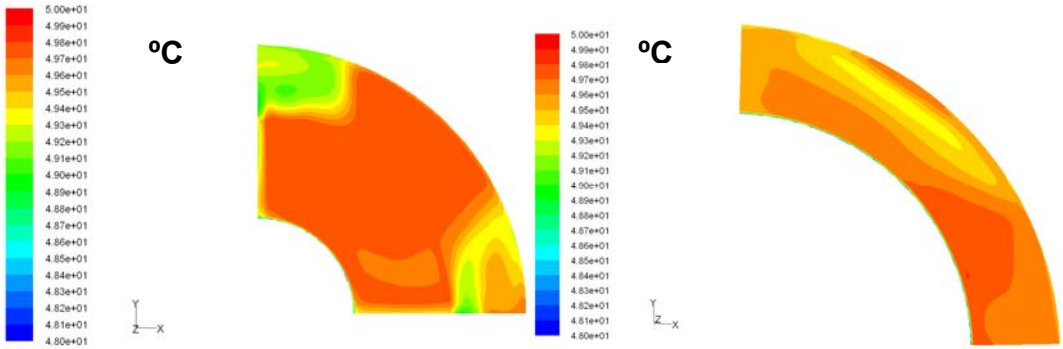

Fig. 4-33. Temperature distribution in a horizontal surface of the outer tank of the reference store for the height of 894 mm (to the left) and of 975 mm (to the right) from the bottom of the tank.

Fig. 4-34 shows temperatures in a quarter of the horizontal cross section of the inner tank for the store with a small DHW tank diameter at two levels 7 minutes after the beginning of the test or 3 minutes and 40 sec after a hot water draw-off with a volume flow rate of 15 l/min, like shown for the reference store. The temperatures close to the tank wall of the inner tank are high in a very narrow region. The temperatures are colder in the other parts of the cross section area of the inner tank. At the higher level, the temperatures are lower than at the lower level again due to the faster heating of a small volume than of a large volume. The temperature level for the store with a small DHW tank diameter is lower than the temperature level for the reference store. The reason is that the hot water discharge will replace the domestic water faster in the tank with the small diameter than in the reference tank.

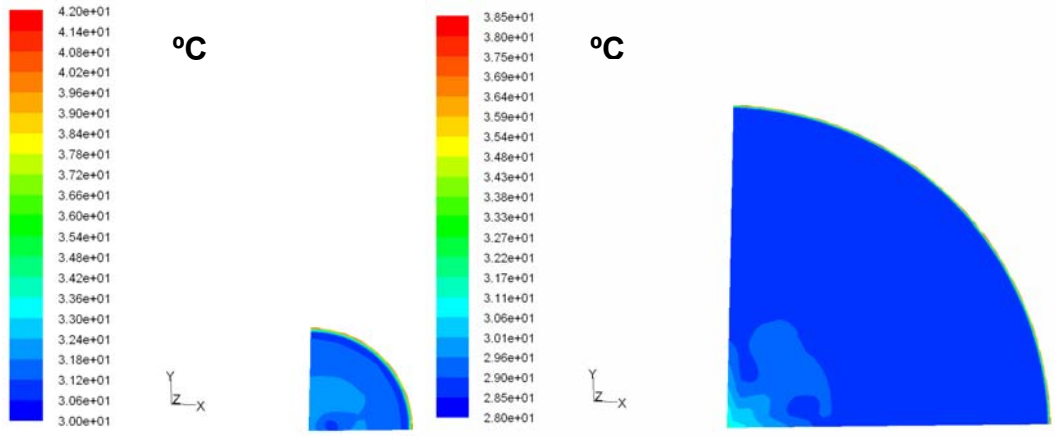

Fig. 4-34. Temperature distribution in a horizontal surface of the inner tank of the store with the small DHW tank diameter for the height of 894 mm (to the left) and of 975 mm (to the right) from the bottom of the tank.

In the outer side of the DHW tank, the temperatures in a narrow region are low close to the tank wall due to the heat loss and heat transfer to the inner tank. There are also lower temperatures in the store with a small DHW tank diameter compared to the reference store.

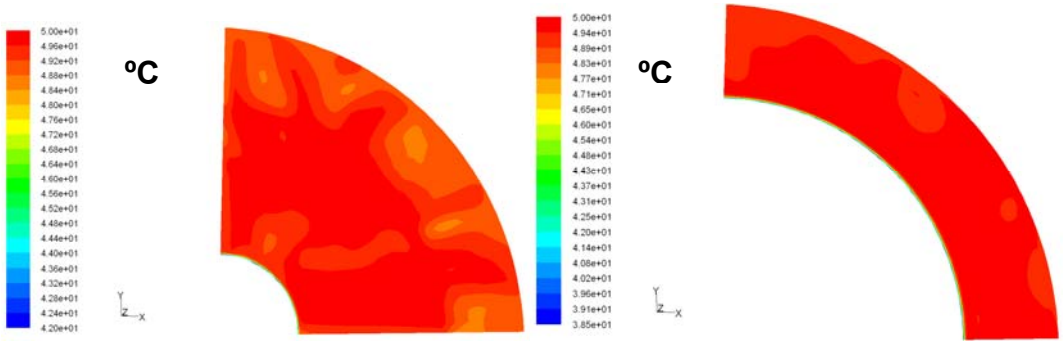

Fig. 4-35. Temperature distribution in a horizontal surface of the outer tank of the store with the small DHW tank diameter for the height of 894 mm (to the left) and of 975 mm (to the right) from the bottom of the tank.

The vertical water velocities in the inner and outer tank are compared in both stores at two different levels below and above the location where the diameter of the tank changes, that is at level 894 mm and level 975 mm during stand by 7 minutes after the beginning of the test or 3 minutes and 40 sec after the discharge. The vertical velocities for the inner tank and outer tank for a tank level of 894 mm for both stores are shown in Fig. 4-36. In the inner tank for the reference store, there is a downward flow at the central parts of the tank. Then there is an upward flow at a radius of 0.057 m. However, again there is a downward flow till a radius of 0.101 m. Close to the tank wall there is a strong upward flow with a velocity of 0.021 m/s due to the high heat transfer close to the tank wall. Then the velocity decreases to zero on the tank wall. In the outer tank of the reference store, due to the heat transfer to the inner tank, there is a strong downward flow of 0.013 m/s at a radius of 0.116 m. This velocity is lower compared to the upward flow in the inner side. The velocity remains more or less constant at about 0.009 m/s till a radius of 0.235 m. Then there is a stronger downward flow of 0.012 m/s at a radius of 0.248 m.

In the inner tank for the store with a small DHW tank diameter, there is downward flow in the central parts of the tank with a velocity up to 0.016 m/s at a radius of

0.017 m. Then there is an upward flow at 0.042 m of about 0.0008 m/s. However, again there is a downward flow till a radius of 0.0673 m with a velocity of 0.00389 m/s. Close to the tank wall there is a strong upward flow with a velocity of 0.025 m/s due to the high heat transfer close to the tank wall. Then the velocity decreases to zero on the tank wall. In the outer tank, due to the heat transfer to the inner tank, there is a strong downward flow of up to 0.014 m/s at a radius of 0.074 m. However, this velocity is lower compared to the upward flow in the inner side. The downward velocity decreases to 0.0015 m/s at a radius of 0.234 m. Then there is strong downward flow up to 0.011 m/s at a radius of 0.26 m.
At a level of 894 mm, the downward and upward velocities close to the DHW tank wall are higher for the store with a small diameter than for the reference store because the water is heated faster in the lower volume of the DHW tank in the store with a small DHW tank diameter than in the reference store.

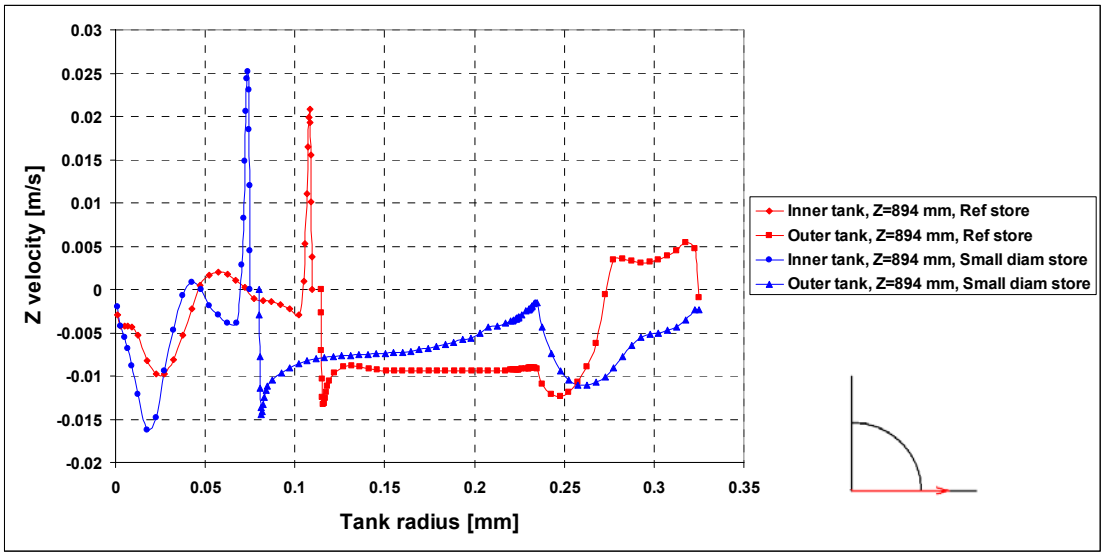

Fig. 4-36. Velocities in the horizontal surface of the inner and outer tank for the height of 894 mm level for the reference store and the store with a small DHW tank diameter (distance from center of the tank).

The vertical velocities for the inner tank and outer tank for a store level of 894 mm for both stores are shown in Fig. 4-37.
In the inner tank for the reference store, there is a downward flow at the center. There is an upward flow of 0.004 m/s at a radius of 0.017 m. The upward flow remains more or less constant till 0.086 m. Then there is a downward flow till 0.2174 m of about 0.0013 m/s. Then close to the tank wall, the upward flow increases to 0.0094 m/s at 0.224 m. The velocity is zero at the tank wall.
In the outer tank, the highest downward velocity is 0.0153 m/s at a radius of 0.2312 m. Then there is an upward flow at a radius of 0.2376 m of 0.0022 m/s. Then the upward flow remains more or less constant till 0.31 m.
In the inner tank for the tank with the small diameter, there is an upward flow at the center to the maximum velocity of 0.0167 m/s at 0.0175 m. Then the upward flow decreases to the downward flow at 0.0623 mm of about 0.0005 m/s. Then it remains almost constant till 0.2174 m. Then close to the tank wall, the upward flow increases to 0.01 m/s at a radius of 0.224 m. The velocity is zero at the tank wall.
In the outer tank, the highest downward velocity is 0.0222 m/s at a radius of 0.2312 m due to the high heat transfer to the inner tank. Then there is a downward flow at

0.2376 m of 0.0007 m/s. Then the downward flow remains more or less constant till the radius of 0.28 m, then the flow rate increases to an upward flow of 0.0003 m/s at 0.3175 m.

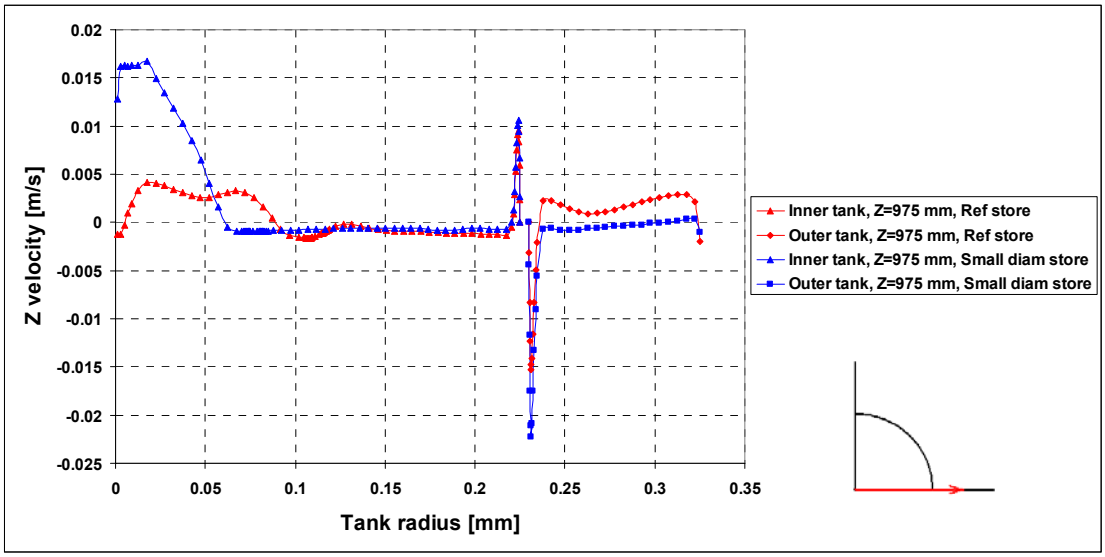

Fig. 4-37. Velocities in the horizontal surface of the inner and outer tank for the height of 975 mm level for the reference store and the store with a small DHW tank diameter (distance from center of the tank).

The vertical heat transfer in the DHW tank wall 7 minutes after the beginning of the test or 3 minutes and 40 sec after the discharge during stand by is shown in Fig. 4-38. Minus heat transfer means that the heat is going downward and vice versa. There is high heat transfer at the bottom of the tank. However it decreases till 853 mm. At 894 mm, the heat is going upward, therefore the positive heat transfer. At level 975 mm, there is high heat transfer going upward. At a higher level, heat is again transferred downward. At the upper level of the tank from 1200 mm, the heat transfer is close to zero since the wall temperature remains constant as shown in Fig. 4-31. The comparison between the reference store and the store with a small DHW tank diameter shows that there is higher heat transfer in the DHW tank wall for the reference store than for the store with a small DHW tank diameter. However, there is higher heat transfer at 894 mm in the store with a small DHW tank diameter than in the reference store. The peak heat transfer at 975 mm also shows higher heat transfer in the store with a small DHW tank diameter than in the reference store. This result is confirmed by higher temperature difference between level 975 mm and level 853 mm for the store with a small DHW tank diameter than for the reference store after the discharge, during stand by, see Fig. 4-30 and Fig. 4-31. The reason is that the smaller volume of the lower part of the store with a small DHW tank diameter is heated faster than the larger volume of the lower part of the reference store.

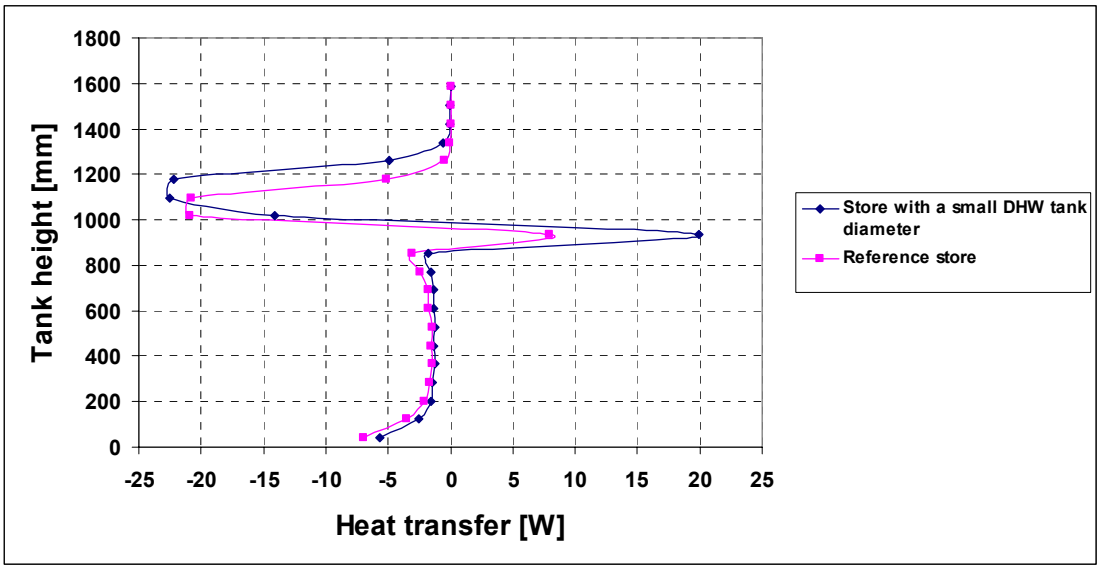

Fig. 4-38. Vertical heat transfer in the tank wall for the reference store and the store with a small DHW tank diameter.

4.4 Conclusions

The simulation study of two different geometries of a reference tank and a tank with a small diameter is investigated in this chapter. The temperature distributions, heat flux, heat transfer coefficients and velocity vectors are shown for three different hot water draw-off volume flow rates of 5, 10 and 15 l/min. The results show that when the diameter of the inner DHW tank in the lower part decreases, the thermal stratification during and after domestic hot water draw-offs gets worse than for tanks with larger diameters.

Most likely thermal stratification is established in a better way in the store with a small DHW tank diameter during charge periods and during space heating discharge periods. This is however not investigated in the current study.

It is shown that there are higher temperatures at a lower level than at a higher level where the diameter of the inner DHW tank changes. The reason for the higher temperatures in the lower level is that the small water volume is heated faster than the larger water volume by the heat transfer from the outer tank.

5 TRNSYS calculations for two solar combisystems and one SDHW system

5.1 Comparison between bikini solar combisystems and mantle tank SDHW systems

5.1.1 Assumptions

The thermal performance of solar combisystems based on a hot water tank with two mantles is calculated with the simulation program TRNSYS 16 (2005).
The solar collector area used is 3-8 m² solar collectors. The collector tilt is 45° and the collectors are facing south. The mass flow rate in the solar collector loop is 0.15 kg/min/m² collector. A differential thermostat control with one sensor in the solar collector and one in the outlet of the lower mantle is used to control the pump in the solar collector loop with a start and stop temperature difference of 10 K and 0.1 K, respectively. Moreover, if the temperature of the top of the tank is higher than 95°C the pump in the solar collector loop is turned off. The solar collector efficiency, η and the incidence angle modifier, kθ are given by:

$$\eta = 0.772 \cdot k\theta - 2.907 \cdot (Tm - Ta)/G - 0.015 \cdot (Tm - Ta)^2 /G \quad (5.1)$$

$$k\theta = 1 - 0.128 \cdot (1/\cos\theta - 1) \quad (5.2)$$

Weather data of Copenhagen, Denmark from Meteonorm is used. A horizontal electrical heating element is used as the auxiliary energy system. The auxiliary heater is located at the middle of the tank. The hot water tank volume is 300 l and the auxiliary volume is 150 l.
The heat store geometry is shown in Fig. 5-1. The heat loss coefficient of the heat store is 2.4 W/K. The heat transfer coefficient of both top and bottom mantle is kept constant as 200 W/m²K. The relative inlet and outlet height of the top mantle for the space heating system are 0.546 and 0.969. Finally, the relative inlet and outlet height of the lower mantle are 0.489 and 0.031. The relative height is 0 at the bottom of the tank and 1 at the top of the tank.

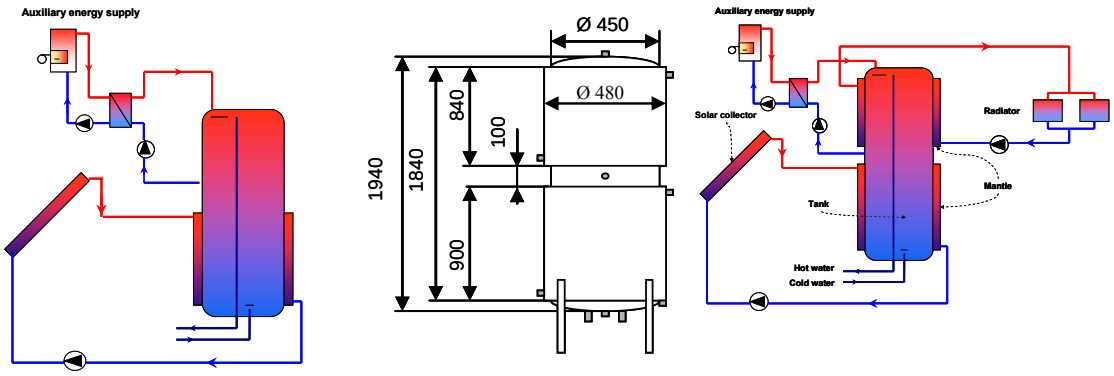

Fig. 5-1. SDHW system (left), Tank dimensions in mm(middle) and bikini solar combisystem.

For simulation of the mantle tank, the non-standard component multiport store-model, Type 340, is used (Drük (2006)). Three different houses with space heating demand of 5000 kWh/year, 9500 kWh/year and 16000 kWh/year are used for the simulations. The house area is 150 m². Fig. 5-2 shows the heat demand throughout the year for the houses.
Four different radiator systems are used. In one of the radiator systems, a variable volume flow rate is used. Fig. 5-3 shows the flow and return temperature during the year. This radiator system is installed in the low energy house with a yearly heat demand of 4818 kWh/year. For the other three radiator systems, the mass flow rate of the systems is constant. The constant mass flow rates of the space heating systems are 215, 280 and 387 kg/hr for radiator sizes of 5000 W, 6500 W and 9000 W, respectively.
The forward and return temperatures versus heat demand are shown in Fig. 5-4 for the three radiator systems. The daily hot water consumption is 100 l with hot water draw offs in the morning, at noon, in the afternoon and in the evening. The cold and hot water temperatures are 10°C and 50°C. The yearly hot water consumption is 1698 kWh/year.
Three different auxiliary heater set temperatures of 50.5, 55 and 60°C in the tank are used. Further, calculations are also carried out for a SDHW system based on the same heat storage, just without the upper mantle. A heat loss coefficient of the mantle tank without the upper mantle of 2.2 W/K is assumed.

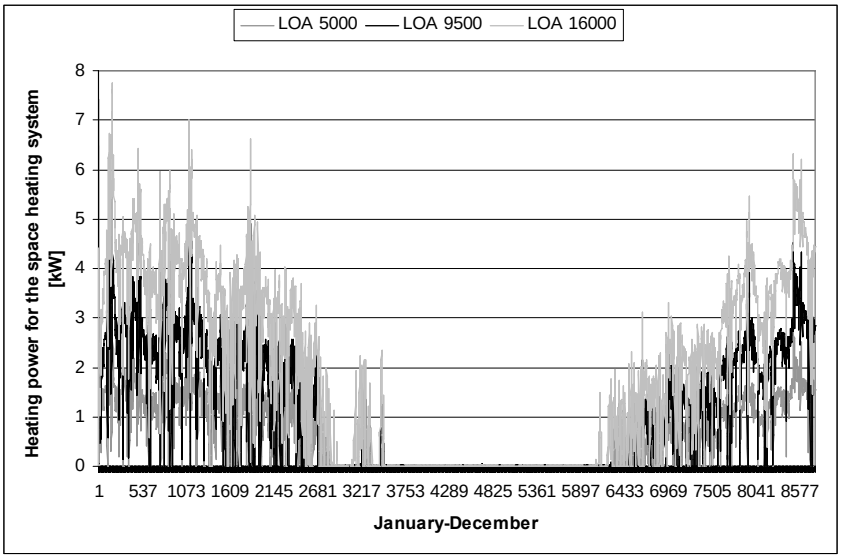

Fig. 5-2.Heat demand for three houses during the year.

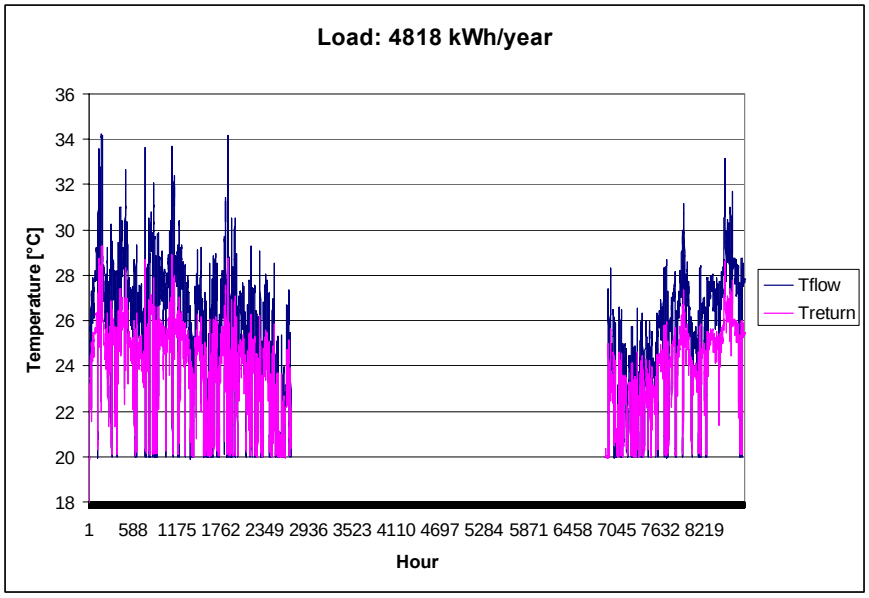

Fig. 5-3.Flow and return for one radiator system in the low energy house.

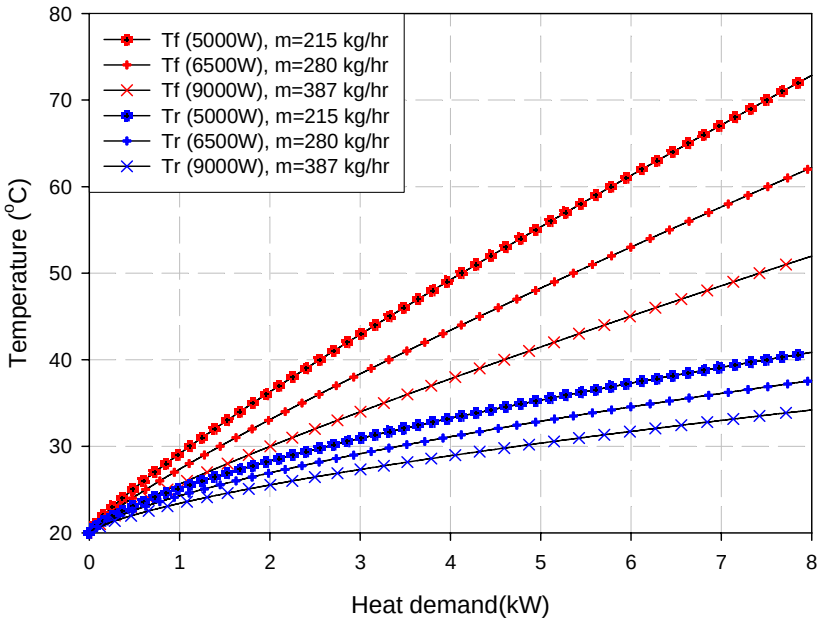

Fig. 5-4.Flow and return temperatures for different radiator sizes.

5.1.2 Results: required set point temperatures

The thermal performance of the system is given as the net utilized solar energy defined as: Domestic hot water consumption + space heating demand - auxiliary energy.

Calculations are carried out in order to determine the required set point temperature for the auxiliary energy supply system in order to fully cover the heat demand of the three houses with the three radiator systems with constant flow rates. Fig. 5-5 shows the required temperature of the auxiliary volume of the bikini tanks for the three houses with a collector area of 3m². The needed set point temperature is decreasing for increasing radiator size and for decreasing yearly heat demand of the house. In the

low energy house (5000 kWh/year), the needed set point temperature to fully cover the space heating demand is lower than 50.5°C. However, the set point temperature must be equal to 50.5°C in order to fully cover the hot water consumption.

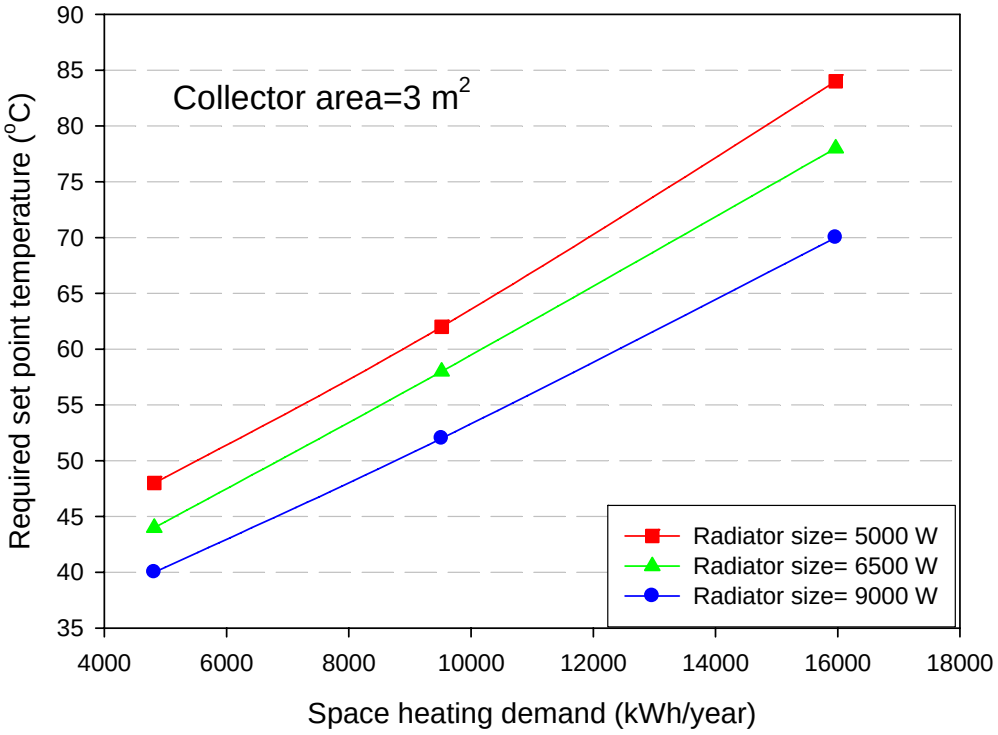

Fig. 5-5. Needed set point temperature for auxiliary volume to fully cover the heat demand.

5.1.3 Results: Different houses and radiator systems

Fig. 5-6 shows the net utilized solar energy for a 3m² solar combisystem based on a bikini tank for different houses with three different radiator systems with constant flow rates. The required set point temperatures from Fig. 5-5 are used in the calculations except for the low energy house where a set point temperature of 50.5°C is used. The thermal performance of the solar combisystem is increasing for decreasing heat demand and increasing radiator size. The reason is that the set point temperature is increasing for increasing heat demand and decreasing radiator size. Consequently, the solar combisystem based on a bikini tank is promising for low energy buildings.

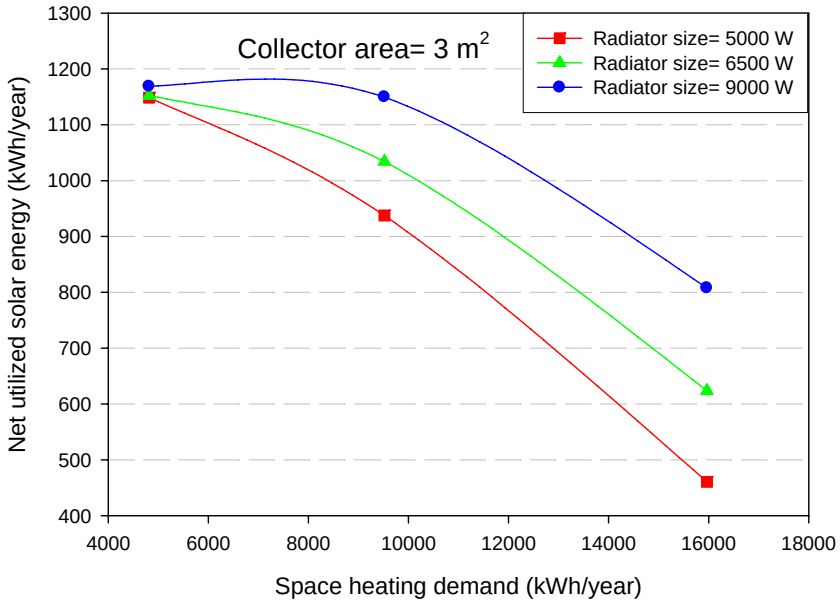

Fig. 5-6. Net utilized solar energy as a function of space heating demand for different space heating systems.

5.1.4 Results: Solar combisystems versus solar domestic hot water systems

In order to compare the solar combisystem with a solar domestic hot water system based on a mantle tank, a series of simulations are carried out. Fig. 5-7 shows the yearly net utilized solar energy as a function of the solar collector area for the low energy house (5000 kWh/year) and the radiator system with variable flow rate as shown in Fig. 5-3. The higher the set point temperature for the auxiliary heater is, the lower the net utilized solar energy will be for both systems. Moreover, solar combisystems has higher net utilized solar energy than SDHW systems. For small collector areas, the difference in the yearly net utilized solar energy of solar combisystems and SDHW systems is small. The difference is increasing for increasing collector area. Clearly, solar combisystems make better use of large collectors than SDHW systems.

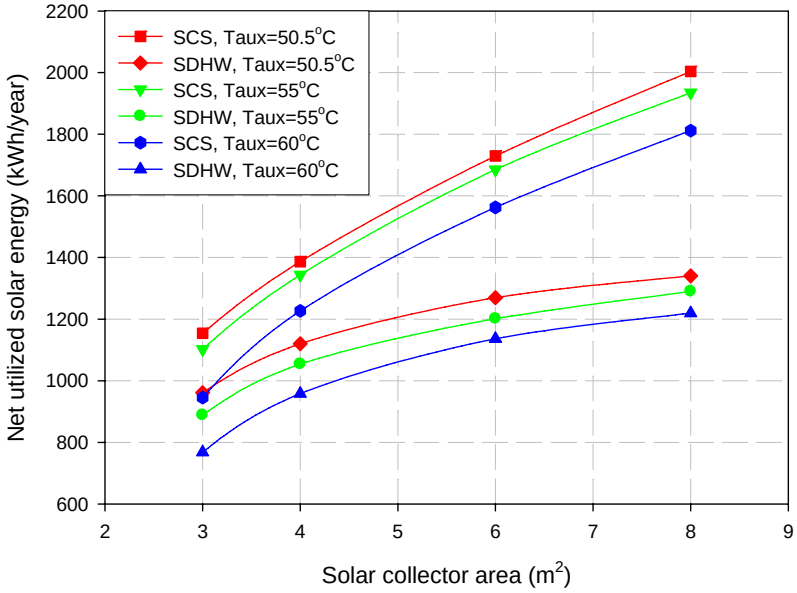

Fig. 5-7. Yearly net utilized solar energy as a function of solar collector area for bikini solar combisystems and SDHW systems based on mantle tank.

5.2 Comparison between solar combisystems based on bikini tanks and tank-in-tank stores

5.2.1 Assumptions

Schematic sketches of the investigated solar combisystems are shown in Fig. 5-8. In the solar combisystem based on a bikini tank, solar heat is transferred from the solar collector fluid to the domestic water by means of a mantle welded around the lower part of a hot water tank. Heat is transferred from the domestic water to the water in the space heating system by means of a mantle welded around the upper part of the hot water tank. The domestic hot water is directly tapped from the tank.
In tank-in-tank solar combisystems, a domestic hot water tank is integrated in the space heating heat store. Solar heat is transferred by an internal heat exchanger spiral placed at the lower part of the tank. The space heating system is connected directly to the tank. Domestic hot water tank is tapped from the domestic hot water tank in the store.

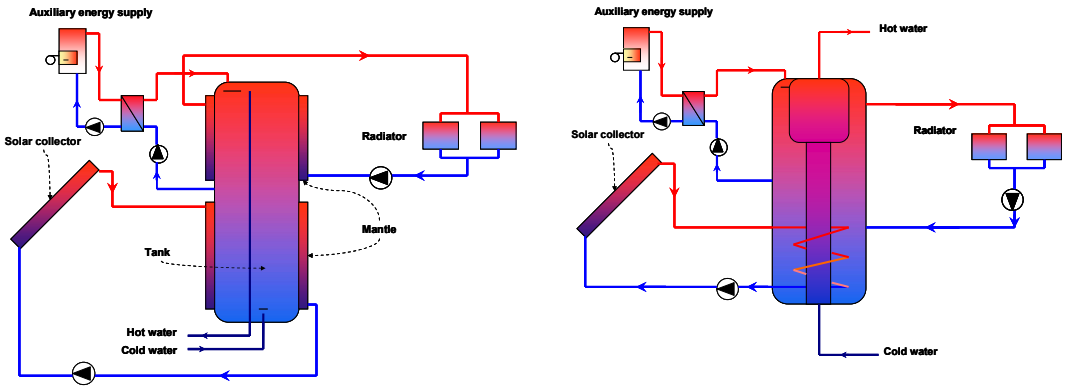

a) Bikini solar combisystem b) Tank-in-tank solar combisystem

Fig. 5-8. Schematic sketches of the investigated solar combisystems.

The tank model multiport store-model; Type 340 (Drük (2006)) is used for both solar combisystems. A previous study by Shah (2001) showed that there is a good agreement between calculated and measured thermal performance for the tank-in-tank solar combisystem.

In order to determine the annual thermal performance for solar combisystems with bikini tanks, a TRNSYS model for a solar combisystem with a bikini tank was developed based on the measurements. The tank model multiport store-model; Type 340 (Drük (2006)) was used for bikini solar combisystems. For the bikini tank model, the dimensions, boundary conditions and operating conditions are adjusted to the bikini tank experiments mentioned in chapter 2. The inlet temperature, the discharge flow rates of 0.5 and 5 l/min, and the heat loss coefficient of the tested tank are used as inputs to the tank model and the calculated outlet temperature and tank temperatures in different levels are compared to the measured data. The limitation of the tank model is that an initial uniform tank temperature is assumed. As shown in Fig. 5-9 and Fig. 5-10, the measured start temperatures are not exactly the same. The measured temperatures at the bottom of the tank are relatively low. However, it is seen that there is a good agreement between measured and calculated temperatures and it is judged that the TRNSYS model is suitable for simulation of the thermal behavior of bikini tanks.

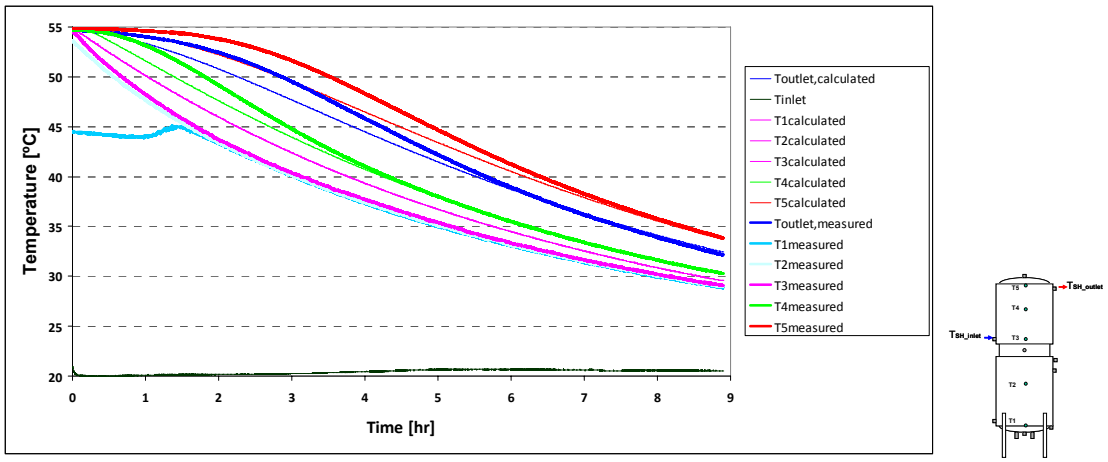

Fig. 5-9. The comparison between measured and calculated temperatures in bikini tank for a discharge volume flow rate of 0.5 l/min.

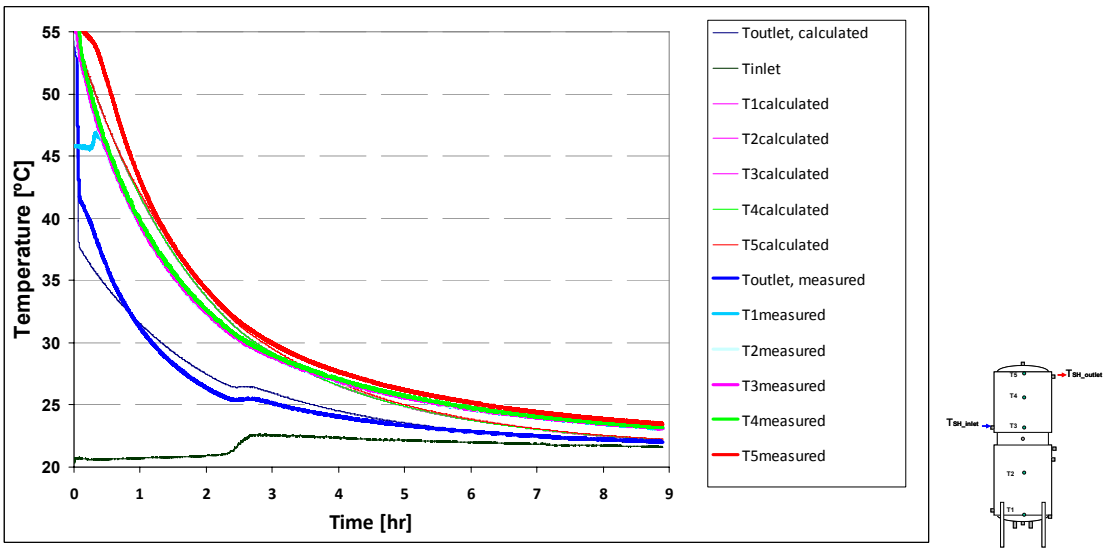

Fig. 5-10. The comparison between measured and calculated temperatures in bikini tank for a discharge volume flow rate of 5 l/min.

The solar collector areas used are 3-8 m². The collector tilt is 45° and the collectors are facing south. The volume flow rate in the solar collector loop is 0.15 l/min.m² for the bikini solar combisystem and 1.2 l/min.m² collector for the tank-in-tank solar combisystems corresponding to low flow and high flow systems. A differential thermostat control with one sensor in the outlet of the solar collector and one sensor in the lower part of the lower mantle for the bikini solar combisystem is controlling the pump in the solar collector loop. For the tank-in-tank solar combisystem, the pump is controlled by a temperature sensor located at the solar collector outlet and a sensor installed in the tank at the level corresponding to 1/3 of the heat exchanger spiral height from the bottom of the heat exchanger spiral. Both systems have start/stop temperature differences of 10/0.5 K.

Moreover, if the temperature of the top tank is higher than 98°C the pump in the solar collector loop is turned off. The solar collector efficiency, η and the incidence angle modifier, $\mathbf{K_\theta}$ are given by Eq. (5.1) and Eq. (5.2).

Weather data of Copenhagen, Denmark from Meteonorm is used. The heat storage volume is 300 l and the auxiliary volume in the heat storage is 150 l. The auxiliary heater inlet and outlet relative height is 1 and 0.5 for both tanks. The relative height of

the space heating inlet and outlet is 0.2 and 0.8 for the tank-in-tank system. Both bikini and tank-in-tank dimensions are shown in Fig. 5-11 and Fig. 5-12. For the tank-in-tank systems, seven different models are considered. Model 1-4 has the same DHW tank volume of 120 litre. In Model 1 and 3, the upper part of the inside tank is located at the same height above the level where the outlet to the auxiliary boiler (middle of the tank) is located. But in Model 2 and 4, the upper part of the inside tank is located at the same level as the inlet of the auxiliary boiler. Model 1 and 2 has a larger tank diameter than Model 3 and 4 in the upper part but a smaller tank diameter at the bottom. In Model 5, 6 and 7, the DHW tank volume is increased to 160 litre and the diameter of the domestic hot water tank is the same. In Model 5, the upper DHW volume of the inside tank is located above the outlet to the auxiliary boiler, in Model 6, it is located at the same level as the outlet to the auxiliary boiler and in Model 7, it is located below the outlet to the auxiliary boiler.
The heat exchange capacity rate of both top and bottom mantle is kept constant as 200 W/m².K for the bikini tank. In the tank-in-tank system, the heat transfer coefficient between the DHW tank and the outer tank is assumed to be 120 W/m².K (Fig. 4-21, Knudsen (2002)). The heat exchange capacity rate for the internal heat exchanger spiral in the solar collector loop is 50 W/K.m² collector area. The tank relative height is 0 at the bottom of the tank and 1 at the top of the tank. The tank is insulated with 5 cm insulation material with a thermal conductivity of 0.037 W/m.K at the tank side, 34 cm insulation material at the top and 1 cm insulation material at the bottom of the tank. The effective thermal conductivity for tank-in-tank store is calculated base on the following equations according to Fig. 5-11.

$$\lambda_{eff,tank} = \frac{A_{insidewater}.\lambda_{water} + A_{insidetank}.\lambda_{steel} + A_{SH}.\lambda_{water} + A_{outertank}.\lambda_{steel}}{A_{insidewater} + A_{insidetank} + A_{SH} + A_{outertank}} \quad (5.3)$$

$$A_{insidewater} = \pi/4.dmi^2,\ A_{insidetank} = \pi/4.(dmo^2 - dmi^2), \quad (5.4)$$
$$A_{SH} = \pi/4.(di^2 - dmo^2),\ A_{SH} = \pi/4.(do^2 - di^2),$$

Model	1	2	3	4	5	6	7
Total tank volume [m³]	0.3	0.3	0.3	0.3	0.3	0.3	0.3
Aux volume [m³]	0.15	0.15	0.15	0.15	0.15	0.15	0.15
Total DHW volume [m³]	0.12	0.12	0.12	0.12	0.16	0.16	0.16
Top volume of DHW tank [m³]	0.05	0.093	0.065	0.065	0.062	0.115	0.153
Bottom volume of DHW tank [m³]	0.07	0.027	0.055	0.055	0.098	0.045	0.007
Aux volume of DHW tank [m³]	0.072	0.093	0.062	0.065	0.093	0.115	0.115
di [m]	0.46	0.46	0.46	0.46	0.46	0.46	0.46
do [m]	0.466	0.466	0.466	0.466	0.466	0.466	0.466
hi [m]	1.828	1.828	1.828	1.828	1.828	1.828	1.828
ho [m]	1.834	1.834	1.834	1.834	1.834	1.834	1.834
dmi [m]	0.36	0.36	0.3	0.3	0.4	0.4	0.4
dmo [m]	0.366	0.366	0.306	0.306	0.406	0.406	0.406
Lti [m]	0.486	0.911	0.486	0.911	0.486	0.911	1.216
Lto [m]	0.49	0.915	0.49	0.915	0.49	0.915	1.22
Lbi [m]	1.336	0.911	1.336	0.911	1.336	0.911	0.606
Lbo [m]	1.34	0.915	1.34	0.915	1.34	0.915	0.61
dbi [m]	0.26	0.194	0.284	0.28	0.306	0.246	0.121
dbo [m]	0.266	0.2	0.29	0.286	0.312	0.252	0.127
Tank heat loss coefficient [W/K]	2.55	2.55	2.55	2.55	2.55	2.55	2.55
Effective thermal conductivity in store [W/mK]	3.302	3.302	3.105	3.105	3.433	3.433	3.433

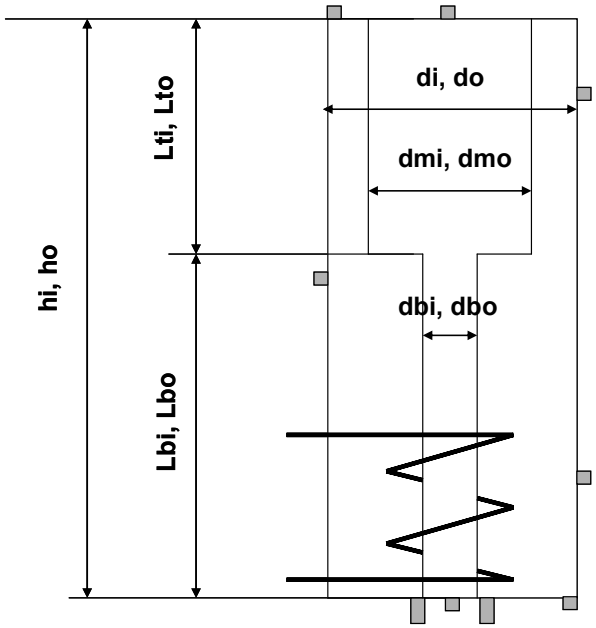

Fig. 5-11. Schematic sketch of the tank-in-tank store and dimensions for store variations.

Total tank volume [m³]	0.3	0.3	0.3
Upper mantle volume [m³]	0.00798	0.00798	0.00798
Lower mantle volume [m³]	0.0081	0.00798	0.00798
Heat transfer area, upper mantle [m²]	0.98	0.98	0.98
Heat transfer area, lower mantle [m²]	1	1	1
H/D	2	3	4
di [m]	0.575	0.503	0.457
do [m]	0.582	0.509	0.463
hi [m]	1.152	1.509	1.828
ho [m]	1.158	1.515	1.834
dmi [m]	0.598	0.525	0.479
dmo [m]	0.604	0.531	0.485
ls [m]	0.019	0.025	0.030
Lti [m]	0.532	0.609	0.670
Lto [m]	0.536	0.613	0.674
Lbi [m]	0.543	0.621	0.683
Lbo [m]	0.547	0.625	0.687
ltm [m]	0.030	0.221	0.406
Tank heat loss coefficient [W/K]	2.43	2.47	2.55
Effective thermal conductivity [W/mK]	2.89	3.19	3.43

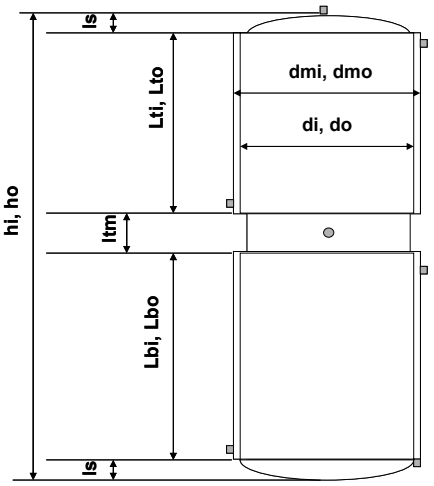

Fig. 5-12. Schematic sketch of the bikini tank and dimensions for store variations.

The effective thermal conductivity for bikini tank is calculated base on the following equations according to Fig. 5-12.

$$\lambda_{tank} = \frac{A_{mantle}.\lambda_{steel} + A_{gap}.\lambda_{glycol.water} + A_{water\,tank}.\lambda_{water} + A_{tank}.\lambda_{steel}}{A_{mantle} + A_{gap} + A_{water\,tank} + A_{tank}} \tag{5.5}$$

$$A_{mantle} = \pi/4.(dmo^2 - dmi^2),\ A_{gap} = \pi/4.(do^2 - dmi^2),$$
$$A_{water\,tank} = \pi/4.di^2,\ A_{tank} = \pi/4.(do^2 - di^2), \tag{5.6}$$

Three different houses with space heating demands of 5000 kWh/year, 9500 kWh/year and 16000 kWh/year are used for the simulations as shown in Fig. 5-2. The house area is 150 m². Fig. 5-13 shows the flow and the return temperature of the assumed space heating systems for three houses with different space heating demands.

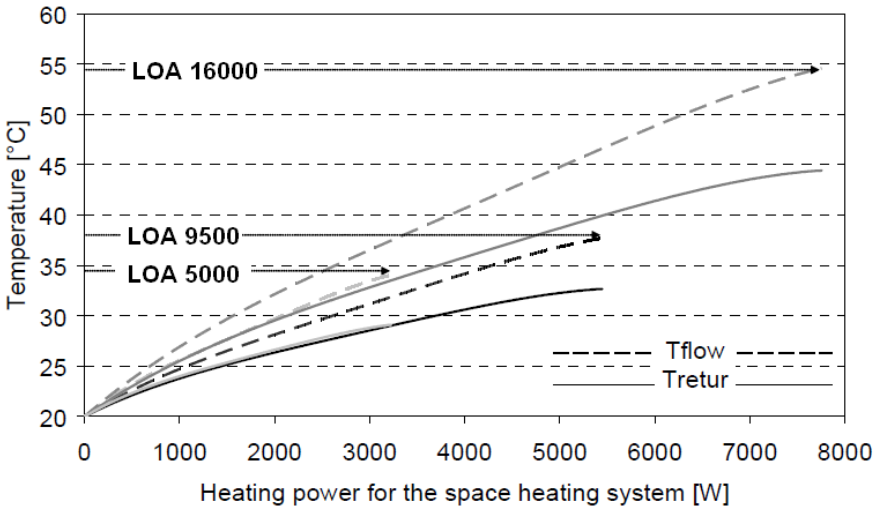

Fig. 5-13. Flow and return temperature of the space heating system for three different houses.

The average daily hot water consumption is 100 l with different hot water consumption patterns. Fig. 5-14 shows three different patterns used every day of the year as well as a strongly variable pattern used in IEA-SHC Tasks 26 and 32 (Jordan and Vajen (2001)). The cold and hot water temperatures are 10°C and 50°C. The yearly hot water consumption is 1698 kWh/year.

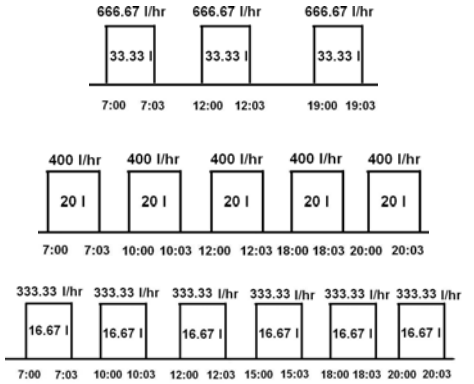

a) high flow rate

b) Medium flow rate

c) Low flow rate

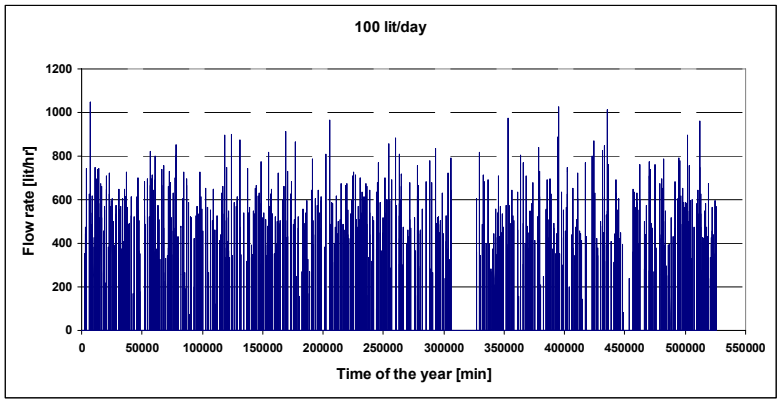

Fig. 5-14. DHW profiles for high, medium and low flow rates DHW draw off during day and Task 26 DHW profile during the whole year.

5.2.2 Results: Set point temperatures

The set point temperature of the auxiliary heater in both bikini and tank-in-tank solar combisystems is determined in such a way that the solar heating system can fully cover the space heating load and the DHW load. Fig. 5-15 shows the set point temperature needed for the tank-in-tank solar combisystem for three different houses and the Task 26 DHW profile. It can be seen that Model 6 and 7 have a low set point temperature due to the large auxiliary volume of the hot water tank.

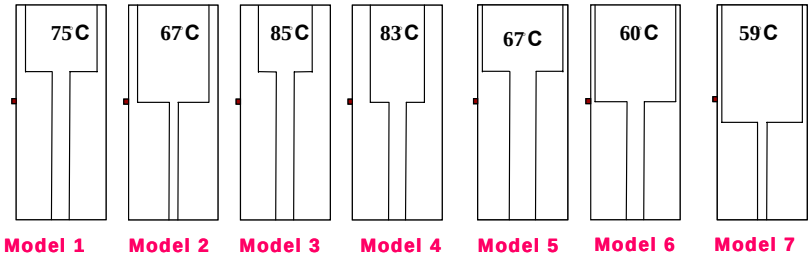

Fig. 5-15. Set point temperature of tank-in-tank system for three houses with the Task 26 DHW profiles.

In Table 5-1, the set point temperatures of the bikini solar combisystem and the tank-in-tank solar combisystem for three different houses with high, medium and low flow DHW profiles are shown. For the tank-in-tank system, the set point temperature is the same for the houses with low and medium heat demand and higher for the old house with a high space heating demand.

Table 5-1. Set point temperature of bikini solar combisystem and tank-in-tank solar combisystem for three different houses and for high, medium and low flow rates DHW profiles for all seven models.

Space heating load [kWh/year]	5000	9500	16000
Set point temperature of tank-in-tank solar combisystems [°C]	50.5	50.5	55
Set point temperature of bikini solar combisystems [°C] #	55	60	75

Also for Task 26 DHW profile

The set point temperature for the bikini tank is higher than the set point temperature for the tank-in-tank store, because the heat transfer from the upper mantle is relatively low in the bikini tank.

5.2.3 Results: Tank-in-tank design

In order to optimize a tank-in-tank system, simulations have been carried out with different DHW profiles and space heating loads. For tank-in-tank systems, the height and diameter of the inside tank might play an important role in the tank design. Therefore, in the current study, the effect of height and diameter of the upper and lower part of the inside tank is investigated by means of the seven different tank-in-tank designs.

Fig. 5-16 shows the net utilized solar energy versus the space heating load for 6 m² solar collector area and different tank-in-tank designs with the Task 26 domestic hot water profile. The net utilized solar energy is the space heating demand + the domestic hot water consumption – the auxiliary energy supply to the top of the heat storage tank. It can be seen that Model 7 has the highest thermal performance

followed by Model 6, 5, 2, 1, 4 and 3. That is: The lower the set point temperature, the higher the thermal performance. It is also seen that the thermal performance of the system is increasing for increasing space heating demand. With the Task 26 domestic hot water profile, the thermal performance is increasing for increasing auxiliary volume of the hot water tank.

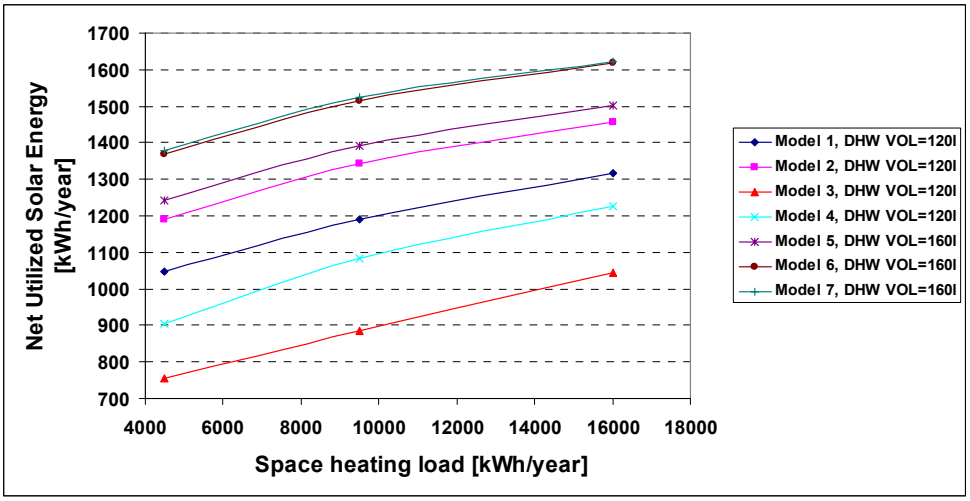

Fig. 5-16. Net utilized solar energy versus space heating load for different tank-in-tank designs with Task 26 DHW profile.

In Fig. 5-8b, the tank-in-tank system has an internal heat exchanger spiral in the solar collector loop and a direct inlet to and outlet from the tank for the space heating loop. Another system with the same tank dimension and model has been investigated and compared when the direct inlet from the space heating system is replaced with an inlet stratifier and the same internal heat exchanger spiral in solar collector loop is assumed. The inlet stratifier is an equipment which helps establishing and maintaining the stratification in the heat store by allowing water to enter the heat store in the right level of the tank where the inlet temperature is equal to the tank temperature. The outlet to the space heating system is positioned with the relative height of 0.8. The best and worst tank-in-tank models from a thermal performance point of view shown in Fig. 5-16 have been used: Model 3 and Model 7. Both tank-in-tank systems have the same boundary conditions and set point temperatures of the auxiliary heater. Task 26 DHW profile has been used for the simulation. Fig. 5-17 is a diagram of the net utilized solar energy as a function of the space heating load. The systems with the inlet stratifier have 3-6% higher thermal performance than the systems with direct inlet in the heat store. The reason for such an increase is the improved thermal stratification in the tank achieved by the inlet stratifier. The higher the thermal stratification in the tank, the lower the consumption of the auxiliary energy and the higher the solar heat production.

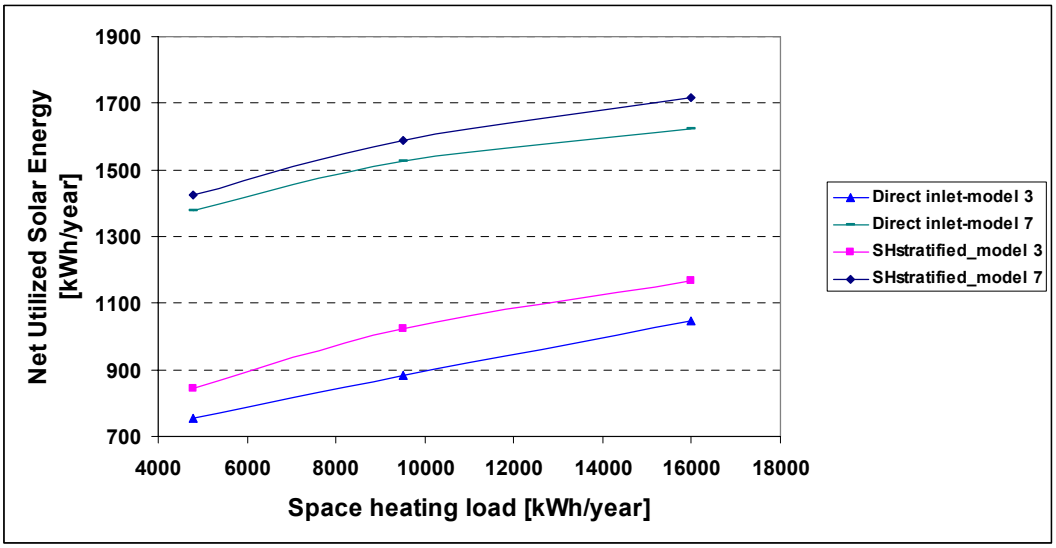

Fig. 5-17. Net utilized solar energy versus space heating demand for two different tank-in-tank designs with Task 26 DHW profile.

The tank-in-tank systems are also investigated with the DHW profiles with high, medium and low flow rates. Fig. 5-18 shows the net utilized solar energy versus the space heating load for the seven models and the high flow rate DHW profile. Model 4 has the highest thermal performance followed by Model 1, 6, 5, 7, 3 and 2. The thermal performances of the systems are increasing for increasing space heating load. The thermal performances of the systems are much higher with the same average daily hot water consumption than with the Task 26 profile. This is caused by the high required set point temperature for the Task 26 profile. For both low and medium flow rate DHW profile, the trend of the net utilized solar energy for the different models is the same as for the high flow DHW profile. The differences of the thermal performances for the three different DHW profiles are small, maximum up to 3%.

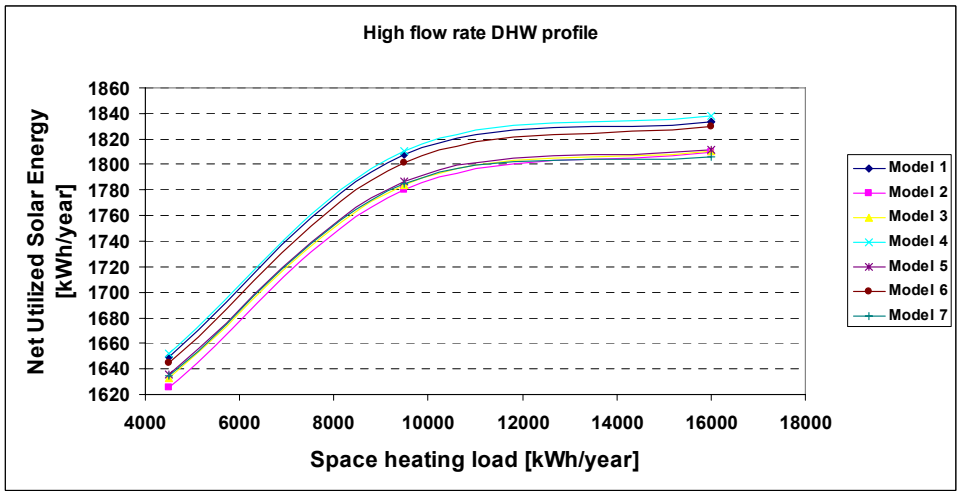

Fig. 5-18. Net utilized solar energy versus space heating demand for different tank-in-tank designs with high flow DHW profile.

5.2.4 Results: Bikini solar combisystem design

The thermal performance of bikini solar combisystems is investigated for the Task 26 DHW profile for different H/D ratios of the tank. The insulation thickness is the same for all H/D ratios. Fig. 5-19 shows the net utilized solar energy for three different space heating systems with three different collector areas and H/D ratios of the tank. The H/D ratio of the tank does not play an important role as long as the H/D ratio is higher than 2. For 3 m² solar collector area a decreased space heating load results in an increased thermal performance of the system. This is due to the decreased set point temperature for the low space heating demands. For a collector area of 5 m², the thermal performance in the house with the medium space heating demand is a little bit higher than the thermal performance of the system in the low energy house while the system has the lowest thermal performance in the old house. For a collector area of 8 m², the thermal performance of the solar heating system in the house with medium space heating demand is a little higher than the thermal performance of the system in the house with low energy demand and higher than the thermal performance of the system in the old house.

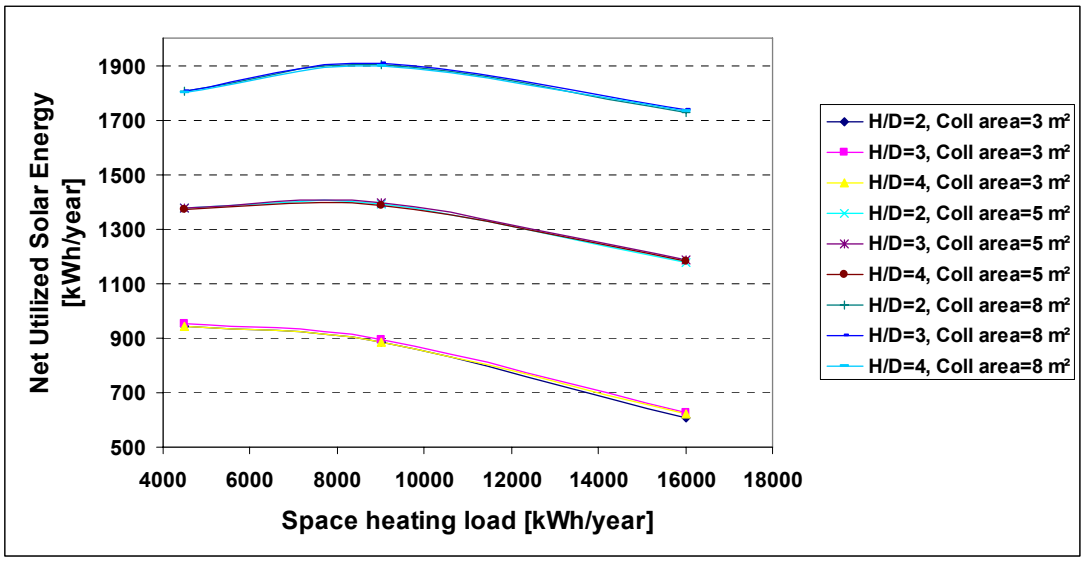

Fig. 5-19. Net utilized solar energy versus H/D ratio for the bikini solar combisystem.

5.2.5 Results: Comparison between tank-in-tank and bikini solar combisystems

In order to compare bikini and tank-in-tank solar combisystems, the best tank-in-tank model system from Fig. 5-16 is compared to a bikini tank system. Thus, Model 7 is used since this tank model performs best among the tank-in-tank models with different space heating loads and the Task 26 DHW profile. Both the bikini and tank-in-tank systems have the same H/D ratio of 4. Fig. 5-20 shows the net utilized solar energy of the solar combisystem installed in the old house, the house with medium space heating load and the low energy house for collector areas of 3, 5 and 8 m². The smaller the collector area, the better the bikini solar combisystems performs compared to tank-in-tank solar combisystems. For a collector area of 3 m², the net utilized solar energy increases for the tank-in-tank solar combisystem and decreases for the bikini

solar combisystem as the space heating load increases. For the bikini solar combisystem, the set point temperature for the auxiliary heater is increased from 55°C for the low energy house to 60°C and 75°C for the houses with medium space heating demand and high space heating demand. For the tank-in-tank system, the auxiliary set point temperature remains constant at 59°C. It can be seen that bikini solar combisystems have higher thermal performance than tank-in-tank solar combisystems as long as the collector area is small. When the collector area increases, the thermal advantage of the bikini tank is decreased especially for houses with high space heating demands. The results are explained by the different required set point temperature for the auxiliary energy supply system.

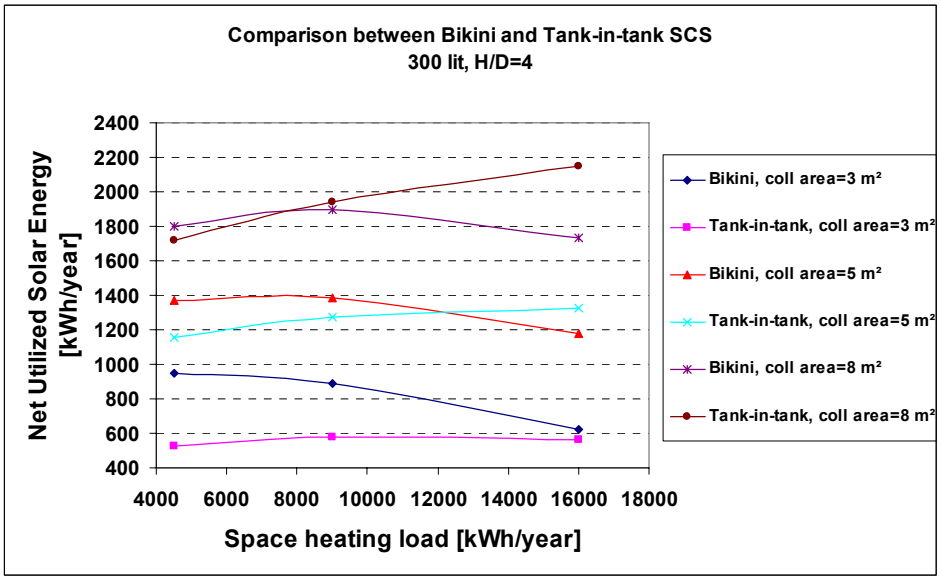

Fig. 5-20. Net utilized solar energy versus space heating demand for Task 26 DHW profile.

5.3 Conclusions

Bikini solar combisystems are investigated numerically and compared to SDHW systems based on mantle tanks. Three different houses with four different radiator systems are considered for the simulations. The needed temperature for the auxiliary heater is determined for different houses and radiator systems. The thermal performance of the solar combisystem is compared to the thermal performance of a solar domestic hot water system based on a mantle tank. The following results are obtained for the investigation

The larger the radiator:

- the lower the required temperature for the auxiliary heater
- the higher the thermal performance of the system

The lower the space heating demand of the house:

- the lower the required temperature for the auxiliary heater
- the higher the thermal performance of the system

Solar combisystems based on bikini tanks and tank-in-tank stores have also been compared. Bikini tank systems require, if installed in low energy buildings, low

auxiliary volume set point temperatures resulting in high thermal performances. High auxiliary volume set point temperatures are required for bikini tank systems installed in houses with a high space heating demand. This results in a relatively low thermal performance. Bikini tank systems are therefore only suitable for low energy buildings with low temperature space heating systems while tank-in-tank combisystems are suitable for normal and old houses. The study has also shown that when the direct inlet from the space heating to the tank is replaced with an inlet stratifier in the store, the thermal performance will increase by 3-6%. Tank-in-tank stores with domestic hot water tanks with large auxiliary volumes are recommended for normal variable domestic hot water consumption patterns in order to achieve a high thermal performance.

6 Conclusions and suggestions for further investigations

6.1 Conclusions

Solar combisystems based on bikini tanks and tank-in-tank solar combisystems are compared experimentally and theoretically in this PhD thesis. Thermal experiments with a bikini tank during space heating discharge are carried out with the aim to elucidate how different discharge volume flow rates through the upper mantle influence the thermal stratification and the thermal behavior of a bikini tank. Five different flow rates of 0.5, 1, 2, 3 and 5 l/min through the upper mantle were tested for a bikini tank in a heat storage test facility. The experiments showed that when the discharge volume flow rate through the upper mantle is high, thermal stratification inside the tank is destroyed. For low volume flow rates, thermal stratification can be created at the beginning of the test but thermal stratification is destroyed at the end of the test. The duration of the period in which thermal stratification is created is increasing for decreasing volume flow rates. The thermal behavior of the bikini tank during the discharge through the upper mantle is not strongly influenced by the temperature level of the tank and the temperature level of the water flowing into the upper mantle. The discharge efficiencies of the bikini tanks are determined for two different initially mixed conditions. The higher the volume flow rate, the lower the discharge efficiency.

Thermal experiments were also carried out for a tank-in-tank store with different DHW discharge volume flow rates of 2.3, 4.0 and 6.5 l/min. The results showed that thermal stratification is higher for lower DHW discharge volume flow rates compared to higher volume flow rates.

The heat transfer and flow structure in tank-in-tank stores are rather complex and the thermal experiments were followed by investigations by means of advanced numerical and experimental techniques. Computational Fluid Dynamics (CFD) models were used to model the convection process in the inner and outer side of the tank-in-tank store. A CFD program solves the Navier-Stokes and energy equations and thus, detailed information of the heat transfer and flow structure can be obtained.

The CFD calculations show that during DHW discharge, turbulent model can be applied for modeling of the inner DHW tank and for the outer tank, laminar model can be used. When the DHW discharge is stopped, that is during stand by periods, laminar model can be applied in both the inner and the outer tank.

The comparison between the CFD calculation and thermal experiments shows a good agreement between calculated and measured temperatures. And also there is a very good agreement between PIV measurements and CFD calculations on flow velocities.

Based on the theoretical and experimental investigations, it can be concluded that the CFD model has the capability to predict and simulate the heat transfer, flow velocities and temperature distribution in the tank-in-tank store in a reasonable way. That is: The CFD model was validated by means of the thermal experiments and by the PIV measurements.

A real steel tank-in-tank heat store is modeled with the validated CFD model. The thermal stratification, heat transfer and flow structure for two different geometries of

the tank-in-tank heat store are investigated: Stores with two different hot water tank diameters are investigated. The temperature distributions, heat flux, heat transfer coefficients and velocity vectors are investigated for three different hot water draw-off volume flow rates of 5, 10 and 15 l/min. When the diameter of the inner DHW tank in the lower part decreases, the thermal stratification during and after domestic hot water draw-offs gets worse. Further, there are higher domestic water temperatures at the lower level than at the higher level where the diameter of the inner DHW tank changes. The reason for the higher temperatures in the lower level is that the small water volume is heated faster than the larger water volume by the heat transfer from the outer tank. Thermal conduction in the DHW tank wall and natural convection will transfer heat upwards in this part of the tank after draw-off periods.
The yearly thermal performance of two solar combisystems and one SDHW system are determined by means of TRNSYS calculations. Bikini tank solar combisystems are compared to SDHW systems based on mantle tanks. Three different houses with four different radiator systems are considered for the simulations. The needed temperature for the auxiliary heater is determined for the different houses and radiator systems. The following results are obtained for the investigation:

The larger the radiator:
- the lower the required temperature for the auxiliary heater
- the higher the thermal performance of the system

The lower the space heating demand of the house:
- the lower the required temperature for the auxiliary heater
- the higher the thermal performance of solar combisystems based on bikini tanks

Solar combisystems based on bikini tanks and tank-in-tank stores have also been compared. Bikini tank systems require, if installed in low energy buildings, low auxiliary volume set point temperatures resulting in high thermal performances. High auxiliary volume set point temperatures are required for bikini tank systems installed in houses with a high space heating demand. This results in a relatively low thermal performance. Bikini tank systems are therefore only suitable for low energy buildings with low temperature space heating systems, while tank-in-tank combisystems are suitable for normal and old houses. The study has also shown that when the direct inlet from the space heating to the tank-in-tank store is replaced with an inlet stratifier in the store, the thermal performance will increase by 3-6%. Tank-in-tank stores with domestic hot water tanks with large auxiliary volumes are recommended for normal variable domestic hot water consumption patterns in order to achieve a high thermal performance and a good hot water comfort.

6.2 Suggestions for the future work

The investigations showed that small solar combisystems based on bikini tanks are suitable for low energy buildings. The investigations also showed that stratification in bikini tanks is destroyed during space heating discharge with high volume flow rates through the upper mantle. Most likely the thermal performance of solar combisystems with bikini tanks can be strongly increased if the auxiliary energy supply system is controlled in a smart way. It is therefore recommended to focus future research on development of an advanced smart bikini tank and a smart control system for system. The bikini tank can be heated by an oil fired boiler or a natural gas burner from the top in such a way that both the water volume and water temperature at the top of the heat storage heated by the boiler/burner can vary. In periods with a low heating demand the volume can be small. In periods with a high heating demand the volume can be large. Further, investigations could be done on how best to transfer heat from the boiler/burner to the heat storage and how best to control the operation of the boiler/burner. Either an external heat exchanger can be used to transfer heat from the boiler/burner to the water in the heat storage or a built in heat exchanger spiral in the heat storage can be used. The control system might be based on weather forecasts and/or expectations for coming heat demands and solar energy production.
It is also recommended further to develop solar combisystems with tank-in-tank heat storages, since these systems are attractive for most buildings. Also for tank-in-tank heat storages, the research should focus on the smart tank principle and on the interplay between the auxiliary energy supply system and the solar heating system.

References

Andersen, E. & Shah, L.J. & Furbo, S. (2004), "Thermal performance of Danish solar combisystems in practice and in theory", ASME, Journal of Solar Energy Engineering, 126, 744 – 74.

Andersen, E., Furbo, S. (2007), "Theoretical Comparison of Solar Water/Space-Heating Combisystems and Stratification Design Options", ASME, Journal of Solar Energy Engineering, 129, 438-448.

Andersen, E. & Furbo, S. & Fan, J. (2007), "Multilayer fabric stratification pipes for solar tanks", Solar Energy, 81 (10), 1219-1226.

Andersen, E., Furbo, S. (2009), "Theoretical variations of the thermal performance of different solar collectors and solar combisystems as function of the varying yearly weather conditions in Denmark", Journal of Solar Energy, 83, 552–565.

Andersen, N. B. (1988) , "Solvarmeanlæg til rumopvarmning og varmt brugsvand, demonstrationsanlægget i Ejby", Report no. 189, Thermal Insulation Laboratory, Technical University of Denmark.

Baur, J.M. & Klein, S.A. & Beckman, W.A. (1993), "Simulation of water tanks with mantle heat exchangers", proceedings ASES Annual Conference. 286-291.

Bergmann, I. & Weiß, W. (2002), "Fassadenintegration von thermischen Sonnenkollektoren ohne Hinterlüftung", Bericht aus Energie- und Umweltforschung, Wien.

Bindslev, B. (2009), "How ambitious can we be in contributing to the world's energy needs with bioenergy, wind, solar and storage. Targets and road maps from Workshop on Sustainable Energies", Technical University of Denmark, Denmark.

Bliss, R.W. (1955), "Design and Performance of the Nation's only Fully Solar-Heated House", Air Conditioning, Heating and Ventilating, 52 (10), p. 92.

Cristofari, C. & Notton, G. & Poggi, P. & Louche, A. (2003), "Influence of the flow rate and the tank stratification degree on the performances of a solar flat-plate collector". International Journal of Thermal Sciences (42), 455-469.

Davidson, J.H. & Adams & D.A., Miller & J.A. (1994a), "A coefficient to characterize mixing in solar water storage tanks", Transactions of the ASME, Journal of Solar Energy Engineering (116), 94-99.

Davidson J.H. & Adams D.A. (1994b), "Fabric Stratification Manifolds for Solar Water Heating", Journal of Solar Energy Engineering, 116, 130-136.

Drück, H. & Hahne E. (1998), "Test and comparison of hot water stores for solar combistores", EuroSun98, The second ISES-Europe Solar Congress, Portoroz, Slovenia.

Drück, H. (2006), MULTIPORT Store – Model, Type 340 for TRNSYS. Institut für Thermodynamik und Wärmetechnik. Universität Stuttgart.

Duffie, J.A. & Beckman, W.A. (1991), "Solar Engineering of Thermal Processes". 2nd edition. John Wiley and Sons Inc. ISBN 0-471-51056-4.

Ellehauge, K. (1993), "Målinger på solvarmeanlæg til kombineret brugsvands- og rumopvarmning – 5 markedsførte solvarmeanlæg installeret hos anlægsejerne", Report no. 255, Thermal Insulation Laboratory, Technical University of Denmark. (In Danish)

Ellehauge, K. (1993), "Små markedsførte solvarmeanlæge til brugsvandsopvarmning-funktionsafpøvning og ydelsesmålinger". Opbygning af prøvestand. Technical University of Denmark, Thermal Insulation Laboratory. Report 93-37. (In Danish)

Ellehauge, K., et al. (2000), "Erfaringer fra målinger på kombinerede solvarmeog biobrændselsanlæg", Technological Institute, Denmark. (In Danish)

Ellehauge, K. (2002), "Generic System #2: A Solar Combisystem Based on a Heat Exchanger between the Collector Loop and Space Heating Loop", IEA-SHC Task 26 Appendix 1, http://www.iea-shc.org/outputs/task26/C_App1_System2.pdf.

Engebretson, C.D. (1964), "The Use of Solar Energy for Space Heating – M.I.T.: Solar House IV." Proc. of the UN Conference on New Sources of Energy, 5, 159.

Esbensen, & Korsgaard, (1977), "Performance of the Zero Energy House in Denmark", Report no. 64, Thermal Insulation Laboratory, Technical University of Denmark.

Fiedler, F. & Nordlander, S. & Persson, T. & Bales, C. (2006), "Thermal performance of combined solar and pellet heating systems", Renewable Energy, 31, 73-88.

Fluent 6.1 User's Guide. (2003). Fluent Inc. Centerra Resource Park 10 Cavendish Court Lebanon, NH 03766.

Furbo, S. & Mikkelsen, S.E. (1987), "Is low flow operation an advantage for solar heating systems?", Proceedings of ISES Solar World Congress. Hamburg, Germany. Vol. 1, pp.962-966.

Furbo, S. (1993), "Optimum design of small DHW low flow solar heating systems", Proceedings of ISES Solar World Congress. Budapest, Hungary.

Furbo, S. & Vejen, N.K. & Shah, L.J. (2004). Thermal performance of a large low flow solar heating system with a highly thermally stratified tank. Journal of Solar Energy Engineering, 127(1), 15-20.

Furbo, S. & Andersen, E. & Thür, A. & Shah, L.J. & Andersen, K (2005). Thermal performance of a large low flow solar heating system with a highly thermally stratified tank. Journal of Solar Energy Engineering, 79 (5), 431 – 439.

Furbo, S. & Knudsen, S. (2006), "Improved design of mantle tanks for small low flow SDHW systems", International Journal of Energy Research. 30(12) 955-965.

Haller, M.Y. & Cruickshank, C. & Streicher, W. & Harrison, S.J. & Andersen, E. & Furbo, S. (2009). Methods to Determine Stratification Efficiency of Thermal Energy Storage Processes – Review and Theoretical Comparison. Solar Energy, 83(10), 1847-1860.

Haller, M.Y. & Yazdanshenas, E. &Andersen, E. & Bales, C. & Streicher, W. & Furbo, S. (2010). A Method to Determine Stratification Efficiency of Thermal Energy Storage Processes Independently from Storage Heat Losses. Accepted for publication in Solar Energy in February 2010.

Hollands, K.G.T. & Lightstone, M.F. (1989), "A review of low-flow, stratified-tank solar water heating systems", Solar Energy (43), 97-105.

IEA, Task 14 (1996) (Editor: Duff, W.), "Advanced Solar Domestic Hot Water Systems". A report of the Task 14 Advanced Solar Domestic Hot Water Systems Working Group. IEA, Solar Heating and Cooling Programme.

Johannes K. & Fraisse G. & Achard G. & Rusaouen G. (2005), "Comparison of solar water tank storage modelling solutions", Solar Energy, 79, 216-218.

Kays W.M. & Crawford M.E. (1993), "Convective Heat and Mass Transfer". Third Edition. McGraw-Hill.

Knudsen, S. (2002), "Heat Transfer in a 'Tank-in-Tank' Combi Store", Department of Civil Engineering, Technical University of Denmark, Report No. R-025.

Knudsen S. & Furbo S. (2004), "Thermal stratification in vertical mantle heat-exchangers with application tosolar domestic hot-water systems" , Applied Energy 78, 257-272.

Knudsen, S. & Morrison, G.L. & Behnia, M. & Furbo, S. (2005), "Analysis of the flow structure and heat transfer in a vertical mantle heat exchanger", Solar Energy 78(2), 291-300.

Lavan, Z. &Thompson, J. (1977), "Experimental study of thermally stratified hot water storage tanks", Solar Energy (19), 519-524.

Löf, G.O.G. & El-Wakil, M. M. & and Chiou, J. P. (1963), "Residential Heating with Solar Heated Air – the Colorado Solar House", Trans. ASHRAE, 77.

Löf, G.O.G. & El-Wakil, M. M. & and Chiou, J. P. (1964), "Design and Performance of Domestic Heating Systems Employing Solar Heated Air – the Colorado House," Proc. Inst. Mech. Eng., Part J: J. Eng. Tribol., 5, 185.

Metzger, J. & Matuska, T. & Sourek, B. (2007), "Performance of Solar Combisystems with Evacuated Flat-plate Collectors and Different Heating Systems", ISES Solar World Congress 2007, Beijing, China.

Metzger, J. & Matuska, T. & Sourek, B. (2008), "Solar Combisystems with Building-Integrated Evacuated Flat-Plate Solar Collectors", Proceedings of EUROSUN 2008, Lisbon, Portugal.

Oliveski R.D.C. & Macagnan M.H. & Copetti, J. B. & Petroll A.M. (2005), "Natural convection in a tank of oil : experimental validation of a numerical code with prescribed boundary condition," Experimental Thermal and Fluid Science 29, 671-680.

Panthalookaran, V. & Heidemann, W. & Müller-Steinhagen, H. (2007), "A new method of characterization for stratified thermal energy stores", Solar Energy (81), 1043-1054.

Shah, L.J. & Morrison, G.L. & Behnia, M. (1999), "Characteristics of vertical mantle heat exchangers for solar water heaters", Solar Energy (67), 79-91.

Shah, L.J. (2001), "Undersøgelse af et solvarmeanlæg til kombineret rum og brugsvandsopvarmning", Department of Civil Engineering, Technical University of Denmark, Report No. SR-01-19.

Shah, L.J. (2002)," Generic System #4: DHW Tank as a Space-Heating Storage Device", IEA-SHC Task 26, Appendix 3,
http://www.iea-shc.org/outputs/task26/C_App3_System4.pdf.

Shah, L.J. & Furbo, S. (2003), "Entrance effects in solar storage tanks; Solar Energy (75), 337-348.

Tepe, R. & Bales, C. (2003), "Simulation Study of a Dream Systems", Technical Reports of Subtask C, IEA-SHC Task 26, http://www.iea-shc.org/task26.

Thür, A. (2007), "Compact solar combisystem-High Efficiency by Minimizing Temperatures", Ph.D. Thesis, Technical University of Denmark, Rapport R-160.

TRNSYS 16 (2005), User Manual, University of Wisconsin, Solar Energy Laboratory.

van Berkel, J. (1997), "Thermocline entrainment in stratified energy stores", Ph.D. Thesis, Technische Universiteit Eindhoven, The Netherlands, p. 32.

van Koppen & C.W.J., Thomas & J.P.S & Veltkamp W.B. (1979), "The actual benefits of thermally stratified storage in a small and medium size solar system". SUN II, Proceedings of ISES Biennial Meeting. Atlanta, USA, pp. 576-580.

Weiss, W. & Bergmann, I. & Faninger, G. (2009), "Solar Heat Worldwide – Markets and Contribution to the Energy Supply 2007", IEA-SHC, http://www.iea-shc.org.

Weiss, W. (2003), "Solar heating systems for houses- A design handbook for solar combisystems", James and James, London, ISBN 1-902916-46-8.